

# Journal of Energy

ISSN 1849-0751 (On-line)  
ISSN 0013-7448 (Print)  
UDK 621.31

**VOLUME 59** Number 1-4 | 2010 Special Issue

- 03** S. Vujević, P. Sarajčev  
An EMTP extension for computing earthing system transient step and touch voltages
- 11** A. Tokić, I. Uglešić  
Power quality problems due to transformer inrush current
- 19** I. Uglešić, I. Ivanković, V. Milardić  
Transients caused by sequential circuit breaker tripping issued by busbar protection
- 25** Z. Maljković, Ž. Zebić, M. Pavlica  
Measurement and simulation of hydro-generator's asynchronous operation
- 32** B. Polajžer, G. Štumberger, S. Seme  
Evaluation of different methods for voltage sag source detection
- 38** I. Jurić-Grgić, M. Kurtović, R. Lucić  
Numerical analysis of power system electromechanical and electromagnetic transients based on the finite element technique
- 46** K. Deželak, A. Korak, T. Konjic, G. Štumberger, J. Voršič  
The impact of events in the Slovene high – voltage network on the power quality in the distribution networks
- 52** M. Kizilcay, C. Neumann  
Mitigation of common mode failures at multi-circuit line configurations by application of line arresters against back-flashovers
- 61** L. Prikler, G. Bán, M. Kizilcay, G. Tari, A. Tombor, J. Zerenyi  
Influence of the secondary arc on the operation of single phase autoreclosure of the 400 kV interconnection between Hungary and Croatia
- 70** M. Lukić Armstrong, J. R. Martí, P. Kundur  
Detailed transients simulation of a doubly fed induction generator wind turbine system with the EMTP-type OVNI simulator
- 77** I. Uglešić, M. Křepela, V. Milardić  
Solving EMC problems in the design of new HV test laboratory
- 83** S. Bojić, A. Sekso Telento, I. Dolić  
Electromagnetic compatibility in various kinds of substations in Croatian transmission networks and mitigation measures
- 90** M. Osborne, P. Jarman, C. Charalambous, Z. Wang  
The impact of ferroresonance and low frequency phenomena on power transformers and transmission systems
- 97** G. Sarcinelli Luz  
Discussion on the interaction between transformers and the power systems
- 105** M. Stojsavljević, D. Nemec, I. Toljan  
At the edge of voltage collapse in Slovenian power system after outage of NPP Krško and 400 kV node Tumbri
- 113** A.L.J. Janssen, F. Iliceto, Q. Bui-Van, S. Morais, M. Waldron, B. Middleton  
Dielectric, switching and system requirements under out-of-phase conditions, during synchronisation and under comparable stresses

# Journal of Energy

Scientific Professional Journal Of Energy, Electricity, Power Systems

Online ISSN 1849-0751, Print ISSN 0013-7448, VOL 59

## Published by

HEP d.d., Ulica grada Vukovara 37, HR-10000 Zagreb

HRO CIGRÉ, Berislavićeva 6, HR-10000 Zagreb

## Publishing Board

**Robert Krklec**, (president) HEP, Croatia,

**Božidar Filipović-Grčić**, (vicepresident), HRO CIGRÉ, Croatia

## Editor-in-Chief

**Goran Slipac**, HEP, Croatia

## Associate Editors

**Helena Božić** HEP, Croatia

**Stjepan Car** Končar-Electrical Engineering Institute, Croatia

**Tomislav Gelo** University of Zagreb, Croatia

**Davor Grgić** University of Zagreb, Croatia

**Mičo Klepo** Croatian Energy Regulatory Agency, Croatia

**Stevo Kolundžić** Croatia

**Vitomir Komen** HEP, Croatia

**Marija Šiško Kuliš** HEP, Croatia

**Dražen Lončar** University of Zagreb, Croatia

**Goran Majstrović** Energy Institute Hrvoje Požar, Croatia

**Tomislav Plavšić** Croatian Transmission system Operator, Croatia

**Dubravko Sabolić** Croatian Transmission system Operator, Croatia

**Mladen Zeljko** Energy Institute Hrvoje Požar, Croatia

## International Editorial Council

**Franco Barbir** University of Split, Croatia

**Tomislav Barić** J.J. Strossmayer University of Osijek, Croatia

**Anastasios Bakirtzis** University of Thessaloniki, Greece

**Frank Bezzina** University of Malta

**Tomislav Capuder** University of Zagreb, Croatia

**Ante Elez** Končar-Generators and Motors, Croatia

**Dubravko Franković** University of Rijeka, Croatia

**Hrvoje Glavaš** J.J. Strossmayer University of Osijek, Croatia

**Mevludin Glavić** University of Liege, Belgium

**Božidar Filipović Grčić** University of Zagreb, Croatia

**Dalibor Filipović Grčić** Končar-Electrical Engineering Institute, Croatia

**Josep M. Guerrero** Aalborg Universitet, Aalborg East, Denmark

**Dirk Van Hertem** KU Leuven, Faculty of Engineering, Belgium

**Žarko Janić** Siemens-Končar-Power Transformers, Croatia

**Igor Kuzle** University of Zagreb, Croatia

**Niko Malbaša** Ekoner, Croatia

**Matislav Majstrović** University of Split, Croatia

**Zlatko Maljković** University of Zagreb, Croatia

**Predrag Marić** J.J. Strossmayer University of Osijek, Croatia

**Srete Nikolovski** J.J. Strossmayer University of Osijek, Croatia

**Damir Novosel** Quanta Technology, Raleigh, USA

**Hrvoje Pandžić** University of Zagreb, Croatia

**Robert Sitar** Končar-Electrical Engineering Institute, Croatia

**Damir Sumina** University of Zagreb, Croatia

**Elis Sutlović** University of Split, Croatia

**Damir Šljivac** J.J. Strossmayer University of Osijek Croatia

**Darko Tipurić** University of Zagreb, Croatia

**Bojan Trkulja** University of Zagreb, Croatia

**Nela Vlahinić Lenz** University of Split, Croatia

**Mario Vražić** University of Zagreb, Croatia

## INTRODUCTION

**J**ournal of Energy special issue: Papers from International CIGRÉ Symposium "Transient Phenomena in Large Electric Power Systems"

Welcome to this special issue, which is based on selected papers presented at the International CIGRÉ Symposium "Transient Phenomena in Large Electric Power Systems", held in Zagreb, Croatia, on April 18<sup>th</sup>-21<sup>st</sup>, 2007.

The International Symposium was organized by the Croatian CIGRE National Committee and Study Committees C4 (System Technical Performance), A1 (Rotating Electrical Machines), A2 (Transformers), A3 (High Voltage Equipment) and C1 (System Development and Economics). The goal of the Symposium was to examine the various aspects of transient phenomena in large electric power systems.

Seven main topics were covered in the ten sessions. The Symposium extended over three days, organised in half-day sessions during which authors presented their papers and then participated in a panel discussion. Participants from manufacturers and utilities, along with those from universities and research centres, gave their presentations and took part in discussions. Three invited lectures were held and 54 papers were accepted.

Electric power systems are subjected to a wide range of transient disturbances, which impact its overall performance. It is a challenge to build and operate power systems so that the safety of individual equipment, the security of the integrated power system and the quality of power supply are not unduly compromised. The general purpose of the Symposium was to provide a forum for discussing the nature of transient phenomena in electric power systems and how these systems need to be designed to ensure a secure and robust service.

The following topics were covered by Symposium:

- insulation coordination aspects, including temporary, resonance and transient overvoltages in shunt/series compensated OH-lines, shunt compensated cables, mixed OH-line-cable sections, HVDC-converter-stations, interconnection lines and as anticipated for half-wave-length lines;
- transient current and TRV aspects due to long distance transmission;
- EMC problems caused by power system transients and mitigation techniques;
- power quality issues as impacted by power system transients;
- transient behaviour of power systems leading to blackouts: recent experiences and mitigation techniques;
- system security management with regards to lightning;
- experience and management of transients during operation when radio base stations are located on transmission line towers.

From the 54 papers presented at Symposium, 16 papers were accepted for publication in Journal of Energy after having undergone the peer-review process. We would like to thank the authors for their contributions and the reviewers who dedicated their valuable time in selecting and reviewing these papers. It was very challenging to collect a balanced overview of the entire Symposium, but we believe that the papers which were selected represent some of the best research about transient phenomena in power systems. We hope this special issue will provide a valuable insight into power system transients, as well as a pleasant and inspiring reading.

## Guest Editors

*Ivica Pavić*

*Viktor Milardić*

## An EMTP Extension for Computing Earthing System Transient Step and Touch Voltages

S. VUJEVIĆ\*, P. SARAJČEV

University of Split, Faculty of Electrical Engineering,  
Mechanical Engineering and Naval Architecture, Split  
Croatia

### SUMMARY

This paper presents a novel technique for computing dangerous voltages due to lightning transients imposed on earthing system, which is based on the use of the well-known ATP-EMTP software package. Earth surface transient potential distributions, as well as step and touch voltages computations, are performed through extending the widely used EMTP software package with a new post-processor (computer program), developed especially for that purpose. The earthing grid is approximated by the circular cross-section conductors. In numerical model, conductors are subdivided into segments (1D finite elements) and Clark's model with distributed constant parameters is then applied. Leakage conductance of conductor segments is modeled in EMTP as an additional lumped parameter. Analytical expressions for distributed and lumped segment parameters are derived using the average potential method. Due to the limitations of the EMTP, EM coupling between segments is neglected. The earth model is limited to the homogenous earth. Soil ionization effect is not accounted for, but could be incorporated, through some modifications of algorithms. Lightning surge model used is based on the Heidler's model of current source.

### 1. INTRODUCTION

Knowing the transient behavior of the substation's earthing grid is very important in the case of direct lightning strikes. A direct lightning strike can cause dangerous overvoltages, which can result in malfunction of the sensitive equipment, as well as dangerous step and touch voltages. Electromagnetic compatibility issues as well as human safety ones could be investigated using hereafter proposed methods. All parameters necessary for the ATP-EMTP simulations are computed by the separate computer program (pre-processor), developed for that purpose. Earth surface transient potential distribution, as well as touch and step voltages are computed from the simulation results obtained by ATP-EMTP using another computer program (post-processor to the ATP-EMTP).

### KEYWORDS

Average potential method, ATP-EMTP, Earthing grid, Lightning analysis, Step and touch voltages

\*: [slavko.vujevic@fesb.hr](mailto:slavko.vujevic@fesb.hr)

## 2. MODEL OF THE EARTHING GRID

Each conductor of the earthing grid, by applying the finite element technique, can be subdivided into segments (1D finite elements). A Clark's model with distributed constant parameters is then applied on each segment. Input data for Clark's model are, [1]: a) resistance per unit length, b) surge impedance, c) propagation velocity, d) segment length.

Additionally, due to the limitations of the ATP-EMTP software package, the leakage conductance (resistance) of buried segments is modeled as an additional lumped parameter, [1].

**Ad a)** Per unit resistance of earthing grid segment can be computed as follows:

$$R = \frac{\rho_s}{r_o^2 \cdot \pi} \quad (1)$$

where  $\rho_s$  is the resistivity of the segment, [ $\Omega\text{m}$ ], while  $r_o$  represents the equivalent radius of the segment, [m].

**Ad b)** Surge impedance of the earthing grid segment is defined by the following equation, [4]:

$$Z_s = \sqrt{\frac{L}{C}} = \frac{\sqrt{\varepsilon_o \cdot \varepsilon_r \cdot \mu_o \cdot \mu_r}}{C} \quad (2)$$

where:  $L$  – per unit inductance of the segment, [H/m],

$C$  – per unit capacitance of the segment, [F/m],

$\varepsilon_o$  – permittivity of the vacuum,

$\mu_o$  – permeability of the vacuum,

$\varepsilon_r$  – relative permittivity of the earth,

$\mu_r = 1$  – relative permeability of the earth.

Hence, in order to compute the surge impedance, one only needs to obtain the value of per unit capacitance of the earthing grid segment. This capacitance can be computed by the average potential method.

Per unit capacitance of the buried conductor segment depends on the position of the segment respective to the earth surface. It can be computed according to the following expression, [3, 4]:

$$C = \frac{4 \cdot \pi \cdot \varepsilon_o \cdot \varepsilon_r \cdot \ell}{\iint_{\Gamma' \Gamma} \frac{d\ell' \cdot d\ell}{r} + \iint_{\Gamma_s \Gamma} \frac{d\ell_s \cdot d\ell}{r}} = \frac{4 \cdot \pi \cdot \varepsilon_o \cdot \varepsilon_r \cdot \ell}{I_{\text{self}} + I_{\text{mut}}} \quad (3)$$

Double integrals in the above expression are computed analytically, as will be explained later. Integral  $I_{\text{self}}$  stands for the self capacitance, while integral  $I_{\text{mut}}$  accounts for the mutual capacitance between earthing grid's segment and its image.

**Ad c)** Propagation velocity of the lightning surge in the earth can be roughly estimated by the following relation:

$$vp = \frac{c}{\sqrt{\varepsilon_r}} \quad (4)$$

where  $c = 3 \cdot 10^8$  m/s represents the velocity of light, and  $\varepsilon_r$  relative permittivity of the earth.

**Ad d)** Each of the earthing grid segments should satisfy the following relation for the maximum length, in meters:

$$\ell_{\max} = \frac{3160}{6} \cdot \sqrt{\frac{\rho}{f_{\max}}} \quad (5)$$

where  $\rho$  is the resistivity of the earth, [ $\Omega\text{m}$ ], while  $f_{\max}$  equals the maximal frequency of interest found in the lightning surge, [Hz].

**Leakage conductance** of the buried segment is represented in ATP-EMTP with the concentrated resistance on each side of that segment. Double value of the resistance on each side of the segment is chosen ( $2 \cdot R_L$ ) in order to obtain value of  $R_L$  after the parallel connection. Value of the earthing grid conductor's resistance is composed of two terms, as follows, [3, 4]:

$$R_L = \frac{\rho}{4 \cdot \pi \cdot \ell^2} \cdot \left( \int_{\Gamma' \Gamma} \frac{d\ell' \cdot d\ell}{r} + \int_{\Gamma_s \Gamma} \frac{d\ell_s \cdot d\ell}{r} \right) = \frac{\rho}{4 \cdot \pi \cdot \ell^2} \cdot (I_{\text{self}} + I_{\text{mut}}) = R_{\text{self}} + R_{\text{mut}} \quad (6)$$

where:  $R_{\text{self}}$  - self resistance of the segment in homogeneous and unbounded medium (earth),

$R_{\text{mut}}$  - mutual resistance between segment and its image in relation to the earth surface.

Double integrals ( $I_{\text{self}}$  for the self resistance and  $I_{\text{mut}}$  for mutual resistance) are those already introduced. They are analytically computed.

## 2.1 Analytical Solution of Double Integrals

Expressions for computing per unit capacitance of earthing grid segments, and resistance (conductance) of earthing grid segments all involve double integrals. They can be analytically solved which contributes to the numerical stability of the derived method.

Double integral  $I_{\text{self}}$  is given by the expression:

$$I_{\text{self}} = \int_{\Gamma' \Gamma} \frac{d\ell' \cdot d\ell}{r} \quad (7)$$

The integration in equation (7) is performed along the segment axis (curve  $\Gamma'$ ) and along the curve on segment surface, which is parallel to the segment axis (curve  $\Gamma$ ). Analytical solution of this integral is given by the following expression, [3, 4]:

$$I_{\text{self}} = 2 \cdot \left( \ell \cdot \ln \frac{\sqrt{\ell^2 + r_0^2} + \ell}{r_0} - \sqrt{\ell^2 + r_0^2} + r_0 \right) \quad (8)$$

where  $\ell$  represents segment's length, while  $r_0$  represents equivalent radius of the segment's cross-section.

Double integral  $I_{\text{mut}}$  is given by the following expression:

$$I_{\text{mut}} = \int_{\Gamma_s \Gamma} \frac{d\ell_s \cdot d\ell}{r} \quad (9)$$

Analytical solution of integral (9) depends on the position of the segment relative to the earth surface. Three different segment arrangements will be examined: a) segment is parallel to the earth surface, b) segment is perpendicular to the earth surface, c) segment is in an aslope position to the earth surface.

**Ad a)** If a horizontal segment is positioned at distance  $h$  [m] parallel to the earth surface, integral solution is ( $r_0 \rightarrow 2 \cdot h \Rightarrow I_{\text{self}} \rightarrow I_{\text{mut}}$ ):

$$I_{\text{mut}} = 2 \cdot \left( \ell \cdot \ln \frac{\sqrt{\ell^2 + 4 \cdot h^2} + \ell}{2 \cdot h} - \sqrt{\ell^2 + 4 \cdot h^2} + 2 \cdot h \right) \quad (10)$$

**Ad b)** If the segment is perpendicular to the earth surface, the first integration in (9) is carried out along the axis of segment image (curve  $\Gamma_s$ ), while the second integration is carried out along the curve on the segment surface (curve  $\Gamma$ ), which is parallel to the segment axis. Analytical solution to the integral (9) in this case is given by [3, 4]:

$$I_{\text{mut}} = u_1 \cdot \text{Arsh} \frac{u_1}{r_0} - \sqrt{u_1^2 + r_0^2} + u_2 \cdot \text{Arsh} \frac{u_2}{r_0} - \sqrt{u_2^2 + r_0^2} - 2 \cdot u_3 \cdot \text{Arsh} \frac{u_3}{r_0} + \sqrt{u_3^2 + r_0^2} \quad (11)$$

with:

$$u_1 = h_1 + h_2 + \ell \quad (12)$$

$$u_2 = h_1 + h_2 - \ell \quad (13)$$

$$u_3 = h_1 + h_2 \quad (14)$$

where  $h_1$  and  $h_2$  represents distances of the starting and ending points of the segment from the earth surface, respectively.

**Ad c)** If the segment is in an aslope position relative to the earth surface, analytical solution of the double integral can be written as [3, 4]:

$$I_{\text{mut}} = 2 \cdot \left[ B(x_p, z_p) + B(x_k, z_k) - B(x_p, z_k) - B(x_k, z_p) \right] \quad (15)$$

where  $x_p, z_p, x_k$  and  $z_k$  represent  $x$  and  $z$  coordinates of the starting and ending points of the segment and its image, respectively. Terms in (15) are computed using the following expression, [3, 4]:

$$B(x, z) = x \cdot \ln \left( z - x \cdot \cos \alpha + \sqrt{x^2 + z^2 + r_0^2 - 2 \cdot x \cdot z \cdot \cos \alpha} \right) \quad (16)$$

with:

$$x_p = z_p = \frac{\min\{h_1, h_2\}}{|h_2 - h_1|} \cdot \ell \quad (17)$$

$$x_k = z_k = \frac{\max\{h_1, h_2\}}{|h_2 - h_1|} \cdot \ell \quad (18)$$

$$\cos \alpha = \frac{2 \cdot d^2}{\ell^2} - 1 \quad (19)$$

where  $d$  represents the length of the orthogonal projection of the segment onto the earth surface. Length of the segment can be obtained using the following expression:

$$\ell = \sqrt{d^2 + (h_2 - h_1)^2} \quad (20)$$

### 3. EARTH SURFACE POTENTIAL DISTRIBUTION

ATP-EMTP software package applied for the simulations can only give transient potential distribution on the earthing grid itself (in the nodes between segments). More important is an earth surface potential distribution from which step and touch voltages could be computed. In order to overcome this disability of the ATP-EMTP, a separate post-processor (computer program) has been developed.

From inside the ATP-EMTP, user can request to publish (within results) a leakage currents which each of the earthing grid conductors dissipate into the earth. This is a current flowing through the lumped resistances, which represent the leakage resistance of the buried conductor segment. From this current, an earth surface transient potential distribution can be computed. Knowing the earth surface potential distribution, step and touch voltages could be easily obtained.

Figure 1 shows a single buried conductor segment in a local coordinate system, along with the point  $T(u, v)$  for which the potential needs to be computed.

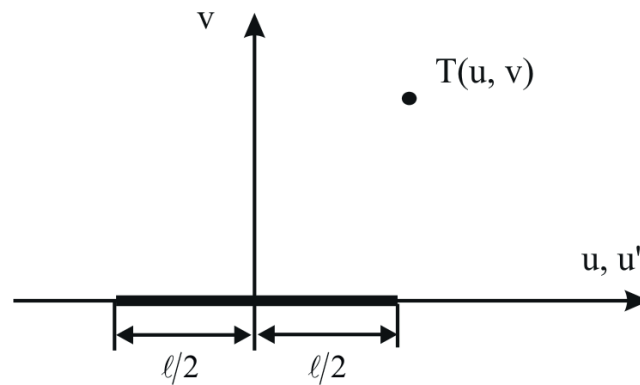


Figure 1. Earthing grid segment in local coordinate system  $(u, v)$ .

Potential at the point  $T(u, v)$  at the time instant  $t$  as a consequence of the current  $I(t)$ , which the segment in the unbounded homogenous medium with resistivity  $\rho$  dissipates into the earth, can be computed according to the following expression:

$$\varphi_T(t) = \frac{\rho}{4 \cdot \pi} \cdot \frac{I\left(t - \frac{r_s}{vp}\right)}{1} \cdot G(u, v) \quad (21)$$

where  $u$  and  $v$  are local coordinates of the point  $T(u, v)$ ,  $r_s$  - distance in the local coordinate system from the middle segment point to the observation point  $T(u, v)$ . Length of the segment is given by  $\ell$ , while  $vp$  stands for the velocity of the surge current in the earth, given by (4). Term expressing the current in the above expression accounts for the potential retardation. Function  $G(u, v)$  in (21) depends on the geometry of the segment and the position of the observation point. It is given by, [7]:

$$G(u, v) = \int_{-1/2}^{1/2} \frac{du'}{\sqrt{(u-u')^2 + v^2}} = \ln \frac{\sqrt{\left(u + \frac{1}{2}\right)^2 + v^2} + u + \frac{1}{2}}{\sqrt{\left(u - \frac{1}{2}\right)^2 + v^2} + u - \frac{1}{2}} \quad (22)$$

Local coordinates of the point  $T(u, v)$  can be computed from the global coordinates of the segment starting and ending points and global coordinates of the observation point. Let the starting point of the segment be  $P(x_p, y_p, z_p)$ , and ending point of the same segment  $K(x_k, y_k, z_k)$ , and let's designate observation point as  $T(x, y, z)$  in the global coordinate system. Origin of the local coordinate system is in the middle segment point with global coordinates  $S(x_s, y_s, z_s)$ . Distance between the middle

segment point and the observation point (expressed with global coordinates) is given by the following expression, [7]:

$$r_s = \sqrt{(x_s - x)^2 + (y_s - y)^2 + (z_s - z)^2} \quad (23)$$

Local coordinates  $u$  and  $v$  of the observation point can be computed as follows, [7]:

$$u = \frac{2}{1} \cdot [(x - x_s) \cdot (x_k - x_s) + (y - y_s) \cdot (y_k - y_s) + (z - z_s) \cdot (z_k - z_s)] \quad (24)$$

$$v = \sqrt{(x - x_s)^2 + (y - y_s)^2 + (z - z_s)^2 - u^2} \quad (25)$$

where the length  $\ell$  of the segment can be computed as follows:

$$l = \sqrt{(x_k - x_p)^2 + (y_k - y_p)^2 + (z_k - z_p)^2} \quad (26)$$

Potential at the observation point T on the earth surface, which is a consequence of leakage currents of N arbitrarily positioned (mutually connected) earthing grid conductors can be computed by the following expression:

$$\phi_T(t) = \frac{\rho}{2 \cdot \pi} \cdot \sum_{k=1}^N \frac{I_k \left( t - \frac{r_{sk}}{vp} \right)}{l_k} \cdot G_k(u, v) \quad (27)$$

where:  $\ell_k$  – length of the k-th segment, computed according to (26), [m],

$G_k(u, v)$  – function joined to the k-th segment, described by (22),

$I_k \left( t - \frac{r_{sk}}{vp} \right)$  – leakage current of the k-th segment with potential retardation, [A].

Discret values of the leakage currents  $I_k$  as a function of time without potential retardation are obtained from the ATP-EMTP output. For each time instant, satisfying the following inequality:

$$t_m \leq t - \frac{r_{sk}}{vp} \leq t_{m+1} \quad (28)$$

current  $I_k$  of the k-th segment as a function of time with potential retardation is given by the following expression:

$$I_k \left( t - \frac{r_{sk}}{vp} \right) = (1 - f_{km}) \cdot I_k(t_m) + f_{km} \cdot I_k(t_{m+1}) \quad (29)$$

where:

$$f_{km} = \frac{t - \frac{r_{sk}}{vp} - t_m}{t_{m+1} - t_m} \quad (30)$$

Thus, according to (29), it can be seen that the current of the k-th segment is linearly approximated between the two successive time-discret values obtained from ATP-EMTP output.

Function  $G_k(u, v)$  depends on the position of the k-th segment in the global coordinate system and can be computed according to relation (22). Thus, a potential at the observation point on the earth surface at the time instant  $t$  is computed by summing the contributions from all the conductors, and their images, taking into account the potential retardation at the same time. In this way, transient temporal and spatial potential distributions on the earth surface can be computed. From those values, step and touch voltages could be easily obtained. In order to carry out these computations, separate computer program (post-processor to the ATP-EMTP) has been developed.

## 4. NUMERICAL EXAMPLE

Figure 2 illustrates the problem analysed in this paper. It consists of a 60 m x 60 m square grid with 10 m x 10 m meshes buried at depth of 0.5 m. The grid is made of copper conductors with 5 mm radius. The soil is assumed to be homogenous with a 1000  $\Omega\text{m}$  resistivity, relative permittivity of 9 and relative permeability of 1. Lightning surge current with following parameters: 1000 A amplitude and 1/20  $\mu\text{s}$  shape has been injected in the lower left corner of the earthing grid. Lightning surge model used for the ATP-EMTP simulation is based on the Heidler's model of current source, [1].

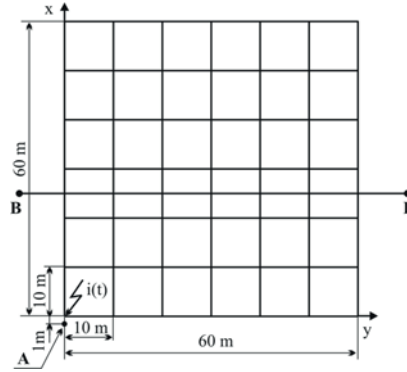


Figure 2. A earthing grid subject to a lightning strike

Observation point for the computation of the transient touch voltage is also shown in the Figure 2 (point A). Touch voltage between this point, located 1 m from the metallic structure at global coordinates (-1; 0; 0), which could be touched, is computed. Single profile on the earth surface has also been selected in order to compute the transient step voltage distribution (profile B–B in the Figure 2). This profile starts at the following global coordinates: (25; -10; 0) and extends to the point with global coordinates (25; 70; 0).

Complete model of the earthing grid presented in Figure 2 has been constructed in ATP-EMTP software package. Parameters of earthing grid elements have been previously computed by means of a separate computer program (pre-processor), according to the above presented model equations. Transient earth surface potential distribution, transient touch and step voltages have been computed from the leakage current distribution obtained from ATP-EMTP by means of specially developed post-processor.

Figure 3 presents two "screen-captures" from the post-processor animation showing a 3D perspective of the transient earth surface potential distribution over the earthing grid at two distinct time instants:  $t = 0.5 \mu\text{s}$  at the left portion and  $t = 5 \mu\text{s}$  at the right. Computations were carried out at various observation points located on the earth surface along several Y-directed profiles covering the earth grid and its vicinity, i.e. 10 m outside the grid outer loop.

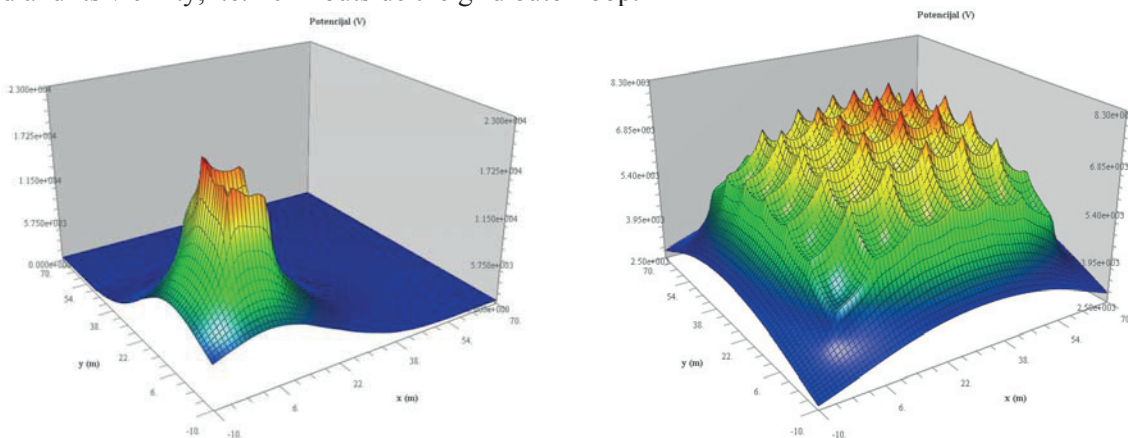


Figure 3. 3D perspectives of transient earth surface potential distribution for two distinct time instants (on the left:  $t = 0.5 \mu\text{s}$ , and on the right:  $t = 5 \mu\text{s}$ ).

Amplitude of the transient voltage (z axis) on the left portion of Figure 3 approximates to 23 kV, while on the right portion of Figure 3 it is approximately 8.3 kV.

Figure 4 presents on the left portion a transient touch voltage at the observation point A defined in Figure 2. At the right portion of the Figure 4, a transient step voltage along profile B–B for the time instant  $t = 10 \mu\text{s}$  is presented. This profile has been defined in the Figure 2 as well.

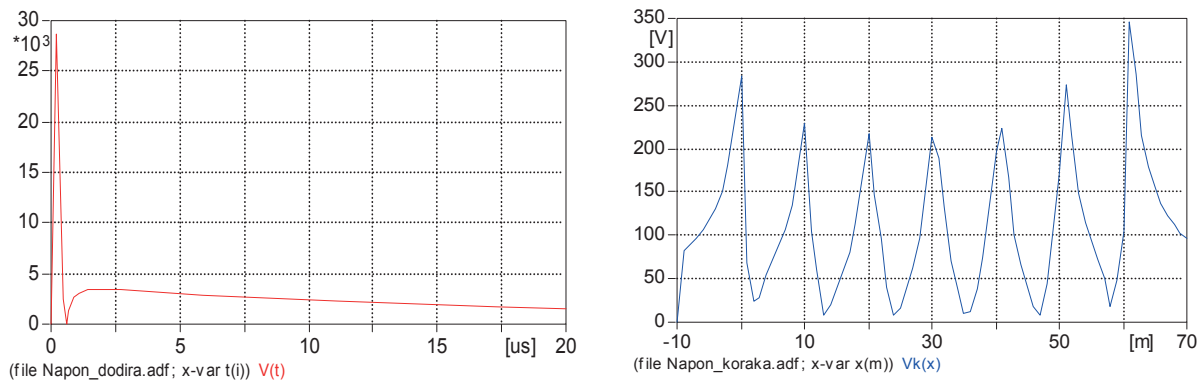


Figure 4. Transient touch voltage at the observation point A (on the left), and transient step voltage along profile B–B at the time instant  $t = 10 \mu\text{s}$  (on the right).

## 5. CONCLUSION

Advantage of the presented TLM based approach for transient step and touch voltages computation is its relative simplicity, and acknowledged good agreement [4] with results obtained from more complex EM fields theory based models.

Earth surface transient potential distributions, as well as step and touch voltages computations, are performed through extending the well-known ATP-EMTP software package with a new post-processor (computer program), developed especially for that purpose.

Due to the limitations of the applied transmission line model approach and the application of the ATP-EMTP software package, electromagnetic coupling between segments could not be taken into account. The earth model is limited to the homogenous earth. Soil ionization effect is not accounted for here.

## BIBLIOGRAPHY

- [1] Dommel, H. W.: "Electromagnetic Transients Program Theory Book", MicroTran Power System Analysis Corporation, Vancouver, British Columbia, 1992.
- [2] Dommel, H. W. et al.: "MicroTran Reference Manual", MicroTran Power System Analysis Corporation, Vancouver, British Columbia, 1992.
- [3] Vujević, S.; Sarajčev, P.; Sarajčev, I.: "EMTP Modeling of Direct Lightning Strikes to the GSM Base Station", SoftCOM 2005, Marina Frapa, Croatia, 2005.
- [4] Vujević, S.; Sarajčev, P.; Petrović, J.: "TLM Model for the Lightning Transient Analysis of the GSM Base Station", COST 286: Electromagnetic Compatibility (EMC) in Diffused Communications Systems, 2005, (<http://www.emc.york.ac.uk/cost286/Splitreports.htm>).
- [5] Xiong, W.; Dawalibi, P. F.: "Transient Performance of Substation Grounding Systems Subjected to Lightning and Similar Surge Currents", IEEE Transactions on Power Delivery, Vol. 9, No. 3, pp. 1412-1420, July 1994.
- [6] Grcev, D. L.: "Computer Analysis of Transient Voltages in Large Grounding Systems", IEEE Transactions on Power Delivery, Vol. 11, No. 2, pp. 815-823, 1996.
- [7] Vujević, S.: "Numerical Computation of Earthing Electrical Field in Rocky Earth" (in Croatian), Master's Thesis, Faculty of Electrical Engineering, University of Zagreb, Zagreb, 1987.

## Power Quality Problems Due to Transformer Inrush Current

A. Tokić\*

Faculty of Electrical Engineering,  
Tuzla  
Bosnia and Herzegovina

I. Uglešić

Faculty of Electrical Engineering and  
Computing, Zagreb  
Croatia

### SUMMARY

Transformer energization can produce a large nonsinusoidal inrush current which contains both odd and higher order harmonic components that can put transformer winding under mechanical stress. Additionally, they can cause irregular tripping of harmonic protection relays. Furthermore, in relatively weak power systems, such as is the Bosnian system, the superposition of harmonic components with system resonance frequencies may produce temporary overvoltages (TOV). Transformer winding failures and metal oxide surge arrester (MOA) energy stresses can occur due to TOV. The paper demonstrates a case study of an energization of a 220/110 kV transformer and power quality problems that can appear due to higher harmonics. Energy stresses of MOA provoked by transformer energization are considered in the paper.

### KEY WORDS

Power quality, transformer, inrush current, temporary overvoltage, surge arrester

### 1. INTRODUCTION

Transformer energization is a regular operation in an electric power system which can lead to large transformer inrush current. The basic characteristic of inrush current is relatively slow decay time to reach its steady state value, determined by transformer and power system parameters. The magnitude and duration of inrush current have a strong dependence from transformer saturation curve. Since the magnetizing inductance in unsaturated region of this curve is high, the inrush current can take a long time to reach its steady state. On the other way, the magnetizing inductance in saturated region is dominant parameter in determination of inrush current magnitude. In addition, inrush current characteristics are depended on the switching breaker time, magnitude and polarity of residual flux [1]. These currents can provoke false operation of protective relays and fuses [2] and mechanical damage to the transformer windings due to magnetic forces [3], cause voltage sags [4], establish temporary harmonic overvoltages [5] and generally reduce power quality on the system. This paper is focused on the analysis and consequences of temporary overvoltages that result from transformer inrush current.

\* e-mail: [amir.tokic@untz.ba](mailto:amir.tokic@untz.ba)

## 2. TEMPORARY OVERVOLTAGES DUE TO TRANSFORMER INRUSH CURRENTS

During transformer energization, the inrush current is asymmetrical and contains DC and fundamental components as well as all odd and even harmonics of the fundamental power frequency. In weak systems, i.e. in systems with relatively low short circuit power, transformer energization through an overhead line can produce resonance with a low frequency. If this resonance occurs and coincides with one of the harmonics produced during transformer energization, overvoltages can be provoked. The most important characteristics of these overvoltages are their relatively long duration, usually 0.1 to 1 sec, extremely 10 sec [6]. Namely, during energization, transformer behaves like a harmonic current source and flows through the lowest impedance point in the power system. Harmonic voltage at a certain point of the system can be expressed as:

$$U(n) = I(n) \cdot Z(n) \quad (1)$$

where  $n$  is order of the harmonic component,  $Z(n)$  is the impedance seen from the given system point at the harmonic frequency of order  $n$ , and  $I(n)$  is the injected harmonic current to the system of order  $n$ . Based on the relation (1), during resonant conditions, when resonant frequency of system impedance  $f_r = n \cdot f_0$ ,  $f_0 = 50 \text{ Hz}$ , coincide with corresponding harmonic current source, temporary overvoltages which contain high voltage harmonic will be established. Magnitude of harmonic voltage has a strong dependence on the corresponding magnitude of the harmonic current. If a magnitude of harmonic current at the resonant frequency of impedance has a relatively low value, then temporary harmonic overvoltage will no appear. Mentioned temporary harmonic overvoltages may considerably energy stress metal-oxide arresters which are located close to the transformers [7]. Energy stresses depended on the network configuration, transformer and arreseter parameters and initial conditions (breaker switching time and residual transformer flux). Magnitude and duration of these temporary overvoltages as well as energy stresses of surge arrester are sustained significantly in weak power systems.

## 3. CASE STUDY

Temporary harmonic overvoltages generated during transformer energization via an overhead line (Figure 1) will be analyzed in this paragraph.

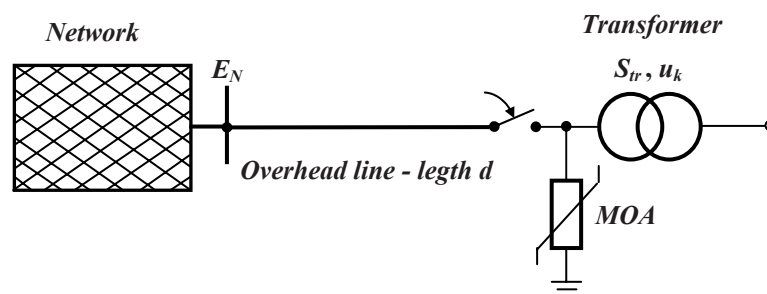


Figure 1. Transformer energization via overhead line, with MOA

In the first step the analyses will be conducted without connected surge arrester. The simplified model, while the transformer energizes through the overhead line, is shown in Figure 2. The network is represented by the ideal voltage source  $e(t) = E_N \cos \omega t$ , with corresponding network impedance  $\bar{z}_N = R_N + j\omega L_N$ . The equivalent network inductance  $L_N$  is evaluated from the 3-phase short circuit power  $S_{SC} \omega L_N = (E_N \sqrt{3} / \sqrt{2})^2 / S_{SC}$ , while the resistance  $R_N$  is determined on the recommended short-circuit relationship  $X_N / R_N$ . The overhead line is represented with distributed parameters  $R'_L, L'_L, C'_L$  and its length  $d$ . The transformer model comprises the constant parameters:  $R_p, L_p, R_m$  and magnetizing inductance  $L_m$ , defined by nonlinear saturation curve. The transformer energization starts at the moment  $t = T_0$ .

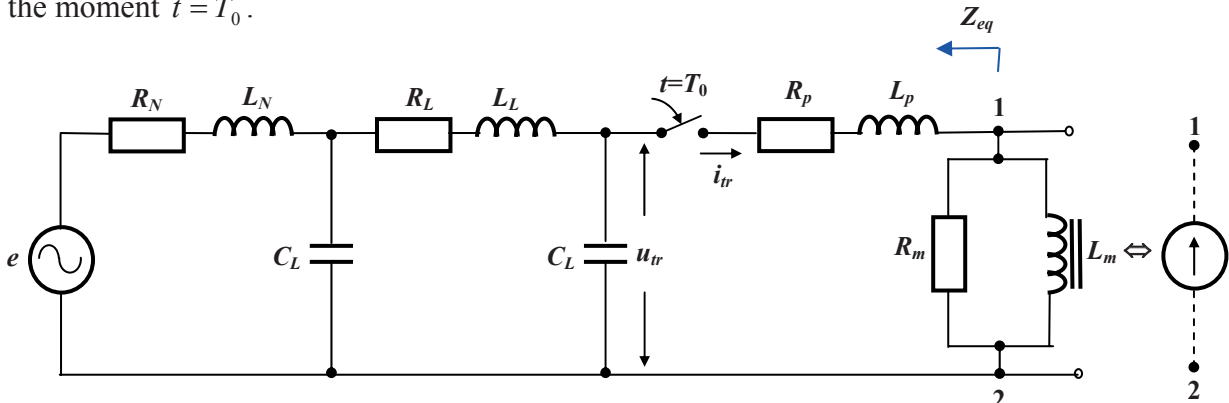


Figure 2. Transformer energization – simplified equivalent model, without MOA

Real data from the Power Utility of Bosnia and Herzegovina (220 kV voltage level) were used in order to investigate the possibility of generation of temporary overvoltages:

Transformer parameters of the Gradacac substation are:

- nominal power  $S_{tr} = 150 \text{ MVA}$ ,
- short circuit voltage  $u_{k\%} = 11\%$ ,
- resistance per winding phase  $R_p = 0.292 \Omega$ ,
- leakage inductance  $L_p = 0.113 \text{ H}$ ,
- iron core losses  $R_m = 1.124 \text{ M}\Omega$ .

Table I: Magnetization curve of 150 MVA transformer

$i_m$ [p.u.]	0	0.00102	0.00187	0.0035	0.00683	1.0
$\Phi$ [p.u.]	0	0.95	1.0	1.05	1.1	1.3185

Network parameters (Tuzla):

$$E_N = 220\sqrt{2} / \sqrt{3} \text{ kV}, X_N / R_N = 15, S_{SC} = k \cdot S_{tr} \text{ MVA}, k \text{ is natural number}$$

Parameters of the Tuzla - Gradacac overhead transmission line, per phase, per km are:

- resistance  $R'_L = 0.022 \Omega / \text{km}$ ,

- inductance  $L'_L = 1.067 \text{ mH} / \text{km}$ ,
- capacitance  $C'_L = 0.03032 \text{ } \mu\text{F} / \text{km}$ ,
- line length  $d = 52 \text{ km}$ .

### 3.1 SIMULATIONS OF TEMPORARY OVERVOLTAGES

All simulation results are obtained by the software MATLAB/SimPowerSystem. The simulation tool has been developed using state-variable approach and the simulation runs in the MATLAB/Simulink environment. The worst case of the switching condition is presumed in all performed simulations and it implies that the breaker switching-in occurs at the same moment as the source voltage crosses the zero.

In Figure 3 are shown system impedances as seen from magnetizing inductance terminals 1 and 2, for different values of the ratio between the transformer nominal power  $S_{tr}$  and the short circuit power of the system  $S_{SC}$  (i.e. rate  $S_{tr} / S_{SC}$ ).

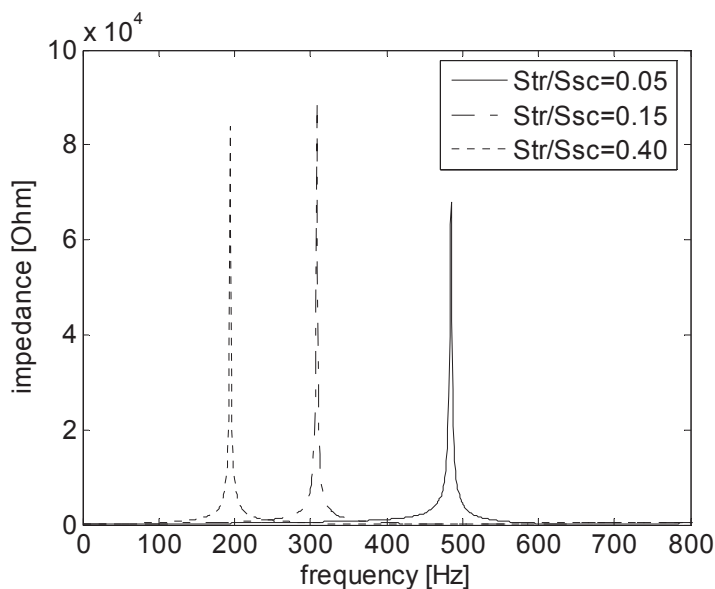


Figure 3. Impedance at magnetizing inductance terminals  $Z_{eq}$ . Resonant frequency are: 194 Hz for  $S_{tr}/S_{SC}=0.40$ , 308 Hz for  $S_{tr}/S_{SC}=0.15$ , 485 Hz for  $S_{tr}/S_{SC}=0.05$

It is obvious that resonant frequency is lower for larger ratio  $S_{tr} / S_{SC}$  i.e. for lower short circuit power of the system (weaker system). Figure 4 depicts the waveform of the typical transformer inrush current obtained for the rate  $S_{tr} / S_{SC} = 0.15$ . Furthermore, Figure 5 shows corresponding harmonic content of this inrush current. Resonant frequency for this case is 308 Hz, i.e. close to 6th harmonic component. However, inrush current harmonic level of order 6th as well as near harmonics order 5th and 7th are very low and sustained temporary harmonic overvoltages are not expected in this case of transformer energization. This is clearly shown in Figure 6, where transformer overvoltage has relatively low magnitude and relatively short duration.

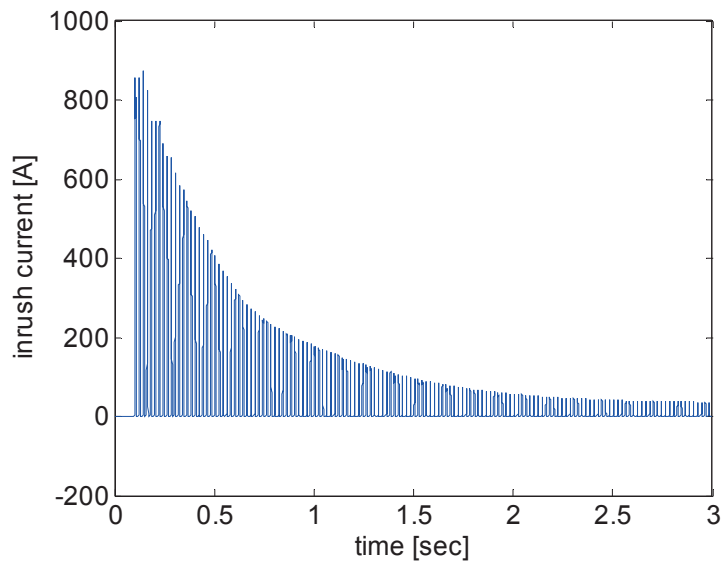


Figure 4. Transformer inrush current, case  $S_{tr}/S_{SC}=0.15$

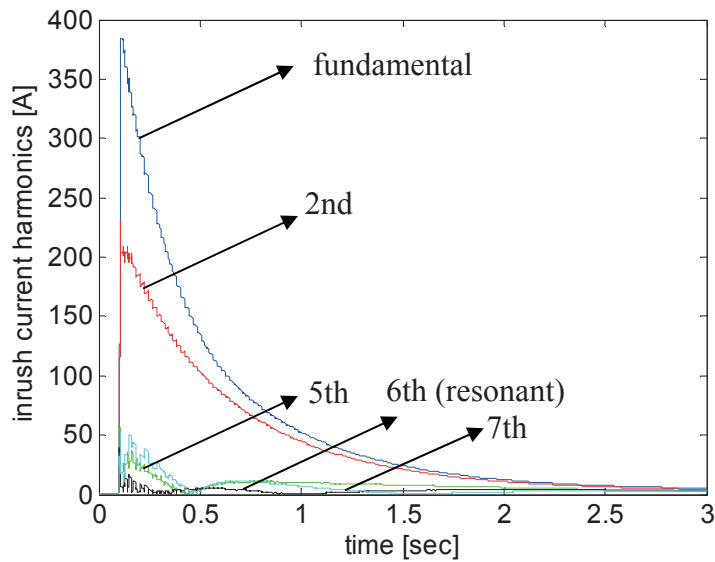


Figure 5. Harmonic content of inrush current, case  $S_{tr}/S_{SC}=0.15$

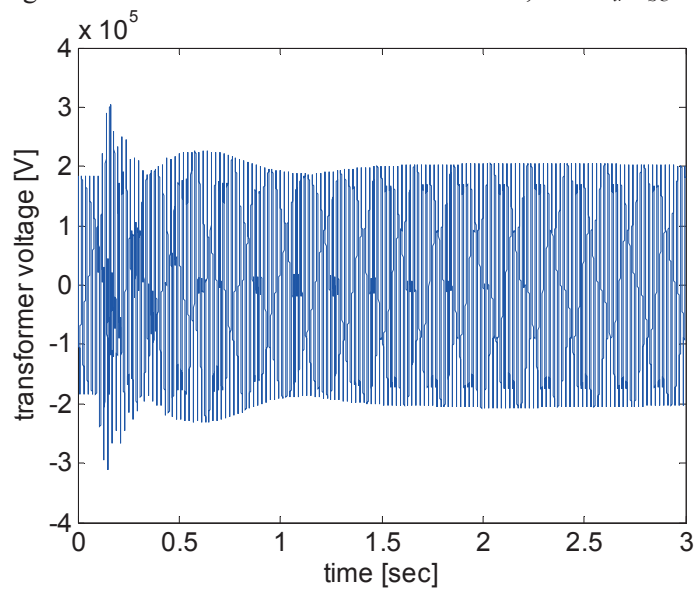


Figure 6. Temporary transformer harmonic overvoltages, case  $S_{tr}/S_{SC}=0.15$

On the other hand, different simulation results are obtained for the rate case  $S_{tr}/S_{SC} = 0.40$ . Figure 7 shows harmonic content of transformer inrush current for this case. Now, resonant frequency is 194 Hz, i.e. close to 4th harmonic component. It is interesting to note relatively large level of corresponding 4th harmonic compared to others harmonics. This harmonic is close to fundamental inrush current component. Sustained temporary harmonic overvoltages are expected in this case of transformer energization. This is clearly shown in Figure 8, where transformer overvoltage has relatively large magnitude and relatively long duration.

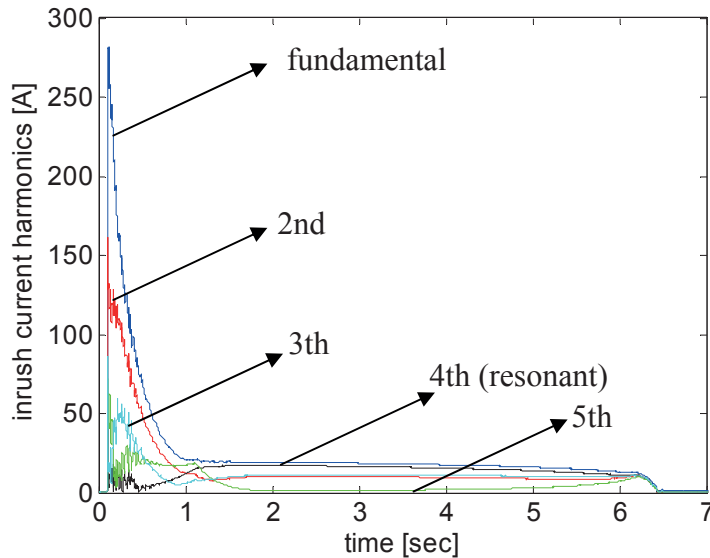


Figure 7. Harmonic content of inrush current, case  $S_{tr}/S_{SC}=0.40$

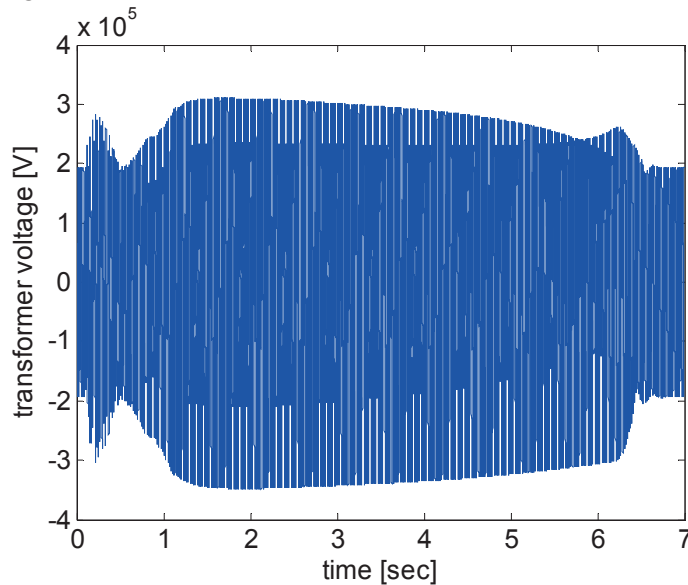


Figure 8. Temporary transformer harmonic overvoltage, case  $S_{tr}/S_{SC}=0.40$

In addition, temporary harmonic overvoltages would have larger values with enlarged length of the line. For example, for the double line length ( $d = 104 \text{ km}$ ), the impedance at terminals 1 and 2 has shape shown in Figure 9. In these cases, resonant frequencies are lower than mentioned for the initial line length, and these conditions are critical for the generation of transformer temporary overvoltages. In the other words, overvoltage values rapidly increase with the rise of the line length due to approaching to the resonant state.

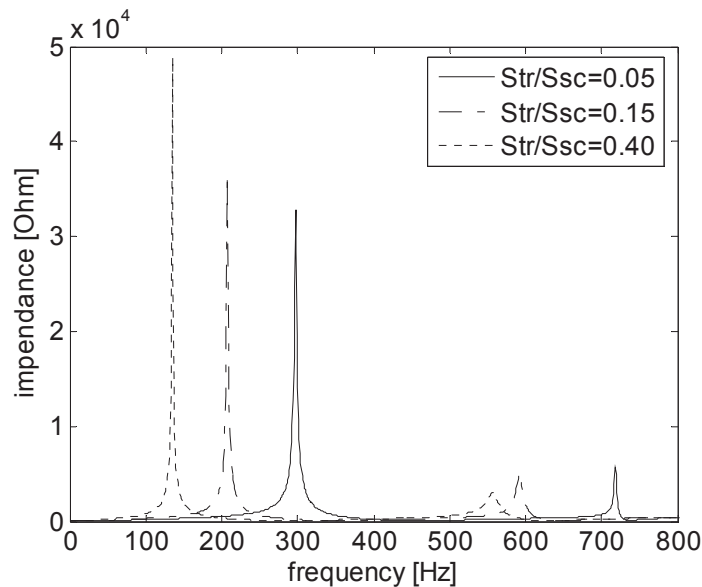


Figure 9. Impedance at magnetizing inductance terminals  $Z_{eq}$ , line length  $d=104 \text{ km}$

### 3.2 ENERGY STRESSES OF MOA

Temporary harmonic overvoltages may considerably stress metal-oxide arresters located close to the transformers [7]. For the MOA the following residual current-voltage characteristic was assumed:

$i \text{ [kA]}$	0.1	1	10
$u \text{ [kV]}$	356	392	476

Others MOA parameters:

- discharge energy capability  $E = 900 \text{ kJ}$
- rate voltage  $U_{prot} = 180 \text{ kV}$

Simulations results are illustrated in Figure 10 which depicts discharge energies of the MOA obtained for different rate values  $0.05 \leq S_r / S_{SC} \leq 1$ . Discharge energies of MOA increase when the residual flux  $\Phi_r$  rises in “direction” to the instantaneous initial transformer current. In addition, discharge energies that MOA has to absorb rapidly increase for the double line length, Figure 11.

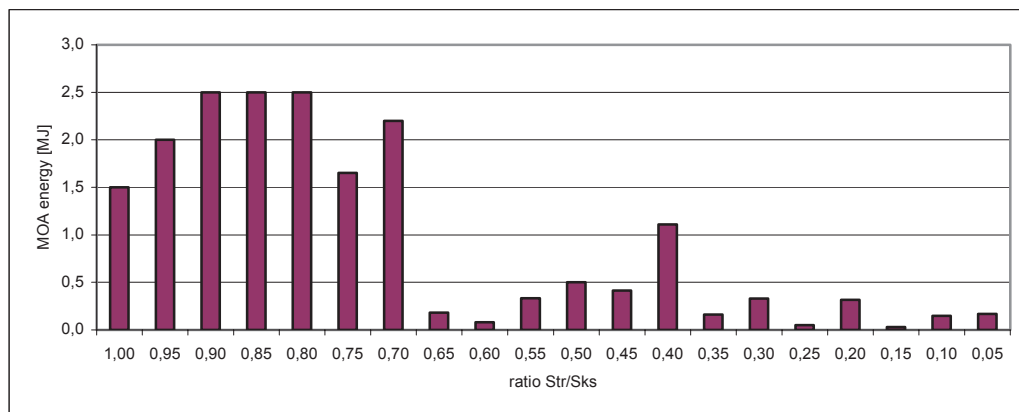


Figure 10. MOA discharge energies for line length  $d=52 \text{ km}$ ,  $\Phi_r=0$

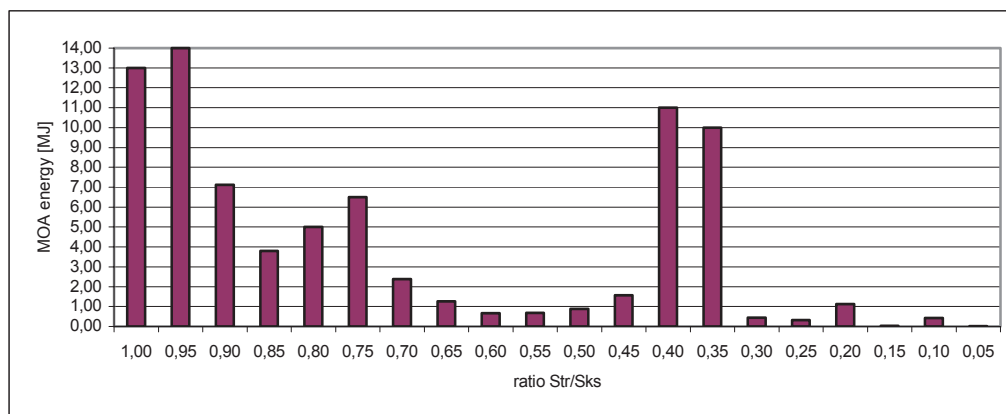


Figure 11. MOA discharge energies for line length  $d=104\text{ km}$ ,  $\Phi_r=0.8\Phi_{nom}$

#### 4. CONCLUSIONS

The transformer energization may produce a large inrush current that contains high order harmonic components. These currents generally reduce power quality in the system and may have unfavourable effects, as is an irregular tripping of transformer differential protection relays, a deterioration of the insulation and mechanical support structure of transformer windings. Furthermore, in a relatively weak power systems, such as is the Bosnian system, inrush current harmonic components may coincide with system resonance frequencies, producing sustained temporary harmonic overvoltages, whose main characteristics are the relatively long time duration and slowly decreasing magnitude.

The case study is demonstrated and the energization of the 220/110 kV transformer is considered. Different influences on TOV are analyzed for the radial network of Bosnia and Herzegovina, which is divided into three separate subsystems. It is shown that overvoltage magnitudes rapidly grow when approaching to the resonant state. This happens with enlarged length of the line and it increases discharge energies that MOA has to absorb.

#### BIBLIOGRAPHY

- [1] J. H. Brunke, K. J. Fröhlich „Elimination of Transformer Inrush Currents by Controlled Switching—Part I: Theoretical Considerations“ (IEEE Transaction on Power Delivery, Vol. 16, No. 2, April 2001, pages 276-280)
- [2] M.E. Golshan, M. Saghaian, A. Saha, H. Samet „A New Method for Recognizing Internal Faults from Inrush Current Conditions in Digital Differential Protection of Power Transformers“ (Electric Power Systems Research, Number 71, 2004, pages 61–71)
- [3] M. Steurer, K. Fröhlich „The Impact of Inrush Currents on the Mechanical Stress of High Voltage Power Transformer Coils“, (IEEE Transaction on Power Delivery, Vol. 17, No. 1, January 2002, pages 155-160)
- [4] M. Nagpal, T. G. Martinich, A. Moshref, K. Morison, P. Kundur „Assessing and Limiting Impact of Transformer Inrush Current on Power Quality“ (IEEE Transaction on Power Delivery, Vol. 21, No. 2, April 2006, pages 890-896)
- [5] O. Bourgault and G. Morin, “Analysis of Harmonic Overvoltage Due to Transformer Saturation Following Load Shedding on Hydro-Quebec-NYPA 765 kV Interconnection” (IEEE Transaction on Power Delivery, Vol. 5, January 1990, pages 397–405)
- [6] D. Povh, W. Schultz „Analysis of Overvoltages Caused by Transformer Magnetizing Inrush Current“ (IEEE Transaction on Power Delivery, Vol. PAS 97, No. 4, 1978, July/August 1978, pages 1355-1362)
- [7] A. Schey, K. H. Weck „MO Arresters in AC Systems“ (Electra 128, 1990, pages 101-125)

## Transients Caused by Sequential Circuit Breaker Tripping Issued by Busbar Protection

Ivo Uglešić<sup>1</sup>, Igor Ivanković<sup>2</sup>, Viktor Milardić<sup>1</sup>

<sup>1</sup>University of Zagreb, Faculty of Electrical Engineering and Computing, Unska 3  
10000 Zagreb, Croatia

<sup>2</sup>HEP-Transmission System Operator, Kupska 4  
10000 Zagreb, Croatia

### SUMMARY

A study of transients in a high voltage substation 400/110 kV is presented in the paper. An analysis was carried out after a fault on the 110 kV busbar, which caused severe damage in the substation. Investigation was focused on a time frame of several sequential circuit breaker trippings. A first step of the study was collection of data from the primary and secondary system in the substation and the control centre. After numerous analyses of data an attempt was made to construct a precision model, which could be used in the computation. Appropriate models were developed for circuit breakers, voltage (potential) and current metering transformers, power transformers, surge arresters, overhead lines and an equivalent grid. The components of the power system can be modelled for the very particular purpose, which means that a different frequency model should be used and each element in this analysis has a specific frequency response. An attempt was made at very detailed modelling of a power transformer, air blast and SF<sub>6</sub> circuit breakers. Computed results of fault currents were compared with measurements captured by the disturbance recorders in the field, mainly in differential numerical relays. Different switching schemes and different tripping sequences of several 110 kV circuit breakers were analysed with a constructed model in the millisecond range. Models of circuit breaker with different types of media, air blast and SF<sub>6</sub> gas were used in the cases investigated. Modelling of the circuit breakers' electrical arc was an important item in all cases in order to take into account the interaction between electrical arc and circuit current during the process of current interruption. The Schwarz/Avdonin equation is applied to model the dynamic behaviour of an electric arc. The fault studied was accompanied by a large short circuit current. For this particular case two types of circuit breaker, air blast and SF<sub>6</sub> were modelled. An important conclusion from those analyses was that sequential tripping of several circuit breakers does not cause superposition of overvoltages, because interruption the current happens when it is passing through the zero. Even the record from the substation and the disturbances recorder proves that each particular circuit breaker was successfully opened. On that basis, focus was put only on the final opening of the breaker and its arc extinction. The conclusion can be drawn that such a substation fault should have no influence on excessive overvoltages that can threaten the insulation of components in the substation.

### KEYWORDS

Switching - Overvoltage - Circuit Breaker Model - Disturbance Recorder - Arc - Extinction - Computation

<mailto:ivo.uglesic@fer.hr>

## 1. INTRODUCTION

The detailed analysis was carried out after one fault that happened on the 110 kV busbar, which caused tripping of several circuit breakers in a few tens of milliseconds. The consequence of the fault was damage on the 110 kV circuit breaker and the power transformer 300 MVA. An effort was undertaken to form a model, which can reconstruct the dynamic of the fault in order to get an insight into transient currents and voltages provoked by the fault. Special attention was dedicated to select and form suitable models for elements in the substation. Several models (Cassie, Mayres, Schwarz and Schwarz/Avdonin) were implemented in the detailed study of the interaction between electrical arc and circuit current during the process of current interruption. Current wave shapes during the switching off operation were recorded by transformer differential protection devices and those data were compared with results of short circuit currents that were computed with the help of the developed model.

## 2. MODELS FOR TRANSIENTS CALCULATION

The models were developed in the calculation of switching overvoltages for circuit breakers, voltage (potential) and current metering transformers, power transformers, surge arresters, overhead lines and equivalent high voltage network. Each element in the analysis has a specific frequency response, which means that a different frequency model should be used.

The model for overhead lines should take into account their frequency dependence.

Metering transformers in a transient state can be modelled in accordance with the standard IEC 60044 [1], [2] and [3].

A power transformer represents an important component in transient processes. A general model of the power transformer, when calculating switching overvoltages in the frequency range of 50 Hz – 20 kHz comprises, besides linear R, L, C elements, the nonlinear inductance of the core, whose influence should be taken into consideration when the eddy currents hinder the magnetic flux to pass through the core. This effect can already appear with frequencies of 3-5 kHz. The nonlinear inductance of the core is connected to the tertiary winding of the transformer model.

The fault studied was accompanied by a large short circuit current and modelling of the circuit breakers' electrical arc was an important item in all cases.

The current interruption requires that the interelectrode gap changes from conductive plasma into an insulating gas, [4] and [5]. This transition occurs around the current's passing through zero.

Black-box models give a mathematical description of the process and they are appropriate for digital simulation of transients, although most of these models actually have no real physical justification [6]. They describe the interaction of the switching arc and the corresponding electrical circuit during the interruption process. The models of Cassie, Mayer and Schwarz can be implemented in the detailed study of the interaction between electrical arc and circuit current during the process of current interruption.

The short circuit current flows through the hot arc until it crosses natural zero [7]. In this way current chopping is not possible when interrupting the short circuit current. The speed of current falling to zero depends on the type of circuit breaker and its corresponding heat and time constants. However the interaction between the electrical networks on the arc can be significant and in most cases it finishes with a relatively natural current drop to zero. A large heat constant influences the faster current drop to zero. Eventually the small post-arc current flows when the arc resistance takes values of a few thousand ohms.

The Schwarz/Avdonin equation is applied to model the dynamic behaviour of an electric arc:

$$\frac{1}{g} \cdot \frac{dg}{dt} = \frac{d \ln g}{dt} = \frac{1}{\tau_0 g^\alpha} \cdot \left[ \frac{u \cdot i}{P_0 g^\beta} - 1 \right]$$

Where:

g - arc conductance;

$u$  - arc voltage;  
 $i$  - arc current;  
 $P$  - removed power (by conduction, convection, radiation)  
 $\tau_0$  - time constant  
 $\alpha, \beta$  - constants

Circuit breakers with different types of media, i.e. air blast and SF<sub>6</sub> gas, were investigated in order to study their influence on the transient's processes [8].  
 The model on an electric arc is validated with the experimental results obtained on the test circuit [9].

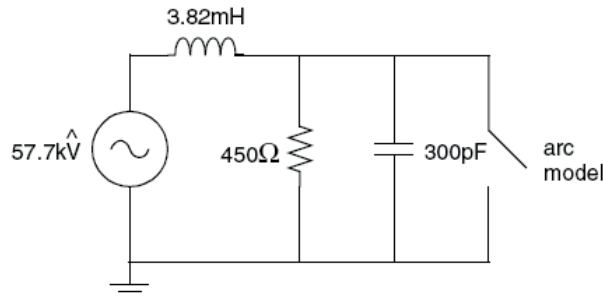


Fig. 1. Test circuit used for the validation of the applied model

The following constants were used for the SF<sub>6</sub> gas circuit breaker model:

$P_0 = 4 \text{ MW}$ ,  $\beta = 0.68$ ; arc time constant:  $\tau = 1.5 \mu\text{s}$ ;  $\alpha = 0.17$ .

Constants for the air blast circuit breaker according to the reference [5] are:

$P_0 = 16 \text{ MW}$ ,  $\beta = 0.5$ ;  $\tau = 6 \mu\text{s}$ ;  $\alpha = 0.2$

The dynamic behaviour of the arc is studied on the simple test circuit in order to avoid undesirable influences. The time dependence of the arc voltages are calculated and depicted in Fig. 2. and Fig. 3.

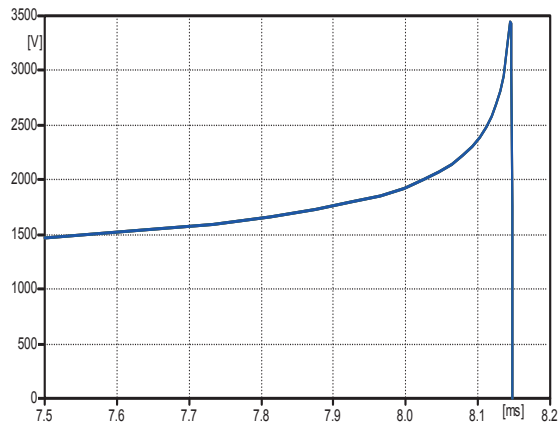


Fig. 2. Arc voltage in the SF<sub>6</sub> circuit breaker

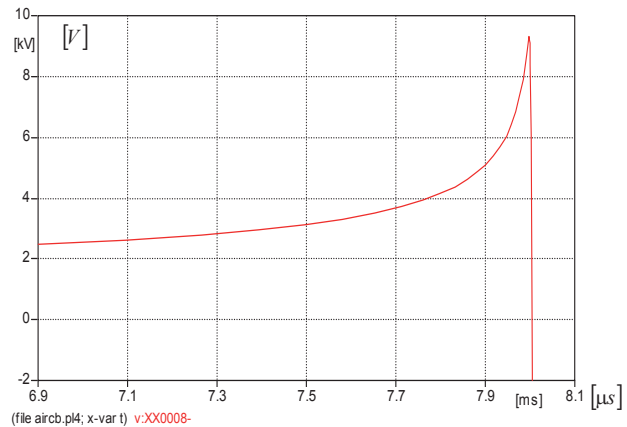


Fig. 3. Arc voltage in the air-blast circuit breaker

The peak values of the arc voltage of the SF<sub>6</sub> gas and air-blast circuit breaker were 3.4 kV and 9.3 kV respectively. The post-arc current of the air-blast was approximately 5.4 greater than the post-arc current of the SF<sub>6</sub> circuit breaker.

### 3. ANALISYS OF SWITCHING OPERATIONS

Transient's processes were studied in a substation during the switching off operation of several circuit breakers of different type in a time interval of some tens of milliseconds.

The fault which happened on the 110 kV busbar was initiated by a breaker fault in the zone of busbar relay protection. An air-bushing exploded on a 110 kV breaker of line 7. Operating status in that time was normal; two busbar systems were connected with the bay coupler breaker (Fig. 4.).

Busbar relay protection switched off the faulty busbar system. The transformer T3 was also switched off. In such conditions, both transformer circuit breakers (on 110 kV and 400 kV voltage side) were

switched off. Altogether, seven circuit breakers on 110 kV voltage level were switched off and one on 400 kV voltage level, red colour on Fig. 4.

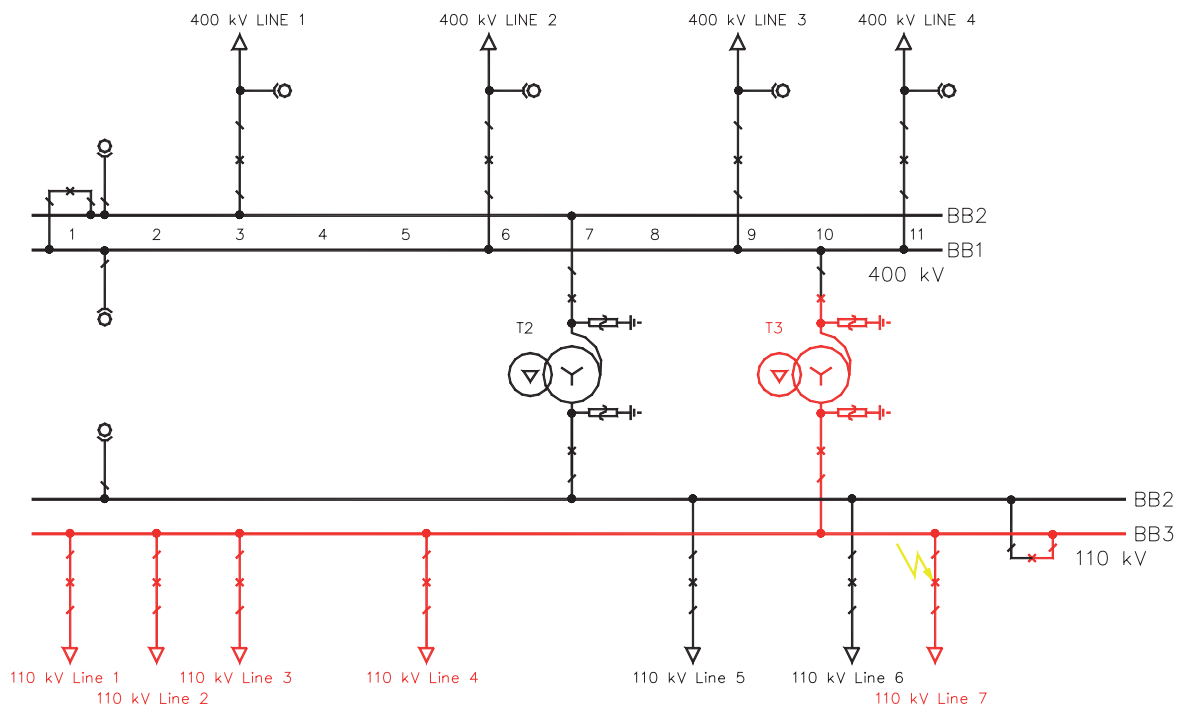


Fig. 4. Operating status of the 400/110 kV substation before fault [8]

### 3.1. SHORT CIRCUIT IN THE SWITCHYARD

Transformer differential relay protection was activated by the fault that happened in the substation and the currents captured by the disturbance recorder are shown in Fig. 5. The fault clearance times were short; the duration of the fault was less than 100 ms in the 110 kV switchyard as can be seen in Fig. 5., and the fault lasted a little longer in the 400 kV switchyard.

This dynamic sequence of events was simulated on the computational model with the aim of reconstructing the transients provoked by the fault. The main intention was an attempt to calculate voltages and currents in the switchyard and in the power transformer during transient's processes.

Fig. 5. presents currents captured by the disturbance recorder and Fig. 6. depicts currents resulting from computation.

Transformer 110 kV circuit breaker was opened after 4.5 periods of 50 Hz (Fig. 5.), and the same time was chosen in the computation (Fig. 6.). After 85 ms the current exceeded the zero value on the 110 kV side of the power transformer. The circuit breaker on the 400 kV side was slower and the tripping took place at 102 ms. The current  $I_{L3}$  does not fall to zero immediately as can be seen in Fig. 5., but in reality the circuit breaker had successfully opened the contact and it was estimated that this part of the current recording is false due to the saturations in the current transformer.

A big impact on the initial value of the short circuit current is caused by a DC component, which strongly depends on the time instant of the fault's initiation. The difference between the real and computed currents at the end of the fault remains less than 10% (peak values of the field and computed currents are 10500 A and 9500 A respectively).

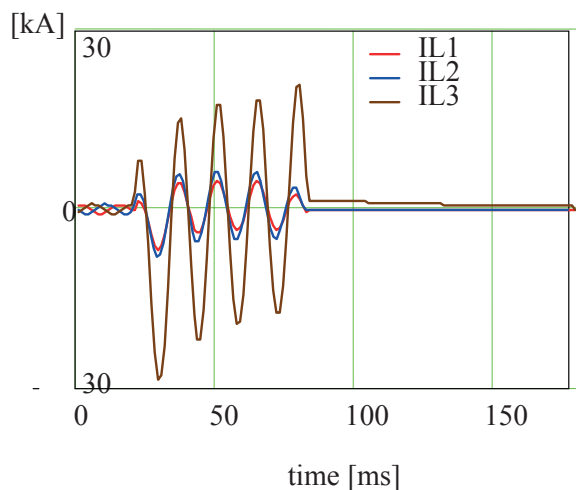


Fig. 5. Recorded currents

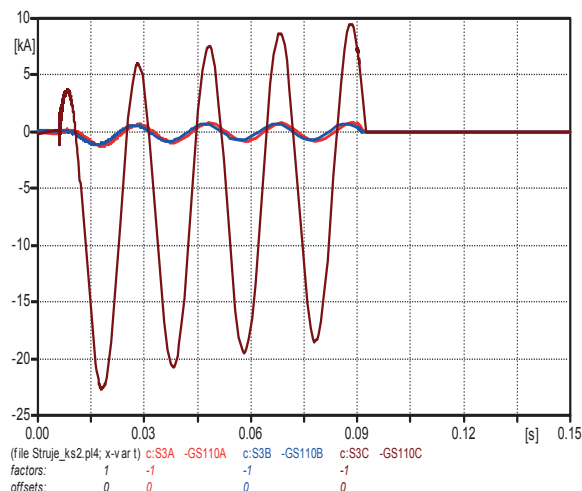


Fig. 6. Computed currents

### 3.2. SEQUENTIAL TRIPPINGS OF CIRCUIT BREAKERS

The simulation is conducted for the real case of tripping five 110 kV line circuit breakers (line 1, line 2, ...line 5) and one bay coupler circuit breaker. The complete power transformer model (inrush nonlinear branch, surge arresters on tertiary winding, windings capacitance, and leakage capacitance) is used in computation for this purpose. In order to calculate the maximum overvoltages that can appear on both sides of the power transformer many possible occurrences that could happen in the switchyard were examined, simulated and analysed [8].

Focus was put on the sequential tripping of circuit breakers and in that circumstance the maximal computed overvoltage at 110 kV side reached a very moderate value of 148 kV (Fig. 7.), which was calculated in the simulation of opening the 110 kV circuit breaker. Fig. 8. depicts transient voltages on the 400 kV side for the same case, and no overvoltages could be noticed (Fig. 8.). After the relay had tripped on the 400 kV transformer side, all voltages were oscillatory falling to zero.

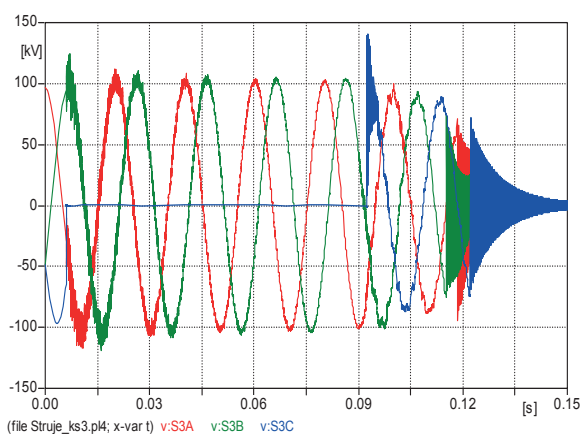


Fig. 7. Voltages on 110 kV side of transformer

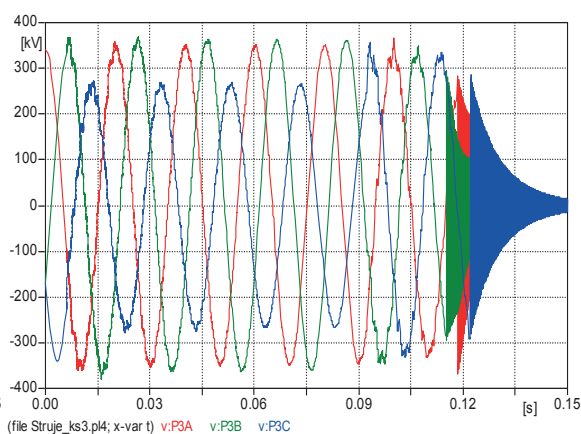


Fig. 8. Voltages on 400 kV side of transformer

Overvoltages were also observed on the tertiary transformer windings where the internal surge arresters were connected and the analysis of computational results did not show any excessive overvoltages caused by sequential trippings of circuit breakers.

The study [8] in which two types of the circuit breaker (air-blast and SF<sub>6</sub> gas) were compared has shown that the type of breaker has not very strong influence on the overvoltages in the switchyard and on the power transformer. Slightly higher overvoltages were noticed when the tripping was done with the air-blast circuit breaker.

## 4. CONCLUSION

The busbar fault in the switchyard was successfully captured by the differential relay disturbance recorder and on this occasion the busbar protection tripped seven 110 kV circuit breakers.

An attempt to reconstruct the whole fault was undertaken and the fault in the switchyard is analysed on the basis of the conducted computer simulations. For this purpose detailed models of all switchyard components, power transformers and overhead lines were built and very special attention was devoted to form the model of an air-blast and SF<sub>6</sub> circuit breaker.

The comparison between the recorded and computed fault currents showed relatively good correspondence.

On the basis of the list of events and disturbance recorder in the switchyard it was concluded that every breaker successfully opened its contacts. The analysis of the fault showed that sequential breaker tripping had not generated excessive overvoltages because the current in each breaker was interrupted when crossing zero. The opening stage of the final breaker is decisive for the transient overvoltages in the substation and its arc extinguishing was analysed for two breaker types. The current chopping and associated overvoltages are not possible when interrupting the short circuit current, while the short circuit current flows through the hot arc until it reaches natural zero crossing. Calculated overvoltages on the power transformer bushing during the dynamic phenomena do not have values that can damage the transformer insulation.

The final conclusion is drawn that the circuit breakers of both types (air-blast and SF<sub>6</sub> gas) generate moderate overvoltages, when breaking short circuit currents, which normally should not threaten the insulation of the components in the switchyard.

## BIBLIOGRAPHY

- [1] IEC 60044-6 - Ed. 1.0: Instrument transformers - Part 6: Requirements for protective current transformers for transient performance, 1992-03.
- [2] IEC 60044-2 - Consol. Ed. 1.2 (incl. am1+am2): Instrument transformers - Part 2: Inductive voltage transformers, 2003-02-13.
- [3] IEC 60186: Voltage transformers, 01-Jan-1987.
- [4] IEC 62271-100 - Consol. Ed. 1.1 (incl. am1): High-voltage switchgear and control gear - Part 100: High-voltage alternating current circuit-breakers, 2003-05-23.
- [5] CIGRE, Working Group 13.01 of Study Committee 13: State of the Art of Circuit-Breaker Modelling, December 1998.
- [6] V.I. Phaniraj, A.G. Phadke: Modeling of circuit breakers in the EMTP, IEEE Transactions on Power Systems, Vol. 3, No. 2, 799-805, May 1988.
- [7] C.H Flurscheim, et Al: Power circuit breaker theory and design, IEE, 1982.
- [8] I. Uglešić, S. Hutter, V. Milardić, I. Ivanković, M. Mandić, A. Tokić: Switching Overvoltages as Consequence of Sequential Switching off a Number of Circuit Breakers (in Croatian), Study, 2005.
- [9] P. H. Schavemaker, L. Van Der Sluis: The Arc Model Blockset, Proceedings of the Second IASTED International Conference, POWER AND ENERGY SYSTEMS (EuroPES), June 25-28, 2002, Crete, Greece

## Measurement and Simulation of Hydro-Generator's Asynchronous Operation

Z. MALJKOVIĆ, Ž. ZEBIĆ, M. PAVLICA

University of Zagreb, Faculty of Electrical Engineering and Computing  
Croatia

### SUMMARY

The extended testing of hydro-generator with Pelton turbine (rated 35 MVA) was performed on a generator whose lifespan expired and it was going to be replaced. This was the perfect opportunity to do some specific and uncommon testing. The complex testing plan was designed in order to enable recording of as much relevant data as possible (electrical, electromechanical, mechanical). Therefore, in some phases of testing, 29 to 44 quantities were measured simultaneously. Among the tests, there are short circuits with lowered voltage, bad synchronization at approximate angle of 15 degrees, asynchronous operation, generator over-speed and operation with short circuited field winding on one pole.

The most interesting and the most critical operation during this testing is asynchronous operation of hydro-generator [1, 2, 3, 4, 5], which is also very dangerous for generator and drive equipment. During such operation synchronous generator operates at a speed unequal to rated speed. This slip causes increased damping winding currents, which increases the thermal stress of this winding beyond the designed level. This makes these tests very infrequent. Asynchronous operating was achieved by decreasing the excitation current.

Complex mathematical model for computer simulation of hydro-generator's asynchronous operation has been made, taking into consideration the magnetic saturation, damper winding and generator transformer's influence. Results obtained by simulations have been compared to those obtained by measurements.

### KEYWORDS

Hydro-Generator, Asynchronous Operation, Testing, Simulation

[zlatko.maljkovic@fer.hr](mailto:zlatko.maljkovic@fer.hr)

## 1 INTRODUCTION

Asynchronous operation of synchronous machines connected to a power system can be caused by loss of excitation, slow clearing of faults, sudden and large change in load or when synchronization conditions are not fulfilled. The most frequent cause for asynchronous operation is the loss of excitation. Conventional practice in such conditions is disconnection of the machine from the power system. The downside of this is the period of generator's unavailability during the resynchronization process and possible significant disturbance in the power system.



Figure 1 - Hydro-generators (35 MVA) with Pelton turbines

## 2 MEASUREMENTS AND SIMULATIONS

Asynchronous operation of hydro-generator is very dangerous for generator and drive equipment. This makes these tests very infrequent. The extensive testing was performed on a hydro-generator (Table I) whose lifespan expired and it was going to be replaced. This was the perfect opportunity to do some specific and uncommon testing. Asynchronous operation in this case was achieved by decreasing the excitation current.

Table I – The main generator parameters

Manufacturer	SECHERON
$S_n$ [MVA]	35
$U_n$ [kV]	10.5
$I_n$ [A]	1925
$\cos\phi_n$	0.8
$n_n$ [rpm]	500
$f_n$ [Hz]	50
$U_{fn}$ [V]	300
$I_{fn}$ [A]	510

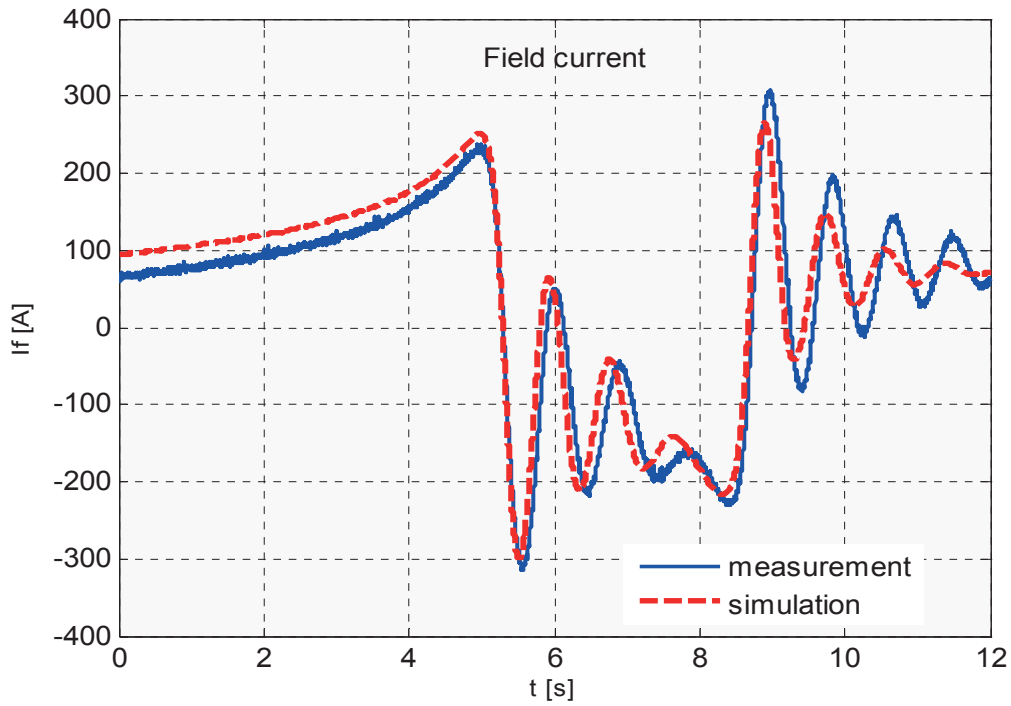


Figure 2 - Measured and simulated field current

Figure 2 shows the measured and simulated field currents. This is a case of the short term asynchronous operation and return of the loaded generator to synchronism. The field current barely exceeds half the rated field current value. It can be concluded that the field winding is not overheated. In case of the higher excitation current value, its thermal capacity and duration of asynchronous operation should be taken into consideration.

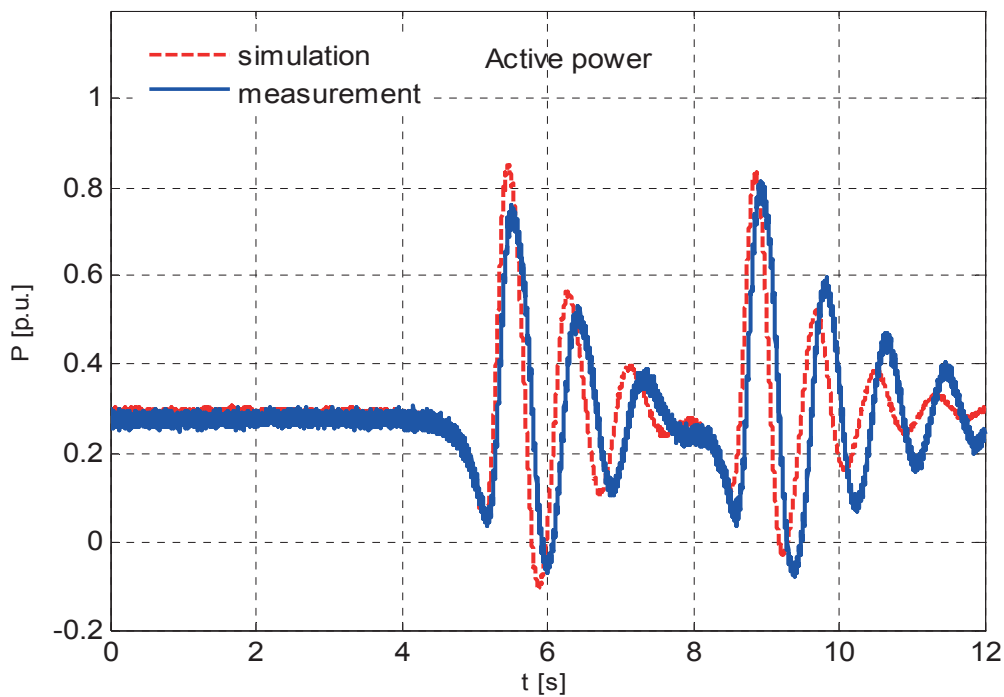


Figure 3 - Measured and simulated active power

Figure 3 shows the measured and simulated active power. Before the asynchronous operation the active power was 0.3 p.u. During the asynchronous operation it reaches the rated value. Such large active power changes cause dangerously high torsional strain of the shaft.

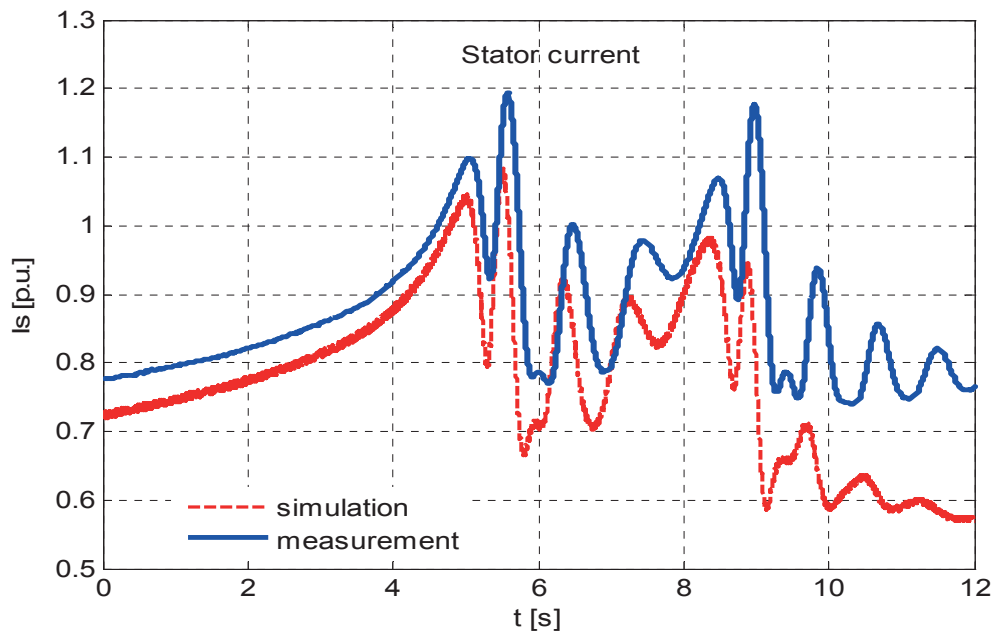


Figure 4 - Measured and simulated armature current

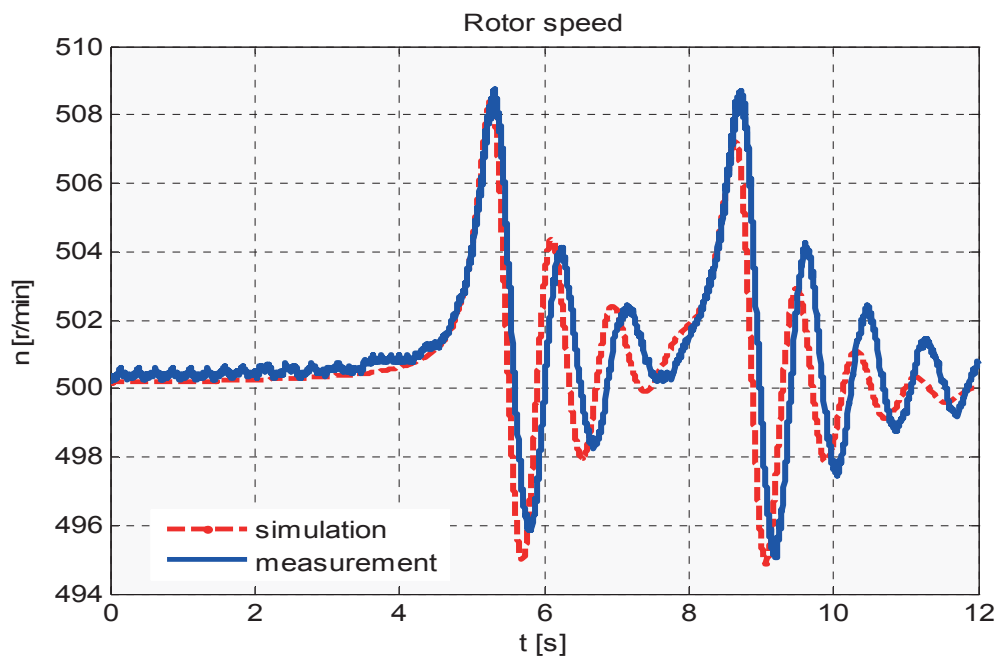


Figure 5 - Measured and simulated rotor speed

Figure 4 shows measured and simulated armature current (rms). During the asynchronous operation the armature current increases above its rated value, even though the active power is relatively small (0.3 p.u.). The underexcited generator draws current for magnetization from the network. This leads to additional heating of armature winding and causes voltage drops which can be harmful to the generator and also to power system stability.

Figure 5 shows the measured and the simulated rotor speed. This relative small change of rotor speed still causes a huge torsional stress on the shaft.

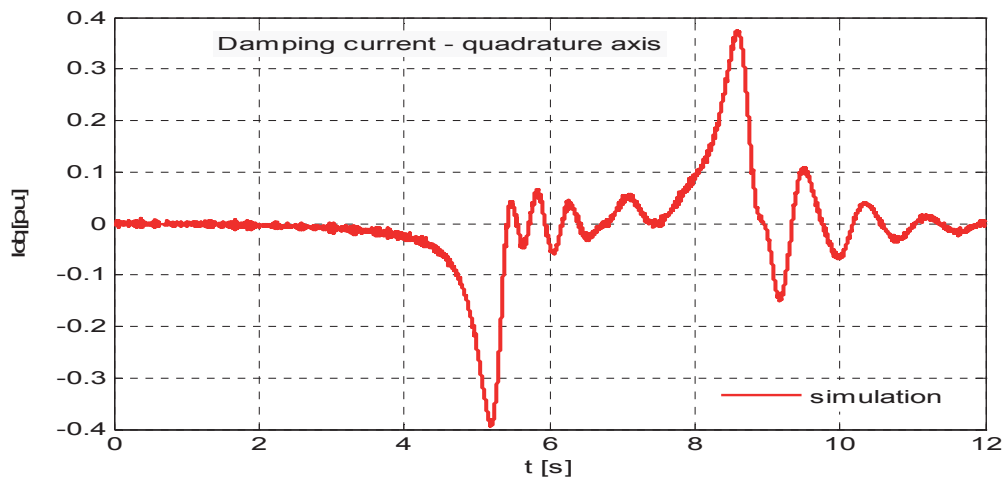


Figure 6 - Simulated damping current in q-axis

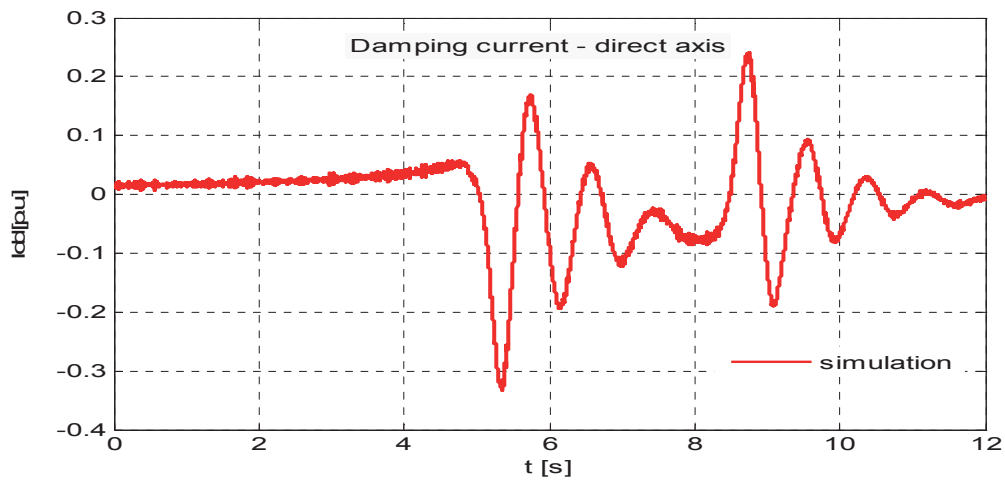


Figure 7 - Simulated damping current in d-axis

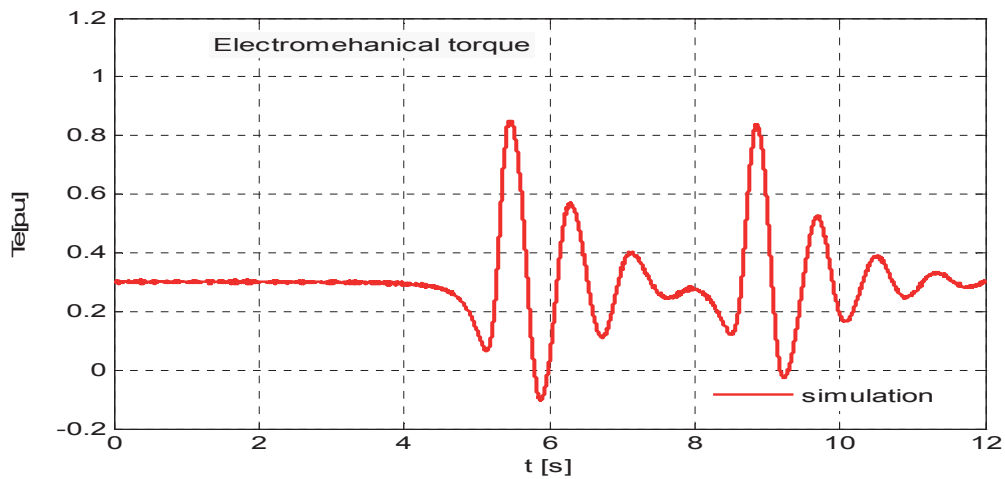


Figure 8 - Simulated electromechanical torque

During asynchronous operation the damping winding of synchronous generator is additionally heated (especially in case of hydro-generator). This winding is not designed for such

additional heat strain. It is almost impossible to measure this current. Figures 6 and 7 show damping winding currents in quadrature and direct axes acquired by simulation.

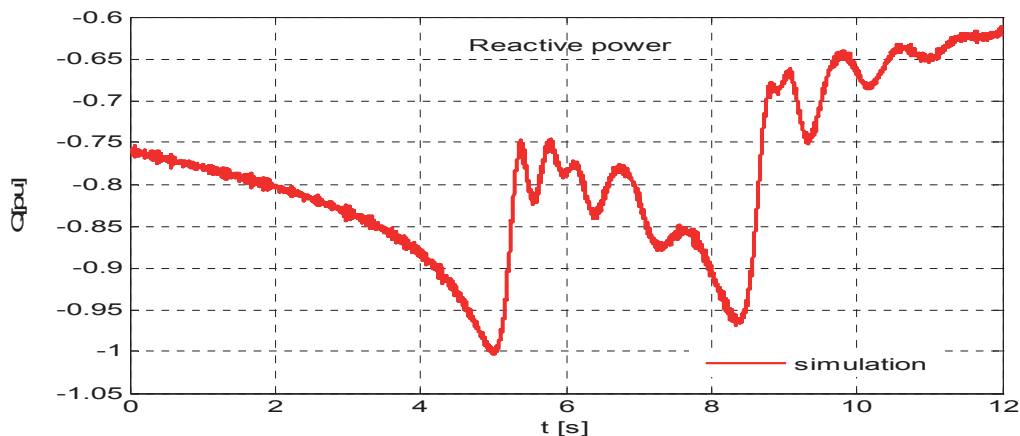


Figure 9 - Simulated reactive power

Figure 9 shows the reactive power which the generator draws from network. It can become a serious problem for power system, if there is not enough backup of reactive power.

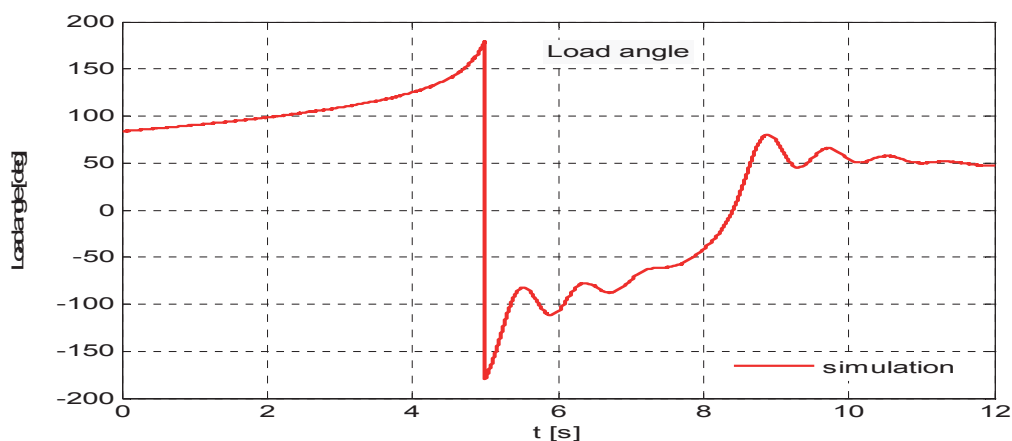


Figure 10 - Simulated load angle

Figure 10 shows a load angle determined by simulation. The same figure also shows one pole skipping at fifth second and generator's return to synchronism.

All simulations were carried out using a “MatLab” software package. Mathematical model for computer simulation of hydro-generator's asynchronous operation has been created, taking into consideration the magnetic saturation, damper winding and generator transformer's influence [2, 3, 5].

Besides these “standard” measured quantities, the whole variety of the quantities was measured. Among them are measurements of the vibrations and displacements during asynchronous operation. Table II shows the comparison of the vibration accelerations during asynchronous operation of the generator and during 3-phase short circuit. Vibration accelerations are measured on one of the foot screws [7].

Table II – Vibration amplitudes (in frequency domain)

ACC. [mm/s <sup>2</sup> ]	50 Hz	100 Hz	200 Hz
3 phase short circuit	2.7	0.5	0.7
Asynchronous operation	0.1	1.18	0.9

Vibration accelerations at frequencies above the base frequency (50 Hz) are larger during the asynchronous operation than in case of 3 phase short circuit.

### 3 CONCLUSION

This paper presents results of measurements during the asynchronous operation of the 35 MVA synchronous generator. Acquired results are compared to ones obtained by numerical simulation. Special emphasis is put on case of loss of excitation, the most frequent reason for asynchronous operation.

The generator that has lost its excitation is operating both asynchronously and underexcited. The asynchronous operation has strong influence on the currents, electromagnetic torque and heating. The underexcited operation can, by itself, cause additional temperature increase in the end region stator segments.

The measurements and simulations indicate that the asynchronous operation is particularly harmful to dampening winding, armature winding, shaft and subsequently to the power system generator is connected to.

Therefore, the asynchronous operation is not desirable and in many countries not allowed. The analyses of this operation and applied protection measures have a significant influence on stability and normal operation of power system.

### BIBLIOGRAPHY

- [1] F. L. Kogan, Features of Asynchronous Mode of Modern Turbogenerators and Protection Requirements, CIGRE, 11-103, 1996.
- [2] M. Jadrić, B. Frančić, Dynamics of Electrical Machines, Zagreb, Graphis, 1995. (in Croatian)
- [3] Z. Sirotić, Z. Maljković, Synchronous Machines, Zagreb, 1996. (in Croatian)
- [4] S. P. Verma, A. M. El-Serafi, Operation of Synchronous Generators in the Asynchronous Mode, Paper No. T 73 519-6, Presented at the IEEE PES Summer Meeting & EHV-UHV Conference, Vancouver, Canada, July 15-20, 1973
- [5] Z. Zebić, Z. Maljković, M. Pavlica, Asynchronous Operation of Hydro-Generator Calculation Verification by Test on Old Hydro-Generator in Power Plant, MELECON, 2004.
- [6] J. V. Mitsche, P. A. Rusche, Shaft Torsional Stress Due To Asynchronous faulty Synchronization, IEEE Transactions on Power Apparatus and Systems, Vol. PAS-99, No. 5 Sept/Oct 1980
- [7] I. Gašparac, Z. Maljković, M. Vražić, Vibrations Measurement During Hydrogenerator Testing, XVII IMEKO

## Evaluation of Different Methods for Voltage Sag Source Detection

**Boštjan POLAJŽER, Gorazd ŠTUMBERGER, and Sebastijan SEME**  
University of Maribor, Faculty of Electrical Engineering and Computer Science  
Slovenia

### SUMMARY

This paper compares and evaluates three different methods for voltage sag source detection. First method (method I) is based on the assumption, that the energy flow at the monitoring point increases during downstream events and decreases during upstream events. Second and third method (methods II and III) are both based on the assumption that currents measured at the monitoring point increase during downstream events and decrease during upstream events. The slope of a current-voltage trajectory is investigated in method II, while a real current component is observed within method III. Both current-based methods (II and III) require fundamental harmonic components of sampled voltages and currents, which are extracted using discrete orthogonal series expansion, such as Fourier or Walsh. Algorithms of this type are especially appropriate for studying steady-state and periodically repeating conditions. Voltage sags are, on the contrary, transient disturbance events. Thus, usage of the discussed algorithms may not be appropriate. Furthermore, criteria within methods II and III are checked for each phase individually. In the cases of asymmetrical voltage sags exact interpretation of the obtained results, therefore, might not be possible. Method I is, on the contrary, based on instantaneous values of line voltages and currents, while three-phase criterion is used. An exact interpretation of the results obtained by this method is, therefore, also possible in cases of asymmetrical voltage sags. All the discussed methods for voltage sag source detection have been tested by applying extensive simulations and field tests. The results for ground faults, asymmetrical voltage sags, upstream events and motor starting have been analyzed in order to evaluate all the discussed methods. The obtained results show that all discussed methods are very successful in cases of heavy motor starting and other symmetrical voltage sags. In cases of asymmetrical voltage sags the methods II and III do not work well, especially for those originating from the upstream side, while the method I is not successful only in particular cases of voltage sags due to upstream ground faults. Based on the performed evaluation it can be concluded, that further development is still needed to increase the degree of confidence in the discussed methods.

### KEYWORDS

Power – System, Power – Quality, Voltage Sag, Source, Detection.

[bostjan.polajzer@uni-mb.si](mailto:bostjan.polajzer@uni-mb.si)

## 1. INTRODUCTION

Among the wide range of power quality disturbances voltage sags are the most frequent ones, since they can be provoked by different events throughout the network, such as faults, motor starting, transformer energizing and heavy load switching [1]. Despite their relatively short duration – usually less than one second [2], voltage sags might be detrimental to several industrial loads. The detection and measurement of voltage sags is, therefore, essential for possible mitigation [3],[4], as well as for further analysis [5]. Reliable information about a voltage sag source is indispensable in order to identify the responsible party for production losses or interruptions in the power supply. It has already been reported that it is possible to use sampled voltage and current waveforms to determine on which side of the recording device voltage sag originates, i.e. from the upstream or downstream side [6]-[8]. However, a methodology for pinpointing the exact locations of voltage sags does not yet exist.

This paper compares and evaluates three different methods for voltage sag source detection. The method proposed in [6] (method I) is based on the assumption, that the energy flow at the monitoring point increases during downstream events and decreases during upstream events. The methods proposed in [7] and in [8] (methods II and III) are both based on the assumption that currents measured at the monitoring point increase during downstream events and decrease during upstream events. The slope of a current-voltage trajectory is investigated in method II, while a real current component is observed within method III. All the discussed methods have been tested by applying extensive simulations. The results for ground faults, asymmetrical voltage sags, upstream events and motor starting have been analyzed in order to evaluate all the discussed methods for voltage sag source detection. Results obtained from the field test are also included.

## 2. METHODS FOR VOLTAGE SAG SOURCE DETECTION

Let us consider the monitoring point shown in Fig. 1. Voltage sags might originate either from point A or from point B. In regard to energy flow direction in the steady-state, upstream and downstream events are defined in points A and B, respectively. A power-quality monitor or another recording device is placed at the monitoring point. Based on the recorded line voltages  $u_k(t)$  and currents  $i_k(t)$ , where  $k \in \{a, b, c\}$  ( $a$ ,  $b$  and  $c$  denote individual phases), it is possible to determine on which side of the recording device the voltage sag originated.

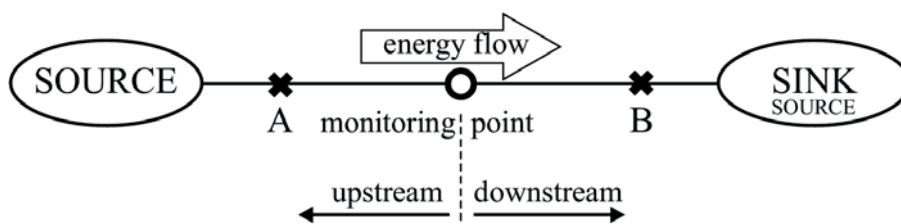


Fig. 1. Upstream event (A) and downstream event (B)

### 2.1 Energy-based method

The method which is based on the assumption, that the energy flow at the monitoring point increases during downstream events and decreases during upstream events is proposed in [6] (method I). The disturbance power  $\Delta p(t) := p(t) - p_{ss}(t)$  is calculated, defined as the difference

between the total three-phase instantaneous power  $p(t)$  and the steady-state three-phase instantaneous power  $p_{ss}(t)$ . The disturbance energy  $\Delta w(t)$  is used as the criterion (1).

$$\Delta w(t) = \int_0^t \Delta p(\tau) d\tau \begin{cases} < 0 \Rightarrow \text{upstream} \\ > 0 \Rightarrow \text{downstream} \end{cases} \quad (1)$$

## 2.2 Current-based methods

Two methods, proposed in [7] and in [8] (methods II and III), are based on the assumption that currents measured at the monitoring point increase during downstream events and decrease during upstream events, as it is shown in Fig. 2.

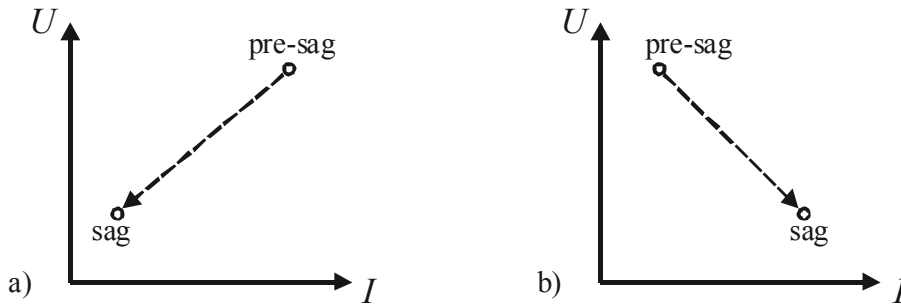


Fig. 2.  $U$ - $I$  characteristics in case of upstream event (a) and downstream event (b)

Phasors for fundamental harmonic components of line voltages  $\underline{U}_k = |\underline{U}_k| e^{j\varphi_{u,k}}$  and currents  $\underline{I}_k = |\underline{I}_k| e^{j\varphi_{i,k}}$  are calculated within both methods, where  $|\underline{U}_k|$  and  $|\underline{I}_k|$  are phasor lengths, while  $\varphi_{u,k}$  and  $\varphi_{i,k}$  are phasor angles, where  $k \in \{a, b, c\}$ . A phase angle is defined as  $\varphi_k := \varphi_{u,k} - \varphi_{i,k}$ . In method II [7] the points of  $(|\underline{I}_k|, |\underline{U}_k \cos \varphi_k|)$  are approximated during the voltage sag using the linear function. The slope of the obtained voltage-current characteristic is investigated for each phase individually (2).

$$\text{slope} \left( |\underline{I}_k|, |\underline{U}_k \cos \varphi_k| \right) \begin{cases} > 0 \Rightarrow \text{upstream} \\ < 0 \Rightarrow \text{downstream} \end{cases} \quad (2)$$

Within method III [8] waveform of a real current component is calculated for a few cycles prior and during the voltage sag. The sign of its first peak at the beginning of the voltage sag is used as the criterion for each phase individually (3).

$$\text{first peak} \left( |\underline{I}_k| \cos \varphi_k \right) (t) \begin{cases} < 0 \Rightarrow \text{upstream} \\ > 0 \Rightarrow \text{downstream} \end{cases} \quad (3)$$

## 3. NUMERICAL SIMULATIONS AND FIELD TESTING

A testing-network, shown in Fig. 3, was selected for numerical simulations of voltage sags. MATLAB/Simulink-based calculations were performed using a sampling time of 0.1 ms. An extensive number of tests were performed for different combinations of loads and for different events. Different types of loads were used in the cases of voltage sags due to faults:

RL-load, induction motor (IM), induction generator (IG), synchronous motor (SM) and synchronous generator (SG). Four types of faults were applied in four different locations (FL1-FL4): ground fault, phase-to-phase-to-ground fault, phase-to-phase fault and three-phase fault. Voltage sags due to motor starting and loading were also calculated, where IM was used. Line voltages and currents were captured at all four monitoring points (MP1-MP4). All discussed methods for voltage sag source detection were, thus, tested for altogether 417 different examples of voltage sags.

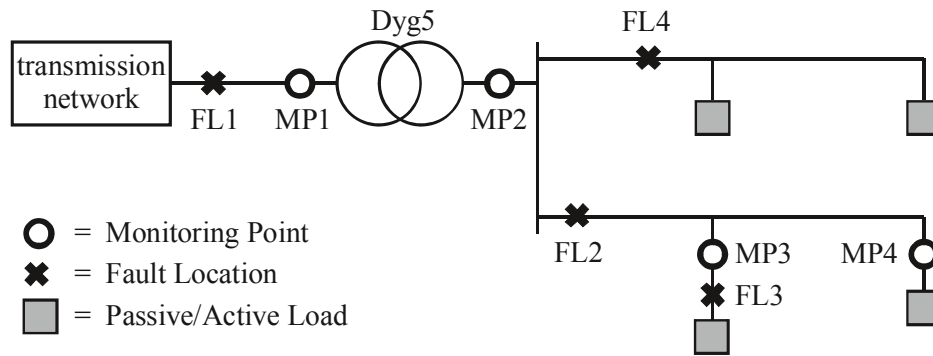


Fig. 3. Testing-network for simulations of voltage sags

Field tests of the discussed voltage sag source detection methods were also performed, as shown in Fig. 4. Voltages and currents were captured in a 20 kV network and in the neighbouring 100 kV and 0.4 kV networks (MP1-MP3). A sampling frequency of 5 kHz was used. During the field test a ground fault was generated in the 20 kV network, provoking extremely deep voltage sag at the 20 kV bus (MP2). This event lead to the protection-relay trip and then to the successful auto-reclosure. Consequently, a power transformer 110/20 kV, connected to the 20 kV bus, was energized. Another voltage sag was thus provoked through the 20 kV bus and a 20/0.4 kV transformer in the neighbouring 0.4 kV network (MP3).

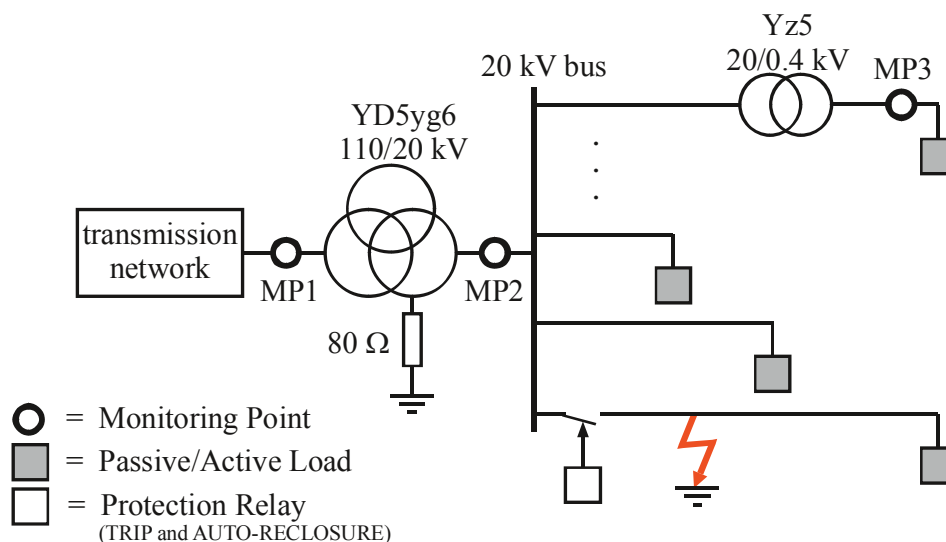


Fig. 4. Field testing

## 4. RESULTS

A typical example of the simulation results is shown in Fig. 5a for the upstream phase-to-phase-to-ground fault in location FL2 (Fig. 3). Voltages and currents were captured at MP3, while SM, IM and IG were used as active loads. The results obtained using methods II and III can not be interpreted exactly, since they are different for individual phases. On the contrary, method I gave us an exact and correct result for this case.

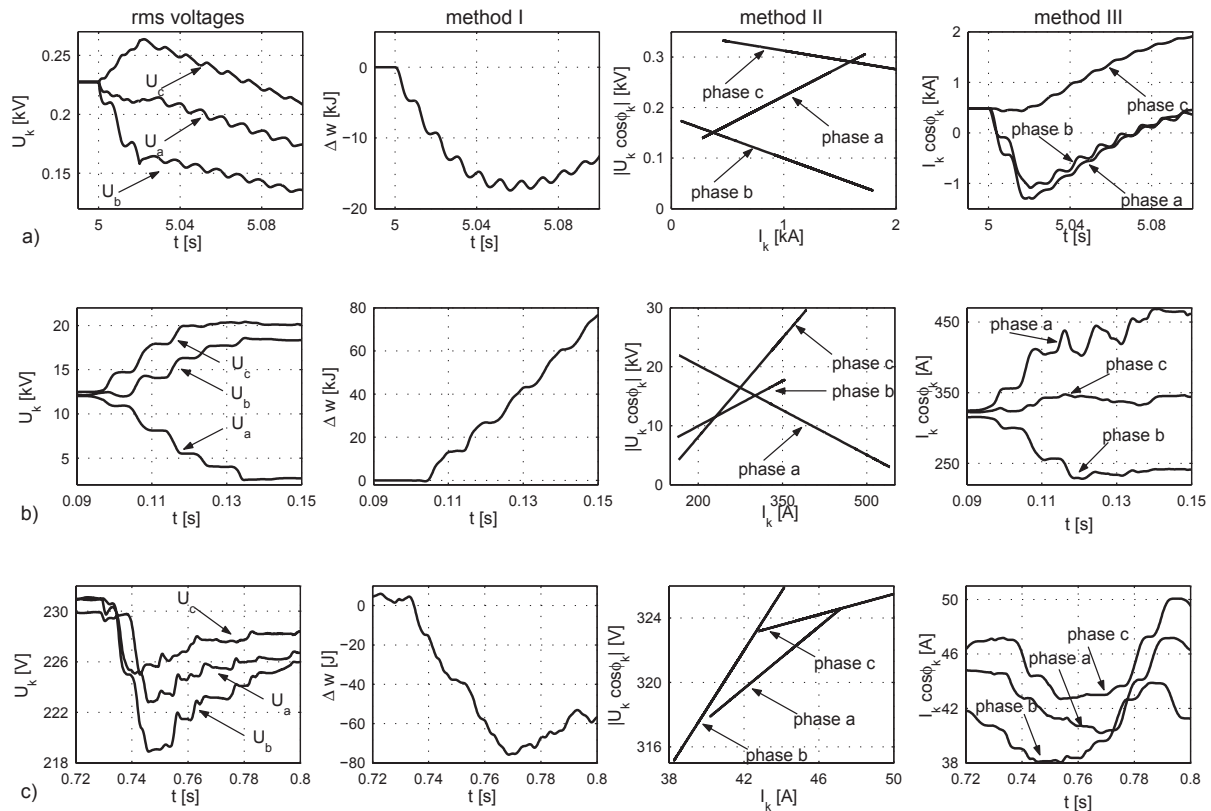


Fig. 5. Simulation results for the upstream phase-to-phase-to-ground fault (a), and field testing results for the downstream ground fault (b) and the upstream transformer energizing (c)

Field testing results are presented in Figs. 5b and 5c. Results for the downstream ground fault (voltage sag at the 20 kV bus – MP2 in Fig. 4) are shown in Fig. 5b, where an extremely deep voltage sag can be noticed in phase *a*. Method I gave us an exact and correct result for this case, while the results obtained using methods II and III can not be interpreted exactly, since they are different for individual phases. Results for the upstream transformer energizing (voltage sag at the 0.4 kV level – MP3 in Fig. 4) are shown in Fig. 5c. Even though the resulting voltage sag was quite shallow, the obtained results show typical waveforms for the rms voltages during the transformer energizing, while all methods gave us correct results.

All the discussed methods for voltage sag source detection were tested by applying extensive numerical simulations and measurements of voltage sags. Successfulness was determined for all three methods, where all 417 different examples of simulation-based voltage sags were considered. The obtained results are shown in Fig. 6, where the results for the total successfulness are given for all types of faults (ground fault, phase-to-phase-to-ground fault, phase-to-phase fault and three-phase fault) in all fault locations (FL1–FL4) and for all

monitoring points (MP1–MP4 in Fig. 4). It can be concluded, that method I works fine in almost all cases, except in particular cases of voltage sags due to upstream ground faults. Methods II, and III, as already mentioned, do not work well in cases of asymmetrical voltage sags, especially for those originating from the upstream side. However, let us emphasize that all discussed methods are very successful in cases of heavy motor starting and other symmetrical voltage sags.

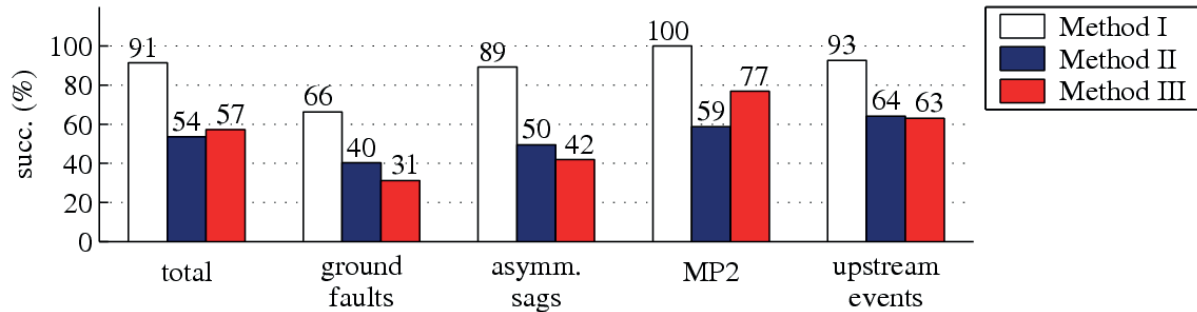


Fig. 6. Successfulness of the discussed methods for voltage sag source detection

## 5. CONCLUSION

Three different methods for voltage sag source detection are studied in this paper. For this purpose, the discussed methods for voltage sag source detection are tested by applying extensive simulations and field tests. The obtained results show that methods II and III do not work well, particularly in cases of asymmetrical voltage sags due to upstream events. Furthermore, methods II and III are both phasor-based and might, therefore, give us questionable results. Method I works fine in almost all cases, except in particular cases of voltage sags due to upstream ground faults. Based on the performed evaluation it can be concluded, that further development is still needed to increase the degree of confidence in all the discussed methods.

## BIBLIOGRAPHY

- [1] M. J. H. Bollen, "Voltage sags in three-phase systems" (IEEE Power Engineering Review, no. 9, September 2001, pages 8-11).
- [2] IEEE recommended practice for monitoring electric power quality (IEEE Standard 1159-1995, June 1995).
- [3] M. Karimi, H. Mokhtari and M. R. Irvani, "Wavelet based on-line disturbance detection for power quality applications" (IEEE Transactions on Power Delivery, no. 4, October 2000, pages. 1212-1220).
- [4] C. Fitzer, M. Barnes and P. Green, "Voltage sag detection technique for a dynamic voltage restorer" (IEEE Transactions on Industry Applications, no. 1, January 2004, pages. 203-212).
- [5] J. Arrillaga, M. J. H. Bollen and N. R. Watson, "Power quality following deregulation" (Proceedings of the IEEE, no. 2, February 2000, pages 246-261).
- [6] A. C. Parsons, W. M. Grady, E. J. Powers and J. C. Soward, "A direction finder for power quality disturbances based upon disturbance power and energy" (IEEE Transactions on Power Delivery, no. 3, July 2000, pages 1081-1086).
- [7] C. Li, T. Tayjasanant, W. Xu and X. Liu, "Method for voltage-sag-source detection by investigating slope of the system trajectory" (IEE Proceedings: Generation, Transmission and Distribution, no. 3, May 2003, pages 367-372).
- [8] N. Hamzah, A. Mohamed and A. Hussain, "A new approach to locate the voltage sag source using real current component" (Electric Power Systems Research, no. 2, December 2004, pages 113-123).

## Numerical Analysis of Power System Electromechanical and Electromagnetic Transients based on the Finite Element Technique

I. JURIĆ-GRGIĆ, M. KURTOVIĆ, R. LUCIĆ

University of Split, Faculty of Electrical Engineering,  
Mechanical Engineering and Naval Architecture  
Croatia

### SUMMARY

This paper presents a novel technique for numerical analysis of electromagnetic transients and electromechanical oscillations in a power system. The proposed method is based on the finite element method (FEM). The finite element technique so far used for numerical analysis of continuum field problems here has been adopted to analyse electromagnetic and electromechanical transients in a power system. According to the finite element technique in the field problem, where the region of interest is divided into finite elements, in the proposed method power system is also divided into electric power system (finite) elements. Each finite element (generator, transformer, transmission line, load etc.) is characterized by a system of governing differential equations. Using generalized trapezoidal rule, also known as theta-method for time integration, the system of differential equations of each electric power system (finite) element can be transformed to the system of algebraic equations for every time step. Once when a system of algebraic equations of each electric power system element is obtained, assembly procedure has to be done. The main contribution of the proposed approach is in an assembly procedure. With the proposed approach, in case of any disturbances in power system or in a part of power system, nodal voltage and branch currents will be obtained, as well as all other interesting variables. The proposed method will be tested on the example of the single-phase short circuit in the power system.

### KEYWORDS

Electromagnetic transients, Electromechanical oscillations, Power system, Finite Element Technique

[ijuricgr@fesb.hr](mailto:ijuricgr@fesb.hr)

## 1. INTRODUCTION

The finite element technique has been widely used in 2D and 3D field problems. To the best of our knowledge, it is not known, that the finite element method is used for electrical network analysis in electrical power system. For power system electromechanical analysis, software package EMTP and Matlab-Simulink are commonly used. On the other hand as the result of our research, the papers [1] and [2] report successful use of the finite element technique for power system analysis. The main contribution of the proposed method over the other known methods is simplification of algorithm by using assembly procedure in a sense of the finite element technique. Each finite element (generator, transformer, transmission line, load etc.) is characterized by a system of governing differential equations. Using generalized trapezoidal rule, also known as theta-method for time integration, the system of differential equations of each electric power system (finite) element can be transformed to the system of algebraic equations for every time step. The entire power system is modeled by assembling the system of algebraic equations of all finite elements. The finite element matrices of electric power system are obtained in natural (a,b,c) coordinates. With such approach the solution of the multimachine problem in a power system is natural and straightforward.

## 2. SYNCHRONOUS GENERATOR AS FINITE ELEMENT

The three phase synchronous generator with field and damper windings is represented as one finite element with three nodes namely 1,2,3.

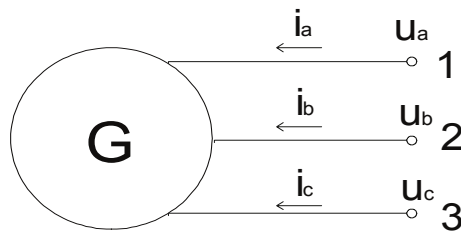


Fig. 1. Synchronous generator finite element

The starting point to obtain the local matrix and vector of synchronous generator finite element is a system of the following equations :

$$\{u\} = [R] \cdot \{i\} + \frac{d}{dt} [\Psi] \quad (1)$$

$$\omega = \frac{d\gamma}{dt} \quad (2)$$

$$T_m \frac{d\omega}{dt} = m_m - m_{el} \quad (3)$$

where are:

$$\{i\}^T = [i_a \ i_b \ i_c \ i_f \ i_D \ i_Q]$$

$[\Psi]$  - (6,6) magnetic flux matrix

$\omega$  - electrical angular frequency

$t$  - time

$i_f$  - field coil current

$u_f$  - field coil voltage

$$\{u\}^T = [u_a \ u_b \ u_c \ u_f \ 0 \ 0]$$

$[R]$  - (6,6) resistance matrix

$\gamma$  - electrical angle of rotor position

$i_Q$  - damper winding current in axes q

$i_D$  - damper winding current in axes d

Time integration of equations (1), (2) and (3) by  $\theta$ - method, yields equations (4), (5) and (6) :

$$\begin{aligned} \{\Psi\}^+ - \{\Psi\} + [R] \theta \Delta t \{i\}^+ + [R] (1-\theta) \Delta t \{i\} \\ - \theta \Delta t \{u\}^+ - (1-\theta) \Delta t \{u\} = 0 \end{aligned} \quad (4)$$

$$\gamma^+ = \gamma + \omega \Delta t \quad (5)$$

$$\omega^+ = \frac{\theta \Delta t}{T_m} m_m^+ + \frac{(1-\theta) \Delta t}{T_m} m_m - \frac{\theta \Delta t}{T_m} m_{el}^+ - \frac{(1-\theta) \Delta t}{T_m} m_{el} + \omega \quad (6)$$

System of equations (4) need to be rearranged to the system of the algebraic equations which will be suitable for assembling procedure with the rest of the power system :

$$\{i_1^+\} = [E_1] \{u_1^+\} + [E_2] \{u_2^+\} + [D_1] \{u_1\} + [D_2] \{u_2\} + [C_1] \{i_1\} + [C_2] \{i_2\} \quad (7)$$

$$\{i_2^+\} = [E_3] \{u_1^+\} + [E_4] \{u_2^+\} + [D_3] \{u_1\} + [D_4] \{u_2\} + [C_3] \{i_1\} + [C_4] \{i_2\} \quad (8)$$

The finite element local system of the generator is given by the system of algebraic equations (5), (6), (7) and (8). The voltage regulator as an essential part of synchronous generator is modeled by the system of appropriate equations and is shown in [2]. The other power system elements used in this paper such as transmission line, transformer, power system network equivalent and three-phase load are also given in the papers [1] and [2].

### 3. NUMERICAL EXAMPLE

In order to verify the proposed method, electromagnetic transients and electromechanical behavior of the electric power system, shown in Figure 2, have been analyzed. In the considered power system at the certain moment of time the single-phase short circuit occurs in the middle of double transmission line system. This caused opening of the circuit breakers at the both ends of faulted system of double transmission line system. As the result of mentioned switching operation overvoltages and electromechanical oscillations due to sudden short circuit on the transmission line have been occurred.

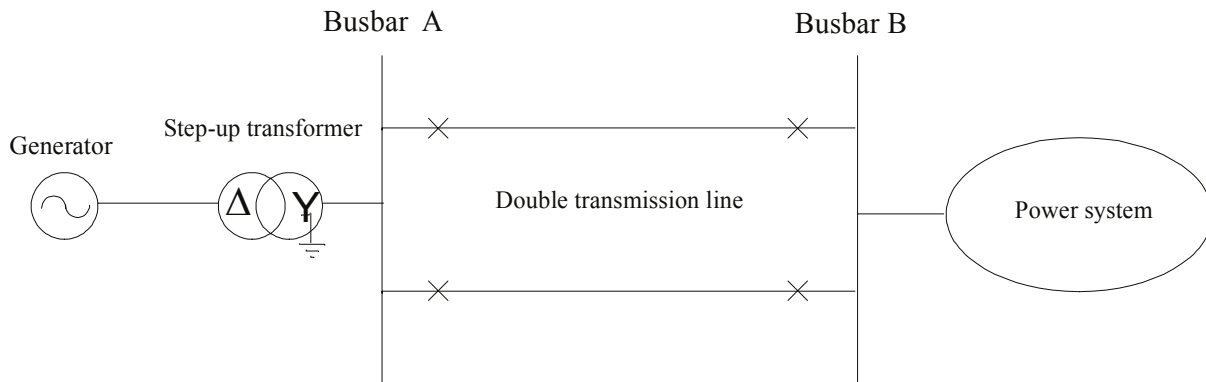


Fig.2. Single-phase scheme of the power system

The generator data are:  $S_n = 120$  MVA,  $P_n = 108$  MW,  $Q_n = 52.3$  Mvar,  $U_n = 14.4$  kV,  $I_n = 4811$  A,  $I_{f0} = 690$  A,  $I_{fn} = 1192$  A.

Available parameters of generator are:

- reactance's (pu)  $x_d = 1.01$ ,  $x_q = 0.666$ ,  $x_q'' = 0.287$ ,  $x_d' = 0.421$ ,  $x_d'' = 0.268$ ,  $x_\sigma = 0.198$
- armature resistance (pu)  $r = 0.00236$
- time constants  $T_d' = 3.4$  s,  $T_{d0}' = 7.5$  s,  $T_d'' = 0.0554$  s,  $T_q'' = 0.0876$  s
- mechanical time constant  $T_{mG} = 8.63$  s

Step-up transformer data are:  $S_n = 120$  MVA, dY5,  $U_{n1}/U_{n2} = 10.5/220$  kV,  $u_k = 12.06$  %,  $P_k = 270$  kW

On the basis of transmission line characteristics, calculated parameters are:

$$[R] = \begin{bmatrix} a & b & c & a_2 & b_2 & c_2 \\ a & 0.18 & 0.09 & 0.09 & 0.09 & 0.09 & 0.09 \\ b & 0.09 & 0.18 & 0.09 & 0.09 & 0.09 & 0.09 \\ c & 0.09 & 0.09 & 0.18 & 0.09 & 0.09 & 0.09 \\ a_2 & 0.09 & 0.09 & 0.09 & 0.18 & 0.09 & 0.09 \\ b_2 & 0.09 & 0.09 & 0.09 & 0.09 & 0.18 & 0.09 \\ c_2 & 0.09 & 0.09 & 0.09 & 0.09 & 0.09 & 0.18 \end{bmatrix} (\Omega/km)$$

$$[L] = \begin{bmatrix} a & b & c & a_2 & b_2 & c_2 \\ a & 2.2 & 0.796 & 0.796 & 0.796 & 0.796 & 0.796 \\ b & 0.796 & 2.2 & 0.796 & 0.796 & 0.796 & 0.796 \\ c & 0.796 & 0.796 & 2.2 & 0.796 & 0.796 & 0.796 \\ a_2 & 0.796 & 0.796 & 0.796 & 2.2 & 0.796 & 0.796 \\ b_2 & 0.796 & 0.796 & 0.796 & 0.796 & 2.2 & 0.796 \\ c_2 & 0.796 & 0.796 & 0.796 & 0.796 & 0.796 & 2.2 \end{bmatrix} (\text{mH}/km)$$

$$[C] = \begin{bmatrix} a & b & c & a_2 & b_2 & c_2 \\ a & 7.76 & -0.76 & -0.76 & -0.76 & -0.76 & -0.76 \\ b & -0.76 & 7.76 & -0.76 & -0.76 & -0.76 & -0.76 \\ c & -0.76 & -0.76 & 7.76 & -0.76 & -0.76 & -0.76 \\ a_2 & -0.76 & -0.76 & -0.76 & 7.76 & -0.76 & -0.76 \\ b_2 & -0.76 & -0.76 & -0.76 & -0.76 & 7.76 & -0.76 \\ c_2 & -0.76 & -0.76 & -0.76 & -0.76 & -0.76 & 7.76 \end{bmatrix} (\text{nF}/km)$$

Transmission line length is 82 km.

Parameters of power system network equivalent are obtained from single and three-phase short circuit current data on the busbar "B":

- rated voltage  $U_n = 220 \text{ kV}$
- subtransient three-phase short circuit current  $I''_{k3} = 15.15 \text{ kA}$
- subtransient single-phase short circuit current  $I''_{k1} = 16.46 \text{ kA}$

In order to model considered power system by the finite element technique, the power system has been divided into the 11 parts (finite elements), shown in the Figure 3. This enables us to define a connection matrix of a power system in a sense of the finite element method.

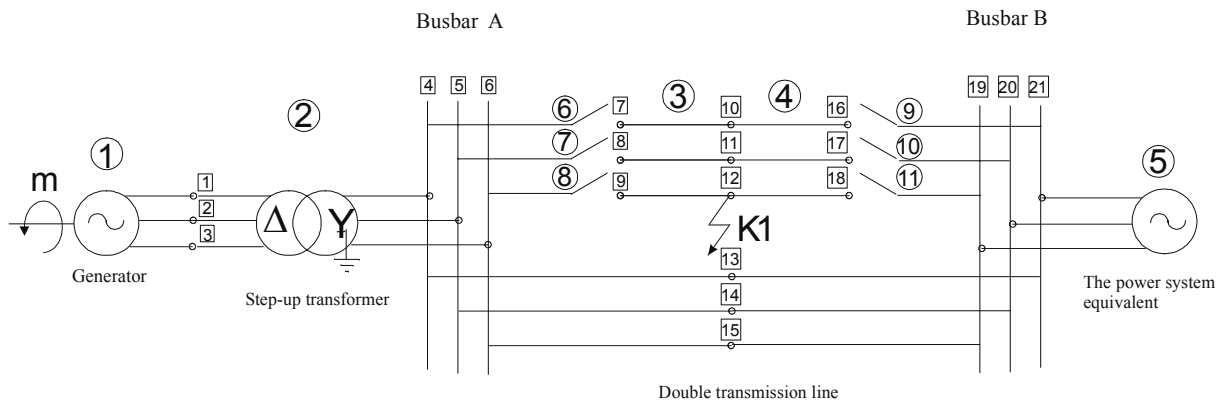


Fig.3. The power system divided to the finite elements

The double transmission line system has been split into two finite elements numbered 3 and 4 with equal lengths of 41 km. The finite elements numbered from 6 to 11 represent single poles of the three phase breakers at the ends of the faulted system of the double transmission line system.

In the beginning of simulation the generator is in nominal operating mode. At the moment  $t=0.885 \text{ [s]}$  the single-phase occurs in phase "a" of transmission line. Approximately 100 ms after single-phase short circuit had occurred, the circuit breakers opened at the both ends of the faulted line system.

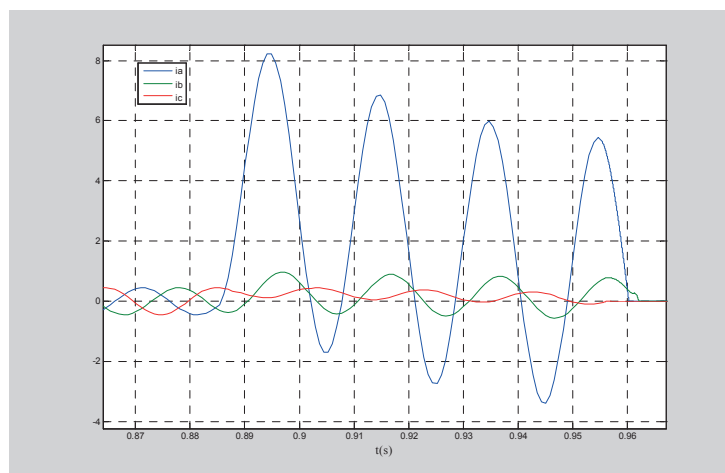


Fig.4. Short circuit currents contributed from busbar "A"

In Figure 4 single-phase short circuit currents of faulted phase “a” and the phases “b” and “c” contributed from busbar “A” are shown. In the Figure 5 overvoltages at the HV-side of the transformer at the busbar “A” after circuit breaker opening are shown.

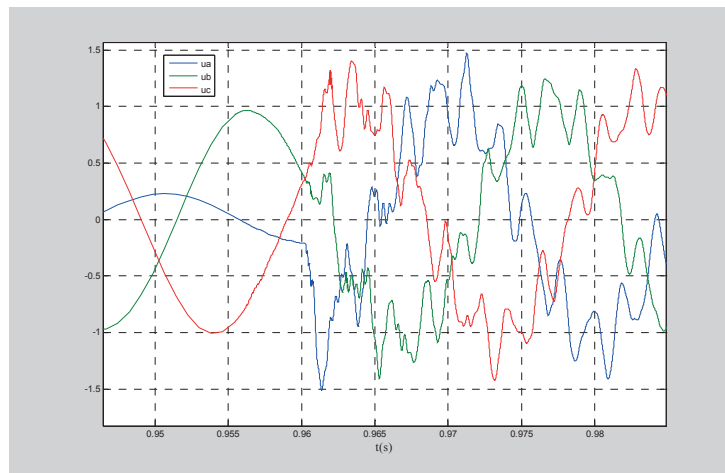


Fig.5. Overvoltages at the HV-side of the transformer at the busbar “A” after circuit breaker opening

According to Figure 5, it can be clearly seen that switching operations at HV-side of the step-up transformer causes approximately 50 % voltage increasing. Due to switching operation, the faulted transmission line of the double transmission line system has been switched off and new steady – state has to be reached. This approach allows us to calculate every interesting variable in all finite elements. For instance, in Figure 6, 7 and 8 electromagnetic moment, field coil current and angular frequency of the generator are shown during entire transient operation.

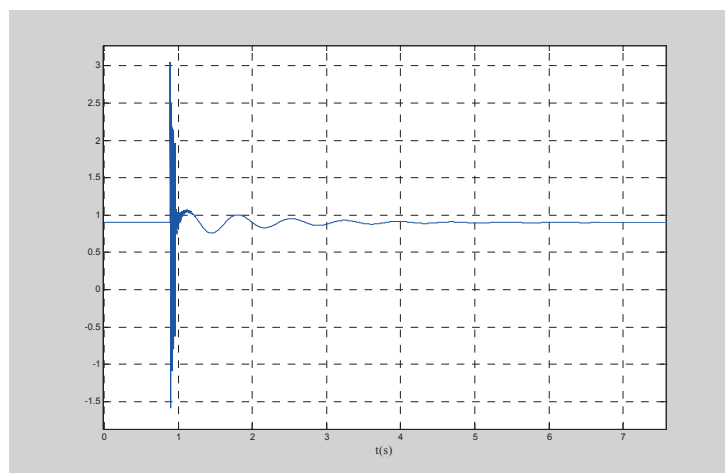


Fig.6. Electromagnetic moment of generator during transient operation

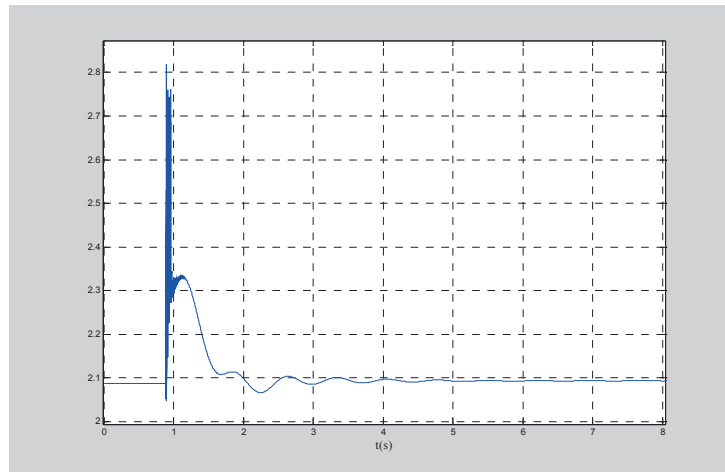


Fig.7. Field coil current of generator during transient operation

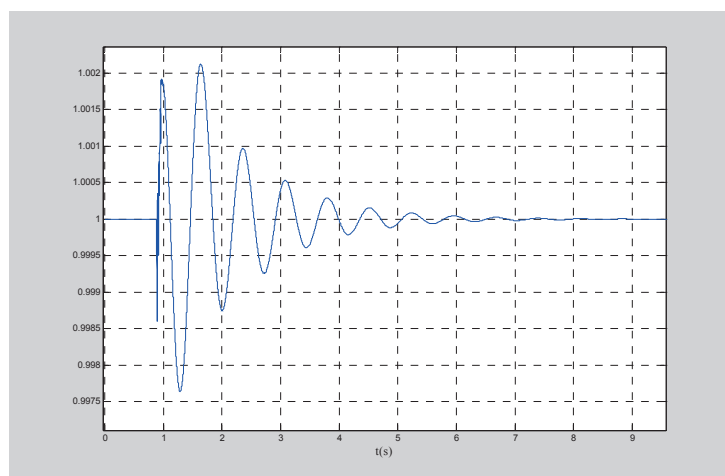


Fig.8. Angular frequency of generator during transient operation

#### 4. CONCLUSION

In this paper the novel method based on the finite element technique has been presented. The proposed method has been successfully applied on short circuit power system analysis. As it has been shown, this approach enables us to calculate currents, voltages as well as other interesting variables in each part of a power system such as generators, transmission lines, transformers etc. Attractive side of this method is a possibility to make a simple algorithm for the multimachine system analysis. The proposed method is competitive, even simpler, than other widely used methods due to elegance of the FEM assembly procedure. As the power system has been built assembling the three phase finite elements, the solution of the multimachine system problem is natural and straightforward.

## BIBLIOGRAPHY

- [1] I. Juric-Grgic, R. Lucic, M. Kurtovic "Transients Analysis of Synchronous Generator Using the Finite Element Technique " (Electrical Engineering and Electromagnetics VI, September 2003, pages 137-146)
- [2] I. Juric-Grgic, R. Lucic, M. Kurtovic "Electromagnetic Transients Modeling in Power Systems Using the Finite Element Technique " (Computational Methods and Experimental Measurements XII, 2005, pages 631-639)
- [3] J. Arrillaga, N. Watson "Power Systems electromagnetic transients simulation", The Institution of Electrical Engineers, 2003.
- [4] J. Arrillaga, N. Watson "Computer Modelling of Electrical Power Systems ", 2001.

## The impact of events in the Slovene high – voltage network on the power quality in the distribution networks

<sup>1</sup>Klemen Deželak, <sup>1</sup>Andrej Korak, <sup>2</sup>Tatjana Konjic, <sup>1</sup>Gorazd Štumberger, <sup>1</sup>Jože Voršič

<sup>1</sup>University of Maribor, Faculty of Electrical Engineering and Computer Science,  
Slovenia

<sup>2</sup>University of Tuzla, Faculty of Electrical Engineering  
Bosnia and Hercegovina,

### SUMMARY

This work analyses the impact of different events in Slovene high-voltage network on power quality in the 20 kV and 0.4 kV distribution networks. In order to perform the analysis a simplified dynamic model of the Slovene power system was build in the program package Matlab/Simulink, using toolbox PowerSys. The obtained model is appropriate for simulation of electromagnetic transients in duration up to a few seconds. It contains simplified dynamic models of all main generators and power transformers installed in the Slovene power system, detailed models of 400 kV, 220 kV and 110 kV networks, simplified models of the neighboring power systems and models of important consumers. The 20 kV and 0.4 kV distribution networks are modeled in the details only in the area of interests. Everywhere else, they are represented as constant loads connected to the 110 kV network.

The aforementioned dynamic model was applied to analyze the impact of different events in the Slovene power system on power quality in the 0.4 kV distribution network during transients and in steady states. The power quality in distribution network was analyzed on 0.4 kV busbars in five substations (Cerkno, Škofja Loka, Vevče, Šentjur, Rače) for the following set of events: a switch-off of a 300 MVA (400 kV/110 kV) power transformer in the substation Okroglo; a three-phase short circuit on 110 kV busbars in the substation Kleče; a three-phase short circuit on 20 kV busbars in the substation Rogaška Slatina and a switch-on in a pumping regime of pump-turbine plants Avče and Kozjak which are currently at the design stage. The results obtained show that aforementioned events in some points of Slovene distribution network can cause power quality distortion over that allowed by the power quality standards.

### KEYWORDS

Power system – Dynamic Model – Voltage Sag – Simulation – Power Quality .

[klemen.dezelak@uni-mb.si](mailto:klemen.dezelak@uni-mb.si)

## 1. INTRODUCTION

This work analyses the impact of different events in Slovene high-voltage network on power quality in the 20 kV and 0.4 kV distribution networks. In order to perform the analysis an appropriate dynamic model is needed. It must be appropriate to handle electromagnetic power system transients that appear in the same frequency range as voltage sags treated in [1]-[3]. According to the time frame of various power system phenomena [4], this range must be between 10  $\mu$ s and a few seconds. An appropriate and simplified dynamic model of Slovene power system is briefly presented in this work. It is applied to evaluate the impact of different events in the power system on power quality in 0.4 kV distribution networks.

## 2. A SIMPLIFIED MODEL OF SLOVENE POWER SYSTEM

This section gives a short description of a simplified dynamic model of Slovene power system build in the program package Matlab/Simulink using toolbox PowerSys. Initial conditions for simulations are normally determined by calculating load flow.

### 2.1 Generator model

It is reasonable to use the complete Park's two-axis generator model with considered magnetic nonlinearities of the iron core only in the cases when turbine, excitation system and control models too are included in the dynamic power system model. However, the simplified model of Slovene power system is used for study of electromagnetic transients which appear relatively far away from the generator's terminals. In such cases generator model can be represented with sufficient accuracy by a voltage source with generator internal impedance in series. The generator output power can be adjusted by the amplitude and angle of the voltage source. Of course, the complete Park's generator dynamic model can be used together with turbine, excitation system and control models if their structures and parameters are known.

### 2.2 Power transformer model

A variety of three phase transformer models can be used. All of them are composed of connected single phase transformers with two or three windings. Required transformer data are nominal voltages and resistances of all windings and rated power. Iron core losses and magnetically nonlinear iron core characteristic can be included in the model if they are available. In the simplified power system model magnetically nonlinear transformer models are used when magnetically nonlinear iron core characteristic is available. In all other cases magnetically linear models are used. A substantial difference between results obtained by the magnetically linear and nonlinear transformer dynamic models can be noticed only when a switch-on of an unloaded transformer is studied.

### 2.3 Models of transmission and distribution lines

The transmission and distribution lines are accounted for by  $\pi$  models. They require resistance, inductance and capacity for positive and zero symmetric components sequences per kilometer and length of the entire line.

## 2.4 Models of transmission and distribution networks and loads

The discussed simplified dynamic power system model contains models of all important generators, transformers, power lines and loads. The 400 kV, 220 kV and 110 kV networks are modeled in details. Lower voltage networks are modeled in details only in the area of interest while everywhere else they are presented as constant loads. In order to achieve the best possible agreement between the measured and calculated results, the exact loading conditions for each individual point of the power system at given instant must be known before simulation is started. Usage of average loading conditions measured for a given time interval in simulations normally leads to disappointing results.

## 2.5 Considering neighboring power systems

Slovene power system is connected to the neighboring power systems in 13 high voltage points. The short circuit impedance in these points is low due to high apparent power. In the simplified model of Slovene power system the neighboring power systems are accounted for passively by voltage sources connected in series with short circuit impedance in given point. The correct power flow is achieved by appropriate amplitude and angle of the voltage source.

## 3. MODEL EVALUATION

The proposed simplified dynamic model of Slovene power system was confirmed in two ways. The steady state accuracy of the dynamic model was confirmed through the comparison of calculated results with those obtained by the professional program for steady state analysis and network optimization NEPLAN. The agreement of steady state voltages during normal operating conditions is very good, while the steady state voltages during the three-phase faults can differ up to 4 % in 0.4 kV network. The dynamic response of the model was partially confirmed by the comparison of calculated results with the results of field testing performed on 20 kV in the substation Rogaška Slatina. The agreement between measured and calculated results is very good for the three-phase faults as well as for the line to line and line to ground faults. Thus, the dynamic responses of the model are confirmed for the tested substation and its vicinity, while the entire model is confirmed only for the steady state operation by the results calculated with NEPLAN.

Table 1 shows decrease of voltage RMS values on 110, 20 and 0.4 kV busbars in substation Cerknò caused by a three-phase short circuit in the middle of 110 kV overhead line Divača – Ajdovščina. The results calculated by NEPLAN and by proposed simplified dynamic model are given for the steady state during aforementioned short circuit.

Table 1: Comparison of voltage drops calculated by NEPLAN and by dynamic model on 110, 20 and 0.4 kV busbars in substation Cerknò caused by a three-phase short circuit in the middle of 110 kV overhead line Divača – Ajdovščina.

Substation Cerknò	Dynamic model	NEPLAN	Differences[%]
110 kV	14,6 kV	14,54 kV	0,41
20 kV	2,27 kV	2,27 kV	0,00
0,4 kV	57 V	55 V	3,63

## 4. RESULTS

The proposed simplified dynamic model of Slovene power system was applied to evaluate the impact of different events on power quality in 0.4 kV distribution networks. Simulations were performed for the following list of events:

1. a three-phase short circuit on a 110 kV busbars in the substation Kleče,
2. a switch-off of a 300 MVA power transformer in the substation Okroglo,
3. a three-phase short circuit on a 20 kV busbar in the substation Rogaška Slatina,
4. switch-on in a pumping regime of pump-turbine plant Kozjak and
5. switch-on in a pumping regime of pump-turbine plant Avče.

The impact of these events on the power quality in 0.4 kV distribution networks is in this work analyzed in the following points:

1. 0.4 kV busbars in the substation Cerkno,
2. 0.4 kV busbars in the substation Škofja Loka,
4. 0.4 kV busbars in the substation Šentjur and
5. 0.4 kV busbars in the substation Rače.

Figure 1 shows results calculated for the three-phase short circuit on 110 kV busbar in the substation Kleče. The three-phase short circuit appears in the time interval between 0.04 s and 0.12 s. The calculated line voltages on 0.4 kV busbar in substations Cerkno, Škofja Loka, Šentjur and Celje are shown in Figure 1. The left hand side of the Figure 1 shows calculated time dependent wave forms of all three voltages, while the right hand side of the same figure shows the time dependent RMS values for voltages in line L1. Only the last type of presentation is used for the presentation of results that follow.

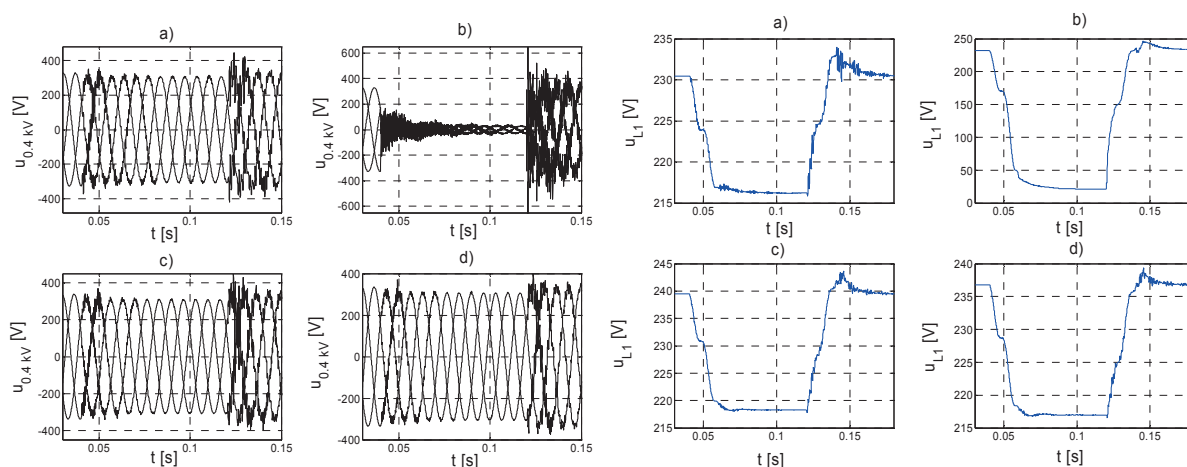


Figure 1: Voltages on 0.4 kV busbar in substations a) Cerkno, b) Škofja Loka, c) Šentjur and d) Rače, during a three-phase short circuit on 110 kV busbar in substation Kleče.

The results presented in Figure 1 show that the three-phase short circuit on 110 kV busbar in the substation Kleče can substantially influence power quality in Slovene 0.4 kV distribution networks. The depth of the voltage sag on 0.4 kV busbar in the substation Škofja Loka, caused by this event, is much higher than it is allowed by the Slovene standard for power quality SIST EN 50160.

The next example shows the impact of switch-off of a 300 MVA power transformer (400 kV / 110 kV) situated in the substation Okroglo. The switch-off appears in the time interval between 0.04 s and 0.12 s. Figure 2 shows time dependent RMS values for line L1 voltage on 0.4 kV busbar in substations Cerkno, Škofja Loka, Šentjur and Celje.

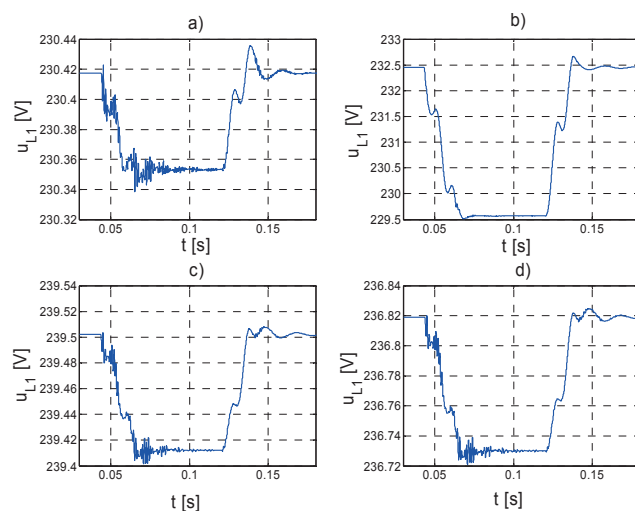


Figure 2: Voltages on 0.4 kV busbar in substations a) Cerknó, b) Škofja Loka, c) Šentjur and d) Rače, during switch-off of 300 MVA power transformer (400kV / 110 kV) in substation Okroglo.

Figure 3 shows time dependent RMS values for line L1 voltages on 0.4 kV busbar in substations Cerknó, Škofja Loka, Šentjur and Celje for the case of a three-phase short circuit on 20 kV busbar in the substation Rogaška Slatina. Again, the short circuit appears in the time interval between 0.04 s and 0.12 s.

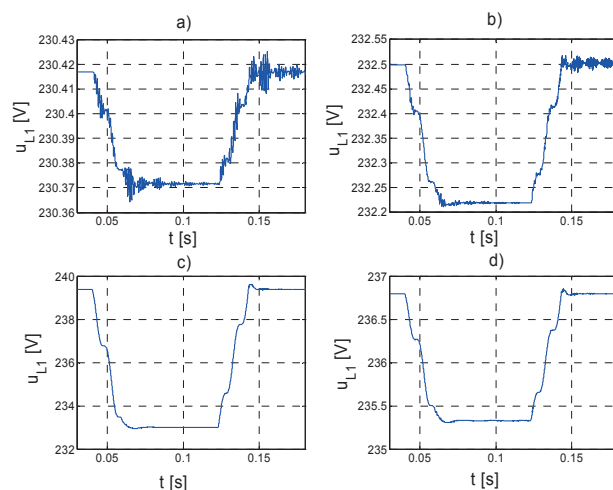


Figure 3: Voltages on 0.4 kV busbar in substations a) Cerknó, b) Škofja Loka, c) Šentjur and d) Rače, for the case of a three-phase short circuit on 20 kV busbar in the substation Rogaška Slatina.

Results presented in Figures 4 and 5 show the impact of pump-turbine plants Kozjak and Avče during their switch-on in the pumping regime. The pump-turbine plant Kozjak is at present at the design stage. It will be build above the Drava valley. The pump-turbine plant Avče is under construction close to the Soča valley. Both pump-turbine plants will use so called var-speed technology to limit the pumping regime switch-on currents. In the simulations, their switch-on is considered as a switch-on of a constant load  $180+j30$  MVA for Avče and  $400+j80$  MVA for Kozjak. In both cases the switch-on appears in the time interval between 0.04 s and 0.12 s. The time dependent RMS values for line L1 voltages on 0.4 kV busbar in substations Cerknó, Škofja Loka, Šentjur and Celje are shown in Figure 4 for the pump-turbine plant Kozjak and in Figure 5 for the pump-turbine plant Avče.

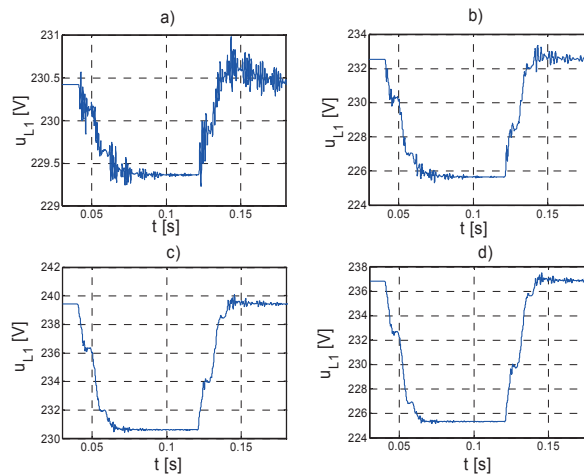


Figure 4: Voltages on 0.4 kV busbar in substations a) Cerčno, b) Škofja Loka, c) Šentjur and d) Rače, calculated for pumping regime switch-on of pump-turbine plant Kozjak.

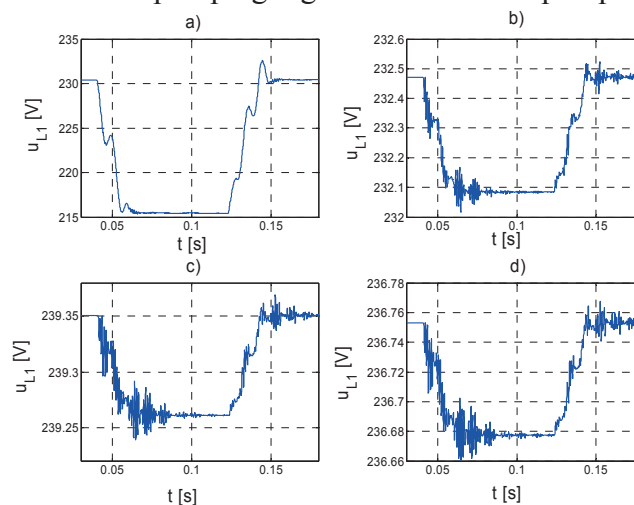


Figure 5: Voltages on 0.4 kV busbar in substations a) Cerčno, b) Škofja Loka, c) Šentjur and d) Rače, calculated for pumping regime switch-on of pump-turbine plant Kozjak.

## 5. CONCLUSION

A simplified dynamic of Slovene power system is presented in this paper. The proposed dynamic model is appropriate for study of electromagnetic transients in the power system. It is applied to evaluate the impact of different events in the power system on power quality in 0.4 kV distribution networks. The results presented show that the impact of some events presented in this paper on power quality in distribution networks is much higher than it is allowed by the national power quality standard.

## BIBLIOGRAPHY

- [1] EN 50160: Voltage characteristics of electricity supplied by public distribution systems.
- [2] IEEE 1564: Voltage Sag Indices
- [3] M. Tesarova, P. Hejtmankova, E. Dvorsky: Voltage sag site indices, Power Engineering Conference, UM-FERI, Maribor, Slovenia, 2003.
- [4] N. Watson, J. Arrillaga, Power system electromagnetic simulation, IEE, 2003.



## 1. INTRODUCTION

Three-phase tripping of a 110 kV double-circuit overhead line has been increased in a certain region, where relatively tall multi-circuit transmission towers were installed. The lightning strokes registered in this region showed a maximum stroke current of 90 kA. The high-frequency measurement of the tower footing resistance with a 26 kHz measuring current has revealed that the resistance value is relatively high at the some towers.

A back-flashover analysis should indicate which towers of that 5.2 km line route are rather prone to back-flashovers of the 110 kV insulator strings depending on different factors like tower footing resistance, tower surge impedance, tower height, etc. There are various methods published before to model lines, towers, lightning strokes and flashover mechanism over the insulators. Since measurements on real towers [1] are costly, various simulation models should be compared with each other to validate the simulation results.

The transients program EMTP-ATP [2] with the integrated simulation language MODELS is well suited to analyze lightning surge phenomenon on overhead lines as reported in numerous publications [3], [4]. Nearly all system components can be represented by built-in elements in EMTP-ATP like overhead lines with phase and ground wires and towers [5]. The flashover criteria or sophisticated representation of tower footing resistance and lightning stroke current can be modelled preferably using MODELS or TACS.

A measure to prevent back-flashovers is to apply line surge arresters. The protective level of the surge arrester for lightning strokes should be selected such that the limiting voltage of the surge arrester is smaller than the flashover voltage of the insulator. Furthermore, it is important to equip a series of towers with surge arresters without leaving out a tower in-between. Otherwise back-flashover at that tower without surge arresters may be expected due to discharging of surge arresters at the adjacent tower.

## 2. MODELING METHOD

The modelling method for the back-flashover analysis used in this paper is based upon various publications on this field [3], [6 – 9].

### 1.1. Towers

The height of multi-circuit towers varies in the range of 55 ... 88 m. The tower structure also varies from tower to tower along the 5.2 km route. The layout of a typical suspension tower is shown in Fig. 1. The distances are given in meters. The upper two cross-arms carry at left and right side a 220 kV and 380 kV single-circuit line, respectively. A 110-kV double-circuit line is suspended from the lowest cross-arm.

The tower is represented by loss-less *Constant-Parameter Distributed Line* (CPDL) model [2]. The propagation velocity of a travelling wave along a tower is taken to be equal to the light velocity,  $c = 300 \text{ m}/\mu\text{s}$  [3], [8]. The tower

travelling time is  $\tau_t = \frac{h}{c}$ .  $h$  is the tower height.

There are several formulas to calculate the surge impedance of the tower [3], [8]-[10]. As a basis, the formula

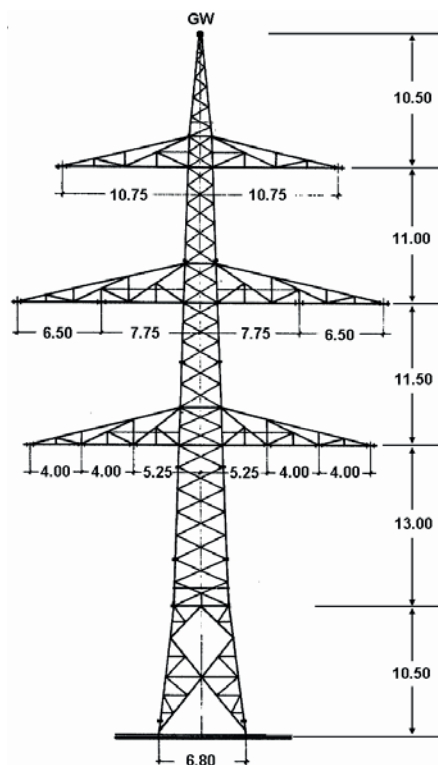


Fig. 1: Layout of a typical multi-circuit suspension tower

given in [10] for “waisted tower shape” (Fig. 2) and recommended by IEEE and CIGRE [8] is used:

$$Z_{t-waist} = 60 \cdot \ln \left[ \cot \left\{ 0.5 \cdot \tan^{-1} \left( \frac{R}{h} \right) \right\} \right] \quad (1)$$

where  $R = \frac{r_1 h_2 + r_2 h + r_3 h_1}{h}$  and  $h = h_1 + h_2$

For a tower of 76.5-m height the equation (1) delivers following value:

$$Z_{t-waist} = 233.3 \Omega .$$

It is recommended in Japan [3] to consider frequency-dependent effects for wave propagation along towers, when the tower footing impedance is represented by a linear resistance, which is the case in this study, because the influence of the surge impedance and the frequency-dependent effect of a travelling wave along the tower becomes rather noticeable. As an alternative, the tower model consisting of CPDL model sections is added by  $RL$  parallel circuits at each section to represent travelling wave attenuation and distortion as shown in Fig. 3.

The  $RL$  values are determined as functions of surge impedance  $Z_t$ , travelling time  $\tau_t$ , distances between cross-arms  $x_1, x_2, x_3, x_4$ , and attenuation factor,  $\alpha = 0.89$  as recommended in [3] by following equations:

$$R_i = \frac{x_i}{h} \cdot 2Z_t \cdot \ln \left( \frac{1}{\alpha} \right) \quad (2)$$

$$L_i = 2\tau_t \cdot R_i \quad (3)$$

### 1.2. Number of Modelled Towers

Total 19 towers of a part of a line route shown in Fig. 4 are represented including all overhead line circuits. Direct lightning strokes to towers between tower #1 and #12 are analyzed.

### 1.3. Transmission Lines

All overhead lines at the same tower are represented by the CPDL model at  $f = 400$  kHz. The ground wire is represented like a phase wire, which is connected to the top of the towers (see Fig. 1). Data of the conductors are:

- 380 kV: 4 conductors/phase, ACSR 265/35 Al/St
- 220 kV: 4 conductors/phase, ACSR 265/35 Al/St
- 110 kV: 1 conductor/phase, ACSR 265/35 Al/St
- ground wire: AY/AW 216/33 (aerial cable)

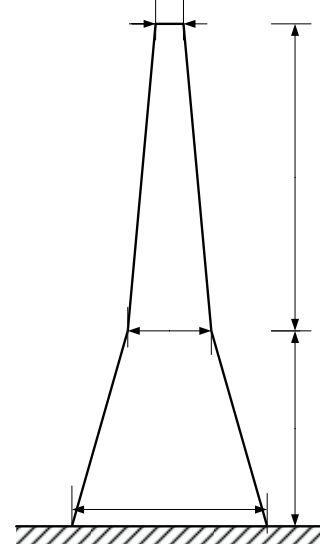


Fig. 2: Waisted tower shape as approximation to calculate tower surge impedance

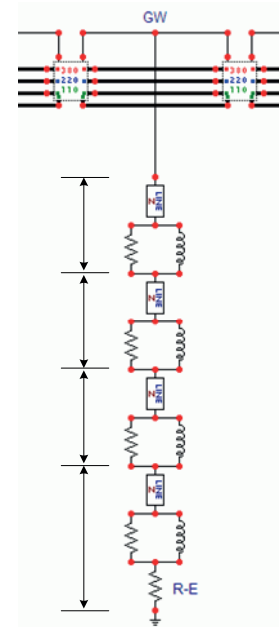


Fig. 3: Tower model with  $RL$ -circuits

In order to take into account the effect of the AC steady-state voltage of the lines on a lightning surge, the transmission lines are connected to AC voltage sources via multiphase matching impedance (surge impedance matrix).

#### 1.4. Lightning Current and Impedance

The lightning stroke is modeled by a current source and a parallel resistance, which represents the lightning-path impedance (Fig. 5). Lightning-path impedance is selected as 400 Ω according to [3].

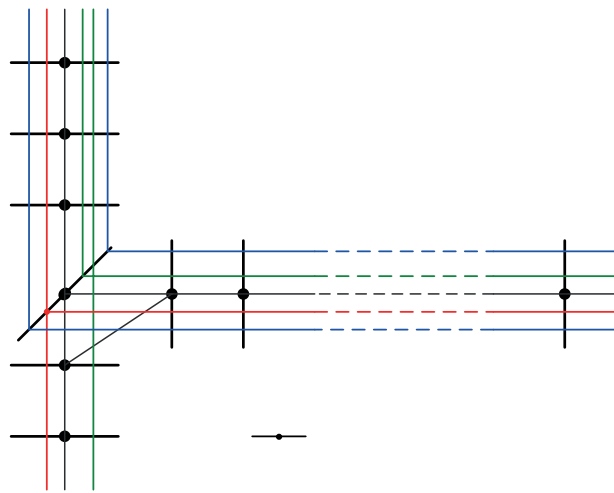


Fig. 4: Modelled part of the transmission line route

Two different lightning current waveforms are used to represent a) first stroke and b) the subsequent strokes:

- CIGRE waveform of concave shape with front time,  $T_f = 3 \mu\text{s}$  and time to half value,  $T_h = 77.5 \mu\text{s}$ .
- Linear ramp waveform with  $T_f = 1 \mu\text{s}$  and  $T_h = 30.2 \mu\text{s}$

In fact, according to [8] the front time of the first stroke depends on the peak value of the lightning current. In this study  $T_f$  and  $T_h$  are assumed to be constant. Fig. 6 shows both current waveforms with a magnitude of 50 kA.

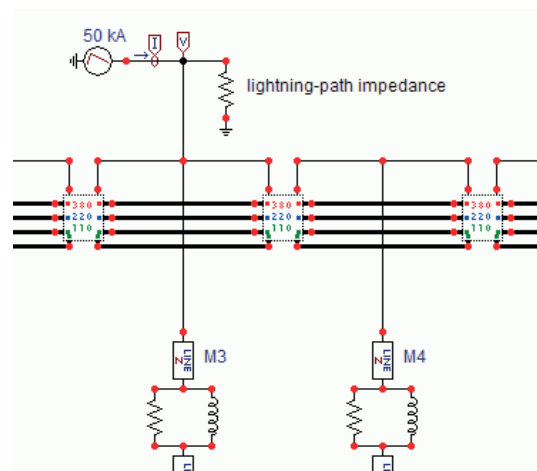


Fig. 5: Lightning stroke model consisting of current source and parallel lightning-path resistance

#### 1.5. Flashover Models

Flashover or back-flashover models estimate the breakdown of the air between the arcing horns of the line insulators under non-standard wave forms. In the literature mainly two methods are known besides the simple flashover estimation by means of a voltage-time curve of an insulator [7], [8]. There are integration methods and Leader development methods. In this study following three flashover models are applied for comparison purposes.

- Equal-area criterion by Kind [6], [8], [14];
- Leader development method by Motoyama [4], [12];
- Leader development method by Pignini et al. [8], [13].

The gap length of the 110 kV phase insulators is 0.965 m. Wave deformation due to corona is not considered in the lightning surge simulations [3]. In this paper it is assumed that the lightning stroke terminates at the tower. The surge

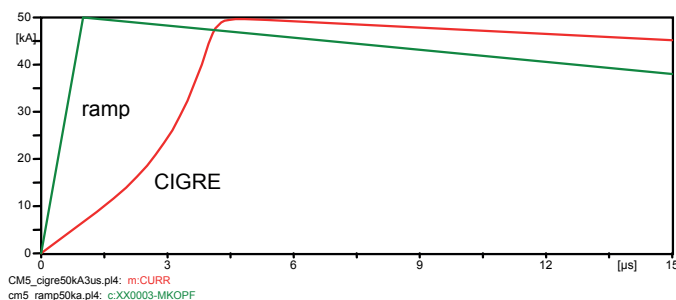


Fig. 6: Lightning current waveforms; CIGRE concave waveform, linear ramp function

propagating on the ground wire can normally be deformed by corona. Simulation results neglecting the corona are expected to be higher than considering corona. Consequently, the results will be on the safe side from the insulation viewpoint.

## 2. BACK-FLASHOVER PERFORMANCE ESTIMATION

In order to estimate roughly which towers on the route from tower #1 to #12 (Fig. 4) are endangered by back-flashovers across 110 kV insulators, the same lightning stroke is applied to each tower. Based on the equal-area criterion by Kind the time integral of the voltage across the 110 kV insulator is evaluated using the following integral on the left-side of equation (4)

$$\int_0^{t_{fo}} [u(t) - U_0] dt \geq F \quad (4)$$

where  $U_0 = 475.42$  kV and  $F = 0.304$  Vs. Following two lightning current waveforms are adopted:

- CIGRE waveform,  $I = 50$  kA;  $3 \mu\text{s}/77.5 \mu\text{s}$
- Linear ramp function,  $I = 50$  kA;  $1 \mu\text{s}/30.2 \mu\text{s}$ .

Two different tower models are taken into consideration. The simulation results are summarized in Figures 7 and 8 for the different lightning current waveforms. The horizontal red line indicates the limiting value  $F$  according to flashover criterion by Kind. Focusing on Fig. 7, it can be said that a back-flashover can occur more likely at the towers #3, #5, #8, #9 and #10. Similar tendency is shown with a steep ramp lightning current in Fig. 8.

There is a clear correlation between the flashover tendency – higher values of voltage-time integral – and the tower footing resistance, and a rather weak correlation between the flashover tendency and tower surge impedance can be observed as shown in Fig. 9.

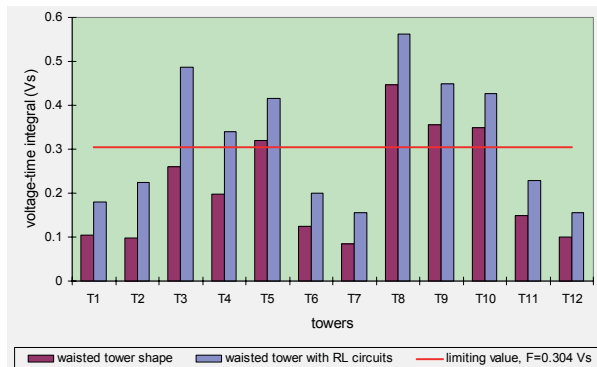


Fig. 7: Voltage-time integral values for the applied CIGRE current waveform

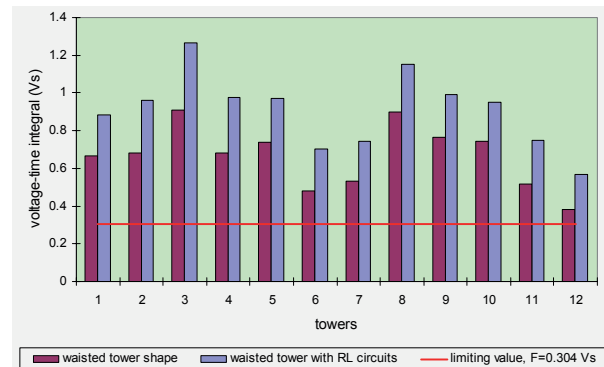


Fig. 8: Voltage-time integral values for the applied current as ramp function

As a simulation example, the computed waveforms of the voltage across the 110 kV insulator at tower #8 with flashover are shown in Fig. 10 and 11 for the three flashover models. With CIGRE lightning current waveform of magnitude 45 kA, a flashover is expected to occur according to Kind and Pignini et al. as shown in Fig. 10. Motoyama's model causes a flashover, when the magnitude of the lightning current is 50 kA (Fig. 11). Note that the voltage waveform before flashover has been deformed in the case of Motoyama, because a pre-discharge current already flows as shown in Fig. 11.

For the selected three towers #3, #7 and #8 the lightning current magnitude is varied in steps of 5 kA and several simulations have been performed. Taking the probability distribution relation for lightning crest current magnitudes according to IEEE [9]

$$p(i > I) = \frac{1}{1 + \left(\frac{I}{31 \text{ kA}}\right)^{2.6}} \quad (5)$$

into consideration, it can be said that at the mostly endangered towers #3 and #8 with an average magnitude of  $I = 35 \text{ kA}$ , 42 % of lightning strokes would cause a back-flashover across 110 kV insulator. Tower #7 has a relatively low footing resistance. Hence at this tower higher current magnitudes are required for a back-flashover. In case of CIGRE current waveform at least a 60 kA lightning stroke can cause a flashover. The corresponding probability of lightning strokes with  $I > 60 \text{ kA}$  is about 15 %.

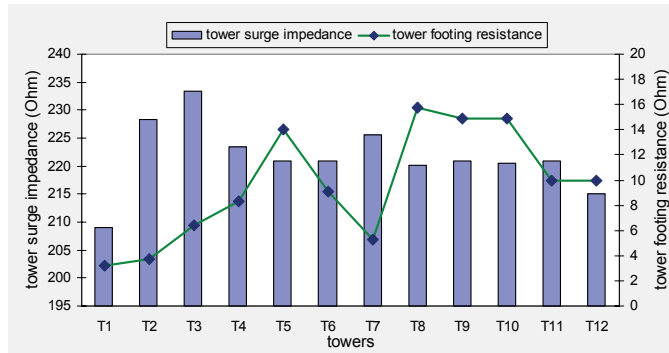


Fig. 9: Tower surge impedances and measured footing resistances

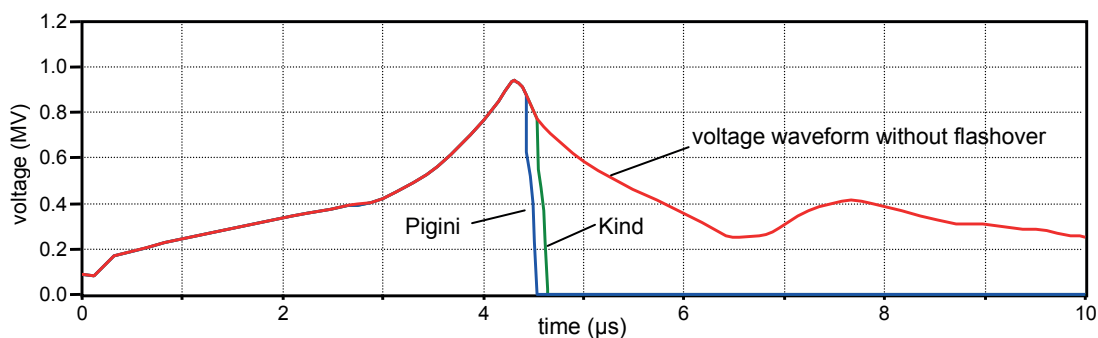


Fig. 10: Flashover across 110 kV insulator at tower #8 according to Kind's and Pignini's model

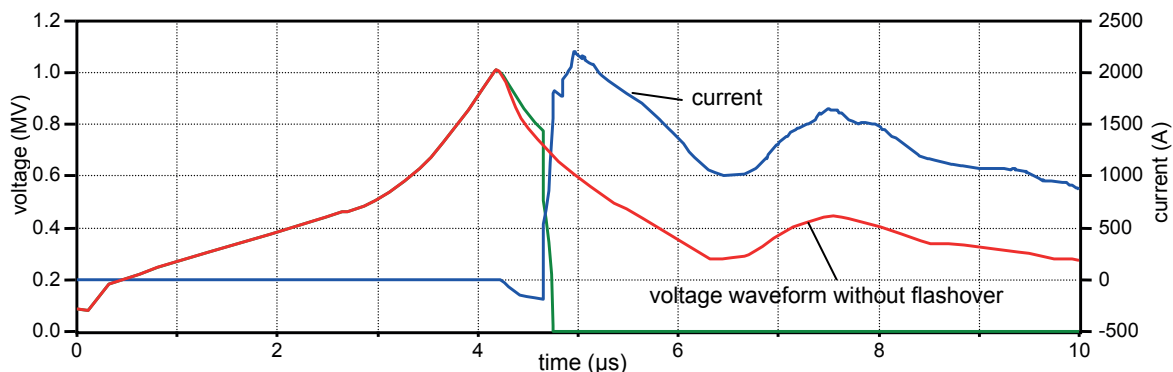


Fig. 11: Flashover across 110 kV insulator at tower #8 according to Motoyama's model

### 3. MITIGATION OF BACK-FLASHOVERS BY LINE SURGE ARRESTERS

Line surge arresters parallel to the phase insulators of 110 kV circuits can prevent back-flashovers at those towers [16]. Towers #3, #5 and #8 are selected as mostly endangered towers by back-flashovers of the 110-kV lines and are equipped with line surge arresters. The model referring to [15] of the selected surge arrester with rated voltage of 156 kV and its nonlinear voltage-current characteristic are shown in figures 12 and 13, respectively.

It can easily be checked by the Kind equal-area criterion that no flashover can occur across the insulator string parallel to the surge arrester, because the voltage across the insulator will be limited by surge arresters below  $U_0$  in equation (4) as shown in Fig. 14 for a lightning stroke with  $I = 100 \text{ kA}$ ;  $3 \mu\text{s} / 77.5 \mu\text{s}$ .

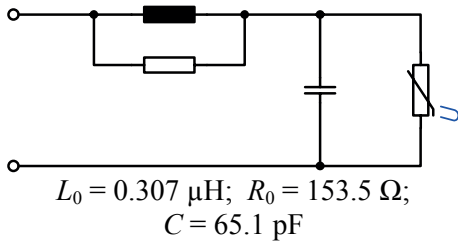


Fig. 12: Surge arrester model

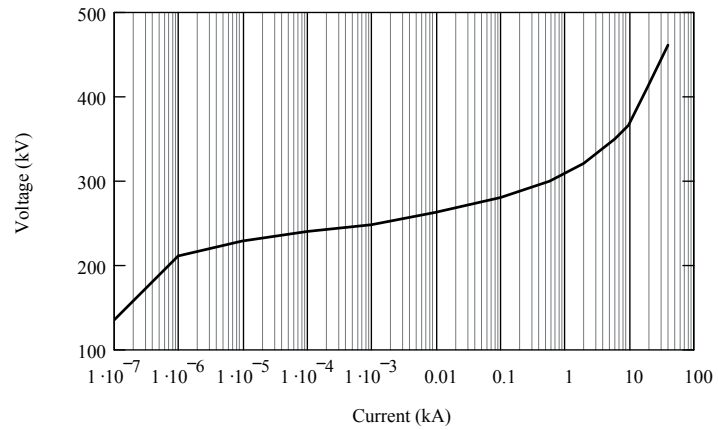


Fig. 13: Voltage-current characteristic of the surge arrester

The simulations of lightning strokes with  $I = 200 \text{ kA}; 3 \mu\text{s}/77.5 \mu\text{s}$  at the towers #3 and #8 also confirmed that no breakdown can occur across parallel insulators according to the other two flashover models by Pignini et al and Motoyama.

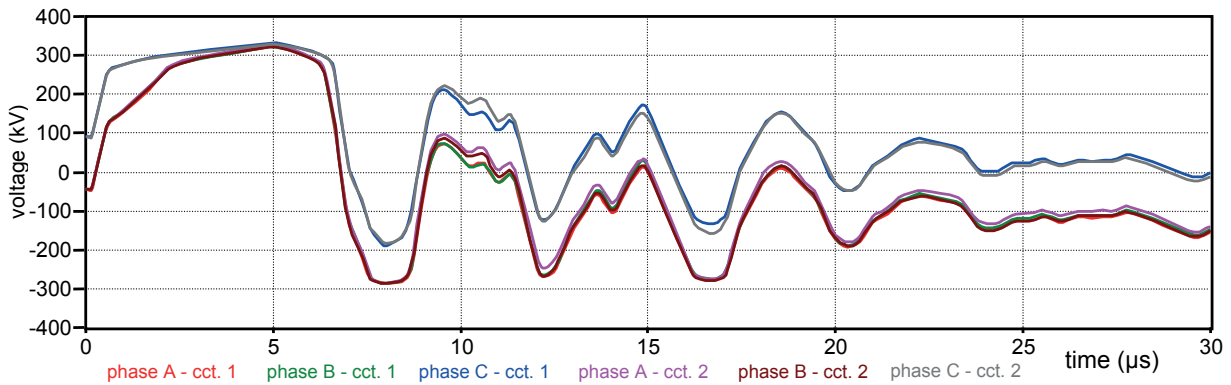


Fig. 14: Voltages across six 110 kV phase insulators at tower #3 which are limited by line surge arresters (no flashover at adjacent towers is assumed)

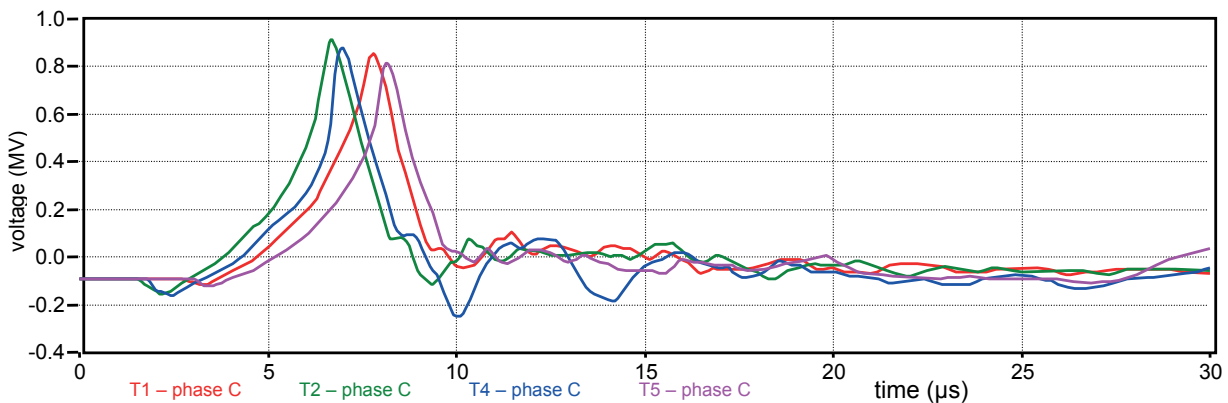


Fig. 15: Voltages between phase *c* and the tower at towers #1, #2, #4 and #5 of the 110 kV line due to discharging of line surge arresters at tower #3. No flashover at adjacent towers is assumed.

Due to discharging of the surge arresters the voltage of the 110 kV phase conductors temporarily increases significantly. Fig. 15 shows voltages between phase *c* and tower at the towers #1, #2, #4 and #5, when a lightning stroke with  $I = 100 \text{ kA}; 3 \mu\text{s}/77.5 \mu\text{s}$  hits the top of the tower #3. The operating

50-Hz voltage of phase  $c$  is at moment of the lightning stroke equal to the negative peak value ( $-90$  kV). Depending on the amplitude of the discharge current of surge arresters, a flashover may take place at other towers, which are not equipped with surge arresters. In this respect two cases have been studied: lightning stroke to towers #3 and #8, which are equipped with line surge arresters for 110 kV. Adjacent towers do not contain any line surge arresters.

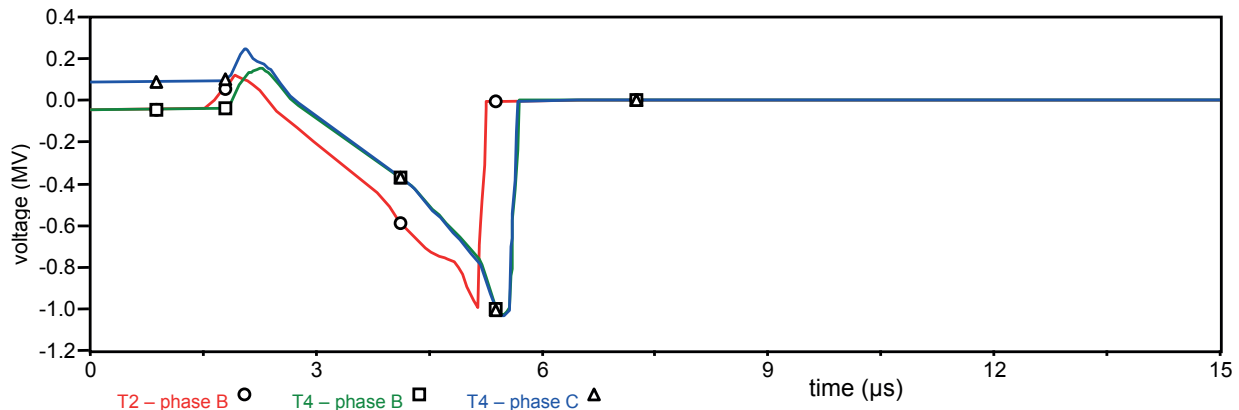


Fig. 16: Waveforms of voltages across 110-kV phase insulators with flashovers at towers #2 and #4 (It is assumed that no line surge arresters are installed at those towers)

The CIGRE current waveform with  $3/77.5$   $\mu\text{s}$  as lightning stroke is used by increasing the amplitude in 5 kA steps. The flashover condition is checked by the Kind equal-area criterion. At tower #3, when  $I > 95$  kA and at tower #8, when  $I > 90$  kA, a flashover is expected at the adjacent towers across the 110 kV phase insulators. Waveforms of the voltage across flashed-over insulators are shown in Fig. 16 for the case of lightning stroke to tower #3 with 110 kA. At tower #2 the phase  $b$  and at tower #4 the phases  $b$  and  $c$  attain flashover. Therefore the installation of line surge arresters at the towers #1 - #5 and #8 - #10 is recommended to avoid flashovers when adjacent towers are hit by strokes in the range of 90 kA.

An important question is, how well the surge arresters will perform in terms of energy absorption. A lightning stroke with  $I = 200$  kA;  $3 \mu\text{s}/77.5 \mu\text{s}$  is applied as worst-case to the top of towers #3 and #8. It is assumed that no line arresters are installed at adjacent towers. Consequently, flashover takes place in all phases of the 110-kV double-circuit line at adjacent towers. Maximum energy absorption computed is 34 kJ, which is uncritical.

#### 4. CONCLUSION

A flashover analysis has been performed for a 110 kV double-circuit overhead line, which is a part of a multi-circuit transmission route. The towers at which back-flashover is more likely than at others are identified in order to take countermeasures like installation of line surge arresters at those towers.

Multi-circuit tower system is modeled with the graphical preprocessor *ATPDraw* and the simulations are performed using *EMTP-ATP*. Three back-flashover models are used to test the performance of line surge arresters, which can be successfully used to prevent back-flashovers at endangered towers. It is shown that for lightning stroke current amplitude from 90 kA upwards flashover occurs at the adjacent towers, when the phase conductors at those towers are not equipped with surge arresters due to discharge current of stressed surge arresters. Energy absorption of the selected 110 kV line arresters remains uncritical.

## BIBLIOGRAPHY

- [1] Yamada, T.; Mochizuki, A.; Sawada, J.; Zaima, E.; Kawamura, T.; Ametani, A.; Ishii, M.; Kato, S.: “Experimental Evaluation of a UHV Tower Model for Lightning Surge Analysis”, IEEE Trans. on Power Delivery, Vol. 10, No. 1, pp. 393-402, Jan 1995.
- [2] Canadian/American EMTP User Group: *ATP Rule Book*, distributed by the European EMTP-ATP Users Group Association, 2005.
- [3] Ametani, A.; Kawamura, T.: “A Method of a Lightning Surge Analysis Recommended in Japan Using EMTP”, IEEE Trans. on Power Delivery, Vol. 20, No. 2, pp. 867-875, April 2005.
- [4] Mozumi, T.; Baba, Y.; Ishii, M.; Nagaoka, N.; Ametani, A.: “Numerical Electromagnetic Field Analysis of Archorn Voltages During a Back-Flashover on a 500-kV Twin-Circuit Line”, IEEE Trans. on Power Delivery, Vol. 18, No. 1, pp. 207-213, Jan. 2003.
- [5] Dommel, H. W.: *EMTP Theory Book*, Bonneville Power Administration, conversion into electronic format by Can/Am EMTP User Group in 1995.
- [6] Schmitt, H.; Winter, W.: “Simulation of Lightning Overvoltages in Electrical Power Systems”, Proceedings IPST 2001 (International Conference on Power System Transients), Rio de Janeiro, June 24-28, 2001.
- [7] IEEE Fast Front Transients Task Force, Modeling and Analysis of System Transients Working Group: “Modeling Guidelines for Fast Front Transients”, IEEE Trans. on Power Delivery, Vol. 11, No. 1, pp. 493-506, Jan. 1996.
- [8] CIGRE WG 33-01: “Guide to Procedures for Estimating the Lightning Performance of Transmission Lines”, Technical Brochure, October 1991.
- [9] IEEE Working Group on Lightning Performance of Transmission Lines: “A Simplified Method for Estimating Lightning Performance of Transmission Lines”, IEEE Trans. on Power App. & Systems, Vol. PAS-104, No. 4, pp. 919-927, April 1985.
- [10] Chisholm, W. A.; Chow, Y. L.; Srivastava, K. D.: “Travel Time of Transmission Towers”, IEEE Trans. on Power App. and Systems, Vol. PAS-104, No. 10, S. 2922-2928, Oktober 1985.
- [11] IEEE Working Group on Estimating the Lightning Performance of Transmission Lines: “IEEE Working Group Report – Estimating Lightning Performance of Transmission Lines II – Updates to Analytical Models”, IEEE Trans. on Power Delivery, Vol. 8, No. 3, pp. 1254-1267, July 1993.
- [12] Motoyama, H.: “Experimental study and analysis of breakdown characteristics of long air gaps with short tail lightning impulse”, IEEE Trans. on Power Delivery, Vol. 11, No. 2, pp. 972-979, April 1996.
- [13] Pignini, A.; Rizzi, G.; Garbagnati, E.; Porrino, A.; Baldo, G.; Pesavento, G.: “Performance of large air gaps under lightning overvoltages: Experimental study and analysis of accuracy of predetermination methods”, IEEE Trans. on Power Delivery, Vol. 4, No. 2, pp. 1379-1392, April 1989.
- [14] Fernandes, M.; Correia de Barros, M. T.; Ameida, M.E.: “Statistical Study of the Lightning Overvoltages at a Gas Insulated Station Transformer”, Proceedings IPST 1995 (International Conference on Power System Transients), Lisbon, 3-7 September 1995.
- [15] IEEE Working Group 3.4.11-Surge Protective Devices Committee: “Modeling of Metal Oxide Surge Arresters”, IEEE Trans. on Power Delivery, Vol. 7, No. 1, pp. 302-309, Januar 1992.
- [16] Tarasiewicz, E. J.; Rimmer, F.; Morched, A. S.: “Transmission Line Arrester Energy, Cost, and Risk of Failure Analysis for Partially Shielded Transmission Lines”, IEEE Trans. on Power Delivery, Vol. 15, No. 3, pp. 919-924, July 2000.

## Influence of the Secondary Arc on the Operation of Single Phase Auto-reclosure of the 400 kV interconnection between Hungary and Croatia

L. PRIKLER, G. BÁN<sup>1</sup> M. KIZILCAY<sup>2</sup> G. TARI, A. TOMBOR, J. ZERENYI<sup>3</sup>

<sup>1</sup>Budapest University of Technology and Economics, Hungary

<sup>2</sup>University of Siegen, Germany

<sup>3</sup>MAVIR Hungarian Transmission System Operator Company Ltd., Hungary

### SUMMARY

Faults on EHV lines are generally single-phase-to-ground ones and not permanent in the majority of cases. Thus single phase auto reclosure (SPAR), at which the faulty phases are tripped for a short time, eliminates the predominant part of the faults [1,2]. The secondary arc, which follows the high power arc after tripping the faulty phases at both side of the line may endanger the successfulness of reclosing if the duration of the switched off interval (dead time) is not long enough to ensure the extinction of the arc. The secondary arcing times recorded on different EHV lines or measured in laboratory tests show significant spread, consequently, to select a dead time according to the longest experimental secondary arc extinction time is not feasible.

During commissioning of the double circuit 420 kV interconnection between Hungary and Croatia several staged faults were initiated to analyze the arc extinction performance. Initially the line was in operation by connecting the two circuits in parallel along the 1/3<sup>rd</sup> of the full length. In this configuration the longest secondary arc extinction time was 4 seconds and the secondary arc has not extinguished in 27s in one of the tests, so the line had to be tripped out to clear the staged fault. Later on, the length of the Croatian section of the line has been significantly shortened after putting a new substation into service. The increased performance of SPAR of the new arrangement has been proved with field tests.

A realistic representation of the secondary arcs is essential in determining the auto-reclosure performance of EHV transmission lines. As shown in the paper, the random variation of the arc parameters influences significantly the arc extinction time. The results of the field tests confirmed the importance of the distributed nature of the transmission line and the nonlinear characteristic of the arc resistance in the intermittent region of arcing, where temporary extinctions and sudden re-ignitions in the arc channel produce transient wave processes along the line.

### KEYWORDS

Line fault, secondary arc, reclosing, simulation, measurement, EMTP-ATP.

prikler@vmt.bme.hu

## 1 INTRODUCTION

To find a new right-of-way is rather difficult today. Using compact tower construction and upgrading existing lines offer a possibility to overcome these constraints. However reducing the phase-to-phase clearances has a strong impact on the lightning and switching performance of the line. The increasing number of faults contradicts another key expectation of the public today: the *quality of supply*. These conditions emphasize the importance of reclosing efficiency, which may compensate the less favourable lightning performance of compact line designs of reduced insulation clearances [3,4,5,6].

The successfulness of SPAR is endangered by long duration secondary arcs and reclosing overvoltages that can re-ignite the arc at the place of the fault. Single or three-phase reclosure produces high switching overvoltages and the heaviest stresses in line insulation. These overvoltages may endanger in particular those lines running in polluted areas or operating in foggy zones. Contamination usually extends to a large area, and it can be presumed that an intensive partial arc activity is going along the surface of many line insulators. The fault occurs when one of them flashes over by the normal operating voltage stress. As a rule, the heating effect of the primary arc dries out the faulted insulator, but a high reclosing overvoltage is able to initiate partial arcs on some other insulators. The temporary overvoltage and the normal operating voltage which follows the reclosing transient may then sustain and elongate the partial arcs further till a full flashover occurs.

Increasing number of unsuccessful reclosing can be observed especially at winter period in operation of the Hungarian HV and EHV lines. Table 1. shows aggregated data for a 4-year period. The ratio of the unsuccessful reclosing to the total ones is 0.26 in summer and 0.53 in winter. Transmission line faults originate mainly from lightning in summer and predominantly from foggy weather in winter. Considering that the ratio of unsuccessful/total reclosing is twice as high in winter as in summer, a significant limitation of the reclosing overvoltages is recommended for the lines containing polluted or foggy sections to keep the line operating performance high.

**Table 1:** Number of reclosings on the Hungarian HV/EHV lines within a 4-years period.

Voltage level	Summer		Winter		Line length (km)
	successful	unsuccessful	successful	unsuccessful	
750 kV	5	0	1	2	479
400 kV	48	20	28	9	1530
220 kV	83	28	23	47	1687
$\Sigma$	136	48	52	58	3696

## 2 SECONDARY ARC AND RECLOSING EFFECTIVENESS

The fault arc can be classified according to the fault state: *primary arc* is effective after fault inception till single-phase tripping of the faulty phase. The *secondary arc* follows the primary arc in the ionized, hot plasma channel after isolating the fault by single-phase tripping and is sustained by the capacitive and inductive coupling to the sound phases. The secondary arc self-extinguishes usually, but its lifetime may have a strong influence to the reliability of the operation of the line. On the one hand a non self-extinguishing secondary arc endangers the efficiency of the single-phase reclosing; on the other hand prolonging the dead time (switched-off interval of the faulty phase) is limited by dynamic stability constraints. This limit is usually less than 1.5 - 2 seconds for a long EHV/UHV interconnection. Considering that line faults are mostly non-permanent ones, a significant percentage of them can be cleared by single-phase auto-reclosure. In particular for compact lines with reduced clearances the smaller phase-to-phase clearances make the capacitive coupling between conductors more substantial, which may result in higher secondary arc currents and longer arcing times.

### 3 EXPERIMENTAL DATA ABOUT SECONDARY ARC EXTINCTION TIMES

The secondary arcing times recorded on real lines and laboratory tests show a significant spread [1,14]. This spread can be explained by the extremely random character of the arc formation and the strong influence of many parameters (wind velocity, the movement of the hot plasma generated by the primary arc, magnetic force due to the current, convection of the plasma cloud and surrounding air, presence and degree of shunt compensation –if exists-, etc.) to the arcing time.

#### 3.1 Staged fault tests on the 400 kV double-circuit interconnection between Croatia and Hungary

As part of commissioning of the new interconnection, the secondary arc extinction parameters have been checked by initiating staged faults with and w/o primary arc in different meteorological conditions at both end of the line. The one-line schema of the corresponding 400 kV network is given in Fig. 1. Initially, the operating length of the line was 230 km without shunt compensation, connecting Heviz 400/132 kV and Tumbri 400/110 kV substations in Hungary and Croatia, respectively. Currently, the line connects Heviz and Žerjavinec 400/220/110 kV substations. At the beginning of operation the interconnection has been operated by connecting the two circuits in parallel along the 1/3<sup>rd</sup> of the full length to reduce transmission losses. The remaining sections of the second circuit had been operated then at 220 kV or were grounded. Seven staged faults have been carried out, aiming to predict the secondary arcing times. The measuring arrangement and the length of the faulty phases are shown in Fig. 2. The location of the staged fault is indicated by a grounding symbol.



Fig. 1 – Overview of the 400 kV interconnection between Hungary and Croatia

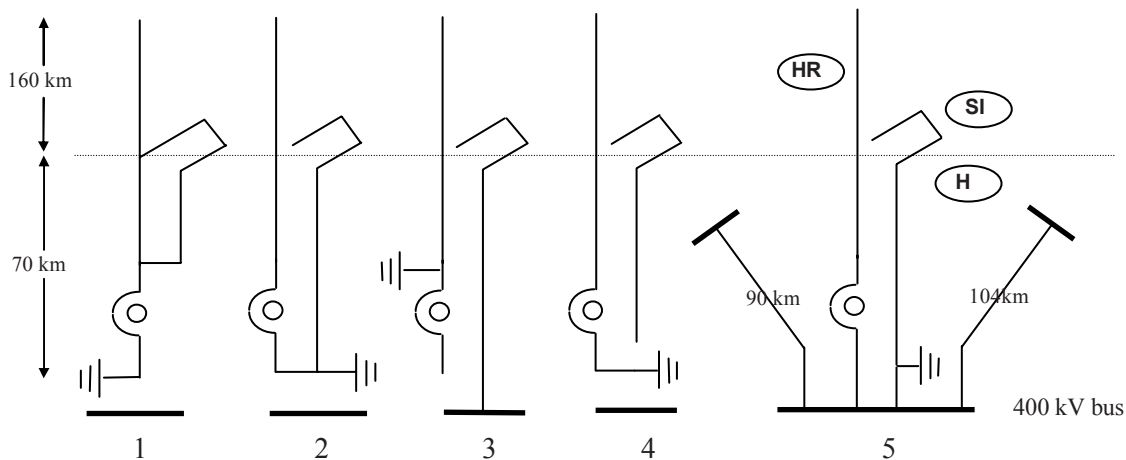


Fig. 2 – Measuring arrangements at fault tests. 1-4 fault w/o primary arc, 5 with primary arc.

In majority of tests the arc has been initiated by a thin wire connecting the phase conductor of an already isolated phase to the substation ground or to metallic structure of transmission line tower, i.e, the primary arc has been omitted in these tests. According to [14] such an arc ignition technique provides comparable results to tests with primary arc if the expected secondary arcing time exceeds 700 ms because the plasma cloud of the primary arc certainly has strong influence to quickly extinguishing secondary arc. However such a self-extinguishing short duration arc does not endanger the SPAR successfulness.

### 3.2 Test results

The shortest arc extinction time was 0.05 s and the longest one was 4 s during the tests. The secondary arc did not extinguish during 27 s at one of the tests. 4 s and 27 s extinction times have been measured in arrangement “1” of Fig. 2 where the fault was created inside the substation at calmness. As Fig. 3 shows, at calmness no significant arc channel elongation is seen. Ions generated during the intermittent arc interval remain in the environment of the arc. These circumstances make the self-extinction time very long. The secondary arcing times recorded at moderate (3 - 4 m/s) wind velocities were in the range of 0.05 s – 0.69 s. As Fig. 3/d shows the elongation of the arc is slow and many loops occur in the arc channel due to the electromagnetic forces. The big spread of the extinction times and very long arcing times experienced in two cases correspond to the data about extinction times published in former papers containing generalized diagrams [1].

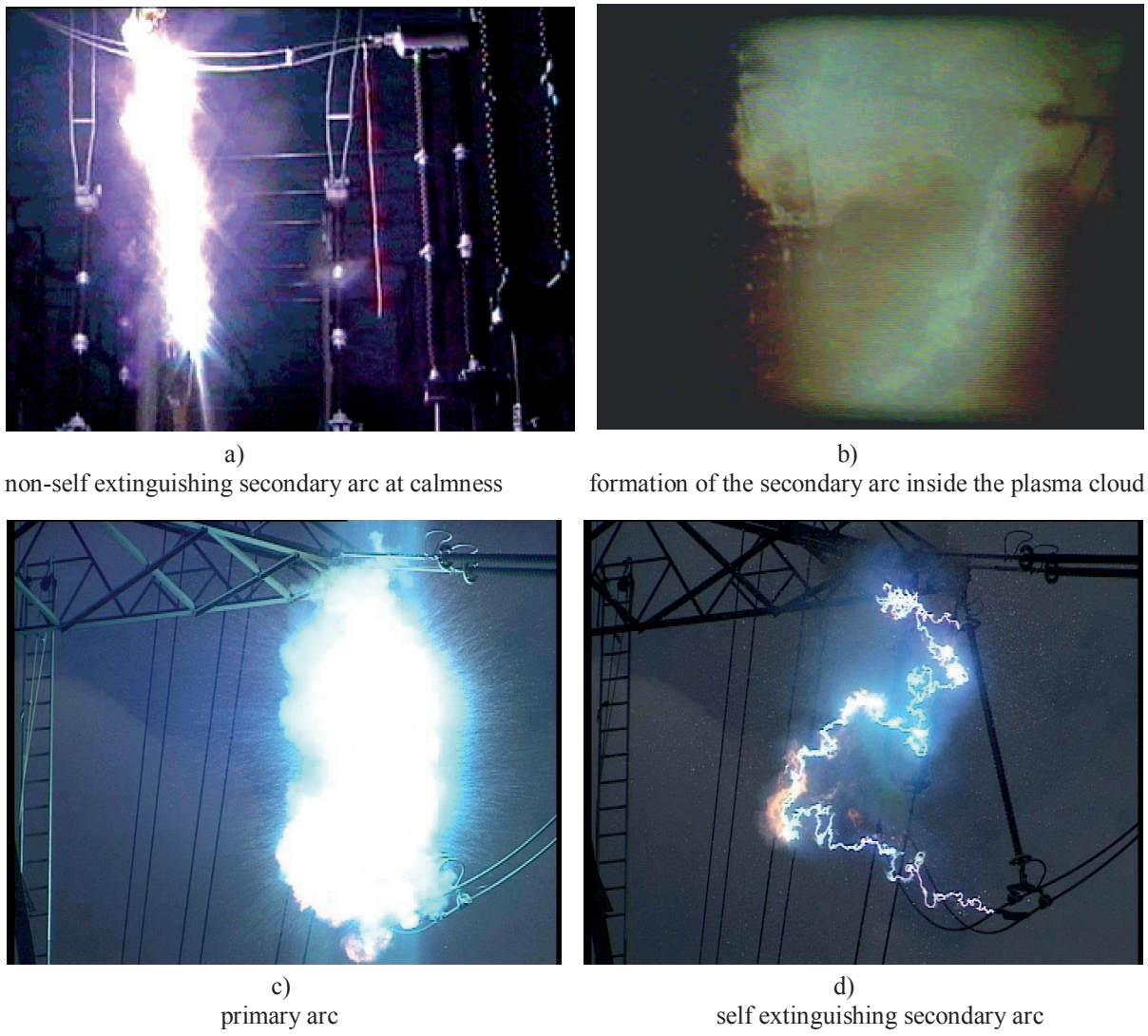


Fig. 3 - Pictures taken at the staged fault tests.

### 3.3 Secondary arc extinction

The main condition of the spontaneous extinction of the secondary arc is a strong air movement, which makes the arc to elongate quickly. The hot plasma generated by the primary arc moves upward with a high velocity, resulting in an initial vertical component for the secondary arc elongation (Fig. 3/b/d). Wind has the same effect on the secondary arc.

The elongation of the secondary arc causes a linear increase of arc voltage. If the arc elongation is rather smooth without steep rise then the secondary arc extinguishes as the arc voltage reaches the magnitude of recovery voltage [7]. A steep rise of arc length can be caused by a gust of wind. In that case the arc may extinguish sooner. Consequently, the arc duration may be estimated by the elongation speed of the arc.

Besides the arc elongation, re-ignitions inside the arc channel may have a significant role in the process. The speedy elongation of the arc separates the conducting plasma clouds by high resistance channel zones. When number of high resistance zones increases, the amplitude of the operating frequency component of the current decreases and high amplitude impulses occur as a consequence of the growing re-ignition voltage. If the recovery voltage is sufficient to produce a breakdown bridging these high resistance zones, the arcing process may return to the steady-state condition, remarkably prolonging the self-extinction time as shown on Fig. 4. The final extinction of the secondary arc is very often preceded by an intermittent interval, when high current impulses are superimposed on the low amplitude operating frequency component of the current. As can be seen on Fig. 4 the amplitude of these impulses is much higher than the peak value of the steady-state current.

The sudden re-ignitions in the arc channel initiate electromagnetic wave phenomena along the line. The length of the current impulses depends on the place of the fault. For the predominant part of the fault displacement, the duration of these impulses is twice of the line travel time. The superposition of the reflected waves produces a current zero in the arc channel resulting in partial arc extinction. The amplitude of these current impulses are sufficiently high to re-ionize a large amount of plasma, resulting in a fallback into the quasi-sinusoidal phase of the arcing process which elongates the secondary arc duration.

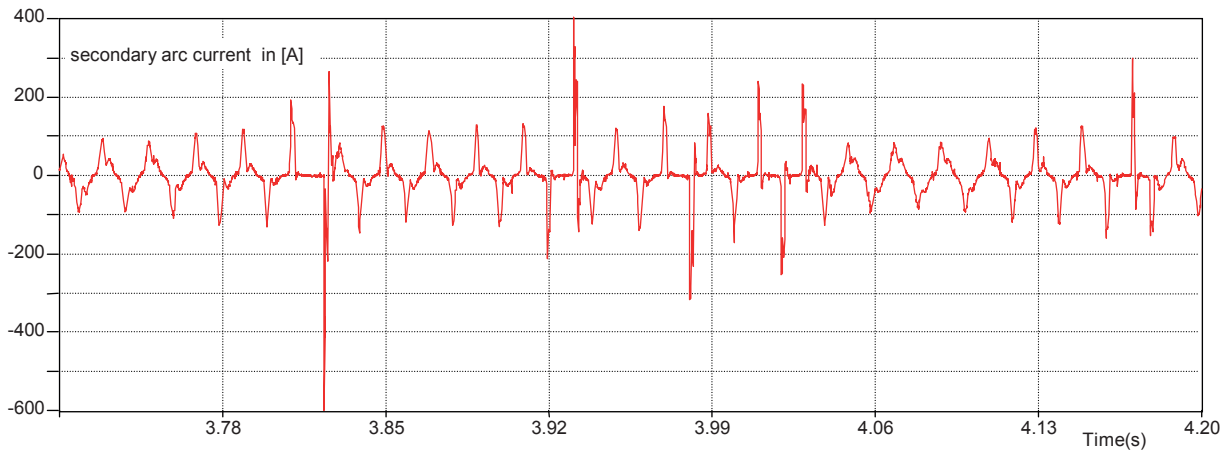


Fig. 4 - Secondary arc current (measurement).

## 4 EMTP-ATP MODEL OF THE 400 KV INTERCONNECTION

The ATP-EMTP model of the interconnection has been assembled by using ATPDraw graphical preprocessor [16]. The model has been elaborated to prove the main characteristics of the recorded signals at the staged fault test. Initially the model corresponded to the measuring arrangement "case 5" of Fig. 2. Later the model has been improved by completing it with an arc model based on

identification of arc parameters [17, 18]. And finally, after commissioning Žerjavinec substation, the model has been further improved to take into consideration the new arrangement of the line and to represent the supply network configuration and influence of the magnetic voltage transformers at both end of the line in more detail. The complete model is shown on Fig. 5.

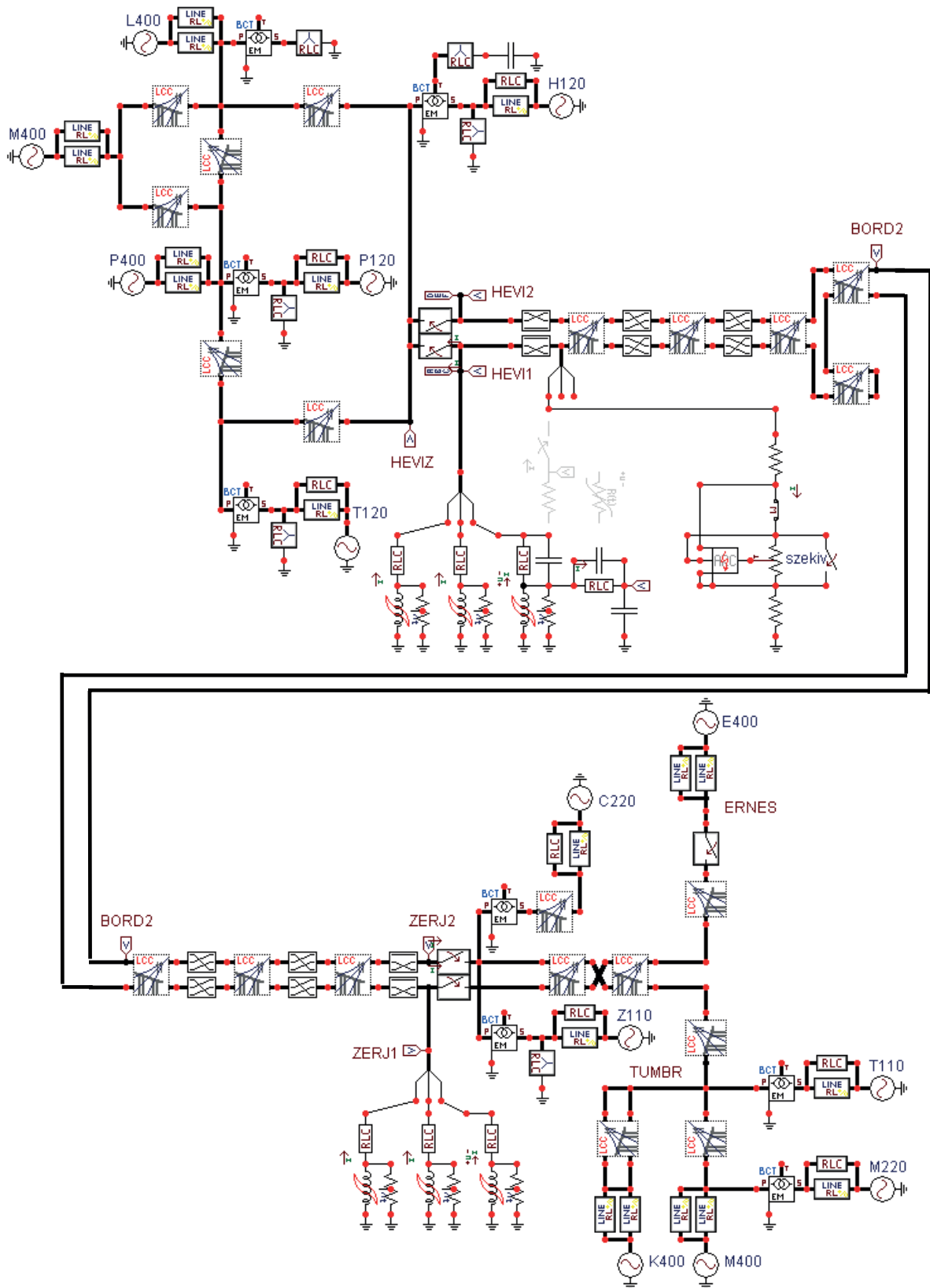


Fig.5 – EMTP simulation of the Heviz - Žerjavinec 400 kV interconnection.

#### 4.1 Fault arc modelling

Whereas the primary arc shows generally a deterministic behavior as observed at field and laboratory tests [7, 8, 9, 10, 11], the secondary arc has extremely random characteristics effected by the external conditions around the arc channel like ionized surrounding air, wind, thermal buoyancy and electrodynamic forces. A numerical arc model may be a useful tool to identify the main influencing factors and the interaction of the arc with the electric circuit, and to estimate the worst-case arcing time.

The arc model used in this work is based on the energy balance of the arc column and describes an arc in open air by a differential equation of the arc conductance  $g$  [7, 15, 17]:

$$\frac{dg}{dt} = \frac{1}{\tau}(G - g) \quad (1)$$

where  $\tau$ : is the arc time constant,  $g$ : instantaneous arc conductance,  
 $G$ : stationary arc conductance.

The stationary arc conductance is defined as:

$$G = \frac{|i_{arc}|}{u_{st}} \quad \text{with} \quad u_{st} = u_0 + r_0 |i_{arc}| \quad (2)$$

where  $i_{arc}$ : instantaneous arc current,  $u_{st}$ : stationary arc voltage,  
 $u_0$ : characteristic arc voltage,  $r_0$ : characteristic arc resistance.

Arc parameters  $u_0$  and  $r_0$  are dependent on arc length  $l_{arc}$ . The dependence of the arc time constant  $\tau$  on  $l_{arc}(t)$  can be defined by the inverse relation

$$\tau = \tau_0 \cdot \left( \frac{l_{arc}}{l_0} \right)^\alpha \quad (3)$$

where  $\tau_0$ : initial time constant,  $l_0$ : initial arc length,  $\alpha$ : coefficient of negative value.

#### 4.2 Arc representation in EMTP - ATP

The arc as a nonlinear dynamic element can be represented by the *Thevenin type*, Type-94 component in the ElectroMagnetic Transients Program EMTP-ATP [12]. The arc is described in MODELS language [13]. The interaction of the electric arc with the remaining circuit is shown in Fig. 6. The use of Type-94 component in EMTP-ATP enables simultaneous solution of arc equations together with the equivalent system of the electric network.

Since the arc parameters are expressed as functions of the instantaneous arc length, the random arc behavior can be reproduced by varying the arc length in a random way. It is physically reasonable to describe a global arc length increase – either piecewise-linear or any predefined function – superposed by a local random length variations that should imitate the local breakdowns along the elongated secondary arc.

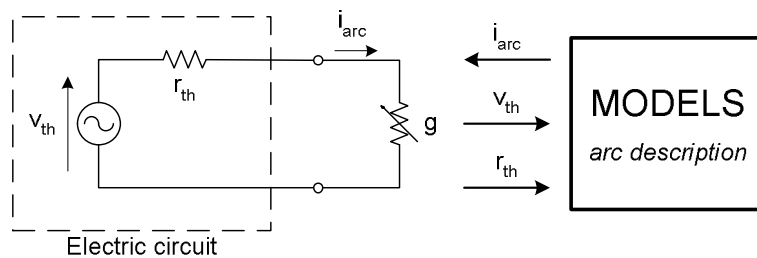


Fig. 6 - Interaction between the electric circuit and the arc model.

### 4.3 Simulation results

Measuring arrangement “5” of Fig. 2 has been selected to compare the simulation results with measurements. In this test the phase-to-ground fault has been cleared by disconnecting phase *a* of circuit breakers at the receiving end of the lines connected with the 400 kV busbar of Heviz substation.

Piece-wise linear arc length variation superimposed by a random signal has been used in the simulation [18]. Fig. 7 and 8 show the measured and computed arc voltages and currents, respectively.

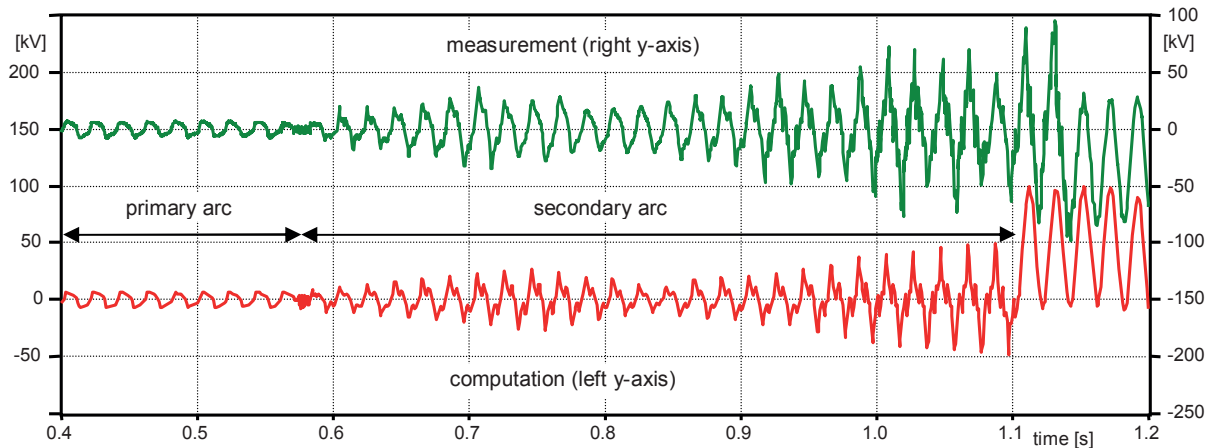


Fig. 7 - Measured and computed arc voltages.

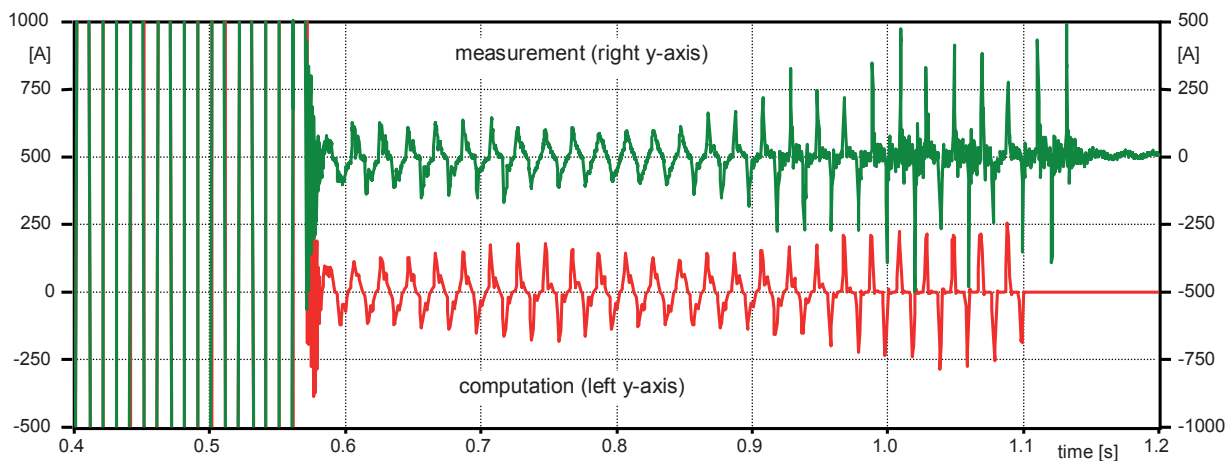


Fig. 8 - Measured and computed arc currents.

## 5 CONCLUSIONS

Secondary arcing times recorded at field tests spread to a great extent due to the differences in the wind velocities, arc initiation technique, line construction etc. Recording the wind velocity in the environment of the secondary arc and a detailed description of the way of arc initiation would reduce the spread of the experimental data.

The staged fault tests proved that the distributed nature of the transmission line plays an important role during the intermittent stage of arcing and that the final extinction of the secondary arc is often preceded by an intermittent interval, when high current impulses are superimposed on the power frequency component of the secondary arc current. The extinction time of the secondary arc is affected by the shape and amplitude of the recovery voltage arising in the transient current zeros at the place of the fault.

Due to highly random behavior of the secondary arc it is difficult to reproduce exact arc duration by digital simulations. The speed of arc elongation plays a significant role regarding arc duration and extinction. In addition the arc time constant depends inversely on arc length. The arc tends to extinguish faster as the arc time constant becomes smaller. This behavior is based on the fact that the arc is an energy storage element. In spite of these uncertainties in the modeling, the arc model can be successfully utilized to find main factors influencing the secondary arcing process.

## 6 ACKNOWLEDGEMENT

The activity reported in this paper has been partly supported by the Hungarian Research Fund under contracts OTKA T-035178 and T-046355. Authors acknowledge the contribution of the Hungarian Power Companies Ltd. to the field measurements.

## BIBLIOGRAPHY

- [1] Haubrich, H.J. et al.: "Single-Phase Auto-Reclosing in EHV Systems" CIGRE 1974, Rep. 31-09
- [2] IEEE Committee Report: "Single-Phase Tripping and Auto Reclosing of Transmission Lines ()", IEEE Trans. Power Delivery, vol. 7, No 1. pp. 182-192, January 1992
- [3] Prikler, L., Bán, G., Bánfai, G., Handl, P.: "Testing and Simulation of EHV Secondary Arcs" Proc. of the European EMTP-ATP Conference, Bristol, UK, Sept 3-5, 2001
- [4] Ban, G.: "Single-phase Reclosing EHV Trans-mission Lines" Proc. of the 17th Hungarian – Korean Seminar, EHV Technologies - II, Keszthely-Lake Balaton, Hungary, October, 2001
- [5] Ban, G., Prikler, L., Banfai, G.: "Testing EHV Secondary Arcs" IEEE Porto Power Tech'01 Conference, Porto, Portugal, Sept 9 – 13, 2001
- [6] Ban, G., Prikler, L., Banfai, G. "The Use of Neutral Reactors for Improving the Successfulness of 3-phase Reclosing" IEEE Budapest Power Tech'99 Conference, Budapest, Hungary, Aug 29 – Sept 2, 1999
- [7] Kizilcay, M., Pniok, T.: "Digital Simulation of Fault Arcs in Power Systems" ETEP Journal, vol., 1 (1991), no. 1, pp. 55-60
- [8] Kizilcay, M., Koch, K-H.: "Numerical Fault Arc Simulation based on Power Arc Tests" ETEP Journal, vol. 4 (1994), no. 3, pp. 177-186
- [9] Terzija, V.V., Wehrmann, S.: "Long Arc in Still Air: Testing, Modelling and Simulation" EEUG News, vol. 7, no. 3 (August 2001), pp.44-54
- [10] Johns, A.T., Aggarwal, R.K., Song, Y.H.: "Improved Techniques for Modeling Fault Arcs on Faulted EHV Transmission System" Proc. IEE – Generation, Transmission and Distribution, vol. 141 (1994), no. 2, pp. 148-154
- [11] Kizilcay, M.: "Evaluation of Existing Secondary Arc Models" EEUG News, vol. 3, no. 2, May 1997, pp. 49-60
- [12] Alternative Transient Program Rule Book, Can/Am EMTP User Group, USA, 1997.
- [13] Dubé, L.: "Models in ATP", Language manual, Feb. 1996
- [14] Rashkes, V.S.: "Generalization of the Operation Experiences, Connected with the Efficiency of Single-Phase Reclosing, Experimental Data about the Extinction Time of the Secondary Arc" Elektricheskije Stancii 1989. No.3 (in Russian)
- [15] Danyek, M., Handl, P.: "Improving the Reliability of Experimental Data about Secondary Arc Duration" Proc. of the 17th Hungarian – Korean Seminar, EHV Technologies - II, Keszthely-Lake Balaton, Hungary, October, 2001
- [16] Prikler, L., Høidalen, H-K.: ATPDraw version 3.5 for Windows9x/NT/2000/XP-User's Manual, SINTEF Energy Research AS, Norway, TR F5680, ISBN 82-594-2344-8, Aug 2002
- [17] Prikler, L., Kizilcay M., Bán G., Handl P.: "Modeling secondary arc based on identification of arc parameters from staged fault test records", Int. Journal of Electrical Power & Energy Systems, Elsevier Science (UK), Vol. 25, (2003) pp. 581-589
- [18] Kizilcay M., Bán G., Prikler L., Handl P.: "Interaction of the Secondary Arc with the Transmission System during Single-Phase Autoreclosure" IEEE Bologna PowerTech Conference, June 23-26, 2003 Bologna, Italy, Paper 471

## Detailed Transients Simulation of a Doubly Fed Induction Generator Wind Turbine System with the EMTP-Type OVNI Simulator

**Mažana Lukić Armstrong\***  
University of British Columbia  
Canada

**José R. Martí**

**Prabha Kundur**  
University of Toronto  
Canada

### SUMMARY

Doubly fed induction generator wind turbines are increasingly used in new wind turbine installations all over the world. Growing concerns about the impact of a large number of these generators on transient and voltage stability of power system networks has led engineers to revisit modelling and simulation practices used for system stability analyses. In this paper, the latest advancements in design of the general purpose power system simulator OVNI developed at the University of British Columbia are presented, and its application to the simulation of a doubly fed induction generator (DFIG) wind turbine system is shown. Because OVNI is based on the EMTP methodology for accurate detailed modelling, and the Multilevel MATE (Multi-Area Thévenin Equivalent) concept, which, combined with hardware solutions, allows for fast simulation of large power system networks, it represents an ideal tool for testing and developing benchmark models of different wind turbine installations. Using the EMTP approach for modelling of a DFIG wind turbine system and its feeding power network we were able to study the responses of the wind turbine generator to different network events. The ultimate goal of our investigations is the development of a benchmarking process for testing different models of wind turbine generators and determining the range of validity of various degrees of approximations normally used for stability simulation purposes. Due to the rapid development of wind generation technology, it is essential to determine the minimum requirements for dynamic modeling of wind turbine generators for assessing impacts of their installations on the dynamic security and stability of power systems.

### KEYWORDS

power systems – EMTP – modelling – simulations – stability – wind turbine generators (WTG) – doubly fed induction generator (DFIG)

\*mazanal@ece.ubc.ca

## 1. INTRODUCTION

The Object Virtual Network Integrator (OVNI) is a simulation tool aimed at obtaining very fast, real-time solutions of power system networks [1], [2], [3]. OVNI is based on the EMTP program (Electromagnetic Transients Program) used to simulate electromagnetic transients [4]. OVNI is built around the MATE ("Multi-Area Thévenin Equivalent") network partitioning framework [1] that extends the main ideas of Diakoptics [5] by recognizing that the subsystems split by the branch links can be represented by Thévenin Equivalents. The multilevel MATE concept [6] further extends the concept of MATE and provides a computationally efficient solution framework for the inclusion of controllers and non-linear elements, as well as power system components such as phase-domain synchronous and induction machines.

The advantages of the detailed modelling and simulation of DFIG wind turbine generators (WTG) with OVNI include: (1) three-phase representation allowing for accurate simulation of balanced and unbalanced network conditions; (2) phase-domain full-detail machine modelling, including the modelling of torsional shaft oscillations; (3) simultaneous solution of the WTG control systems and network equations; (4) and phase-domain modelling of power electronic voltage source inverters. This paper will demonstrate how an experimental DFIG wind turbine system from [7] is modelled in OVNI with the full time-domain (EMTP-type) solution.

## 2. DOUBLY FED INDUCTION GENERATOR WIND TURBINES

Variable-speed turbines with doubly fed induction generators have become a new standard for wind turbines of installed capacity above 2 MW. As the ratings of such wind farms connected to the power system grid become closer to the ratings of traditional generating units, and their share in the total installed generating capacity of the power system becomes considerable, it becomes necessary to perform studies of the impact of large wind farm connections to the power system network. The main concern is to study the responses of wind farms to power system faults and their impact on overall system stability.

Variable-speed operation of the turbines is achieved through the use of power electronic converters that can also be used to improve the grid integration aspects. It is anticipated that in the future it may be possible to require specific responses of wind farms to network disturbances from the manufacturers to help in the system recovery. Detailed model parameters of converter-controlled wind turbines can only be provided by manufacturers, and these control details are usually confidential and not readily available. However, efforts are being made to create reasonably accurate general models of doubly fed induction generators that can produce realistic results of wind farm responses to system disturbances and the influence of the associated controls.

Physically, the machine of a doubly fed induction generator is a conventional wound rotor induction machine. The key distinction is that this machine is equipped with a solid-state AC excitation system. The AC excitation is supplied through an AC-DC-AC voltage converter. Doubly fed induction machines have a significantly different dynamic behaviour than conventional synchronous or induction machines. The fundamental frequency electrical dynamic performance of a doubly fed induction generator is completely dominated by the field converter. Conventional aspects of the generator's performance related to the rotor angle, excitation voltage and synchronism are largely irrelevant. The electrical behaviour of the generator and converter is that of a current-regulated voltage-source inverter. The converter makes the wind-turbine behave like a voltage behind a reactance that produces the desired active and reactive current delivered to the device terminals. A schematic of a doubly fed wind turbine system with two voltage-source inverters and accompanying controls is depicted in Figure 1.

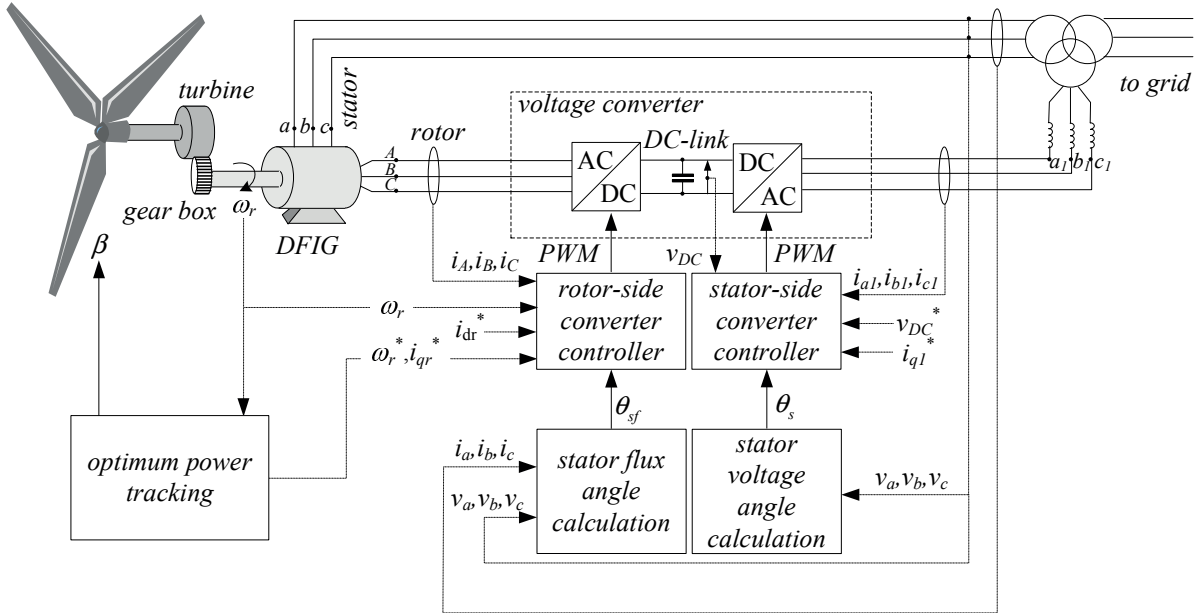


Figure 1. Schematic of a doubly fed induction generator wind turbine system

### 3. DFIG MODEL STRUCTURE

To construct a DFIG wind turbine system model, the following structure is considered:

- A doubly fed induction generator model based on a phase-domain induction machine model
- A voltage converter model based on an average model of a back-to-back PWM voltage-source inverter with stator and rotor-side converter control
- A wind model that maps the wind speed to the shaft mechanical power for the turbine
- A crowbar protection scheme
- Mechanical controls, including blade-pitch control and over/under speed trips

A doubly fed induction generator can be modelled as an induction machine in phase coordinates [8]. A phase-domain induction machine model is especially convenient for the implementation in the EMTF-type of simulators such as OVNI because it can be naturally interfaced with a three-phase network representation. The phase-domain model can be simulated more efficiently, with time steps in the order of milliseconds, than the commonly used EMTF dq0 model. The difference between a conventional induction machine and a doubly fed induction machine is that the rotor of a doubly fed induction machine is connected to the grid via a voltage converter. The electrical equations of the two machines are identical and in the general form, for discretization with the trapezoidal rule, are shown in (1):

$$\begin{bmatrix} \mathbf{e}_{abc} \\ \mathbf{e}_{ABC} \end{bmatrix} = \begin{bmatrix} \mathbf{R}_s & 0 \\ 0 & \mathbf{R}_r \end{bmatrix} + \frac{2}{\Delta t} \begin{bmatrix} \mathbf{L}_s & \mathbf{L}_{sr} \\ \mathbf{L}_{sr}^T & \mathbf{L}_r \end{bmatrix} \begin{bmatrix} \mathbf{i}_{abc} \\ \mathbf{i}_{ABC} \end{bmatrix} + \begin{bmatrix} \mathbf{e}_{habc} \\ \mathbf{e}_{hABC} \end{bmatrix} \quad (1)$$

where  $\mathbf{e}_{abc}$  and  $\mathbf{e}_{ABC}$  represent vectors of stator and rotor voltages across the windings,  $\mathbf{R}_s$  and  $\mathbf{R}_r$  are diagonal matrices of stator and rotor winding resistances,  $\mathbf{L}_s$ ,  $\mathbf{L}_{sr}$  and  $\mathbf{L}_r$  are matrices of stator and rotor windings self and mutual inductances, and  $\mathbf{e}_{habc}$  and  $\mathbf{e}_{hABC}$  represent vectors of stator and rotor windings history voltages. A discrete phase-domain induction machine electrical model is depicted in Figure 2.

With respect to the mechanical equations, detailed modelling of DFIG wind turbines requires a two-mass shaft representation. When analyzing the system response to heavy disturbances (such as

short circuits in the network), the generator and turbine acceleration can be simulated with sufficient accuracy only if shaft oscillations are included in the model.

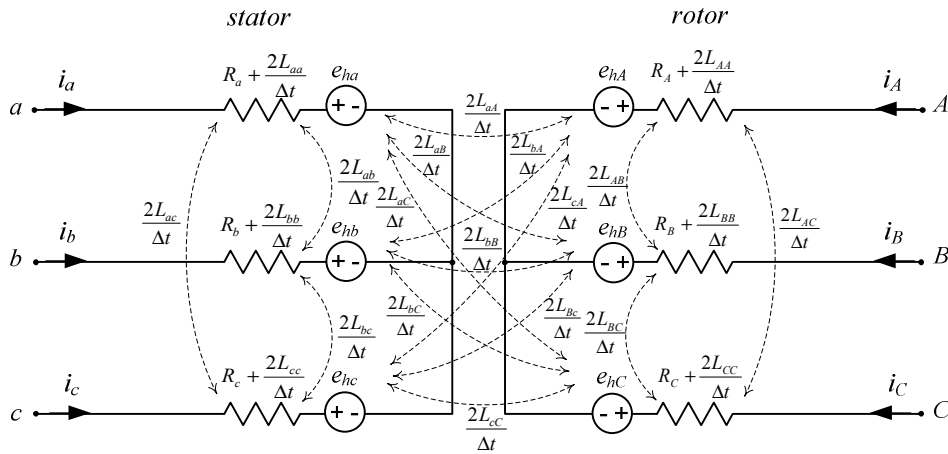


Figure 2. Discrete phase-domain induction machine electrical model

The converter and its controls highly influence the dynamic response of a DFIG. The voltage converter that supplies the rotor of a doubly fed induction generator consists of two voltage-source inverters linked via a DC-link capacitor, as shown in Figure 1. The stator-side voltage-source inverter is connected to the network and to the DFIG stator terminals. The rotor-side voltage-source inverter is connected to the DFIG rotor circuit. The approximate fundamental frequency modelling approach of PWM converters (average model) neglects all switching operations occurring within the voltage-source inverters and represents the converter as an ideal, lossless DC-to-fundamental-frequency AC converter. The high-frequency ripple due to switching harmonics caused by the PWM operation of the voltage converter is of little significance for studying the performance of DFIG WTG in response to network events [9], and in practice is small and further limited by the inclusion of supply-side inductors [7]. In this study, the average model of a PWM converter is implemented in OVNI in phase coordinates. A more complex and detailed model of a PWM converter could be used as well. However, high frequency switching would require the model to be solved with smaller discretization time steps than the one used in the test case described in this paper. The concept of Multilevel MATE [6] allows a common simultaneous solution of power system networks and components modelled individually with different size discretization time steps (latency exploitation) [10].

Rotor- and stator-side converters are vector controlled in the stator flux- and stator voltage-oriented dq reference frame, respectively. Vector control of the stator-side converter enables decoupled active and reactive power control at the machine's terminals, maintaining the converter's DC voltage at the set value. Vector control of the rotor-side converter enables decoupled control of electrical torque, and therefore rotor speed, used for extracting optimum power available from the wind (optimum power tracking). Algorithms for the calculation of stator flux and stator voltage positions are based on the instantaneous values of fundamental frequency stator flux linkages and phase voltages. For the stator-side converter control the angular position of the stator voltage ( $\theta_s$ ) can be calculated from the instantaneous values of stator voltages ( $v_a$ ,  $v_b$  and  $v_c$ ) as:

$$\theta_s = \tan^{-1} \left( \frac{\frac{\sqrt{3}}{2} v_b - \frac{\sqrt{3}}{2} v_c}{v_a - \frac{1}{2} v_b - \frac{1}{2} v_c} \right) \quad (2)$$

The objective of the tracking control is to keep the turbine speed fixed to the optimum power curve as the wind velocity varies. For wind velocity higher than the turbine's rating, the turbine energy captured has to be limited by applying pitch control or driving the machine to the stall point. Optimum power tracking can be realized by either speed-mode or current-mode control [7].

The implementation of DFIG control and non-linear functions with the Multilevel MATE concept [6] enables an efficient, simultaneous solution of its equations with the system equations. With this

approach we avoid instabilities and inaccuracies in the computation reported when a time step delay in the control system solution is introduced in, for example, EMTPTACS [11].

#### 4. DFIG WIND TURBINE TEST SYSTEM

A doubly fed induction generator wind turbine system from an experimental setup in [7] was modelled and implemented in OVNI. This reference provides the data necessary for modelling of the wind turbine system in phase domain. The DFIG wind turbine system case was extended to include a step-up transformer and a 10 kV double-circuit transmission line connecting the wind turbine to a strong network modelled as an infinite bus. The single-line diagram of the test network is depicted in Figure 3. Inclusion of the connecting network allows us to study the response of the wind turbine to a three-phase fault applied in the middle of Circuit 2 of the transmission line.

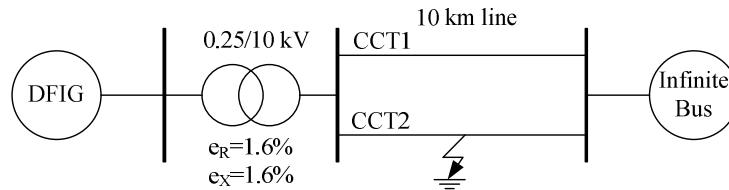


Figure 3. DFIG wind turbine test case

A simulation is first performed for the response of the DFIG wind turbine system to a change in wind velocity following an optimum power tracking system. Initially, the induction machine is operating in steady state with a wind velocity of 9 m/s. The maximum power-tracking system works in current-mode control. At  $t = 2$  s, the wind velocity decreases instantaneously to 5 m/s. Reduced wind power, and therefore mechanical torque, cause the DFIG to decelerate, with the deceleration torque being the difference between the turbine's mechanical torque and the torque given by the optimum power curve. Simulation results for mechanical and electrical quantities for the decrease in wind velocity are shown in Figures 4 and 5.

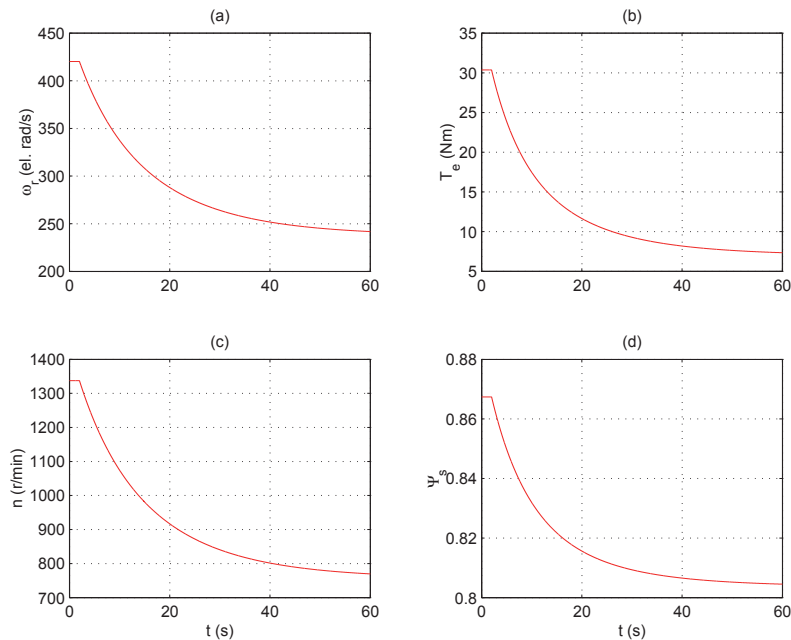


Figure 4. Transient response of the DFIG wind turbine to a step decrease in wind velocity: (a) rotor angular velocity, (b) electromagnetic torque, (c) rotor speed, (d) stator flux

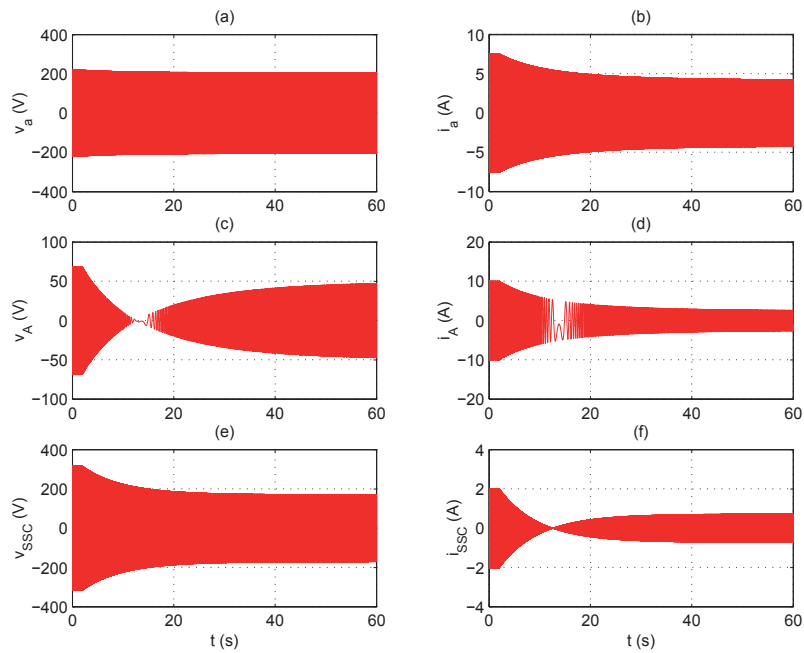


Figure 5. Transient response of the DFIG wind turbine to a step decrease in wind velocity: (a) stator phase to neutral voltage, (b) stator phase current, (c) rotor phase to neutral voltage, (d) rotor phase current, (e) stator-side converter phase voltage, (f) stator-side converter phase current

The second test was done for a three-phase fault at the connecting network. The induction machine operates in steady state with a wind velocity of 8 m/s generating 2700 W of active power that is transmitted to a strong power system modelled as an infinite bus. The DFIG stator-side converter is regulated to maintain its q-axis current at zero, meaning that the reactive power of the induction generator is entirely supplied from the network. At  $t = 0.2$  s, a three-phase fault is applied in the middle of circuit CCT2, Figure 3. The fault is removed after 0.1 s without tripping the circuit. The responses of electrical variables of rotor and stator circuits in corresponding dq reference frames are depicted in Figure 6.

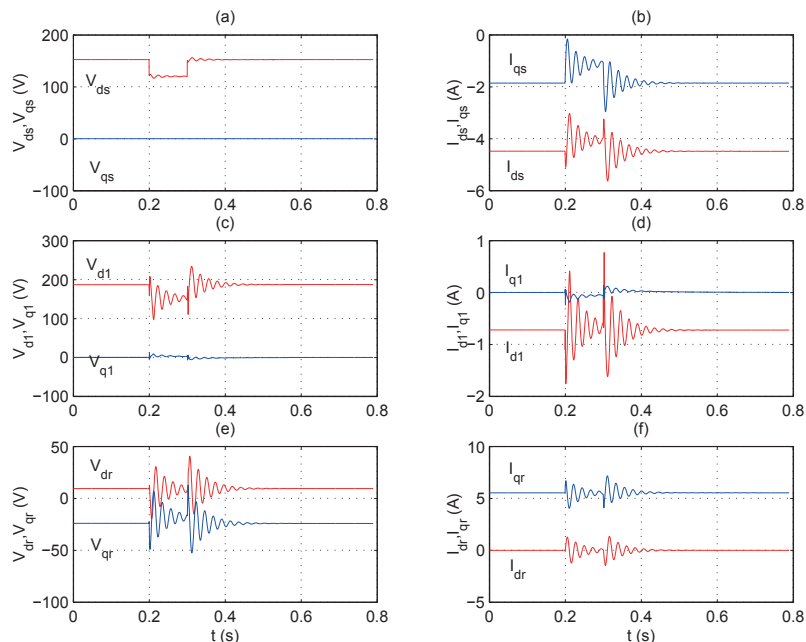


Figure 6. Transient response of the DFIG wind turbine to a three-phase short circuit: (a) stator voltages' dq components, (b) stator currents' dq components, (c) rotor voltages' dq components, (d) rotor currents' dq components, (e) stator-side converter voltages' dq components, (f) stator-side converter currents' dq components

## 5. CONCLUSION

In this paper we describe a detailed EMTP-type of modelling of a doubly fed induction generator wind turbine system implemented in the OVNI simulator. The test system was taken from an experimental setup described in the literature and replicated with our simulation tool. By using a phase-domain induction machine model we were able to simulate the presented test system with a significantly larger time steps (in the order of the milliseconds) than what is traditionally needed with the dq0 model in the EMTP (in the order of microseconds). Also control and nonlinear equations associated with the test system are solved simultaneously with the machine and network equations. This paper presents a new generation of EMTP-type of tools that is not limited to the analysis of electromagnetic transients. The new, more efficient EMTP models and solution methods are based on the principles of MATE and provide unlimited capabilities for developers and users in implementing a wide range of models and types of power system studies. One of the immediate uses of the new simulation tool can be in developing and testing detailed and approximate models of the new types of alternative power generation such as wind power, as described in this paper.

## BIBLIOGRAPHY

- [1] J. R. Martí, L. R. Linares, J. A. Hollman, F. M. Moreira, "OVNI: Integrated Software/Hardware Solution for Real-Time Simulation of Large Power Systems," Conference Proceedings of the 14th Power Systems Computation Conference, PSCC02, Sevilla, Spain, 7 journal pages, June 24th - 28th, 2002.
- [2] J. R. Martí, L. R. Linares, "Real-Time EMTP-based transients simulation," IEEE Transactions on Power Systems, Vol.9, No.3, pp.1309-1317, August 1994.
- [3] S. Acevedo, L. R. Linares, J. R. Martí, Y. Fujimoto, "Efficient HVDC converter model for real time transients simulation," IEEE Transactions on Power Systems, Vol. 14, No. 1, pp. 166-171, February 1999.
- [4] H. W. Dommel, "Digital computer solution of electromagnetic transients in single and multiphase networks," IEEE Transactions on Power Apparatus and Systems, PAS-88(4):388-399, April 1969.
- [5] Gabriel Kron, "Tensorial Analysis of Integrated Transmission Systems, Part III – The Primitive Division," AIEE Transactions, Vol.71, Pt. 3, pp. 814-821, 1952.
- [6] M. Armstrong, J. R. Martí, L. R. Linares, and P. Kundur, "Multilevel MATE for efficient simultaneous solution of control systems and nonlinearities in the OVNI simulator," IEEE Transactions on Power Systems, 21(3):1250-1259, 2006.
- [7] R. Pena, J. C. Clare, and G. M. Asher, "Doubly fed induction generator using back-to-back PWM converters and its application to variable-speed wind-energy generation," IEE Proceedings-Electric Power Applications, 143(3):231-241, May 1996.
- [8] J. R. Martí and T. O. Myers, "Phase-domain induction motor model for power system simulators," In Proceedings of the IEEE Communications, Power, and Computing Conference WESCANEX 95, 1995.
- [9] J. Morren, S.W.H. de Haan, P. Bauer, J.T.G. Pierik, and J. Bozelie, "Comparison of complete and reduced models of a wind turbine with doubly-fed induction generator," In Tenth European conference on power electronics and applications, EPE 2003, Toulouse, France, September 2003.
- [10] F.A. Moreira, J.R. Martí, "Latency techniques for time-domain power system transients simulation," IEEE Transactions on Power Systems, Vol. 20, Issue 1, Feb. 2005 Page(s):246 – 253
- [11] L. Dube and H. W. Dommel, "Simulation of control systems in an electromagnetic transients program with TACS," In Proceedings of IEEE PICA Conference, pages 266-271, 1977.
- [12] Prabha Kundur, Power System Stability and Control, McGraw Hill, 1994.
- [13] Hermann W. Dommel, EMTP Theory Book, 2nd Ed., Microtran Power Systems Analysis Corporation, Vancouver, British Columbia, Canada, pp. 12-3 to 12-9, 1992-1996.
- [14] L. Linares, M. Armstrong, J.R. Martí, "Software Implementation of Controller Representation in the OVNI Simulator," Conference Proceedings of the 15th Power Systems Computation Conference, PSCC05, Liège, Belgium, 6 journal pages, August 22th - 26th, 2005.

## SOLVING EMC PROBLEMS IN THE DESIGN OF NEW HV TEST LABORATORY

Ivo Uglešić<sup>1</sup>, Miroslav Křepela<sup>2</sup>, Viktor Milardić<sup>1</sup>

<sup>1</sup>University of Zagreb, Faculty of Electrical Engineering and Computing, Unska 3  
10000 Zagreb, Croatia

<sup>2</sup>EXOR d.o.o., Bani 73A  
10010 Zagreb, Croatia

### SUMMARY

The paper deals with solving electromagnetic compatibility (EMC) problems in the design of a new, case study, industrial high voltage test laboratory, intended to be used for testing of transformers and other apparatus up to 550 kV rated voltage. Modern high voltage test facilities are equipped, apart from primary test devices like AC, DC and impulse voltage generators etc., also with sophisticated numerical measuring instruments and informatics technology. Since such devices are sensitive to transient overvoltages, the highest degree of EMC is to be secured. This can be achieved by proper earthing and screening of test laboratory, what shall be designed in a way to satisfy all requirements conditioned by building lightning protection, personal protection and system earthing, avoiding electromagnetic compatibility disturbances at the same time. One of the main tasks is solving electromagnetic compatibility problems caused by outdoor electromagnetic disturbances originating from various unknown sources. Those disturbances and interferences may seriously influence measuring accuracy and readings of test devices, what consequently leads to false results. The stated is especially relating to partial discharge measurements. As to avoid such disturbances, the laboratory shall be completely screened with a net forming optimally designed Faraday cage. On the other hand, at high voltage tests with impulse voltages, especially with chopped tail waves, steep transient overvoltages may be generated. As a consequence, high transient potential differences between particular points along the earth electrode may occur, what can even lead to flashovers between parts of it. Therefore is of utmost importance to provide proper earthing and low inductance current return path for impulse high voltage test equipment where high frequency transients are to be anticipated. Improper earthing and bonding may result, apart from mentioned flashovers, in severe induced voltages in secondary cables with consequential influence on test results, possible destruction of measuring instruments and hazardous touch voltages for personnel. For analyzing transient potential differences, it is important to model, with maximum accuracy, impulse test circuit (impulse generator, chopping spark gap, voltage divider, Faraday cage, fundament earth electrode, earthing strips, earthing rods etc.). Magnitude of transient potential difference between particular points is proportional to earth electrode inductance, i.e. low inductance of earth electrode will result in decrease of transient potential difference.

### KEYWORDS

EMC - Earthing - Bonding - Transient - Disturbance - Testing - Measuring.

[ivo.uglesic@fer.hr](mailto:ivo.uglesic@fer.hr)

## 1. INTRODUCTION

Problems of electromagnetic compatibility (EMC) can be very often met in operation of high voltage open-air [1] and gas insulated substations [2]. Very similar problem of EMC exists in high voltage test laboratory where primary system consists of test apparatus and circuits that generate electro-magnetic interferences (EMI). The secondary systems consisting of all the apparatus and circuits for measurement, control and protection should be designed to function satisfactory in EMI conditions.

The paper describes a new industrial HV laboratory and foreseen methods of earthing, bonding and equipotential bonding, aiming to achieve security for personnel and suppression of EMC disturbances. The analysis of possible EMC problems is performed by EMTP-ATP modeling of earth electrode and impulse generator and simulating test with the lightning impulse chopped on the tail, the front time duration  $T_1 = 1,2 \mu\text{s} \pm 30\%$  and time to chopping  $T_c = 4 \mu\text{s}$ . Based on the obtained results, using analytical method [3], the verification and analysis of induced voltages developed at the ends of metal conduits for measuring cables, for the cases of conduit earthing at one end only and at both ends, had been performed.

## 2. DESCRIPTION OF TEST LABORATORY

Internal dimensions of the laboratory are:  $30 \times 35 \times 25 \text{ m}$  ( $w \times l \times h$ ). In order to provide required level of protection against external electromagnetic and noise interferences that might cause partial discharge and noise measurement errors, the high – voltage laboratory is constructed with a double wall with 1400 mm wide air space. As to additionally block an electromagnetic component of external influence, inner sheets of outside wall cladding are mutually galvanically joined.

The laboratory is equipped with one test input for voltage up to 110 kV, one test input for voltage up to 36 kV, two test inputs 12 kV and two low voltage test inputs (0 ... 750 V). The power supply is provided by three generators, one of which with 200 Hz output, and rotating transformer. Test inputs 110 kV and 36 kV are supplied through outdoor HV switchyard with three-coil test transformer 12/4/(40 ... 80) kV and capacitor bank 92 Mvar.

The laboratory will be used, beside for other standardized tests, also for dielectric tests with standard lightning impulses and lightning impulses chopped on tail. Those tests are performed with negative

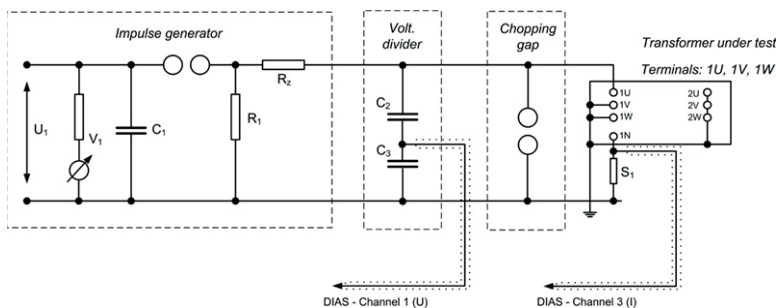


Figure 1. Connection scheme of impulse voltage test circuit

polarity voltages with a view to avoid erratic flashovers in the external insulation and test circuit, since they, under laboratory conditions, present lower insulation stress. Utmost potential danger for insulation originates from chopped on tail impulse wave with front time  $T_1 = 1,2 \mu\text{s} \pm 30\%$  and time to chopping  $T_c = 2 \dots 6 \mu\text{s}$ . Connection scheme of impulse voltage test circuit is presented in Fig. 1 [4].

## 3. EARTHING AND EQUIPOTENTIAL BONDING

Laboratory earthing system is executed in a way to protect life and property in case of supply power system (50 Hz) faults (short circuits) and transient phenomena (lightning, transients resulting from impulse tests). The stated is achieved by equipotential bonding and preventing the unallowed potential rise of earthed metal parts, i.e. transient potential differences between different points of the laboratory earthing system and transfer of earth potential rise to external installations. Analyzed transient phenomena of the order of MHz are characterized with inductive earth electrode resistance, i.e. impulse earth resistance.

The laboratory earthing system consists of grid made of Fe/Zn  $40 \times 4 \text{ mm}$  strips laid in the building foundations, concrete casted, and eight deep – driven copper earth rods, length 10 m each, equally distributed over laboratory ground plan surface [5]. It is galvanic connected with the earthing system

of outdoor HV switchgear dedicated for power supply of test inputs, as well as with the surrounding industrial area earthing system.

Inside the laboratory floor a copper net, being part of its electromagnetic screen is laid. The net is made of metal plate, cut with slots and expanded, with diamond pattern meshes  $10 \times 5$  mm, approx. 2 mm thick. Together with the net inside the inner wall and under the ceiling, made of spot - welded tinned steel wire  $\varnothing 1$  mm, with square meshes  $10 \times 10$  mm, and the net inside the glass of test laboratory control room, it forms the Faraday cage (Fig. 2). The floor net is used as earth return for HF transient currents at execution of lightning impulse tests. All segments of nets inside the floor and the walls are mutually continuously soldered.



Figure 2. Faraday cage

The Faraday cage net is fixed to a grid of wooden slats mounted on a steel construction using screws made of rigid insulation material. Such executed net, galvanic connected to the laboratory earthing, represents an electromagnetic screen which effectively damps magnetic component of disturbances.

All penetrations through the inner wall (e.g. door – posts, gate, bushing sealing flanges, electric cabinets, MV switch panels etc.) are integrated in the screening system by continuous galvanic connection with Faraday cage net along the entire perimeter.

Above-ground connections to lightning protection installation and metal construction connected

thereto are executed via insulated spark gaps. Galvanic connection of Faraday cage and lightning protection installation and metal building construction is executed inside the ground, through foundation earthing grid and earth rods.

Faraday cage net is connected to foundation earth electrode via eight deep – driven copper earth rods. Galvanic connection of earth rods and copper floor net is executed through the copper plate welded to the net with silver solder along the perimeter. At the top of each earth rod, an earth plate electrode is welded, with connection points for earthing test objects and measuring equipment (Fig. 3.). Apart from the described, another 19 auxiliary plate electrodes for the same purpose are foreseen within the laboratory.

Test, measuring and power cables are run through steel conduits laid immediately below the earthed copper net in the laboratory floor. Conduits end in cable connection boxes which are galvanically connected to electromagnetic screen (Faraday cage) by continuous welding along the entire perimeter (Fig. 4). Steel conduits are the same way galvanically connected to cable boxes at both ends.

The test laboratory will be protected against external electromagnetic disturbances, that might cause errors at partial discharges measurements, by means of Faraday cage. Targeted damping [6] of the



Figure 3. Earth plate electrode



Figure 4. Cable connection box

electric component of the order of 1 MHz should be 40 ... 60 dB. For magnetic component lower values have to be accepted. Disturbance level inside the laboratory should be  $\leq 10$  pC, i.e.  $\leq 2,5$   $\mu$ V.

#### 4. TRANSIENTS ORIGINATING FROM CHOPPED LIGHTNING IMPULSE TEST

In this section computation of transients resulting from testing with the chopped lightning impulse is described. Such test can produce dangerous potential differences between different earth points, what can also happen when a lightning stroke hits a laboratory building.

The model of the impulse generator V2800/210 is developed for the computer simulation with the following data:  $C1 = 53.5$  nF,  $R1 = 1560$   $\Omega$ ,  $R2 = 198$   $\Omega$ . The inductance of the impulse generator is 49  $\mu$ H ( $14 \times 3.5$   $\mu$ H). The impulse wave with the voltage peak of 2.2 MV is simulated. The voltage divider is modeled with capacitances  $C2 = 626.25$  pF and  $C3 = 973.8$  nF. The transformer under test is modeled with inductance 100 mH and capacitance 5 nF in parallel. The connection line between the impulse generator and the chopping gap is modeled with the inductance of 12  $\mu$ H on the HV side. On earth side, the chopping gap and the impulse generator are usually connected with a strip or braid of low inductivity. Additionally, there is also current return path through the Faraday cage. All together, current return path on the earth side is of low inductivity. The current return path conductors are defined with the inductance of 0.36  $\mu$ H and the resistance of 0.12 m $\Omega$ .

The length of the connection line on the HV side, from the chopping gap to a transformer under test, is 10 m and it is modeled with the inductance of 10  $\mu$ H. On the earth side, the current path is modeled with the inductance of 0.3  $\mu$ H and the resistance of 0.1 m $\Omega$ . Chopping of lightning impulse occurs at 4  $\mu$ s and the chopping gap is modeled with the switch and the arc resistance of 1  $\Omega$ . Parts of the fundamental earthing grid for the EMTP-ATP [7] simulation are modeled with concentrated parameters as depicted in Fig. 5. Each branch of earthing grid is replaced with its corresponding  $\pi$ -circuit. Values for G, L and R are dependant on a length of the branch. The ATP model of complete grounding system of the test laboratory is shown in fig. 8.

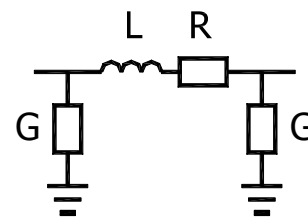


Fig. 5. Part of foundation earth grid electrode

A current which flows through the earth electrode from the transformer under the test to the impulse generator is shown in Fig. 6. Its first peak is the result of the impulse front and second one of the impulse chopping. This current produces transient potential differences between chopping gap and impulse generator earth points, as shown in Fig. 7.

Let us examine theoretically the worst case, when a conduit for secondary test cables, bonded with Faraday cage copper net at one end, is laid in parallel to the earth current path between impulse generator and chopping gap. All calculated voltages and currents are peak magnitudes.

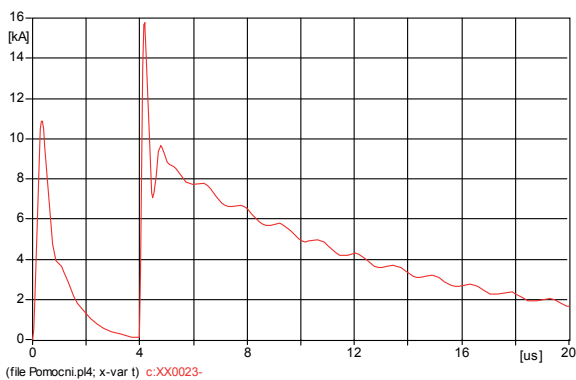


Figure 6. Return current flowing to the impulse generator through the floor copper grid

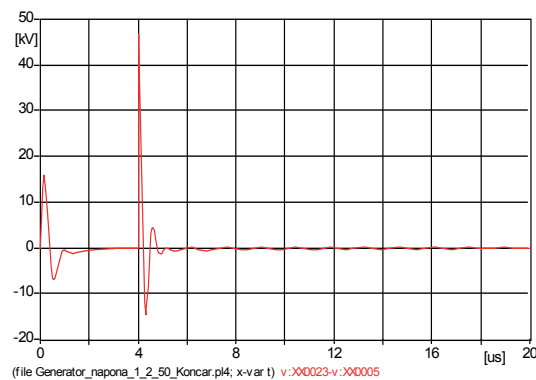


Figure 7. Transient potential difference between earth points of the sphere chopping gap and the generator,  $U_{max} = 46,8$  kV

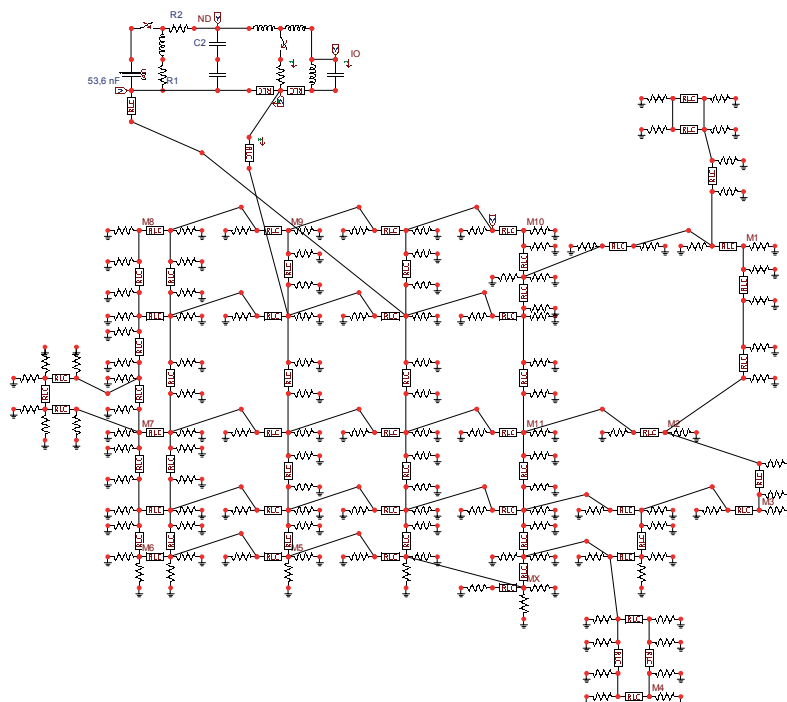


Figure 8. ATP model of impulse generator connected to foundation grid earth electrode

Induced voltage developed across such an open loop may be calculated, using the method described in [3], using the formula:

$$U_{cg} = (j\omega \cdot L_{\sigma} + j\omega \cdot M_g) \cdot \ell \cdot I_g = 2,63MV \quad (1)$$

where are:  $j\omega \cdot L_{\sigma} \cdot \ell \cdot I_g \approx U_{maks} = j46,8kV$  (Fig. 8.)

$$\omega = 2 \cdot \pi \cdot 1,845 = 11,6MHz$$

$\ell = 12m$  - conduit length

$L_{\sigma} \approx 1,7 \cdot 10^{-7} H / m$  - external inductance of a conductor in the copper grid

$M_g \approx 94 \cdot 10^{-7} H / m$  - mutual inductance between the copper grid and the conduit

Mutual inductance between the copper net and the conduit depends, first of all, on geometric dimensions of the expanded net and its meshes and vertical clearance between the net and the conduit. When the conduit is earthed at both ends, current flowing through such a loop is defined by the expression:

$$I_{cg} = \frac{U_{cg}}{Z_{Th}} = 76kA \quad (2)$$

where is:  $Z_{Th}$  - Thevenin impedance of the circuit [3].

Voltage along a steel conduit at HF transient may be calculated by means of formula:

$$U_r = I_s \cdot R_s \quad (3)$$

where are:  $I_s = I_{cp} = 76 kA$  - the current flowing through the conduit;  
 $R_s$  - transfer resistance of the conduit.

While for non-ferrous materials with high conductivity (Cu, Al) resistance  $R_s$  decisive for calculation of induced voltage peak magnitudes caused by HF transient currents with steep slopes is practically equal to ohm resistance, by ferrous materials this resistance has up to five times lower value (16% of resistance against direct current for the example presented in [8]). With regard to the calculation complexity and earth electrode configuration of test laboratory (copper net, foundation earthing grid, concrete armouring), it is performed with DS resistance value, i.e.:

$$R_i = \frac{\rho \cdot l}{\pi \cdot s \cdot (s + 2r)} = 0,71 m\Omega \quad (4)$$

where are:  $\rho = 130 \times 10^{-9} \Omega m$  specific steel resistance  
 $s = 4,5 mm$  conduit wall thickness  
 $r = 75 mm$  internal conduit radius

Finally, inserting  $R_i = R_s$  in (3), voltage level at the conduit in case it was made of non-ferrous material is obtained:

$$U_r = 76 \cdot 10^3 \cdot 0,71 \cdot 10^{-3} = 54V \quad (5)$$

In accordance with stated, peak voltage magnitude expected to be induced in the steel conduit will be up to five times less, i.e. of the order of 10 V. The resistance  $R_s$  of the armour material for transient HF impulse currents is decreasing with lower resistance  $\rho$  and higher relative permeability  $\mu_r$ . As for ferromagnetic materials  $\mu_r$  is significantly higher than 1 (for steel 200 ... 300), without considering relatively high specific resistance  $\rho$ , steel conduits are very efficient armouring against magnetic field penetration and present almost entire protection for signaling cables against electromagnetic interference, i.e. transfer inductive resistance conduit - conductor  $Z_t \approx 0 H/m$ .

The most effective armouring for the entire frequency range is achieved by double armouring – a metallic conduit earthed at both ends and a cable screen earthed at one end, where signaling circuit is earthed too, strictly considering user manuals for test and other equipment.

## 5. CONCLUSIONS

The design and construction of a new industrial high voltage test laboratory demanded solving of EMC problems.

The double wall with an air space is designed in order to provide required level of protection against external electromagnetic and noise interferences. Sheets of outside wall cladding are galvanically joined. The inner Faraday cage of copper and metal net is designed as an additional electromagnetic screen.

The analysis results of transient potential differences indicate that crucial role for their reduction has the inductance of the return current path. Prevention of dangerous high induced voltages in measuring circuits may be achieved by laying of cables through conduits made of ferrous materials bonded at both ends, with minimal distance between the conduit and the floor net. Accordingly, for transient potential differences reduction, mutual bonding of all metal parts using low inductance connections (strips, braids) is of utmost importance.

## BIBLIOGRAPHY

- [1] M. H. B. de Grijp and C. Borm: Electromagnetic Compatibility in Open Air Substations (4<sup>th</sup> IEEE Africon, Stellenbosch, 24-27 Sept. 1996.)
- [2] I. Uglešić, S. Hutter, V. Milardić, I. Ivanković, B. Filipović-Grčić: Electromagnetic Disturbances of the Secondary Circuits in Gas Insulated Substation due to Disconnecter Switching (Conference Proceedings of International Conference on Power Systems Transients - IPST 2003 Hong Kong (New Orleans)).
- [3] Hyltén – Cavallius, N.R., Giao, T.N.: Floor Net Used as Ground Return in High-Voltage Test Areas (IEEE Trans. on PAS, Vol. PAS-88, No. 7, 1969, pp 996 – 1005).
- [4] Lightning impulse test (KPT-QTPT 015E, Končar – Power Transformers Ltd., Issue: 08.2003.)
- [5] M. Křepela & associates: System Earthing of HV Test Laboratory Končar – Power Transformers Ltd., Zagreb, Execution Design (EXOR d.o.o., Zagreb, April 2006)
- [6] Hyltén – Cavallius, N.: High Voltage Laboratory Planning (ASEA HAEFELY & CO.LTD, Basel, December 1986)
- [7] ATPDraw, Windows version 3.6p5 (SINTEF Energy Research, Norway)
- [8] Hasse, P., Wiesinger, J.: Handbuch für Blitzschutz und Erdung

## Electromagnetic compatibility in various kinds of substations in Croatian transmission networks and mitigation measures

S. BOJIĆ\*, A. SEKSO TELENTO, I. DOLIĆ  
Energy Institute Ltd., Zagreb  
CROATIA

### SUMMARY

In the last two decades have been studied the conditions of electromagnetic compatibility (EMC) in different kind of substations in transmission networks of Croatia. Investigations have been done by measuring method using special measuring technique and also by computing simulations. In this paper will be shown conditions of EMC which have been studied by measuring method during normal or fault switching operations of disconnectors and circuit breakers. Conditions of EMC with particular stress on transient voltages in secondary circuits within various kind of transmission network objects have been carefully studied (AIS, GIS, old and new substation design type, rated voltages from 110 kV to 400 kV).

In the paper will be given the review of some main data from those investigations made in the long period of time. Then main findings will be given and the differences in EMC conditions will be shown taking into account various parameters such as: design details of substations (distances, cable types, protective measures etc.). Also, it will be given a review of measuring methods and tools (oscilloscopes with low and deep acquisition memory, statistical tools for data processing, etc.). Generally, it was shown that overvoltage in secondary equipment follows normal or Gaussian statistical distribution from which some typical data have been taken, such as 98% - probability values etc.

Consequently, different kind of the mitigation measures have been proposed in cases of high overvoltages in secondary circuits. Typically, changes in earthing systems, in cable sheets connections etc. have been proposed to utilities. All proposed measures have been tested by measuring methods too and the effects have been very satisfactory in ensuring EMC conditions within substations. Some most interesting ways in reducing high level of TEVR in GIS substations will be shown in pictures.

Given results and effects of mitigation measures in Croatian transmission network substations clearly show that the best method is experimental investigation which usually was followed by some necessary mitigation measures which ensure the conditions of EMC within substations according to international standards and recommendations.

### KEYWORDS

Electromagnetic compatibility, High voltage, Substation, Transmission network, Mitigation measure, Disconnector, Switching operation, Measurements, Statistical analysis

\* [srecko.bojic@ie-zagreb.hr](mailto:srecko.bojic@ie-zagreb.hr)

## 1. INTRODUCTION

In the last 25 years the discipline “Electromagnetic compatibility” (Abb.: EMC) become one important part of design and testing within power substations and power plants [1]. In Croatian electric power system the study of EMC questions passed the way from the first methodology studies [2] and first measurements in high voltage (HV) substations [5, 6] to the mature discipline. The first serious study started practically along with introducing 400 kV voltage in power transmission network.

As have been known, the main problem with EM incompatibility of some electrical equipment in power substations are transient overvoltages in primary or secondary circuits due to lightning strokes, switching operations and different kinds of faults. Overvoltages due to earth faults and lightning strokes are relatively infrequent and in primary circuits they are in majority cases successful suppressed by using of MO arresters and switching control measures.

The most important thing for the occurrence of transients, special in secondary circuits, is automatic or intentional switching of HV disconnectors and circuits breakers, (Fig. 1).



Fig. 1 Arc between contacts of disconnector in AIS 400 kV substation Tumbri, near Zagreb

Travelling current and voltage waves due to disconnector switching influence on sensitive measuring, protective and control circuits. The main part of influence is coming through the measuring transformers because of specific kind of conjugation between primary and secondary circuits (inductive and capacitive). In some cases conductive and radiated components are significant, too.



Fig. 2 View on one of the GIS 110 kV substation Dobri in which EMC conditions have been investigated

It is important to point out the great significance of transient overvoltages in GIS substations, although all AIS substations are not immune on them. But in GIS and in apparatus with compressed SF<sub>6</sub> enclosed by metal cylinders, very high frequency overvoltages are spread in the form of complicated travelling waves, which after few reflections are transferring into very high frequency (up to 50 MHz) and low damped oscillations. The main characteristics of those very fast transients (VFTO) are very steep wave fronts (typical rise time 3 to 5 ns). Such waves may cause significant transient overvoltages in secondary circuits, very high transient voltage rise of metal enclosure (TEVR) and significant transient ground potential rise (TGPR) on different parts of grounding system.

In the beginning of research the EMC problems in Croatian transmission networks it was decided after introducing the first important theoretical studies [4] that the very useful method for determining the level, wave shape, kind and main causes of transient overvoltages are direct measurements within high voltage substations. One of those main reasons for this conclusion is complex structure of substations usually inconvenient for computation, special in secondary circuits.

## 2. EXPERIMENTAL INVESTIGATIONS OF TRANSIENT OVERVOLTAGES IN SECONDARY CIRCUITS OF “AIS & GIS” SUBSTATIONS IN CROATIA

### 2.1 Description of measurements

For experimental study of transient overvoltages it was chosen a typical test configurations of substations which are showed on next two figures (one of 400 kV AIS substations on Fig. 3 and one of 110 kV GIS substations, Fig. 4). In each configuration measuring of transients have been done during disconnectors switching “On” and “Off” on different parts of substations.

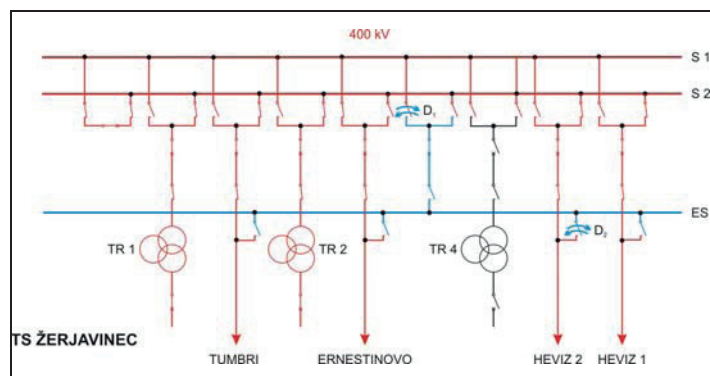


Fig. 3 400 kV AIS substation Žerjavinec with locations of disconnectors which have been switched on and off

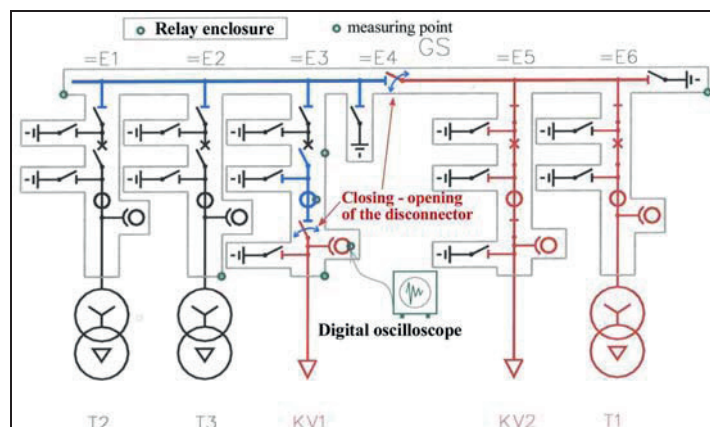


Fig. 4 GIS substation 110 kV Dobri with location of disconnectors during EMC investigation

In AIS substation as a most dangerous was chosen switching of unloaded auxiliary bus-bars (Fig. 3), but in GIS the section of enclosed busbars with sectional disconnecter (Fig. 4).

For each type of measurement the choice of measuring-acquisition equipment was based of expected amplitude and frequency spectrum of studied transients. Because of that are chosen modern digital-storage oscilloscopes with frequency bandwidth of 500 MHz, sample rate from 0.5 to 1 Gs/sec. Also it was necessary to take the instruments with very deep acquisition memory and high voltage measuring probe with 250 MHz frequency bandwidth. Measurements have been done on measuring points in secondary equipment cubicles (Fig. 5a and 5b), but in GIS substations on different points of metal enclosure, additionally.



Fig. 5a Detail of measuring equipment



Fig. 5b Measurements points in relay cubicle

Furthermore, because of stochastic nature of transients measurements have been repeated several times in the same configuration due to statistical processing of collected samples. In intention to find maximum values of transients in each switching cycles it was used sequential memory mode of oscilloscope.

## 2.2 Review of results

The first results of measurements and studies conducted in AIS type of 400 kV substations showed desirable level of overvoltages in secondary circuits in 400 kV substations which was less than  $2 \text{ kV}_{\text{peak}}$  [5, 6]. In some specific cases the level of overvoltages exceeded  $3 \text{ kV}_{\text{peak}}$  and it was to required to make additional EMC measures already through the building process it was found lower level of overvoltages in secondary circuits [3, 10, 12]. On Fig. 6a is shown typical oscillogram of overvoltages in secondary circuits in one of new 400 kV AIS substation. For comparison Fig. 6b shows measured overvoltage in secondary circuits investigated within 110 kV GIS type of substation.

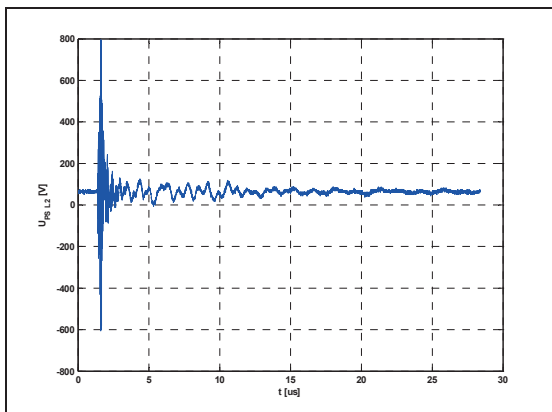


Fig. 6a Transient in AIS 400 kV Žerjavinec

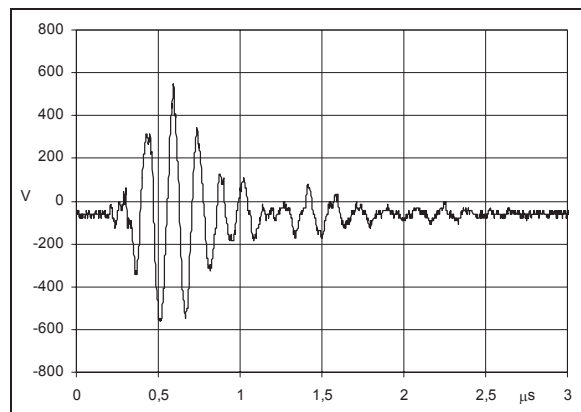


Fig. 6b Overvoltage in 110 kV GIS Dobri

In GIS substations besides of amplitude level more care have to be taken on frequency range of transient overvoltages (usually 5-20 times higher than for AIS) due to some specific properties of GIS (very steep overvoltages, small design distances, superposition of TEVR etc.) In that sense more experimental studies have been performed in Croatian GIS substations in past several years with statistical evaluation of measuring results special because of higher risk of undesirable disturbances in secondary circuits.

In table 2.1 it is given the summary of results of the highest overvoltages recorded in different points of one of representative 110 kV GIS substations during disconnecter switching.

Table 2.1 Overview of the highest overvoltages values recorded in different points of GIS Substation 110 kV Dobri (in town Split), during disconnectors switching-„Switching off” (peak overvoltages values and number of measurements at each measuring point) (red sheded: overvoltages measured in secondary circuits)

Measuring point	Reference point	U <sub>peak</sub>	E1 (Q1)-TR1 Disconnecter, busbar side	E3 (Q0)-KAŠT Switch	E3 (Q1)-KAŠT Disconnecter, busbar side	E3 (Q9)-KAŠT Line disconnecter	E4 (Q11)-SAB Busbar section disconnecter	E5 (Q1)-SUČ Disconnecter, busbar side	E5 (Q9)-SUČ Line disconnecter	E6 (Q1)-TR2 Disconnecter, busbar side
Enclosure-T1	M1	2.438 V (16)					1.750V (11)			2.438 V (5)
Enclosure -T1a	M1	8.438 V (41)	2.969 V (4)	3.125 V (1)	5.438 V (10)	3.813 V (9)	3.813 V (9)		8.438 V (5)	3.813 V (3)
Enclosure -T2	M1	13.750 V (36)		4.063 V (1)	6.750 V (10)		1.781 V (12)		13.750 V (5)	5.063 V (8)
Enclosure -T3	M1	2.250 V (15)					1.563V (11)			2.250 (4)
Enclosure -T3a	M1	3.500 V (22)	2.125 V (4)			2.875 V (9)	3.500 V (9)			
Enclosure -T4	M1	6.000 V (15)					6.000 V (11)			4.019 (4)
Enclosure -T4a	M1	16.456 V (55)	1.425 V (2)	5.450 V (1)	3.363 V (8)	16.456 V (10)	3.450 V (25)	3.925 V (1)	5.700 V (5)	4.163 V (3)
Enclosure -T4b	M1	9.531 V (41)	1.188 V (2)	4.000 V (1)	4.250 V (9)	9.531 V (10)	2.594 V (10)	3.063 V (1)	4.000 V (5)	4.775 V (3)
Enclosure -T4c	M1	2.969 V (15)					2.969 V (15)			
Enclosure -T5	M1	7.313 V (14)					7.313 V (14)			
Enclosure -T6	M1	5.438 V (14)					5.438 V (14)			
SK-Kaštiela	M-E3	1.161 V (82)			651 V (36)	1.161 V (40)				734 V (6)
SK-Sučidar	M-E5	1.198 V (56)	693 V (16)				1.198 V (40)			
SK-T1	M-E1	938 V (53)					917 V (44)			938 V (9)
SK-T2	M-E6	1.646 V (60)					1.646 V (60)			

The highest peak overvoltages measured on different points of secondary circuits are not exceeding value of 2 kV<sub>peak</sub>, but the measured values of transient enclosure voltage rise (TEVR) are significant on some points of enclosure. The last findings lead to introduction of various kinds of mitigation measures.

### 3. MITIGATION MEASURES FOR EMC FULFILMENT IN SUBSTATIONS

In accordance with presented results and some other studies [7, 8] it was made in each tested substation evaluation of fulfilment of EMC conditions. In old generation of AIS 400 kV substations it was concluded that disconnecter switching could lead to high transient overvoltages in secondary circuits. In those cases it was necessary to reduce them to levels to assure safe and truly operation of sensitive electronic devices. Desirable level of overvoltages was concluded to be less than 2 kV<sub>peak</sub>.

New generation of AIS and GIS type substation fulfil that and other EMC conditions generally. But, all higher levels of transients cannot be completely eliminated. This is particularly related to transient enclosure voltage rise (TEVR) in GIS type substations which is unique for GIS and can be in some worst cases also significant for disturbances in secondary circuits and EMC condition in related substation.

In that sense and as for example on Fig. 7 is done principal scheme three different kinds of earthing both sides of enclosure-cable connection in tested GIS which have been experimental investigated to quantify the differences and efficiency in decreasing level of TEVR during disconnecter switching, [7, 8].

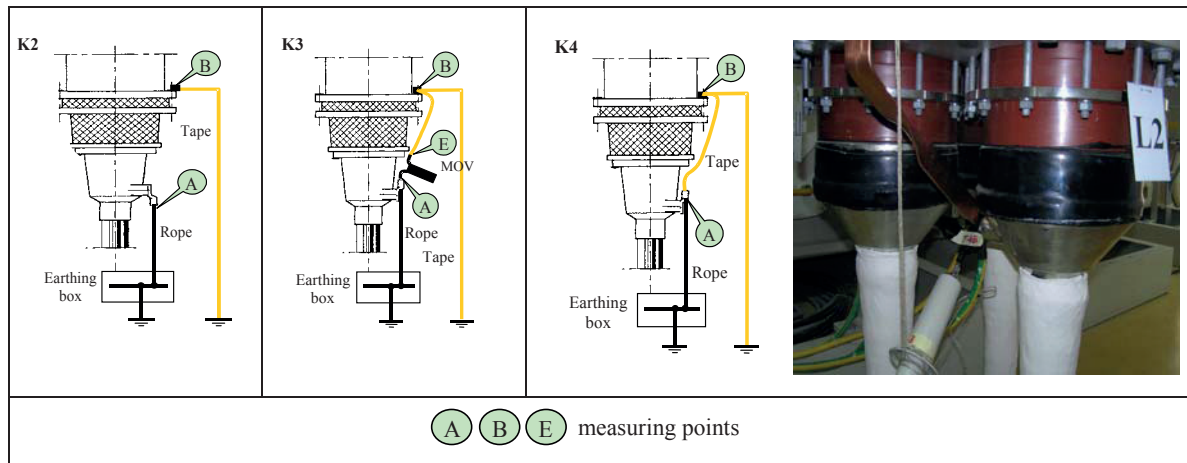


Fig. 7. Test configurations to determine efficiency of different kinds of earthing interconnected GIS enclosure and cable terminals on TEVR level

Measurements have been repeated several times in the same configurations to get representative samples for farther statistical evaluation. Summary of statistical evaluated results is described as bar diagrams Fig. 8 (left part of figure). From the diagrams is evident the influence of low inductance earthing on both sides of enclosure-cable interconnection in significant mitigation TEVR in tested GIS.

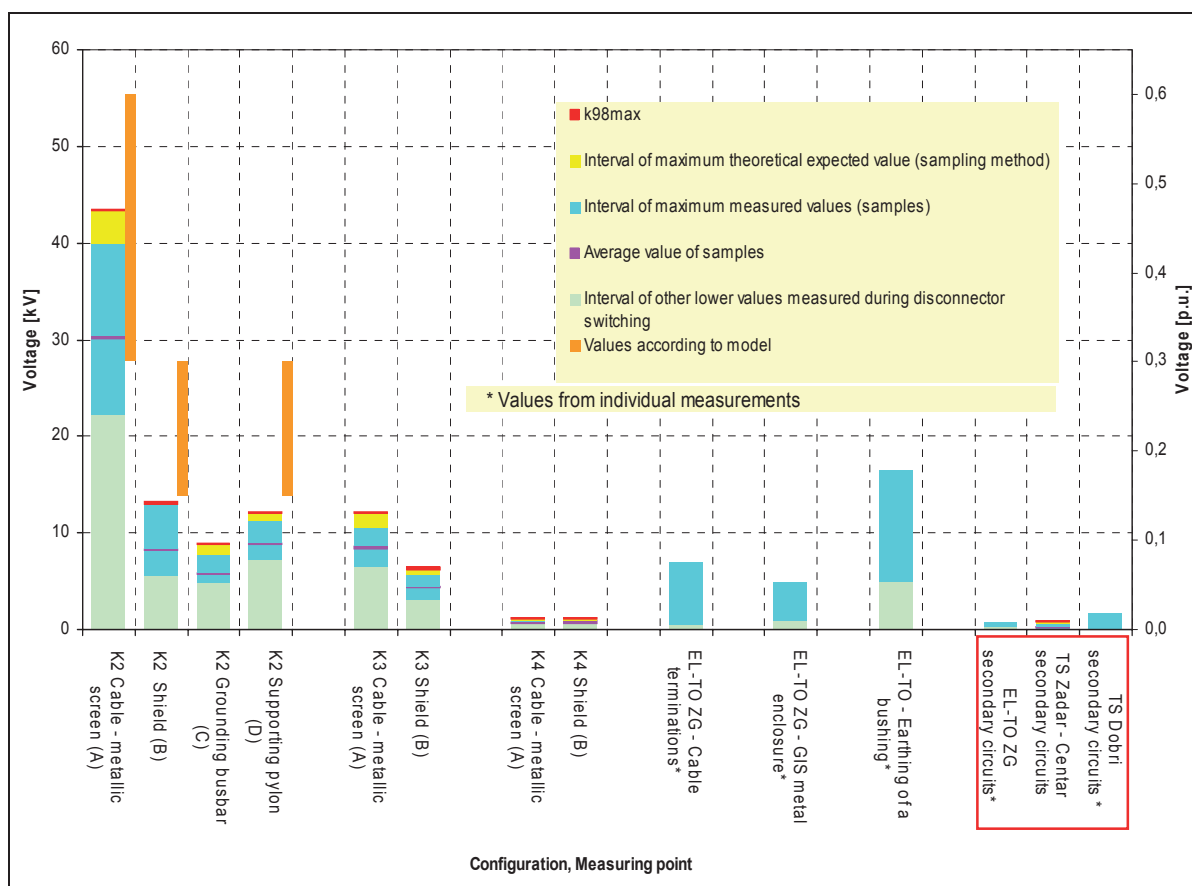


Fig. 7. Summary of results of tested configurations to determine efficiency of different kinds of earthing interconnected GIS enclosure and cable terminals on TEVR level; Transient overvoltages in secondary circuits measured in three different GIS substations (in red frame)

But sometimes it is difficult and expensive to carry out enough effective measures. Because of that the most effective way is to predict ways for reducing of overvoltages already in the phase of design of new substations. In that sense experiences with measurements in existing substations are essential.

#### 4. MAIN CONCLUSIONS AND LESSONS LEARNED

Some main conclusions from measuring investigations of transient overvoltages in secondary circuits in different kind of Croatian 110 kV and 400 kV substations may be briefly stated as follows.

1. Overvoltages within old types of AIS substations are generally higher and often need reductions
2. GIS substations showed lower level of peak values of transient overvoltages in comparison to AIS substations, but generally have higher frequency range and some specific problems (TEVR)
3. Various mitigation measures undertaken after first measurements showed good suppressive effects
4. It was decided to carry out measuring investigations in all type of substations periodically and according to IEC and other regulations
5. Computing methods of investigations of EMC conditions is considered as useful in design phase for new substations and may be validated only through measuring investigations with special and sophisticated equipment.

#### BIBLIOGRAPHY

- [1] CIGRE: Monograph on GIS Very Fast Transients, Presented by Working Group 33/13.09, Paris July 1989
- [2] CIGRE: Earthing of GIS: An application guide, Technical Brochure Ref. 044, Paris 1993
- [3] CIGRE: Guide on EMC in power plants and substations, Technical Brochure Ref. 126, Paris 1997
- [4] A. Sekso: Limitations of overvoltages in secondary circuits of HV substations and EMC problems (Study in Croatian), Institute for Electric Power Industry, Zagreb 1983
- [5] R. Naumov, P. Vukelja, N. Jakanović, A. Sekso: Induced voltages in secondary circuits of 400 kV substation Ernestinovo (Study in Serbian), Institute Nikola Tesla, Belgrade 1985
- [6] R. Naumov, P. Vukelja: Experimental investigations of transient overvoltages in secondary circuits of 400 kV and 220 kV HV substations, CIGRE Symposium "Power system EMC", Paper No. 500-05, Laussane 1993
- [7] S. Bojić, I. Uglešić: Research of the efficiency of measures for decreasing of TEVR in GIS, Proceedings IPST, Paper 090, pp. 25-30, Rio de Janeiro 2001
- [8] S. Bojić: Enclosure voltage rise in HV switchgears due to disconnecter switching, M. Sc. Thesis (Croatian), University of Zagreb, Zagreb 2002
- [9] A. Sekso Telento, S. Bojić: Measurements of overvoltages in secondary circuits for EMC evaluation in transmission network substations, Paper No.P.05.50 on XIII<sup>th</sup> Symposium on High Voltage Engineering, Delft, Netherlands, 2003
- [10] Ž. Štih, S. Berberović, Z. Haznadar, S. Banić: Analysis of EMC in 400 kV substation Ernestinovo, Paper No. C4-12 (in Croatian), Proceedings of 6<sup>th</sup> Session of Croatian NC CIGRE, pp 115-124, Cavtat 2003
- [11] J. Šimić, S. Gross: Electromagnetic environment and immunity of equipment to EM disturbances in power system objects, Ibid. Paper No. C4-11, pp. 105 - 114
- [12] S. Banić, B. Pinčić, B. Glavan, M. Rončević, V. Ilijanić. Analysis of HV substation parameters which influence to EMC, Paper No. C4-07 (in Croatian) on 7<sup>th</sup> Session of Croatian NC CIGRE, Cavtat 2005

## The Impact of Ferroresonance and Low Frequency Phenomena on Power Transformers and Transmission systems

**Mark Osborne, Paul Jarman\***  
National Grid

**Charalambos Charalambous, Zhongdong Wang \*\***  
University of Manchester

(United Kingdom)

### SUMMARY

Ferroresonance is a low frequency phenomenon that can occur when one side of a double circuit transmission line connected to a transformer is switched out. This can result in the transfer of power from the adjacent circuit through mutual coupling into the de-energised circuit. This can lead to saturation of the transformer and stressing of the disconnector during opening. More typically, ferroresonance will affect control and protection functions preventing circuit operations and possibly requiring an unplanned double circuit outage to safely isolate the distressed transformer.

In the UK a number of power transformers are exposed to ferroresonance and remote switching where they are connected to mesh corner and circuit tee configurations. Ferroresonance will continue for a few minutes until it can be detected and quenched. In cases where it cannot be detected, this can be much longer until the transformer is fully isolated. There are a number of ferroresonance modes, which may affect the unit differently, little is known to what degree this is damaging the transformer.

This paper briefly discusses the results of system tests carried out to investigate the effect of ferroresonance and subsequent modelling work. The validation of a detailed transient model has been carried in an attempt to understand the effect of ferroresonance and quantify the energy injected into the transformer core during various ferroresonance modes. The article concentrates on the early stages of this work and the impact of ferroresonance on network infrastructure including transformers, switchgear, protection and control.

### KEYWORDS

Ferroresonance, switching, transformer modelling, saturation, power systems, system tests.

### BACKGROUND

The UK transmission network is a highly integrated system, containing many double circuit lines, terminating in some cases, with mesh design substations [1]. During the 1970's, when the transmission network was built, the prohibitively high cost of circuit breakers drove the development of the mesh substation (Fig. 1). This design maximised the use of the circuit breaker, which was comparable in

cost to the transformer. The air blast circuit breakers were very complex units requiring highly skilled engineering and resource. This cost factor resulted in a design compromise and the mesh substation was established. The banking of transformers with lines exposed transformers to more frequent and higher stresses from remote end switching over-voltage effects, compared to that of transformers in a double busbar substation.

Although technology has changed over the last few decades, substations with mesh corners or circuit ‘tees’ still exist and experience the problems of remote energisation overvoltages and ferroresonance. Remote energisation is more likely to cause a failure mode, but can be managed to some degree by surge arresters. Ferroresonance tends to cause switching complexity issues, albeit damage is possible. As the issue of ferroresonance became more of a problem, intricate control schemes were developed, based on automatic quenching schemes using disconnectors to isolate the transformer from the line to remove the ferroresonance. While this was acceptable for the older and more robust committee design disconnectors, present day equipment with tighter design margins proved less robust and effective as quenching devices and as a result quenching performance has deteriorated.

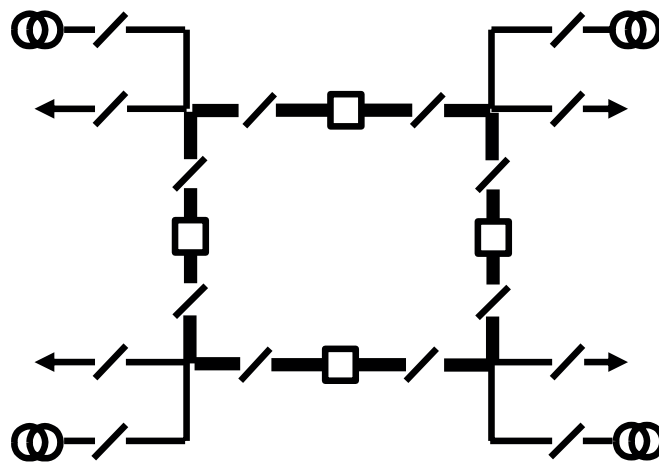


Figure 1. A typical mesh substation layout

## FERRORESONANCE

Ferroresonance is an electromagnetic phenomenon which occurs as a result of the interaction between an iron core inductance and shunt capacitance. This non-linear condition can arise on the transmission system under specific network configurations (Fig. 2). The effect can weaken the security of the network and ultimately damage primary equipment, including power transformers, wound voltage instrument transformers and switchgear exposed to the electro-mechanical stress during the ferroresonance condition [2].

There are three categories of ferroresonance, and in each case mechanical duty will be imposed onto the transformer winding and core, in addition to the consequential dielectric and thermal stress on the insulation materials.

- **Unstable Quasi-Periodic Oscillation (Chaotic)** where a given excitation forces a move between more than one stable equilibrium state. The effect is characterised by a sudden jump of voltage or current from one stable state to another.
- **Fundamental Mode Ferroresonance** can only be sustained in the presence of fundamental excitation (from an adjacent source). Both odd and even harmonic oscillations can occur depending on the system parameters and initial conditions. However, the region of existence of such oscillations is very sensitive to losses in the circuit.
- **Sub-Harmonic Mode Ferroresonance** can occur at an integral sub-multiple of the fundamental frequency, but only in the presence of fundamental excitation. Both odd and even sub-harmonic oscillations are possible. It is also very sensitive to losses in the circuit.

There are two typical scenarios where ferroresonance occurs within the UK Transmission network:

- Power transformer ferroresonance – where the unit is connected to a double circuit overhead line (this can also affect quadrature boosters and shunt reactors),
- Wound electromagnetic voltage transformer (EMVT) ferroresonance – where the unit is connected to an isolated section of busbar and circuit breakers fitted with grading capacitors.

This paper concentrates on the impact associated with power transformers, the issue of electromagnetic voltage transformer ferroresonance is covered in greater detail by other references [3].

This paper examines where power transformer ferroresonance can arise as a result of the following circumstances (Fig 2):

- De-energisation of one circuit of a double circuit over-headline with a transformer feeder
- A live adjacent overhead circuit on the same tower (i.e. part of a double circuit typically longer than 10km)
- Transformer connected with a disconnector (no HV circuit breaker between the transformer and line).

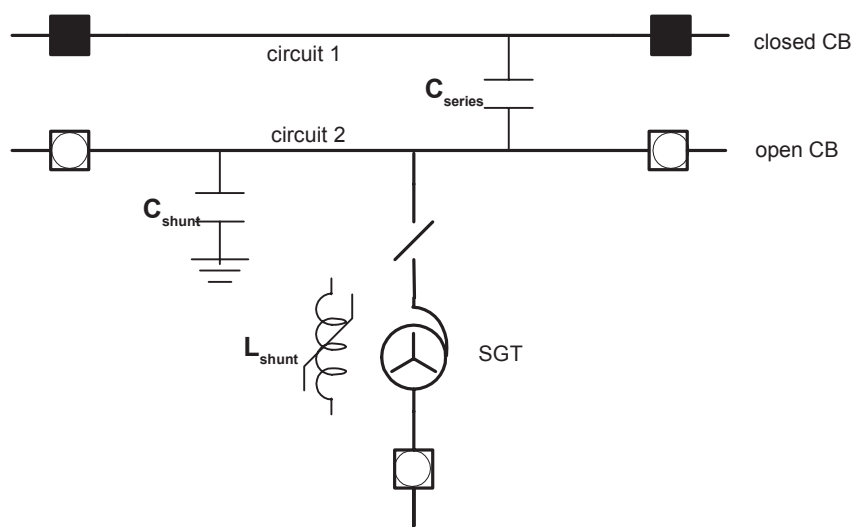


Figure 2. Typical circuit configuration which can exhibit ferroresonance.

The energised adjacent line (on a double circuit tower) is capable of indefinitely supporting an established ferroresonance condition between the non-linear inductance of the transformer and the de-energised line circuit capacitance to ground. This forcing function can cause the transformer magnetic flux to saturate, failure of the core to contain magnetising current, results in stray current flowing into metallic elements of the transformer other than the iron core (such as core bolts or the tank). These components have a higher resistance and rapidly heat up due to the stray currents. This could potentially cause internal thermal damage to insulation local to the parts, this will result in a subsequent reduction in the dielectric strength.

## SYSTEM TESTS

In 1998 a number of system tests were performed on a 400kV circuit which was known to ferroresonate. The feeder circuit is composed of a 1000MVA 400/275kV interbus transformer connected to a double circuit overhead line with only a disconnector. The purpose of these tests was to establish the likelihood of ferroresonance and the quenching performance of the disconnector. The tests successfully established different states of ferroresonance through control of the point on wave switching of the circuit breaker which discharges the circuit containing the transformer.

The results indicated that quite onerous conditions could be generated on a relatively short circuit (37km) if the ideal conditions for ferroresonance prevail. In the case of fundamental mode

ferroresonance, voltages in excess of 1 per unit were established (Fig. 3) and associated non sinusoidal currents with peak values over 200A (Fig. 4). Other tests produced sub-harmonic mode ferroresonance where the voltages and currents were much lower, typically of the order 100kV and 50A. The disconnectors opened successfully to quench and remove the ferroresonance condition and safely isolated the transformer.

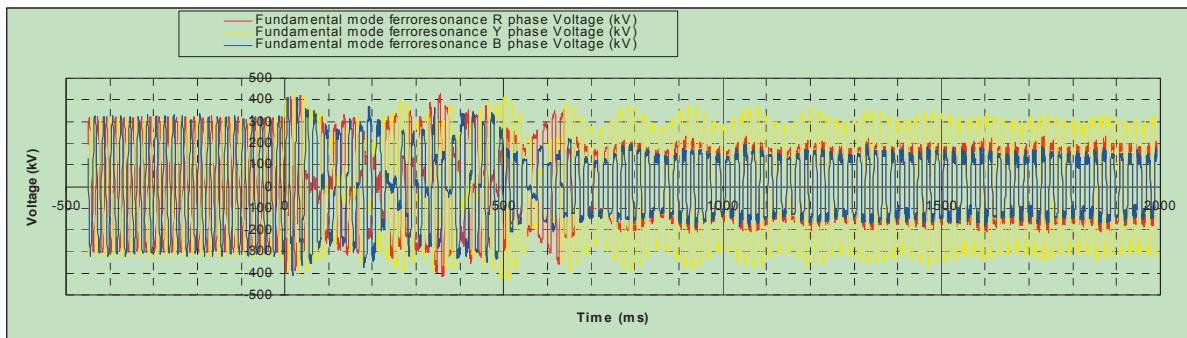


Figure 3. Fundamental mode ferroresonance – voltage (measured)

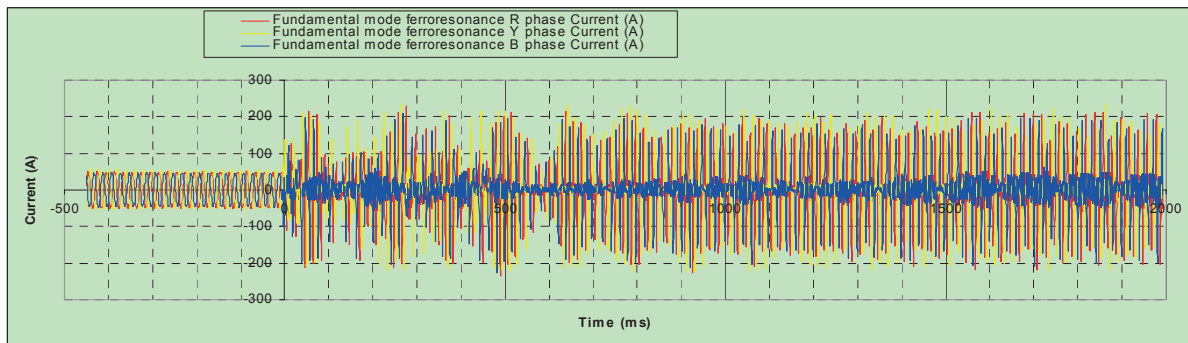


Figure 4. Fundamental mode ferroresonance – current (measured)

## MODELLING FERRORESONANCE

The system tests were replicated in EMTP (ATP) to understand the impact that ferroresonance has on both the switchgear and transformer. This will help to gain further insight into the conditions which increase the likelihood of ferroresonance occurring and the amount of energy being transferred into the transformer.

The overhead line circuit was modelled using the geometric transmission line characteristics. The transformer model adopted the BCTRAN transformer matrix model using data from manufacturer test results. Saturation effects were considered by attaching the non-linear characteristics externally in the form of a non-linear inductive element branch [4]. The results replicated the measured voltage (Fig. 5) and currents (Fig. 6) waveforms to a very good degree [5].

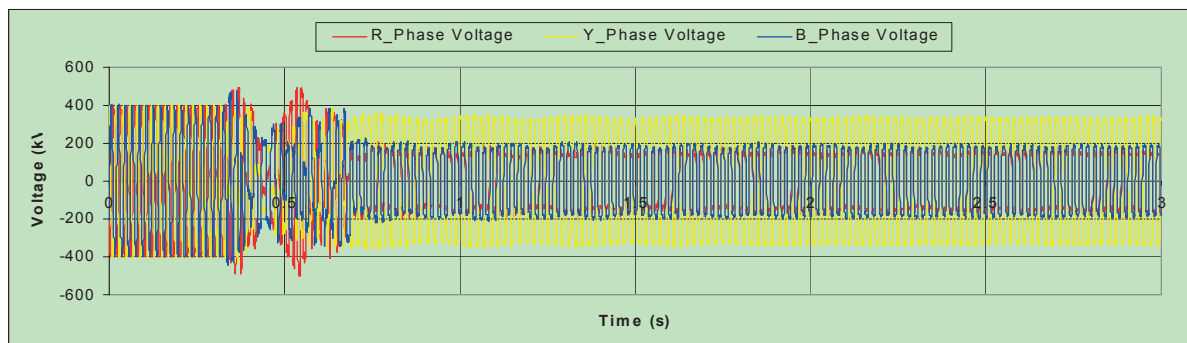


Figure 5. Fundamental mode ferroresonance – voltage (simulated)

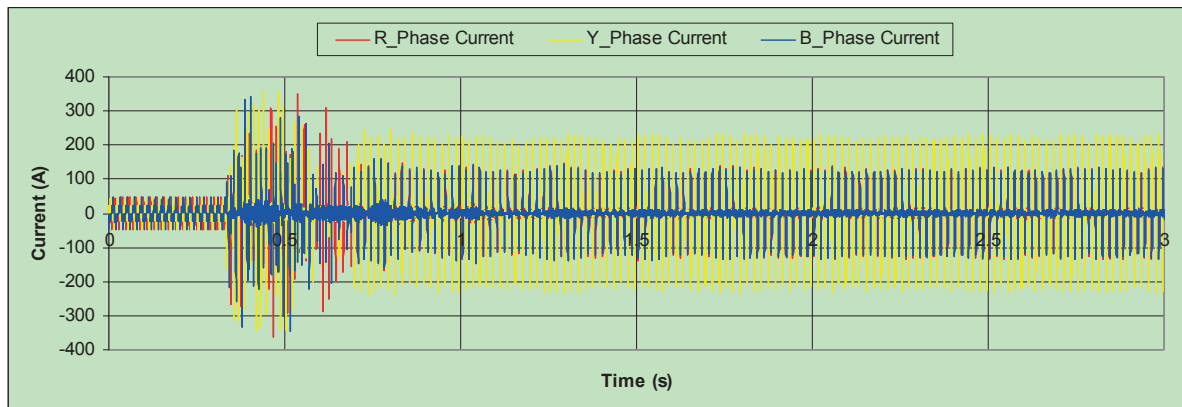


Figure 6. Fundamental mode ferroresonance – current (simulated)

Numerous studies were performed considering various sensitivities including the interaction between point on wave switching, transformer core losses and line length. From this analysis a ferroresonance map (Fig. 7) was developed, which identifies the likely type of ferroresonance to be experienced when a feeder circuit with the relevant conditions is switched. The map suggests that point on wave switching and transmission line length dominates the susceptibility of a transformer to sustain ferroresonance. These results support the concept of energy transfer in the transformer being a likely cause of insulation stressing and possible ageing. Switching studies suggest that, in addition to ferroresonance, large magnitude overvoltages and inrush currents will worsen the condition of the transformer, by further reducing the dielectric strength.

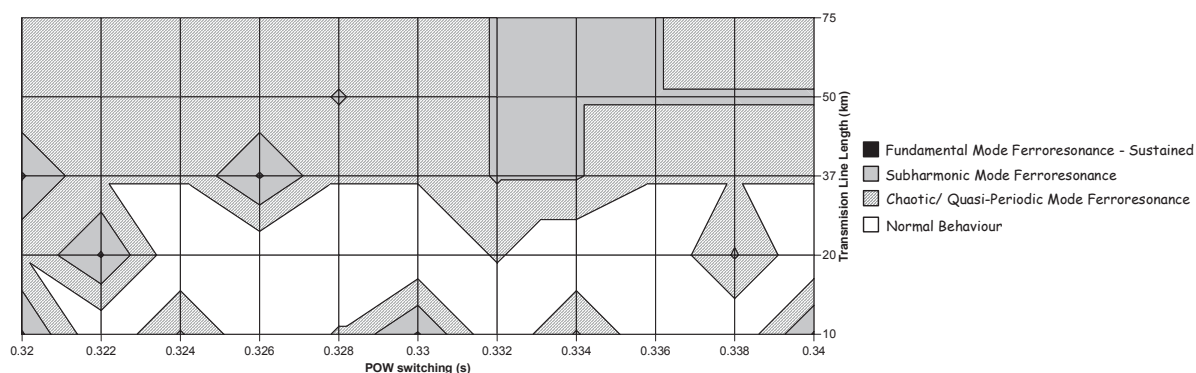


Figure 7. Ferroresonance map - Interaction of point on wave and line length

The information gained from this work can be used in conjunction with fine element analysis to develop a detailed transformer model to understand the magnetic field distribution within a transformer under ferroresonance and any degrading mechanisms on the transformer. This model will help to determine the likelihood of transformer ferroresonance and other low frequency effects including geomagnetically induced currents (GIC) and switching surges.

## IMPACT THE TRANSMISSION SYSTEM

Ferroresonance does not only affect transformers and the effect on the transmission systems is widespread stressing switchgear and interfering with protection and control operation.

### Transformers

The key concern for plant with magnetic iron cores such as transformers, reactors and quadboosters is whether the energy transferred into the transformer body during core saturation by the non-sinusoidal currents is damaging. Saturation and failure of the transformer core to contain the flux, manifests itself

as current induced in parts of the transformer body not designed to conduct current. The ferroresonance fundamental current pulses (up to  $500A_{pk}$ ) can continue indefinitely causing heating in the core bolts and tank. This can thermally damage insulation, creating weaknesses, which cannot be spotted before a failure occurs.

A transformer experiencing ferroresonance generates an uncharacteristic audible grumbling, the fundamental frequency mode is loud and can be heard up to 50m away. Evidence of ferroresonance causing internal heating is indicated by gassing and tripping of the Bucholtz protection.

### **Switchgear**

During the field tests the disconnectors experienced significant arcing during quenching of the fundamental mode ferroresonance. This caused some erosion of the contacts, which suggests that closer inspection and possible replacement is likely should they see frequent ferroresonance quenching duty.

New disconnectors are not rated for ferroresonance quenching duty and are not ideal devices as they draw the arc slowly and in an uncontrolled manner. A modified earth switch is used instead as it is the only other mechanical switching device remaining (other than an expensive circuit breaker). The method is a closing operation which will not draw an arc (although one will be created). Operationally, a standard earth switch is not suitable for ferroresonance quenching, so an enhanced duty device is necessary.

Surge arresters can also be affected if the voltages associated with ferroresonance exceed the rated TOV and cause the arrester to operate and conduct current for long periods (in surge arrester terms). This is a particular issue if an arrester is subject to heating and then exposed to a switching over-voltage when the transformer is remotely energised. This can only be avoided through design by ensuring the MCOV and TOV is greater than anticipated ferroresonance voltages.

### **Control & Protection**

There are a number of problems caused by ferroresonance, firstly it is very difficult to reliably detect and initiate automatic quenching, and secondly ferroresonance can interfere with circuit protection and control operations.

Detection is difficult, especially sub-harmonic modes. The bulk of ferroresonance modes involve current values typically of 100A and below. These are quite low values to detect in terms of protection reliability and dependability and could lead to spurious tripping. Voltage detection is more suitable, however three phase detection is necessary and the frequency response of the CVT can make sub-harmonic ferroresonance detection uncertain. The relay looks for a three phase condition typical of fundamental mode ferroresonance, sub-harmonic mode detection is more variable.

Interference with schemes is probably the main concern surrounding ferroresonance from the Control room perspective. The main problem is lockout of autoreclose schemes following a transient fault. The presence of a ferroresonance voltage inhibits the synchronisation relay, which detects a voltage on what should be a dead circuit. Non routine switching is necessary to quench the ferroresonance before the circuit can be re-energised. If operation of the disconnector is prevented then the adjacent circuit will need to be switched out, creating a double circuit outage. This is quite a serious situation, since what started out as a simple transient fault (e.g. lightning) can start to compromise system security by creating an N-2 condition. Consequently, where ferroresonance can be identified in advance an automated detection and quenching scheme is installed in an attempt to prevent the risk of a double circuit outage.

Mesh corner and transformer tee control schemes require bespoke engineering solutions and are resource intensive, involving significant site-specific functionality. The risks are difficult to quantify at a design stage. Although switchgear costs are reduced, the engineering cost can be significant and introduce problems at commissioning, where various circuit configurations must be tested. Mesh corner protection is complex, adding ferroresonance to this introduces another unreliability factor. The complexity associated with this type of connection should not be dismissed, since any circuit changes throughout the connection lifetime will need to be carefully assessed to identify any interactions or inter-tripping.

## CONCLUDING REMARKS

Ferroresonance is a complex electro-magnetic condition. Through system tests and analytical studies it has been demonstrated that ferroresonance is a stochastic function, dependent upon the initial conditions and circuit parameters. Simulations suggest that the transformer may be exposed to higher energy transfers with long transmission lines or where the core losses are low. The impact of ferroresonance on transmission assets has been discussed and although no transformers have failed during ferroresonance activity, accelerated ageing is likely, but to what extent we do not know at this time.

Ferroresonance has a complex and cumulative impact, since not only do you get the ageing of assets, but there is the problem of reliably detecting the condition and then the interference from ferroresonance on protection and control systems which make secure operation of the system increasingly difficult. In summary utilities should avoid configurations which will create ferroresonance and increase the risks to the system and assets.

## BIBLIOGRAPHY

- [1] National Grid Seven Year Statement. [www.nationalgrid.com/sys](http://www.nationalgrid.com/sys)
- [2] Tong, Y.K. "NGC experience on ferroresonance in power transformers and voltage transformers on HV transmission systems", Warning! Ferroresonance can damage your plant, IEE colloquium on, 12th Nov. 1997
- [3] Z. Emin, B.A.T. Al Zahawi and Y.K. Tong, "Voltage Transformer Ferroresonance in 275kV Substation", 11<sup>th</sup> International Symposium on High Voltage Engineering, August 23-27, London.
- [4] J. A. Martine-Velasco, B. A. Mork, "Transformer Modelling for Low Frequency Transients – The state of the Art, IPST 2003 New Orleans, USA.
- [5] C. Charalambous, Z. Wang, M. Osborne, P. Jarman "Validation of a Power Transformer Model for ferroresonance with system tests on a 400kV circuit" Accepted for Presentation on I.P.S.T 2007, Lyon, France 4<sup>th</sup>-7<sup>th</sup> June 2007.

## Discussion on the Interaction between Transformers and the Power Systems

**Guilherme Sarcinelli Luz\* on behalf of  
Cigré-Brazil Joint Working Group  
JWG – A2/C4-03 – Electrical Transient Interaction between  
Transformers and Power Systems  
Brazil**

### SUMMARY

A general increase in transformer dielectric failures in the Brazilian transmission system, some of them with no specific causes, motivated the start up of a Cigré Joint Working Group JWG A2/C4–03 Electrical Transient Interaction between Transformers and the Power System. This group has been gathered to assess and discuss the different types of electrical transient interaction between transformers and other components of the T&D power system that could explain some of these failures.

The main focus of the JWG is to pursue an improvement of the system reliability based on recommendations regarding the electrical transient interaction between transformers and the power system. This takes into account the necessity of detailed transient studies looking for an upgrade in equipment specifications, system planning and operation criteria. The working group started its activities in May 2005 and is composed of around 30 members, representing utilities, research center, manufacturers, universities and the national grid system operator.

The objective of this paper is to present the work that has been carried out so far by the JWG including the main discussions and the conclusions already reached.

### KEYWORDS

Transformers – Switching transient – Reliability – Electrical System Interaction

\* e-mail: [guiluz@furnas.com.br](mailto:guiluz@furnas.com.br)

FURNAS Centrais Elétricas  
Rua Real Grandeza, 219 Bloco E sala 110 - CEP. 22283-900 - Rio de Janeiro – Brazil

## 1. INTRODUCTION

In recent years some transformer failures due to system interaction have been reported from members of the Brazilian Study Committees A2 and C4. These reports have motivated the engineering teams of utilities, transformer manufacturers and independent research centers to start a Joint Working Group to study this problem named JWG – A2/C4-03 - Electrical Transient Interaction between Transformers and Power Systems.

The main focus of this JWG is to improve the system reliability by suggesting additional recommendations after a better understanding of the oscillatory phenomena resulting from the interaction between the transformer and its surrounding electrical environment after a transient event.

The objective of this paper is to present the work that has been carried out so far by the group, including the main discussions and the conclusions already reached. The main topics are summarized below:

- Brazilian utility experiences regarding transformer failures related to system transients;
- Transient system studies in order to evaluate a range of frequencies that appears during switching in substations of different voltage level and arrangements;
- Presentation of the first results related to circuit breaker switching in substations of different utilities up to 500 kV.

Programs for electromagnetic transient simulation in time-domain have been used for years to calculate system overvoltages and to provide the necessary data for an optimized insulation coordination based on the peak voltage. With the current experience, it is possible to conclude that, peak values, although very important, are not the only risk factor for the transformer. Also the oscillatory excitation involving the specific interaction of each piece of equipment with the system, due to transient events, should be taken into account.

Some oscillatory excitation, even of low amplitude, may occur in frequencies that interact with a transformer winding part resulting in a local amplification due to resonance. As the transformers are constantly exposed to transient events such as lightning, switching operations, short-circuits, etc. the resonances at singular points in the winding may continuously stress its insulation leading to a failure, sometimes hours after the events.

The report of the members' experiences and the simulation of several substation arrangements for different voltage levels frequently used in Brazil provided the basis for the coming discussions. Transformer standards and specifications are asked to be reconsidered in order to establish an adequate compromise between the equipment operational reliability and the necessary clarity and impartiality to evaluate designs of different manufacturers.

## 2. UTILITY EXPERIENCES: TRANSFORMERS AND POWER SYSTEM INTERACTION

Some important transformer failures have occurred in the Brazilian transmission system in the last ten years. In some cases, a clear diagnosis could not be achieved but the evidences led to switching operations as the most probable cause. The analysis of these occurrences motivated the development of large scale electromagnetic transient simulations with the objective of quantifying not only the magnitude but mainly typical frequency ranges of the high frequency transient voltages in the transformer terminals. These voltages were generated by the switching-on operations, in substations of different configurations and voltage levels. The results of these evaluations were a valuable contribution to the CIGRÉ Brazilian JWG-A2/C4-03 and will be discussed in the next items.

The experience of some Brazilian utilities (CEMIG, CHESF, CTEEP, ELETRONORTE, ELETROSUL and FURNAS) with occurrences involving interaction between transformers and power system are described below:

**Case 1:** Unexplained dielectric failures of two 500/345/13.8 kV – 400 MVA autotransformers, a few days from each other, in February 1995, led the utility to review its traditional approach regarding the

transformer reliability. After exhaustive analyses, a common cause suggested for these failures, although not proved, was the occurrence of internal overvoltage due to frequent switching in the substation. This fact showed the necessity to improve discussions with the manufacturer about the electrical system environment and design based on a better understanding of the interaction of the power system and transformers. Some actions have been taken with this aim, including switching transient simulations studies with more realistic transformer models and field measurements to subsidise new transformer specifications and reproduce system disturbances [1].

**Case 2:** During a no-load 230/138/13.8 kV – 55 MVA transformer switching, through the 230 kV bus tie breaker, a flashover occurred in the 13.8 kV bushings leading to a short circuit to earth. The 13.8 kV transformer terminals were operating in an open condition and were not protected by lightning arresters. Failure analysis showed that the dominant frequency of the transient voltages calculated in the 230kV terminals is very close to one of the winding resonant frequencies, which corresponds to the highest amplification factor in the 13.8 kV terminals. The resonant frequencies related to the 230/13.8 kV voltage ratio were determined by field measurements of the frequency response.

**Case 3:** Dielectric failures have been registered in single phase units of different manufacturers, since the 16/16/500 kV – 555 MVA step-up transformer banks started their operation in 1988. Short circuits between turns in the HV winding, between HV and LV windings, and LV winding to ground were observed. Digital simulations of no-load breakers and disconnectors switching in the 500 kV terminals and frequency response measurements showed that the transient voltage dominant frequencies were very close to the windings resonant frequencies for some units, leading to the highest amplification factors in the 16 kV terminals. Simulations and field measurements of the transient voltages presented very close frequency ranges.

**Case 4:** In a group of twelve 765/345/20 kV – 500 MVA single-phase autotransformers of different ages and manufacturers, four units failed within six months in 2005, leading the utility to conduct a detailed investigation to determine possible causes. During this investigation, a new failure occurred in April, 2006. This substation has 9 shunt capacitor banks of 200 Mvar each that were gradually included in the 345 kV sector due to the necessity of voltage control in this system area. The high number of switching of these capacitive units was considered as a possible cause of such failures. However, site measurements and digital analysis have not shown any relation between the failures and these operations so far.

**Case 5:** In 1994 there was a failure in a 13.8/550 kV – 378 MVA step-up transformer due to very fast transients associated with disconnecting switching operation in the 550 kV GIS. The analysis performed by a team composed of utility, manufacturer and research center engineers, with the help of digital simulation, field measurements and analysis of the transformer internal insulation withstanding, confirmed that the very fast transients were the fundamental cause of the failure. The failure involved mainly turn to turn, disk to disk close to the HV terminal and main duct insulation between HV and LV windings.

**Case 6:** In 1988 some minutes after a phase to ground fault in a 460 kV transmission system followed by automatic reclosure, there was a dielectric failure in one phase of a 550/460/13.8 kV – 300 MVA transformer bank. The internal inspection concluded that there had been an electric discharge between contacts of the tap changer. The frequency response measurement carried on the regulation winding showed significant resonance in the range of 4 to 6 kHz which is typical of switching surges. So the transformer failure was considered a direct consequence of the system disturbance mentioned above.

### 3. DIGITAL SIMULATIONS

In accordance with the scope of the Brazilian JWG-A2/C4-03, this item presents the investigations carried out by the Brazilian utilities and research center members of the group, concerning transformers energization at different voltage levels and substation arrangements. A brief description of the modelling guidelines, the studies performed and the results achieved are presented below.

### 3.1 Modeling guidelines

An accurate simulation requires a valid representation of network components for a specific frequency range that usually corresponds to some particular transient phenomenon. An acceptable representation of each component in a wide frequency range is very difficult, and even practically impossible for some components [2]. In this work, the objective of electromagnetic transient studies is to quantify the magnitude and typical frequencies range of the high frequency transient voltages in the transformer terminals produced by the switching-on operations. According to reference [3], these studies can be classified as fast transients and the associated frequencies can vary from 10.0 kHz up to 3.0 MHz. Due to the involved frequency spectrum, the frequency dependence of the parameters should be taken into account, when possible, in models for transmission lines, substation buses and power apparatus. To do this, modeling guidelines based on reference [2] are applied. The present section describes the adopted approach. In all transient studies, digital simulations were carried out using the Alternative Transients Program (ATP) [4].

#### a) Power transformer modeling:

In this work three different power transformer models were considered:

- I) Simple lumped capacitance to ground: This model is traditionally applied in insulation coordination studies;
- II) Network of lumped capacitances: A more accurate model supported by the manufacturer, considering capacitances between windings, windings to core and windings to ground as well as bushing capacitances;
- III) Frequency-dependent equivalent model (black box): An equivalent RLC network obtained from field measurements (admittance curve in the frequency-domain). This model is usefully when frequency responses are available. The black box model was obtained using a recent implementation of the Vector Fitting routine [5, 6], called Matrix Fitting [7] or with the software Sintnet [8].

#### b) Substation and transmission lines modeling:

The substation apparatus, such as circuit breakers, disconnectors and instrument transformers were represented by their stray capacitances to ground, as proposed in [2]. All the equipment locations were derived from the substation layout drawings. Mostly, frequency-dependence of transmission lines parameters were taken into account using ATP JMarti setup [4]. Substation buses and conductors between discontinuity points inside the substation, and connections between substation apparatus were represented by line sections, modeled as three-phase untransposed distributed parameter, taking frequency-dependence into account, if they are long enough. Otherwise, a lumped impedance was used.

### 3.2 Case studies – description and results

The purpose of these studies was to determinate the amplitudes of the high frequency voltages and their frequency range that appear during transformer energization. A brief description of the substation arrangement, the studies performed and the results achieved are presented below:

#### 3.2.1 Description

**Study 1 – CEMIG:** Ouro Preto II substation has an arrangement of breaker-and-a-half with three 345kV line transmission bays. The 500/345/13.8 kV – 400 MVA autotransformers are connected directly to the bus and are switched by either one of the transmission line circuit breakers. The distance between the breakers and the autotransformers varies from 60 to 120 m. In this study, the circuit breaker by which the transformers were energized was varied, considering or not the presence of a 345 kV reactor bank installed at one of the transmission line bays for voltage control. This reactor is around 200 m away from the closest transformer. Circuit breakers has no pre-insertion resistor.

**Study 2 – CHESF:** Campina Grande II 230 kV substation has a main and auxiliary bus arrangement, with ten transmission lines and six transformers. Simulations were performed for the no-load switching-on of a 230/138/13.8 kV – 55 MVA transformer, through the transformer breaker (20 m away) and through the transfer breaker of the substation (128 m away).

**Study 3 – CHESF:** Luiz Gonzaga 500 kV substation has a breaker-and-a-half bus arrangement, with six transmission lines and three links of about 400 m for interconnection with the Luiz Gonzaga hydroelectric power plant. In the power plant there are three step-up transformer banks of 16/16/500 kV – 555 MVA. Simulations were performed for the no-load switching-on of a transformer bank with respective link (400 m away).

**Study 4 – FURNAS:** The 345 kV sector of Tijuco Preto substation has a breaker-and-a-half bus arrangement of 700 m length, ten transmission line bays, four autotransformer banks and four islands of capacitor shunt banks. Each 765/345/20 kV – 500 MVA autotransformer is around 190 m away from two possible breakers for its switching. Simulations were performed for the no-load switching-on of transformer banks of two different manufacturers with and without pre-insertion resistor (R) represented. Autotransformer bank for each manufacturer were represented by two different models.

**Study 5 – CEPEL:** The 230 kV substation studied was a typical double bus, single breaker arrangement, with six lines and one 345/230/13.8 kV – 225 MVA autotransformer bank. The transformer was energized, from the 230 kV side, considering two basic substation configurations: first, switching the breaker that connects the autotransformer directly to the two main buses (i.e., the transformer circuit breaker); second, switching the bus tie breaker, which is located within a longer distance from the switched transformer. Both circuit breakers were not provided with closing resistors. Separating distances between switched breaker and the transformer being energized are, approximately, 60 and 180 m, respectively.

**Study 6 – ELETROSUL:** Campos Novos 525 kV substation has a breaker-and-a-half arrangement with six bays, four transmission lines and two 525/230/13.8 kV – 672 MVA single-phase autotransformer banks. The simulations took into account the autotransformer being switched by the bus circuit breaker (BCB), and by the tie circuit breaker (CCB) with and without the 800 Ω pre-insertion resistors (R). The autotransformer bank was modeled by a 3 nF capacitance which represents its impedance for 150 kHz.

**Study 7 – CTEEP:** Aparecida 230 kV substation has a ring bus, two transmission bays and three 230/88 kV – 60 MVA transformer banks. An analysis of the energization of the third bank from the 230 kV side, 72 m away from the circuit breaker was made. Measurement during its energization and simulation using the ATP program with the transformers modelled as concentrated 2 nF, 3 nF and 4 nF capacitances were performed.

**Study 8 – ELETRONORTE:** Tucuruí I 500 kV substation has a breaker-and-a-half bus arrangement, with three transmission lines and six links of about 1000 m for interconnection with twelve generators of the hydroelectric power plant. Simulations were performed for the no-load switching-on of a 550/230/13.8 kV – 450 MVA transformer bank with respective link (170 m).

### 3.2.2 Results

Figures 1 to 10 typify the results (voltage in the terminal of the corresponding transformer) and Table I summarizes the main parameters and values obtained in the studies.

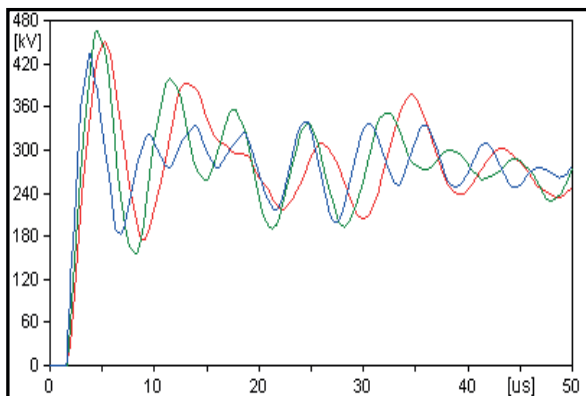


Figure 1: Study 1 – Model I (green); Model II (red) and Model III (blue)

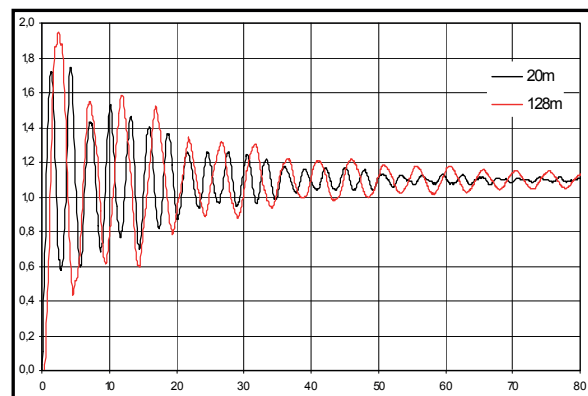


Figure 2: Study 2 – Breaker distance 20 m (black) and 128 m (red)

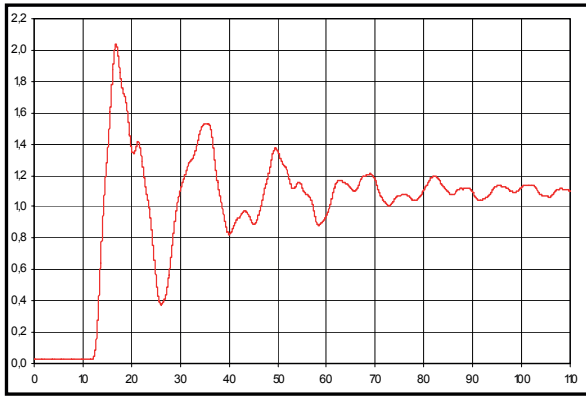


Figure 3: Study 3 – Breaker distance 400 m

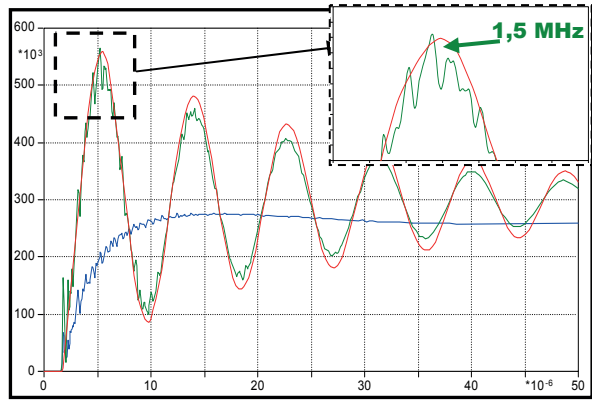


Figure 4: Study 4 – Manufacturer A - Models: I-without R (red); III-without R (green); III-with R (blue)

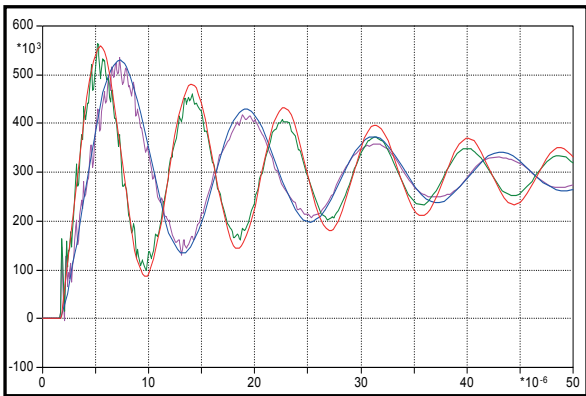


Figure 5: Manufacturer A Models I (red); III (green) (Study 4) Manufacturer B Models I (blue); III (violet)

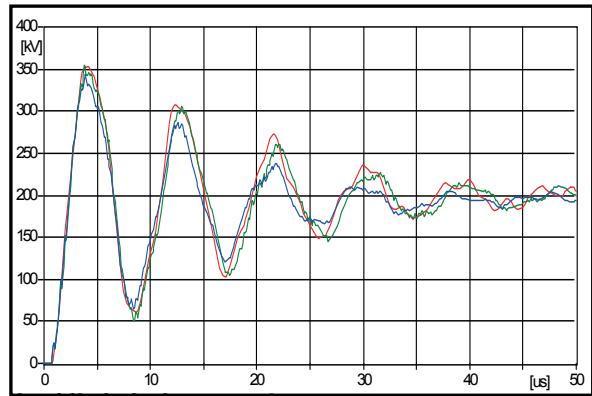


Figure 6: Study 5 – Breaker distance 180 m Models: I (blue); II (green) and III (red)

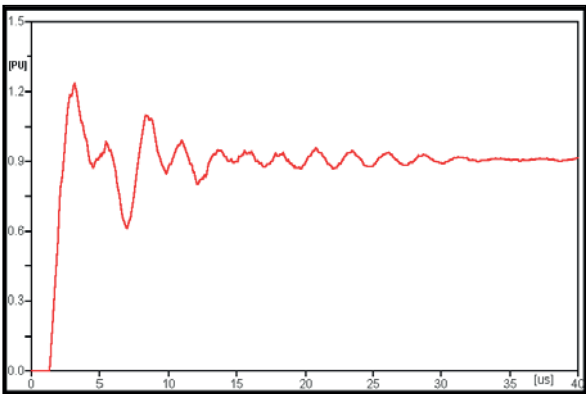


Figure 7: Study 7 – Breaker dist. 170 m (simulation)

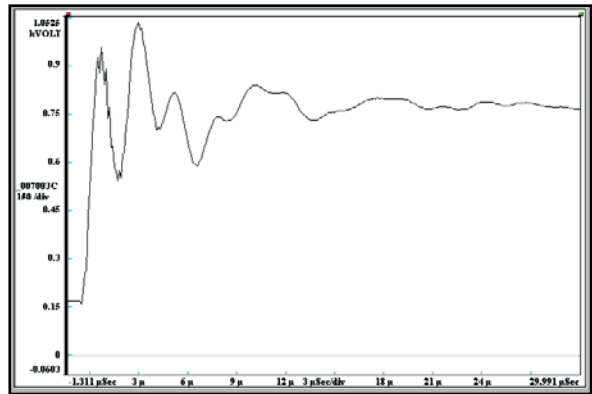


Figure 8: Study 7 – Breaker dist 170 m (measurement)

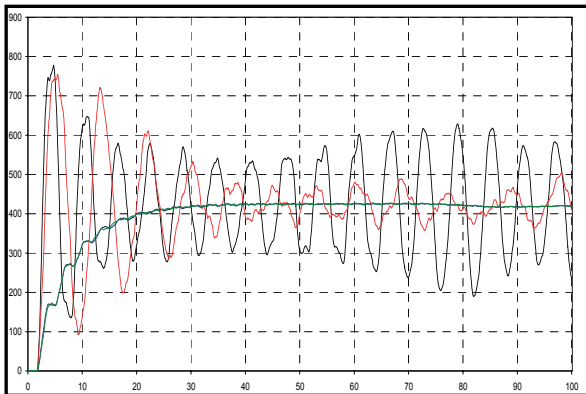


Figure 9: Study 6 – BCB without R (black); with R (blue); CCB without R (red); with R (green)

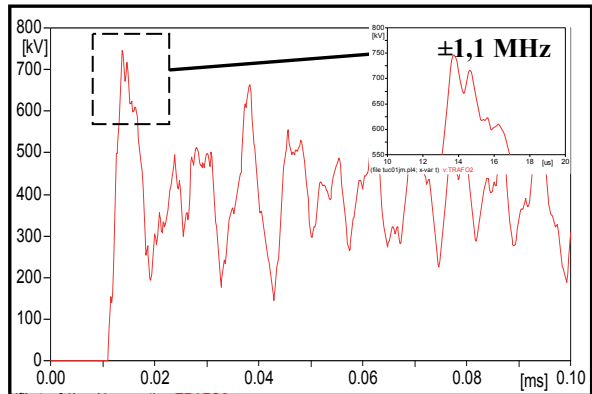


Figure 10: Study 8 – Breaker distance 170 m

**Table I – Summary of simulations results**

<b>Study</b>	<b>Voltage level (kV)</b>	<b>Station layout</b>	<b>Switched equipment</b>	<b>Breaker distance (m)</b>	<b>Maximum overvoltage (pu)</b>	<b>Dominant frequency (kHz)</b>	<b>Model (item 3.1a)</b>
1	345	Breaker-and-a-half	Autotransformer 500/345/13.8 kV – 400 MVA	123	1.60	100	I
					1.65	140	II
					1.54	180	III <sup>(1)</sup>
2	230	Main and auxiliary bus	Transformer 230/138/13.8 kV – 55 MVA	20	1.75	340	I
				128	1.95	210	I
3	500	Breaker-and-a-half	Transformers 500/16/16 kV – 555 MVA	540	2.04	60 -70 140 -170	I
4	345	Breaker-and-a-half	Autotransformer 765/345/20 kV – 500 MVA Manufacturer A	190	1.98	117	I <sup>(3)</sup>
				190	2.00	117	III <sup>(2)</sup>
			Autotransformer 765/345/20 kV – 500 MVA Manufacturer B	190	1.89	85	I <sup>(3)</sup>
				190	1.90	85	III <sup>(2)</sup>
5	230	Double bus, single breaker	Autotransformer 345/230/13.8 kV – 225 MVA	60	1.94	194	I <sup>(3)</sup>
				60	1.93	194	II
				60	1.93	193	III <sup>(2)</sup>
				180	1.88	117	I <sup>(3)</sup>
				180	1.88	117	II
				180	1.87	118	III <sup>(2)</sup>
6	500	Breaker-and-a-half	Autotransformer 525/230/13.8 kV – 672 MVA	186	1.81	157	I
				186	1.76	122	I
7	230	Ring bus	Transformer bank 230/88 kV – 60 MVA	72	1.24	180 380	I
8	500	Breaker-and-a-half	Transformer bank 525/230/13.8 kV – 450 MVA	170	1.84	100	I

<sup>(1)</sup> Using Vector Fitting

<sup>(2)</sup> Using SINTNET

<sup>(3)</sup> Equivalent capacitance obtained from the frequency response model for the dominant frequency

#### 4. CONCLUSIONS

The paper presented the investigation carried out up to now by the Brazilian JWG–A2/C4-03 to study the electrical transient interaction between transformers and the power system. ATP simulations of transformer energization were performed, considering different voltage levels and substation arrangements, and the results pointed out the importance of a better knowledge of transformer behaviour in the range of 40 kHz to 200 kHz. Significant voltage stresses in these frequencies may not be very well represented by the standard dielectric tests or taken into account during the project which can contribute to equipment failures.

Cases where frequencies greater than 200 kHz were observed –were those corresponding to the ring substation arrangement or with very small distance between the transformer and the circuit-breaker. For larger distances between the transformer and the circuit-breaker, the oscillation frequencies presented lower spectrum, considering the same transformer modeling.

As far as the transformer modeling is concerned, application of Vector Fitting and SINTNET routines seemed to give more accurate results with the voltage transients having relatively greater attenuation and smaller amplitudes caused by the resistances of the equivalent RLC circuit provided.

It was also observed that the simple lumped capacitance model representation may lead to similar results if the equivalent capacitance is obtained from the frequency response model for the dominant frequency because, in this case, this dominant component will be well reproduced. The other components, as a consequence of the model simplification, might not be well reproduced.

The application of pre-insertion resistors is one of the conventional solutions to reduce the overvoltage magnitudes on the transformer terminals and to increase the voltage attenuation.

## 5. JWG-A2/C4-03 NEXT STEPS

The group next main task will be to find a reasonable way to use the transient study results to identify risk factors that may increase the probability of transformer failures due to transients and help evaluate the necessity of a case-by-case analysis and propose an upgrade of the transformer specifications design review practices and an improvement of standard dielectric tests to make them more representative.

It is relevant to point out the advantages of joint evaluations involving different experiences such as utilities, research center, manufacturers, universities and the national grid system operator, as the work being done by the JWG-A2/C4-03 of Cigré-Brazil, especially when the solution depends not only on the power system but also on the characteristics of the equipment.

JWG-A2/C4 is composed by the following members:

Angélica da Costa O. Rocha (CEMIG) – Convener; Alecio Barreto Fernandes (ONS); Álvaro Portillo (TRAFO-Consultant); Antonio Carlos S. de Lima (UFRJ); Antonio Roseval F. Freire (CHESF); Camilo Machado Jr. (ELETORNORTE); Carlos Ossamu Kajikawa (ELETROPAULO); Davi Sixel Arentz (FURNAS); Fernando Rodrigues Alves (CHESF); Francisco Salgado Carvalho (CEPEL); Gilson Machado Bastos (FURNAS); Guilherme Sarcinelli Luz (FURNAS); João Maria Fontoura Júnior (COPEL); José Carlos Mendes (ABB); José Francisco Lofrano de Oliveira (TRAFO); José Renato Torrens (WEG); José Toshiyuki Honda (ELETORNORTE); Luiz Henrique S. Duarte (CEMIG); Methodio Varejão de Godoi (CHESF); Roberto Asano Junior (SIEMENS); Roberto Vaisman (CEPEL); Rogério Lima Tompson (CTEEP); Rogério Magalhães de Azevedo (CEPEL); Sebastião Otávio Moreira (CEMIG); Ulisses R. R. Massaro (ELETROSUL); Walter Carvalho Pereira (VONCKEL/DOBLE)

## BIBLIOGRAPHY

- [1] Rocha, A.C.O. et al., “Análise das falhas dos autotransformadores da SE São Gotardo 2 - Enfoque na ressonância parcial de enrolamento”, GSI – XV SNPTEE, 17 a 22 de Outubro de 1999, Foz do Iguaçu – Paraná – Brasil (in portuguese).
- [2] IEEE WORKING GROUP 15.08.09, “Modeling and Analysis of System Transients Using Digital Programs”, Piscataway: IEEE PES Special Publication, 1998.
- [3] Working Group SC 33-02 CIGRÉ, “Guidelines for Representation of Network Elements when Calculating Transients”, Technical Brochure CE/SC GT/WG 02, 1990.
- [4] LEUVEN EMTP CENTER, “ATP – Alternative Transient Program – Rule Book”, Herverlee, Belgium, July 1987.
- [5] Gustavsen, B., Semlyen, A., “Rational Approximation of Frequency Domain Responses by Vector Fitting”, IEEE Trans. on Power Delivery, Vol. 14, Iss.3, pp. 1052-1061, July 1999.
- [6] Gustavsen, B., “Application of Vector Fitting to High Frequency Transformer Modeling”, IPST 2003, New Orleans, USA, 2003.
- [7] Online available: <http://www.energy.sintef.no/produkt/VECTFIT/index.asp>.
- [8] Azevedo, R. M., Junqueira, A. J. S., “Programa Sintnet – Síntese de redes para modelagem de equivalentes em frequência – método de Cauer”, Relatório CEPEL 851/95 – DPP/TEC, 1995.

## At the Edge of Voltage Collapse in Slovenian Power System After Outage of NPP Krško and 400 kV Node Tumbri

M. STOJSAVLJEVIĆ\*, D. NEMEC  
Energy Institute Ltd. Zagreb

I. TOLJAN  
HEP (Croatian Electricity Utility), Zagreb  
CROATIA

### SUMMARY

A major disturbance that resulted in the tripping of the 400 kV line Tumbri (HR) – Hévíz (H) and the entire 400 kV node Tumbri in the Croatian system occurred on 27 August 2003 and almost led to a voltage collapse in that area. The disturbance was initiated by an accidental outage of a generator at NPP Krško (SLO) due to a human error during regular maintenance work. Its further development was the consequence of a hidden fault of the numeric protection at the 400 kV switchyard Tumbri. In the specific system operating conditions (network configuration and generator scheduling) at that moment, the systems of Slovenia and Austria in the central part of the UCTE system were brought near voltage collapse. At the same time the operational security level of the power systems of Croatia and BiH, then at the perimeter of the UCTE system, was also decreased.

The sequence of events is described and discussed in the paper. Recordings of frequency and active power in representative transmission lines, taken at NDC Zagreb, are also given. A simulation analysis was performed first for the real disturbance scenario and then for the hypothetical scenario in which there was no failure of the protection at Tumbri substation and consequently the 400 kV node Tumbri would have remained in operation. The simulations showed that the loss of a NPP Krško generator would have only a local impact and would be barely noticeable at the UCTE level had the 400 kV node Tumbri remained in operation. Simulation results are in accordance with information obtained from the Slovenian power system where severely depressed voltages were recorded, particularly in the area around NPP Krško. It was also observed that the Slovenian system was acting as a reactive power sink while active power was flowing in the opposite direction, i.e. towards Croatia.

Assessment of Croatian system security during the disturbance with respect to voltage stability, frequency and angle stability and congestion criteria was done on the basis of measurements and simulation results. The conclusion was that Croatian system security with respect to all the above mentioned criteria was preserved but it must be stressed that the initial system operating conditions were rather favorable from the stability point of view.

### KEYWORDS

Power system dynamics, power system security, outage, voltage and angle stability, relay protection

\* milan.stojsavljevic@ie-zagreb.hr

# 1. INTRODUCTION

Major disturbances in power systems have serious technical and economic consequences. The analysis of actual disturbances point to technical and/or organizational weaknesses in the system and makes it possible to take measures to remove the observed deficiencies. At the same time, the analysis of how the system behaves during the disturbance enhances the understanding of its characteristics. This is important for predicting possible states and scenarios in which system security is jeopardized.

An especially tricky situation occurs when disturbances occur at such points or with such an intensity that they significantly affect the operation of neighboring systems or even a broader area. The analysis of such events requires close cooperation among operators, including exchange of available information, records and measurements. Large-scale disturbances also mean real primary verification of system protection actions, from local plant level to special protective schemes at system level.

The present paper describes an event which included the outage of a major power plant and several interconnection lines, affecting a number of power systems (principally Slovenia (SLO), Croatia (HR), Austria (A) and Hungary (H)).

# 2. POWER SYSTEM CONFIGURATION AND STEADY STATE

The configuration of Croatia's 220 and 400 kV transmission network and its interconnections with neighboring systems is shown in Figure 1. The nuclear power plant Krško (NPP Krško), a generating facility located near the Croatian-Slovenian border, is used jointly by the Croatian and Slovenian utilities in the ratio 50:50. The 400 kV node Tumbri and/or the 400/110 kV Tumbri substation is a key point for the supply of the local power system of the city of Zagreb (HR) and its surroundings. Incidentally, this fact was actually confirmed by an event that took place on January 22, 2003. On that day, a failure of one 110 kV circuit breaker in Tumbri substation and action of bus protection led to the outage of the 110 kV node Tumbri and subsequent blackout in the city of Zagreb and north-western Croatia.

The interconnections between the Hungarian and Croatian systems, a 400 kV double-circuit line Tumbri (HR) – Hévíz (H), built and operating at that time as a single circuit, is significant for the security of the Croatian power system and it establishes an important electricity transit route, Hévíz (H) – Tumbri (HR) – Melina (HR) – Divača (SLO) – Italy (I), from the northeast to the southwest of the UCTE interconnected system. Consequently, the availability and any disturbance of this interconnection is of special interest for the UCTE interconnected system and for the Croatian system as its part.

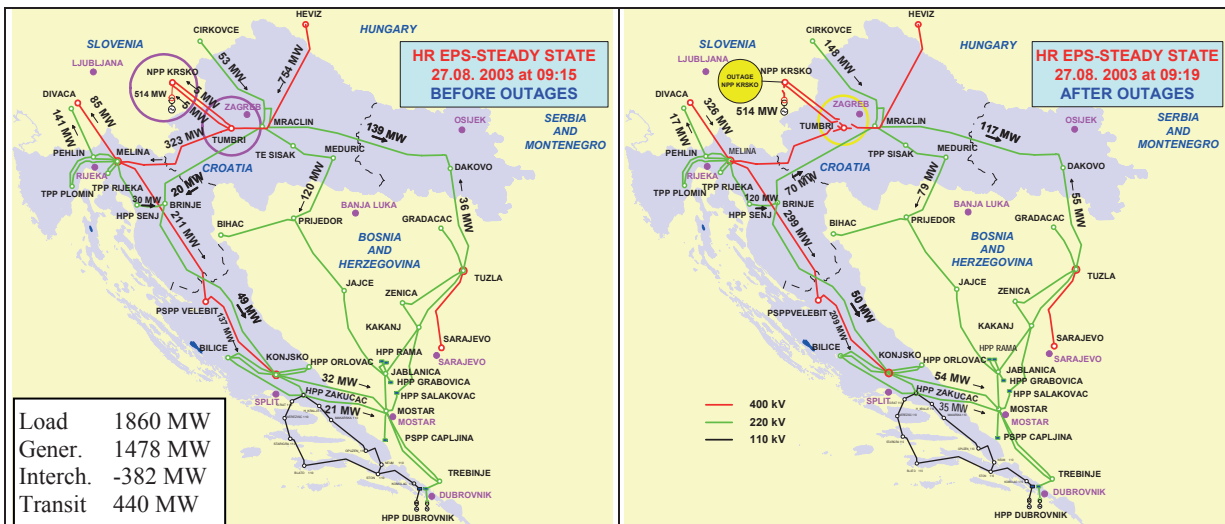


**Figure 1** Configuration and power flows in HR system before outage of NPP Krško and 400 kV node Tumbri

**Figure 2** Configuration and power flows in HR system after outage of NPP Krško and 400 kV node Tumbri

The event considered occurred on August 27, 2003 at 9:15:10.008. The transmission networks of Croatia and BiH and their mutual interconnections at that time (Figure 1) were not built at the today level. In the Croatian system the 400 kV Žerjavinec and Ernestinovo substations did not exist then so that the eastern part of Croatia was connected to the Zagreb area at the 220 kV level (Figure 1, the 220 kV line Mraclin – Đakovo). As mentioned above, in operation was only one circuit of the present-day double circuit 400 kV interconnection TS Žerjavinec – TS Hévíz, introduced into Tumbri substation.

Active power before the event was flowing from the north-eastern toward south-eastern part of the UCTE system through Hungary, Austria, Croatia and Slovenia, with the concentration of demand being in Slovenia, Italy, Croatia and BiH. Interestingly, due to relatively low voltages in Austria (southern part) and Slovenia, reactive power flows had the opposite direction, i.e. from Italy and Croatia through Slovenia to the southern part of Austria. It should be noted that active power flow from Hévíz to Tumbri (Figure 1) immediately before the event was 754 MW.

Following the outage of a NPP Krško unit and subsequent tripping of the 400 kV node Tumbri, active power began to flow through Austria, Germany and Italy toward Slovenia, Croatia and BiH where power imbalance further increased due to the outage of the NPP Krško unit. Voltage conditions deteriorated in Austria and Slovenia especially after the connections between Austria and the Czech Republic were switched off. These connections were in fact switched off by the first action of the system protection (“Sollbruchstelle”) in the Austrian system. The area around the 400 kV node Krško was especially critical and on the brink of voltage collapse. The results of simulation of system dynamics undoubtedly show and confirm that, as illustrated below. Reactive power continued to flow from Italy and Croatia through Slovenia toward the southern part of Austria, now in greater amounts.

Active power flows on the lines before (09:15) and after (09:19) the outage of the Krško NPP unit and the 400 kV node Tumbri are also shown in Figures 1 and 2.

Demand in the Croatian power system immediately before the disturbance was 1860 MW and was covered by production from domestic sources of 1478 MW and from import of 382 MW (including 50% of power from Krško NPP or 257 MW). Roughly two thirds of the import balanced the southern part of HR system and one third was used to balance the wider Zagreb area. The notified transit of active power through HR system for BiH system was 160 MW and the undeclared transit for an unknown user was 280 MW. Due to an especially long dry period most of production within the HR system originated from thermal power plants located in the wider Zagreb area (about 620 MW) and from thermal power plants in the western part of HR system (TPP Rijeka and TPP Plomin 1 and 2 whose total dispatched power was about 600 MW). These sources were connected to the 110 kV and 220 kV levels of the transmission network not affected by the disturbance which proved to be of decisive importance for maintaining the overall stability of the Croatian system in this particular case..

### 3. CHRONOLOGY OF EVENTS

The situation before the disturbance in all power systems considered was normal. The disturbance began by the outage of the NPP Krško unit (09:15:10.008) during a routine testing, whose production at the time was 514 MW. Loss of this production caused power flow to increase on the 400 kV line Hévíz – Tumbri after which circuit breaker failure protection (CBF protection) was quickly activated in the 400 kV bay Hévíz in Tumbri substation (at 09:15:10.374). This protection switched off the circuit breaker in the 400 kV bay Tumbri in Hévíz substation, all 400 kV lines connected to the Tumbri node and all three 400/110 kV transformers through which the local power system of Zagreb and its surroundings is supplied from the 400 kV network. Based on the checking done at operator level, it was concluded that the circuit breaker in the bay Hévíz in Tumbri substation was o.k. and at 09:30 a switching on was attempted of all 400 kV circuit breakers in Tumbri substation with the circuit breaker in the 400 kV bay Hévíz being the last to be switched on. However, when it was switched on (09:35:12.613) CBF protection was activated again (09:35:36.679) and all elements connected to the 400 kV node Tumbri were switched off. It was concluded that the circuit breaker in the 400 kV bay Hévíz needed detailed examination and that it should not be switched on until further notice. In the next attempt, the 400 kV node Tumbri was successfully reconnected without the 400 kV line Tumbri (HR) – Hévíz (H). The system operator compensated for the loss of production (NPP Krško) in the Croatian power system by dispatching hydro generating units in the southern part of the system (Senj, Orlovac and Zakučac hydro power plants).

A specialist checking of the circuit breaker and relay protection (Figures 3 and 4) in the bay Hévíz of Tumbri substation (from 09:40 to 11:15) determined that the circuit breaker was in the proper working order and that the cause of the fault was the welded contact of the auxiliary relay in the line protection REL 531 which starts CBF protection (Figure 4). The contacts of that relay in the line protection REL 531 are not overseen by the watchdog function. The technical defect was removed by switching off in REL 531 the START-signal for CBF protection and at the same time the current threshold in CBF protection (Figure 4) was returned from 1300 A to 1800 A. After that, at 11:21 the 400 kV line Tumbri – Hévíz was also switched on. It remained to be determined at a later point why the “welding” had occurred of the auxiliary relay in REL 531.

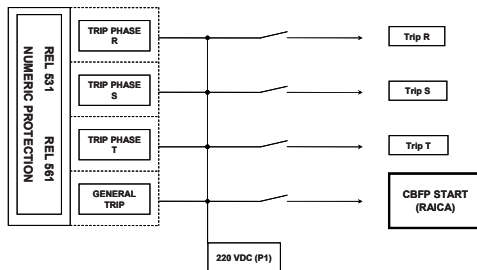


**Figure 3** Binary output configuration of numeric line protection tripping circuits

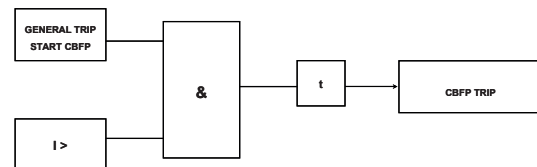


**Figure 4** Block diagram of CBF protection

The redistribution of power flows in the central part of the UCTE system (Hungary, Austria, Czech Republic,...) caused by the outage of NPP Krško and of the 400 kV node Tumbri especially in Austria’s transmission network caused overloading of the 220 kV lines and consequent activation of the system protection ( “Sollbruchstelle”) which at 09:19:14 switched off the 400 and 220 kV connections toward the Czech Republic (Dürnrohr – Slavetice and Bisamberg – Sokolnice). There ensued a dangerous loading of the lines between Austria and Hungary and dropping of voltage in the Austrian system (e.g. to the level of 91% in the node Obersielach 380). At the same time voltage in the Slovenian system fell considerably. For instance, in the 400 kV node Krško, the voltage dropped below 360 kV. The situation in the Slovenian and Austrian power systems was normalized by dispatching reserves and increasing production of reactive power in generating units.

#### 4. SYSTEM DYNAMICS RECORDING IN THE POWER SYSTEM OF CROATIA

During the disturbance described above, active power flows on the lines between Croatia and Slovenia and Hungary (Figure 5) and system frequency (Figure 6) were recorded in the Croatian power system. Figure 4 shows that the outage of a Krško generating unit caused frequency to fall by about 27 mHz. This frequency drop is relatively well correlated with the production loss of 514 MW and the regulation constant of the UCTE system of about 20000 MW/Hz.

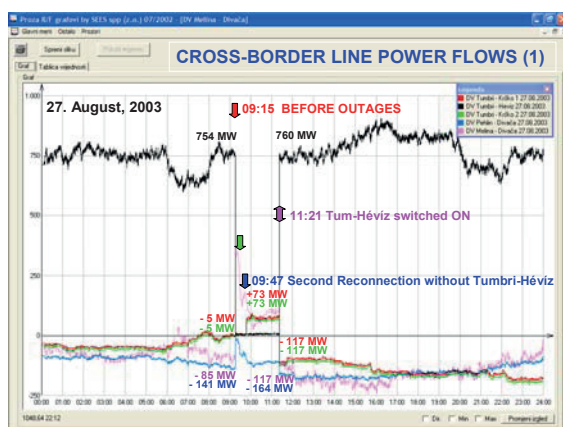


**Figure 5** Active power flows on lines between HR, SLO and H

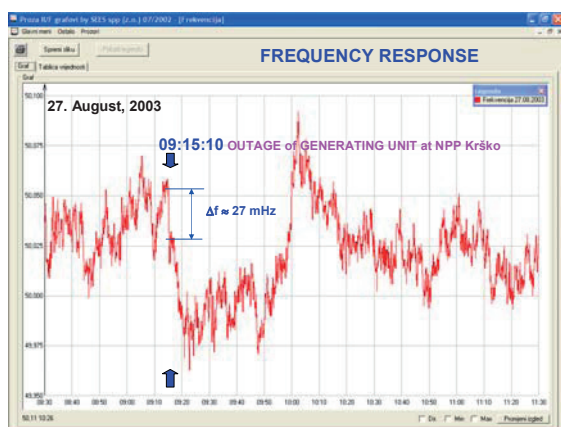


**Figure 6** System frequency chart

## 5. SIMULATION ANALYSIS

A simulation analysis on the dynamic system model has been carried out for the case of the actual sequence of events (outage of a Krško unit and consequent outage of the 400 kV node Tumbri) and for a hypothetical case consisting only of outage of the Krško unit. The objective of the simulation analysis was to preliminarily investigate:

- power flows dynamics on the characteristic lines in the Croatian power system for assessment of congestion risk, and the current dynamics on the 400 kV line Tumbri – Hévíz for analysis of CBF protection action,
- dynamics of the Croatian power system and to assess the security of the Croatian system primarily using the criterion of voltage stability and the criterion of angle stability because at that time Croatian and BiH systems were on the perimeter of the UCTE system with a characteristic mode of inter-area oscillations (with period 1.2 to 1.4 s) of a group of hydro generating units in the southern parts of the Croatian and BiH systems,
- voltage dynamics in the Slovenian system and an assessment of the trend of voltage profiles in the first 15 seconds because this system experienced a considerable loss of production in the immediate proximity of the border with the Croatian system.

The investigations were carried out using an appropriate software package for the calculation of stability on a multimachine dynamic model which comprises the power systems of Croatia and BiH (detailed model at 400, 220 and 110 kV levels), Slovenia, Austria, Hungary, northern Italy, Slovakia and the Czech Republic (400 and 220 kV) and dynamic equivalents of the remaining part of the UCTE system.

The configuration and steady state of the system were so set as to match as much as possible the situation immediately before the event (27 August 2003 at 09:15). Power system dynamics during first 15 seconds was simulated.

Considering dynamics of active power flow (Fig. 7) and current (Fig. 8) on the 400 kV line Tumbri – Hévíz, voltage dynamics of the 400 kV node Tumbri (Figure 11), time needed for current on the line Tumbri – Hévíz to reach the overcurrent threshold of CBF protection (1300 A) following the outage of a NPP Krško unit, and considering response time and delay of CBF protection operation and circuit breaker closing time, it is estimated that active power on the 400 kV line Tumbri – Hévíz at the moment of its switching off was about 900 MW. This is almost 20% higher than the power flow read from the recorded trend curve shown in Figure 5. The results of the simulation show us that the power of the disturbance was considerably greater than the one that could be read from available records. WAMS system would certainly allow a much better insight into the system in this particular and any similar situation.

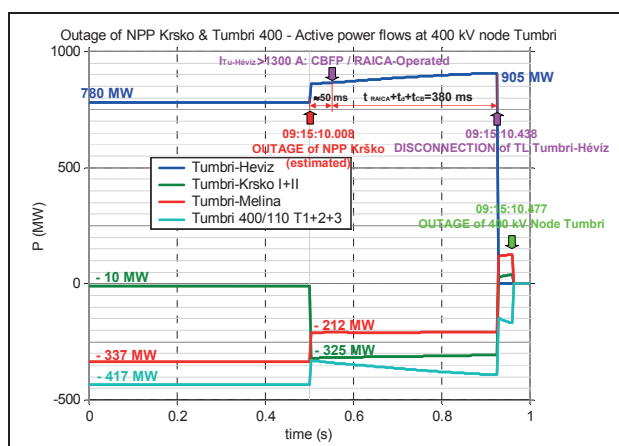


**Figure 7** Active power flow on lines connected to 400 kV node Tumbri (outage of NPP Krško and 400 kV node Tumbri)

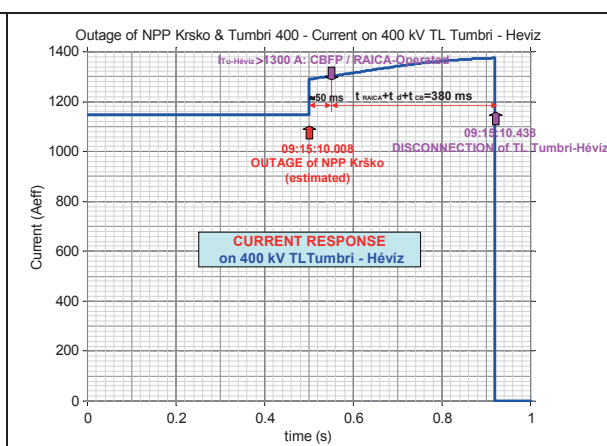


**Figure 8** Current on 400 kV line Tumbri (HR) – Hévíz (H) - (outage of NPP Krško and 400 kV node Tumbri)

The simulation analysis of power flow dynamics for both the actual event (outage of a NPP Krško unit and the 400 kV node Tumbri) as illustrated in Figure 9 and for a hypothetical event (outage of a NPP Krško unit only) as illustrated in Figure 10 shows that the security of the Croatian power system was not jeopardized during the event, neither by congestion/overloading of system elements nor by dangerous lowering of voltages. The results of the simulation analysis of voltage stability are illustrated in Figure 11 for the actual event of outage of the NPP Krško unit and the 400 kV node Tumbri and in Figure 12 for the hypothetical event (outage of the NPP Krško only).

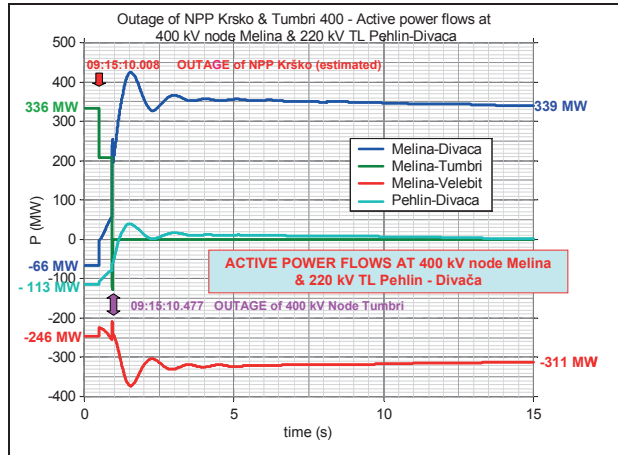


**Figure 9** Active power on characteristic lines (outage of NPP Krško and 400 kV Tumbri)

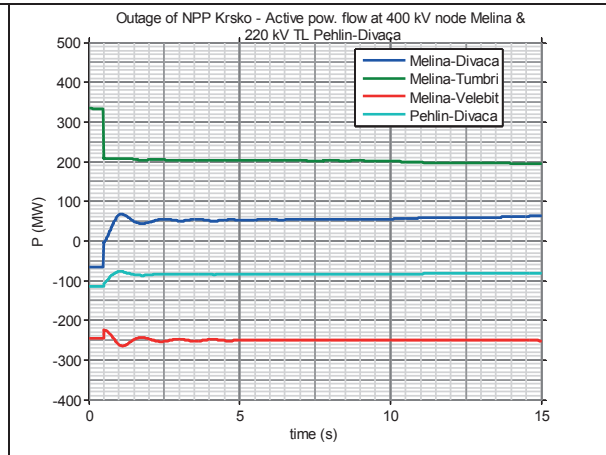


**Figure 10** Active power on characteristic lines (outage of NPP Krško only)

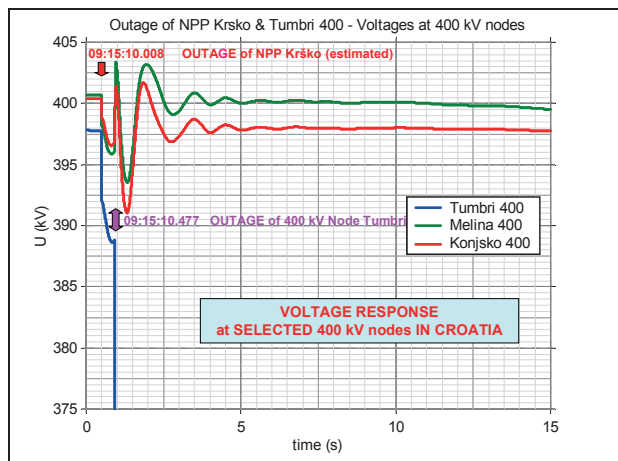


**Figure 11** Characteristic bus voltages in HR system (outage of NPP Krško and 400 kV Tumbri)

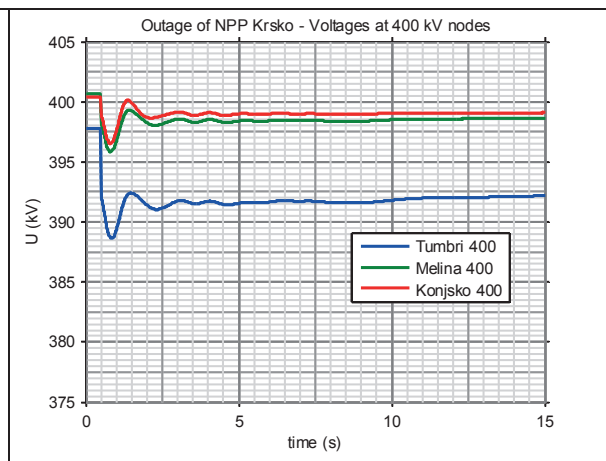


**Figure 12** Characteristic busvoltages in HR system (outage of NPP Krško only)

Regarding the security of the Slovenian system using the criterion of voltage stability, the simulation analysis shows and confirms that for the case of the actual event (outage of a Krško unit and the 400 kV node Tumbri), the critical situation was in the vicinity of the Krško substation. Voltage conditions in the Slovenian system are illustrated by voltage dynamics at characteristic points of the Slovenian system shown in Figure 13 for the case of the actual event and for the case of the hypothetical event (outage of a Krško unit only) in Figure 14. The results of the investigation show that for the case of the actual event the Slovenian system in the vicinity of Krško substation was on the brink of voltage collapse. For example, the rate of voltage decrease in the 400 kV node Krško (Fig. 13) at the end of the simulation period was 4.8 kV/s or 1.2%/s. In the case of outage of a Krško unit only, the simulation analysis shows (Fig. 14) that the voltage stability of the Slovenian system would not be jeopardized. It would be interesting to carry out a simulation analysis aimed at assessing the justifiability of activation of the system protection in the Austrian system in this particular case (outage of a Krško unit and the 400 kV node Tumbri).

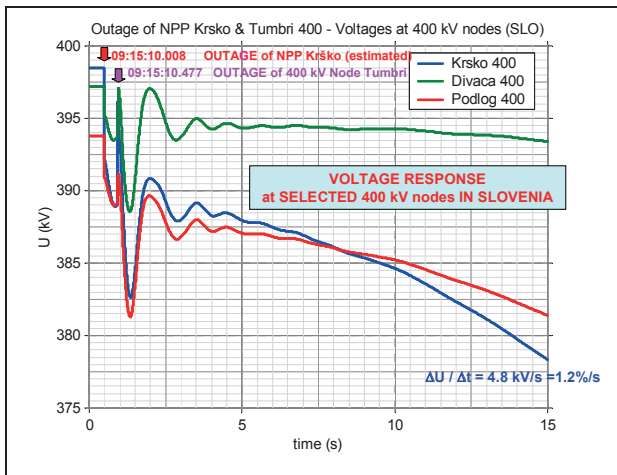


**Figure 13** Voltage at characteristic nodes of Slovenian system (outage of NPP Krško and 400 kV node Tumbri)

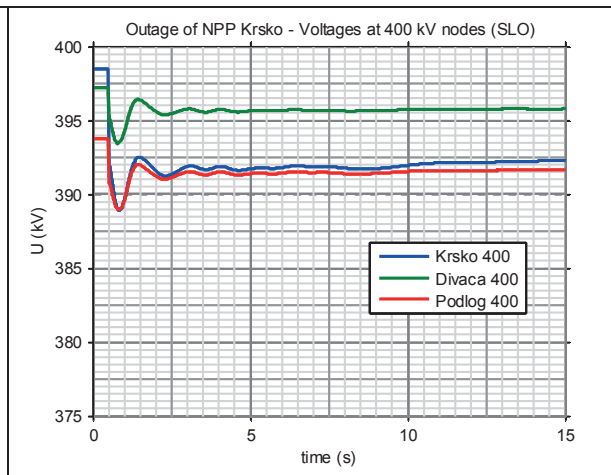


**Figure 14** Voltage at characteristic nodes of Slovenian system (outage of NPP Krško only)

It is characteristic of the Croatian and BiH systems that their hydro units in the southern parts of the system form a coherent group with the mode of inter-area electro-mechanical oscillations whose period varies between 1.2 s and 1.4 s depending on dispatching of these units. This oscillation mode and its characteristics were used to assess system security using the criteria of small signal angle stability. For this purpose the dynamics of system frequency was analyzed at characteristic system points as well as dynamics of power of generating units.

A generating unit of the Dubrovnik hydro power located at system perimeter has been chosen for illustration (Figure 1). The dynamics of active and reactive power of this unit for the case of the actual event (outage of NPP Krško and the 400 kV node Tumbri) is given in Figure 15 and in Figure 16 for the hypothetical case (outage of NPP Krško only). Roughly, based on the dynamics of active power of the unit, for both cases the oscillation frequency of this inter-area mode was 0.89 Hz, oscillations were well damped ( $\zeta_1=0.117$  in the actual event,  $\zeta_2=0.095$  in the hypothetical case) while the maximum elongation of the generator active power was 38 MWpp for the actual event as opposed to 16 MWpp in the hypothetical case.

In conclusion, the security of the Croatian system using the criterion of angle stability was not jeopardized during the actual event.

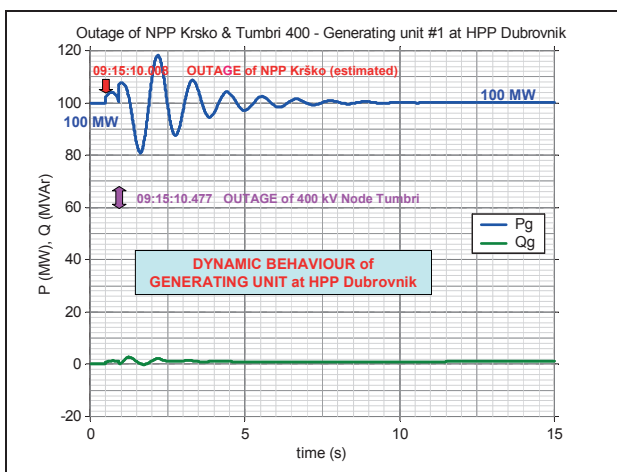


**Figure 15** Dynamic behavior of a generating unit of HPP Dubrovnik (outage of NPP Krško and 400 kV node Tumbri)

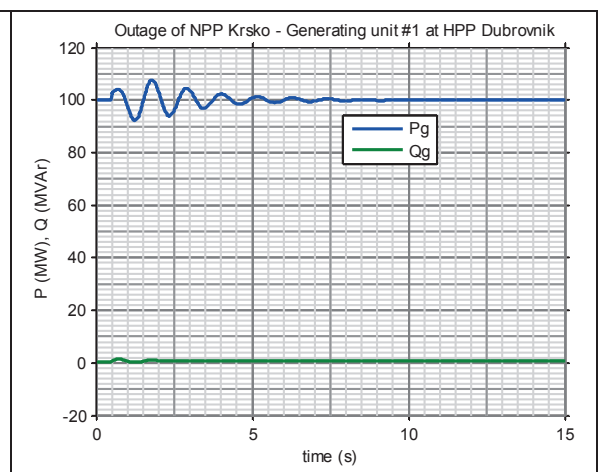


**Figure 16** Dynamic behavior of a generating unit of HPP Dubrovnik (outage of NPP Krško only)

## 8. CONCLUSION

The outage of a generating unit of NPP Krško (SLO) and outage of the 400 kV node Tumbri (HR) was a major disturbance which jeopardized in particular the Austrian and Slovenian systems. The outage of the 400 kV node Tumbri was due to the failure of an auxiliary relay in the line protection of the 400 kV line Tumbri – Hévíz which is not supervised by the watchdog function.

Overloads and consequent tripping of lines led to the weakening of connections within the UCTE system and/or to diminished operational security of all the systems affected.

The security of the Austrian system was jeopardized judging by the line overloads and voltage stability criterion.

The Slovenian system security was jeopardized judging by the voltage stability criterion. Area in the vicinity of the Krško nuclear power plant was on the brink of voltage collapse.

The security of the Croatian system was maintained across all the criteria considered: voltage stability, angle stability and the line congestion / overloads. During the disturbance, the operational security of the Croatian system was diminished due to unavailability in the transmission network.

The simulation analysis has provided a more precise insight into power system dynamics during the first 15 seconds of the disturbance. The results of the simulation for the hypothetical case of outage of NPP Krško show that it would be a local disturbance for the UCTE system. Use of WAMS would greatly enhance observability of power system dynamics.

It would be interesting to carry out a simulation to investigate the justifiability of activation of system protection in the Austrian system in this particular event.

Also, based on the experiences with this event a question arises of how to make a timely determination of hidden faults of relay protection and whether regular testing procedures should be amended accordingly.

## BIBLIOGRAPHY

- [1] Disturbance In UCTE / CENTREL Power System On 27 August, 2003 at 09:15, HEP – Croatian Electricity Utility, Vienna 23<sup>rd</sup> October 2003
- [2] Outage of the line Heviz-Tumbri Wednesday, 27<sup>th</sup> of August 2003, 09:15, and the consequences for the Austrian transmission grid, VERBUND – Austrian Power Grid, Vienna 23<sup>rd</sup> October 2003
- [3] Events on August 27th 2003 – outage of NPS Krško and line Heviz – Tumbri, ELES – Slovenian Transmission System Operator, Vienna 23<sup>rd</sup> October 2003
- [4] Outage of the line Heviz – Tumbri, Wednesday, 27<sup>th</sup> of August 2003, 09:15 and the influence to the Czech Transmission Grid, ČEPS, Vienna 23<sup>rd</sup> October 2003

## Dielectric, Switching and System Requirements under Out-of-Phase Conditions, during Synchronisation and under Comparable Stresses.

**A.L.J. Janssen**<sup>°</sup>   **F. Iliceto**   **Q. Bui-Van**   **S. Morais**   **M. Waldron**   **B. Middleton**  
The Netherlands   Italy   Canada   Brazil   U.K.   Canada

On behalf of CIGRE WG A3.13

### SUMMARY

Recent developments in electrical networks can increase the probability of out-of-phase switching and dielectric stresses being applied to open circuit-breakers, due to asynchronous systems at both sides. This report presents a systematic study of TRV-stresses associated with generator separation and system separation. TRV peak values are higher than required in the Standards, even for relatively small out-of-phase angles (75° to 90°), and the dielectric stresses are high with respect to the short-duration power frequency withstand voltages across a circuit-breaker open contacts, especially taking into consideration the external insulation under pollution and ageing processes. To the opinion of the authors, the Standards should be revised to give users clear and adequate guidance on the assessment and specification of TRV-values and dielectric withstand requirements under out-of-phase conditions.

### KEYWORDS

Out-of-phase, synchronisation, TRV, RRRV, First-Pole-to-Clear Factor (fpcf), longitudinal dielectric stress

### 1. INTRODUCTION

Within CIGRE SC A3 “High-voltage Equipment”, WG A3.13 “Changing Network Conditions and System Requirements” has investigated the impact of developments in electrical networks upon conventional high voltage apparatus. The major relevant trends identified are:

- 1) increasing implementation of distributed generation
- 2) increasing distances of bulk power transmission
- 3) increasing application of power electronics (generation, transmission, distribution and load).

One of the phenomena studied is the increased probability of out-of-phase conditions. Operating of systems closer to their limits may lead to steady-state, transient and dynamic stability problems and the problems are exacerbated by the increasing complexity of the power systems: large distances between load and power generation centres, regional concentrations of wind farms and associated power transmission and reserve problems, the changed nature of distribution grids and a trend to consider island operation of parts of the (distribution) system.

<sup>°</sup> [anton.janssen@continuo.nl](mailto:anton.janssen@continuo.nl)

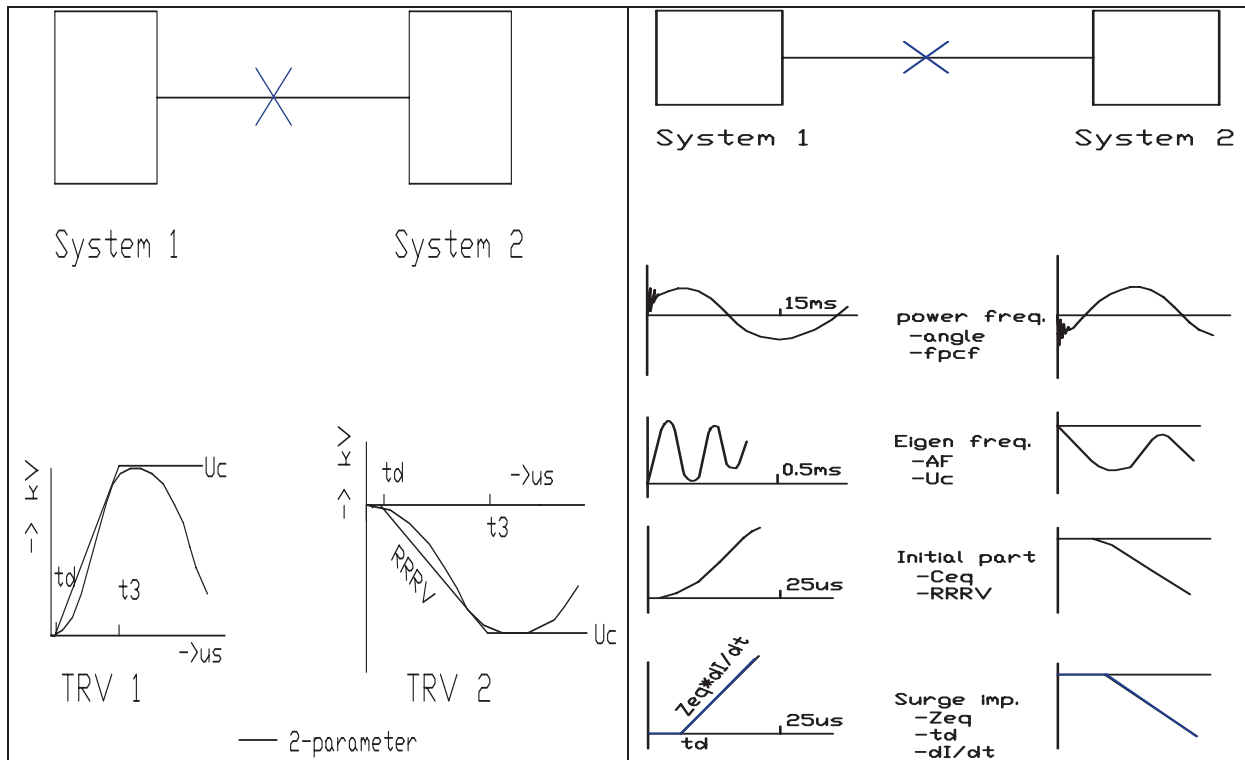


Fig. 1 Longitudinal stresses across the first-pole to clear out-of-phase

Fig. 2 Characteristics of the RV and TRV

The stresses on HV equipment, especially circuit-breakers (figure 1), under out-of-phase conditions and during synchronisation of generators and networks have been investigated and are presented in the following sections. Present Standards [1][2][3][4] define out-of-phase TRV (transient recovery voltage) and RRRV (rate of rise of recovery voltage) conditions on the basis of parameters including out-of-phase angle ( $\psi$ ), out-of-phase current ( $I_{oop}$ ), recovery voltage (RV), natural frequency, damping and amplitude factors (AF) and travelling wave behaviour. Figure 2 shows schematically the different time domains which are relevant for the TRV-studies and reference [5] presents the relation between the different parameters in 3-phase systems. The out-of-phase test duty leads to the highest TRV-peak requirements for circuit-breakers.

WG A3.13 will publish more detailed information in two CIGRE Technical Brochures during 2007.

## 2. SYSTEM CONSIDERATIONS

The circumstances that may lead to system separation, either singly or in combination, include:

- transient instability (slow fault clearing, false synchronisation of large network elements or large power plants)
- voltage instability (inadequate reactive power and/or voltage regulation, poor or adverse tapchanger control)
- small signal instability (amplification of power swings due to negative damping)
- frequency instability (system inability to react to sudden load/generation unbalances)
- cascade trippings (multiple lightning, weather conditions, overloading, vegetation growth, temporary overvoltages)
- protection mal-operation
- false synchronisation of a single generator.

Large increases in distributed generation, including many windmills and windmill parks, and multiple power transfers across longer distances, increase the probability of occurrence of many of these events as detailed in the following examples:

- medium voltage networks typically have fault clearing times which exceed the maximum clearing time for continued stability of small generating plants equipped with synchronous generators
- the optimal control of reactive power supply and voltage regulation by small generators has not been established yet
- windmills are very sensitive for wind variations, especially under high wind conditions, which may result in co-incident tripping of many units
- small cogeneration plants (e.g. for greenhouses) are operated in large groups without consideration of wider network requirements
- systems are more commonly operated up to, or even beyond, their loading capabilities
- (small) generators are tripped and synchronised more regularly than ever before
- certain distributed power generation technologies cannot provide inertial energy required for the immediate dynamic response to sudden load/generation unbalances. This reduces the average inertia constant of the whole system and hence reduces the margin to the dynamic stability
- it is important that dispersed generators remain connected to the network during voltage and/or frequency deviations caused by faults and other disturbances as specified for the large conventional synchronous generators, thus contributing to ride through system disturbances with their active and reactive outputs and their inertia
- on the other hand, the growing use of dispersed generation increases the probability of out-of-phase conditions.

All these trends lead to the conclusion that out-of-phase conditions have to be studied more carefully than in the past. A better understanding of the effects and consequences of out-of-phase conditions and of the present and future probabilities of occurrence is necessary.

### 3. OUT-OF-PHASE PHENOMENA

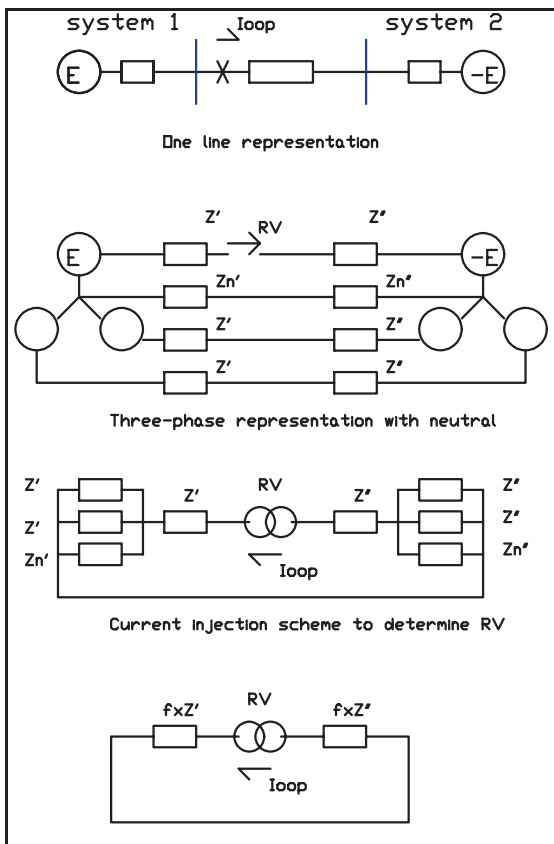


Fig. 3 Out-of-phase RV with  $f = \text{total } fpcf$

In common with the recently published Guide for Application of IEC 62271-100 and IEC 62271-1 [15], two out-of-phase cases are considered here:

- (i) generating units that separate from the network
- (ii) major systems that separate.

Whilst the focus of the above mentioned Guide is to explain the values given in the Standards, a more fundamental approach is taken here with emphasis on the behaviour of system topologies not directly considered in the Standard.

#### 3.1 Case (i)

Out-of-phase switching may be applicable to a generator circuit-breaker at the MV-terminals of a generator, as specified in IEEE Standard C37.013 (1997) [10], or to a generator circuit-breaker at the HV side of the step-up transformer, normally specified as a general purpose circuit-breaker to IEC 62271-100 or ANSI/IEEE C37.04/06/09. In both situations, as shown in figure 4, the total RV is caused by the disappearance of the voltage drop across the reactances of the generator, the step-up transformer and the system and the overall fpcf:

$RV = I_{loop} * fpcf * (Xd'' + X_{tr} + X_s)$ . The overall fpcf is a combination of the fpcf (depending on the neutral treatment  $Z_n$ ) of the systems at both sides of the circuit-breaker and can be deduced from the double Neptune-scheme as shown in figure 3.

The largest voltage drop will generally be across the generator sub-transient reactance. The transformer reactance is in the range from 0.1 to 0.15 pu whilst many modern generators have a sub-transient reactance in the range 0.18 – 0.27 pu; lower values (0.12 – 0.15 pu) were typical in old 2-pole turbine generators. The system reactance is typically five (or more) times smaller than sub-transient generator plus transformer reactance. Further, the natural frequency of the generator windings is 2 to 3 times lower than the natural frequency of the transformer windings. System frequencies usually have the lowest values defined primarily by the travelling waves of the shortest OH-lines. In terms of surge impedances and local capacitances, the generator will offer the lowest surge impedance (in the range of several tens to less than 100 Ohms) with the highest capacitance (typically 0.1  $\mu$ F) and the transformer the highest surge impedance (thousands of Ohm) with the smaller local capacitances. The system's surge impedance does not exceed 300 - 400 Ohm with local capacitances comparable with the capacitance of a transformer (thousands of pF).

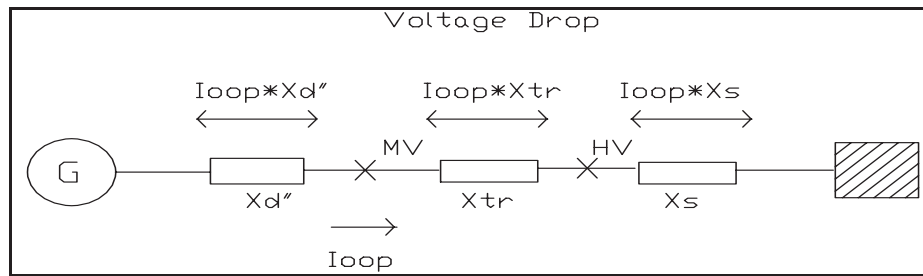


Fig. 4 Generator circuit-breaker RV

Seen from the HV-side of a step-up transformer (winding configuration: YN-D), it is assumed that the earth fault factor and therefore the first-pole-to-clear factor (fpcf) are very low:  $k=Z_0/Z_1$  is 0.7 to 0.9. With  $k$  being about 0.8 the fpcf becomes 0.92, and the second and last pole clearing factors are larger than the fpcf [5]. On the other hand, as shown in figure 3, the total fpcf is to be considered and not the individual fpcf at each side of the circuit-breaker. For  $k=0.8$  at the generator-transformer side and a fpcf of 1.1 at the net-side, the total fpcf is 0.94 to 0.96, depending on the ratio of normal sequence reactance at the generator/transformer side versus the normal sequence reactance at the network side.

With a fpcf of 1.3 at the net-side, the total fpcf becomes 1.06 for a sub-transient generator/transformer reactance which is five times the reactance at the net side. To derive the total RV, this total fpcf has to be multiplied with the out-of-phase voltage which depends on the out-of-phase angle. In this example, the total RV for full phase opposition will reach a value of 2.12 pu, with 5/6 of the voltage appearing at the step-up transformer side of the circuit-breaker and the remaining 1/6 appearing at the network side, in addition to the pre-clearing voltage of 4/6 pu. So, at the step-up transformer side the terminal voltage of the first clearing pole jumps from 0.67 pu to - 1.10 pu ( $\Delta = 1.77$  pu) and at the other terminal from 0.67 pu to 1.02 pu ( $\Delta = 0.35$  pu). For smaller out-of-phase angles  $\psi$ , the total RV, the two parts of the RV and the voltage jumps are smaller in proportion to  $\sin(\frac{1}{2}\psi)$ .

At the generator-transformer side the amplitude factor (over-swing) will be quite large (for instance 80%: amplitude factor 1.8), as the losses will be relatively low ( $X/R$  ratio of 50 or more) and the generator side capacitance large. A significant depression of the voltage at the generator terminals and therefore of the recovery voltage at the HV-side of the transformer can be expected [16], figure F.1 of [1]. This phenomenon leads to a considerable reduction of the voltage at the HV circuit-breaker, typically resulting in a residual voltage of 80% to 90%; i.e. a sub-subtransient source voltage of 0.8 to 0.9 pu, in the first few hundred  $\mu$ s after clearing the out-of-phase current. The effect is larger at larger currents but is not observed for generators with fully laminated poles and a damper winding [16].

The amplitude factor of the RV is determined by the natural frequencies of each side of the circuit-breaker and normally the natural frequencies differ substantially such that the components of the transient recovery voltage at both sides of the circuit-breaker swing independently and their crests do not coincide.

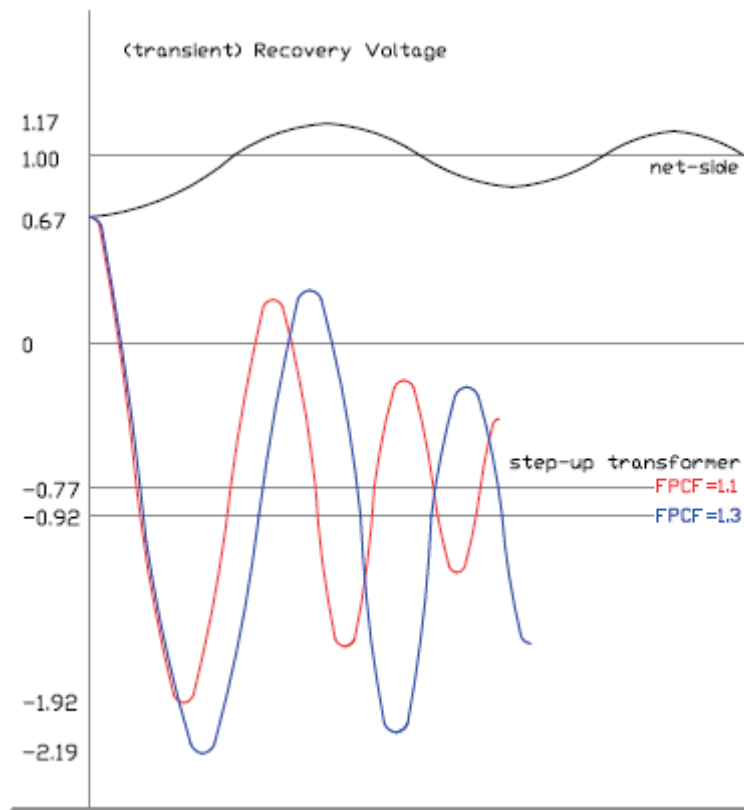


Fig. 5 Out-of-phase Recovery Voltage. Case (i)

Shortly before clearing the voltage at both terminals of the circuit-breaker pole is defined by:  
 $V_{cb} = E_s + (E_g - E_s) * X_s / (X_d'' + X_t + X_s)$ , where  $V_{cb}$  is the circuit-breaker terminal voltage,  $E_g$  is the source voltage at the generator side and,  $E_s$  is the source voltage at the net side. If  $E_g = -1.0$  pu,  $E_s = +1.0$  pu (full phase opposition) and  $X_d'' + X_t = 5 * X_s$  then  $V_{cb} = 0.67$  pu. The net side RV will swing from 0.67 pu to about 1.0 pu (see former page and figure 5). With an over-swing of the voltage jump corresponding to an amplitude factor of 1.5, a peak value of 1.17 pu is reached.

The transformer side will swing from 0.67 pu to -0.92 pu (assuming net side fpcf of 1.3 and 10% depression) with an amplitude factor of 1.8, thus giving a peak value of -2.19 pu. For a net-side fpcf of 1.1 (and 10% depression), the voltage will jump at the transformer side from 0.67 pu to -0.77 pu; with an amplitude factor of 1.8, a peak value of -1.92 pu is reached.

In order to estimate the crest value of the total TRV, the assumption is made that the peak at one side coincides with the power frequency recovery voltage at the other side. In this case,

1. the peak at the net side 1.17 pu coincides with -0.92 pu (resp. -0.77 pu) at the step-up transformer side, summing up to a TRV peak value of 2.1 (resp. 1.9 pu)
2. the peak at the step-up transformer's side -2.19 pu (resp. -1.92 pu) coincides with 1.0 pu at the net side, summing up to 3.2 pu (resp. 2.9 pu).

These peak values are higher than 2.5 pu, as specified in IEC 62271-100 for systems with fpcf = 1.3.

In figure 5, the wave-shapes on both sides of the first clearing pole are schematically given assuming full phase opposition. Reducing the out-of-phase angle will shift  $V_{cb}$  from 0.67 pu towards 1.0 pu, thus decreasing the over-swing at the net side but increasing the over-swing at the step-up transformer side. Moreover, due to the lower out-of-phase current the generator will show less depression and this leads to a higher residual voltage.

At an out-of-phase angle of 90° the out-of-phase voltage is 1.41 pu. Assuming no depression, a reactance ratio of 5,  $k = 0.80$  at the step-up transformer-side and  $fpcf = 1.3$  at the net side, it can be calculated that the peak-value of the TRV is 2.5 pu: a value which is recognised in the Standards. In other words, for these specific assumptions, the Standards do not address out-of-phase angles in excess of 90°.

In a system with a floating neutral, or equipped with Peterson coils, the  $fpcf = 1.5$  and the maximum RV will be 3.0 pu. The total TRV for the same example case can reach 4.55 pu at full phase opposition. Without depression, an out-of-phase angle of 75° gives a RV of 1.83 pu and a peak value of the TRV of 3.1 pu which is close to 3.13 pu as given in the Standards (for systems with  $fpcf$  of 1.5).

For a circuit-breaker at the MV-side of the step-up transformer, the IEEE/ANSI Standard C37.013 [10] is applicable. In this Standard an out-of-phase angle of 90° has been taken as the basic assumption to specify the TRV requirements. It has to be mentioned however that many utilities specify an angle of 180°; see for instance [8].

### 3.2 Case (ii)

When, during out-of-phase conditions, the equilibrium point (virtual short-circuit point) is somewhere on the OH-line that connects the two systems going out of synchronism, protection systems will trip the circuit-breaker. Whilst it is possible to install advanced and complicated out-of-phase blocking systems to delay the tripping command until the beating out-of-phase angle is small, this is uncommon and switching can normally occur over a wide range of out-of-phase angles. The TRV across the first clearing pole is determined by the system parameters on the busbar side of the circuit-breaker and by the line parameters at the line side. As the largest impedance will be on the line side, the largest voltage excursion will also appear at the line side.

The out-of-phase current is, to a large extent, dependent on the out-of-phase angle and the length of the OH-line. Due to the traveling wave effects, the TRV at the line side will exhibit a triangular shape and its peak value can be calculated as twice the wave traveling time along the OH-line multiplied by the RRRV (rate of rise of the recovery voltage). The traveling time is proportional to the line length, but the RRRV shows a decreasing trend with increasing line length due to the decrease in out-of-phase current ( $I_{oop}$ ). Specifically  $RRRV = fpcf * Z_{eq} * dI_{oop}/dt$  where  $Z_{eq}$  is the equivalent surge impedance. Due to the influence of the source impedances of both systems, the amplitude of  $I_{oop}$  is not inversely proportional to the line length. Therefore, the peak value of the line side TRV will still increase with an increasing line length. This effect, however, becomes smaller for OH-lines with longer lengths.

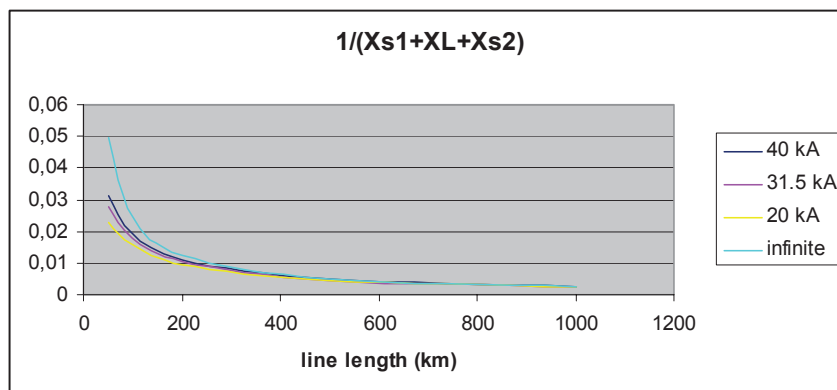


Fig. 6 Total admittance as function of line length

Figure 6 shows the total admittance of both systems and the interconnecting line as a function of the line length, for different (but arbitrarily chosen to be equal at both sides) source impedances of the systems; i.e. for 420 kV systems with a short-circuit power equivalent to short-circuit currents of 40 kA, 31.5 kA and 20 kA in comparison to infinite short-circuit powers.

In addition to the line side TRV, the busbar side TRV should be added. As  $I_{oop}$  is defined to be 25% of rating in the Standards and is often less than this in reality (15%), the system side TRV can be estimated to be 25% (15%) of the TRV associated with, for instance, T100. The peak value is then less than 0.37 pu (0.22 pu). For an OH-line with a length of 100 km, the return traveling time will be roughly 650  $\mu$ s, close to T2, as defined for T100. For a 420 kV/40 kA circuit-breaker, the peak value of the total TRV will be close to 4.1 pu for  $I_{oop} = 25\%$  and 2.5 pu for  $I_{oop} = 15\%$  of the rated short-circuit current.

In figure 7, the TRV peak values (line side) as a function of line length are shown for the example above (figure 6). The out-of-phase currents are based on full phase opposition. As the TRV peak value at the line side is proportional to  $I_{oop}$ , it is also proportional to  $\sin(\frac{1}{2}\psi)$ .

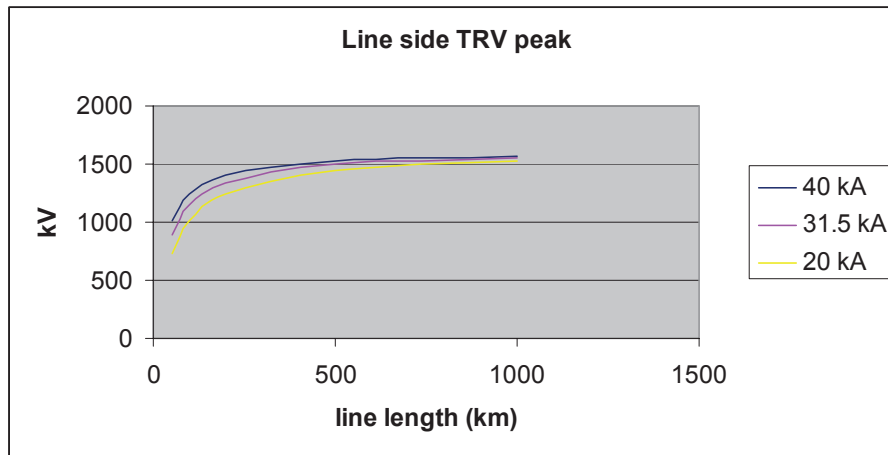


Fig. 7 Line side TRV peak value as function of length in a 420 kV-network

It can be concluded that the TRV peak values can be considerably higher than specified in the Standards (857 kV @ 1335  $\mu$ s for a rated voltage of 420 kV), even when taking into account smaller out-of-phase angles. For instance with a line length of 200 km and source impedances corresponding to a short-circuit current of 20 kA, an out-of-phase angle of 120° will still give a line side peak value of 1075 kV. Combined with a system side RV of roughly 100 kV this results in a total TRV peak of 1175 kV. A line length of 100 km under the same conditions will give 875 kV at the line side and 975 kV in total. The IEC peak value of 857 kV is reached at out-of-phase angles as small as 75° and 90° for 200 km and 100 km lines respectively.

Calculations and simulations for real networks show out-of-phase TRV peak values as high as 3.3 to 3.5 pu [9] or even 3.9 pu [19] for very extended networks (hundreds of km, low currents) and 3.0 to 3.5 pu for meshed networks (hundred or less km, relatively high currents).

#### 4. DIELECTRIC STRESSES ACROSS OPEN CONTACTS

During synchronization the longitudinal voltages applied to open contacts vary from zero to 2 pu in a periodic, beating pattern for periods of seconds or minutes. In case of frequent synchronisation, clause 2.3.2.4 of IEC 60071, part2 [13] recommends consideration of the occurrence of an earth fault during synchronisation (at one side!), thus leading to higher longitudinal voltages: up to 2.5 pu for a short time.

Clause 2.3.2.5 of [13] recommends careful examination of the probability of simultaneous occurrence of circumstances that lead to temporary overvoltages. Examples include an earth fault with consequential line tripping firstly at load side, load rejection with high overvoltage causing an earth fault, load disconnection under heavy pollution conditions, or a failure of a circuit-breaker to trip a line fault with a generator still feeding the earth fault. In such cases a careful system study is required.

Clause 2.3.2.2 of [13] indicates that full load rejection will lead to temporary overvoltages, which are normally less than 1.2 pu for moderately extended systems but which could reach values up to 1.5 pu for large extended networks and even more in case of (ferro)resonance. (Ferro)resonance, however, should be avoided and mitigation measures are suggested (cl. 2.3.2.3 and 2.3.2.6). The longitudinal overvoltages across the circuit-breaker open terminals are equal to the temporary overvoltages when the rejected load was of a static nature. But, in case of generators the longitudinal overvoltage can reach values up to 2.5 pu and in very extended systems even more. A power frequency longitudinal overvoltage as high as 2.5 pu is also given in clause D.1.3.2. of IEC 60694 [11].

With regard to the dielectric requirements under synchronising operations simultaneously with a substantial transient or temporary overvoltage, clause 4.2 of IEC 62271-100 [1] indicates that the standard requirements may be insufficient and the application of the requirements as specified for disconnectors across open contacts is recommended. In clause 4.2 of IEC 60694 [11] different requirements for the longitudinal withstand voltage across open contacts for the safety function (eg. disconnectors) and for the working function (eg. circuit-breakers) are specified for rated voltages  $\leq 245$  kV. The values given in column (2) of the tables 1a and 1b [11], applicable for rated voltages  $\leq 245$  kV, are used for the specification of the longitudinal requirements of circuit-breakers, while the values given in column (3) are used for the longitudinal requirements for disconnectors. For rated voltages  $\geq 300$  kV, the values of column (3) of the tables 2a and 2b are specified for the 1min power frequency type test across open contacts of both circuit-breakers and disconnectors, however the values of column (2) are accepted for routine tests. In the following table the power frequency short-duration withstand voltages are reported for some rated voltages for comparison, including the withstand voltages in pu. For rated voltages  $\leq 245$  kV, the highest class of insulation has been taken from table 1a, and for  $\geq 300$  kV the values given in table 2a:

Rated voltage (kV)	(2) 1min withstand (kV) <sup>+) </sup>	(2) 1min withstand (pu) <sup>+) </sup>	(3) 1min withstand (kV) <sup>Δ) </sup>	(3) 1min withstand (pu) <sup>Δ) </sup>
24	50	3.61	60	4.33
72,5	140	3.34	160	3.82
145	275	3.28	315	3.76
245	460	3.25	530	3.75
420	520	2.14	610	2.52
550	620	1.95	800	2.52
550 °	710	2.24	890	2.80
800	830	1.80	1150	2.49

<sup>o</sup> from table 2b: additional rated insulation levels in North America.

<sup>+)</sup>  Specified for longitudinal insulation of circuit breakers with rated voltage  $\leq 245$  kV

<sup>Δ)</sup>  Specified for longitudinal insulation of disconnectors (all rated voltages) and of circuit breakers with rated voltage  $\geq 300$  kV

IEC-Standard 62271-203 “Gas-insulated metal-enclosed switchgear for rated voltages above 52 kV” [17] (the previous Standard 60517), makes reference to these tables in IEC 60694 but for the highest rated voltages different short-duration power frequency withstand voltages are specified:

Rated voltage (kV)	(2) 1min withstand (kV)	(2) 1min withstand (pu)	(3) 1min withstand (kV)	(3) 1min withstand (pu)
420	650	2.68	815	3.36
550	710	2.24	925	2.91
800	960	2.08	1270	2.75

External and internal flashovers across the open contacts of EHV circuit-breakers have occurred in operation during synchronizing of generating units (due to contaminated wet insulators in live tank circuit-breakers, due to failure of grading capacitor in dead tank breakers, etc.) or during the dead time before line automatic re-closure. These events generally cause a busbar fault, and also explosions of circuit-breaker poles. It is therefore necessary to specify the circuit-breakers to withstand with a reasonable margin the over-voltages liable to occur during these manoeuvres and to preserve this capacity in operation.

Some reported cases of circuit-breaker failures during synchronizing of generating units have been caused by flashovers on contaminated and wet external insulation of the interrupting chambers of live tank circuit-breakers, by failure of the grading capacitor in parallel with one of the contacts, or by inadequately specified power-frequency withstand voltage of circuit-breakers across open contacts eroded by aging or by other reasons. Rare flashovers across the open contacts of line circuit-breakers during the dead time before the automatic re-closure have been reported to be caused by multiple lightning strokes in absence of surge arresters or of special protective air gaps at the open line terminal [18]. Figure 8 shows a special protective gap shaped such as to minimize the influence of polarity and wave shape of LIs and SIs on flashover voltage and to provide a time to flashover shorter in the gap than in the protected open circuit-breaker. For decades, in Italy, there is very good service experience with the application of these special protective gaps.

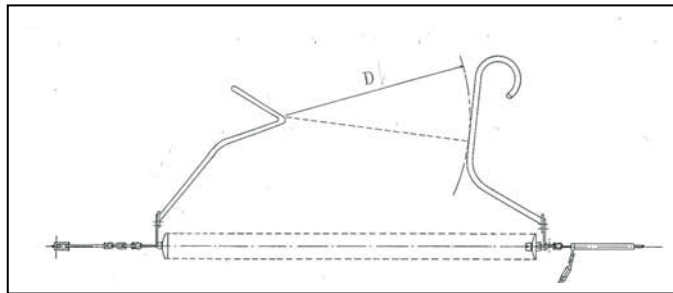


*Fig.8 Special protective spark gap fitted in the line anchor insulator strings to substation gantry;  $D = 1700 \text{ mm}^\circ$  for 380 kV lines;  $D = 800 \text{ mm}$  for 150 kV lines.*

*$^\circ$  SI 50% flashover voltage = 1040 kV(3 pu)*

In live tank circuit-breakers the external insulation between terminals is not energized when the circuit-breaker is closed. It is recommended that for the external insulation across open contacts of live tank circuit-breakers used for synchronizing, the withstand voltages as specified to column (3) of the tables 1a, 1b, 2a and 2b of IEC 60694 [11], should be withstood in a type test under wet test conditions and also under representative artificial pollution conditions.

All the dispersed statements in the Standards support the view point that with respect to out-of-phase conditions and synchronisation, circuit-breakers longitudinal dielectric withstand should be specified to column (3) rather than column (2) for all rated voltages.

## 5. OTHER CONDITIONS LEADING TO HIGH TRV PEAK VALUES

When clearing single or multi-phase faults distant from the substation on an OH-line (instead of at a short distance, as with short-line faults), the well-known triangular wave-shape of the TRV at the line side will rise to high values, depending on the wave travelling time from the circuit-breaker terminal up to the location of the fault and back. This phenomenon is known as long line fault (LLF) and has been discussed in [14]. As the time to the peak value of the TRV is rather long, it is comparable with the TRV for out-of-phase switching. Peak values of 2.4 pu have been reported [14] and LLF is a subject of study for CIGRE WG A3.19.

Clearing faults in series compensated OH-lines leads to TRV values in excess of the values specified in the Standards, due to the charging voltage on the series capacitor banks. Peak values of the TRV as high as 4.6 pu (420 kV-system in Turkey) and 4.8 pu (800 kV system in Canada) could be expected without certain countermeasures. By means of special MOSA with a low SSPL (switching surge protective level) of 1.57 pu, Hydro Québec manages to reduce the TRV peak value to 3.2 pu. In Turkey, MOV parallel to the arcing chambers of circuit-breakers have been applied successfully. Depending on the requirement of re-synchronisation by the circuit-breaker, the TRV peak can be reduced to 2.5 pu or 3.0 pu. These solutions lead nevertheless to TRV peak values comparable with or beyond those given before for out-of-phase conditions.

Although there is no real application of half-wave length lines (HWLL, 3000 km at 50 Hz; 2500 km at 60 Hz), a number of studies on over-voltages and TRVs have been performed for this interesting technology for long distance bulk power transmission. Simulations show that clearing faults in HWLL will lead to TRV peak values as high as 3.2 pu, again comparable with the TRV peak values mentioned before for out-of-phase clearing [9].

Another switching phenomenon giving high TRV values is the de-energization of unloaded OH-lines under high TOV (temporary overvoltages) conditions [15]. For the 800 kV system of Hydro Québec TRV peak values of 3.3 pu to 3.5 pu have been reported under such conditions; see figure 9b. [9]

Out-of-phase switching on series compensated OH-lines has not been addressed yet, but it is evident that the electrical charge on the series capacitors will add to the peak value of the TRV. Unfortunately, right at the moment of current clearing the voltage across the series capacitors is at maximum value, unless the capacitors have been by-passed by the self-triggered or forced triggered spark gaps. The situation is similar to clearing short-circuit currents. In modern series capacitors metal-oxide varistors are installed in parallel to the capacitor bank. Such varistors limit the voltage across the capacitor banks. Moreover special surge arresters connected phase-to-ground or varistors across the arcing chambers of the circuit-breakers are applied, thus limiting the total TRV peak value at clearing short-circuit currents and out-of-phase currents as well. The countermeasures for limiting the peak value of the TRV at clearing short-circuit currents are also effective at clearing out-of-phase currents; see figure 9a. [9]

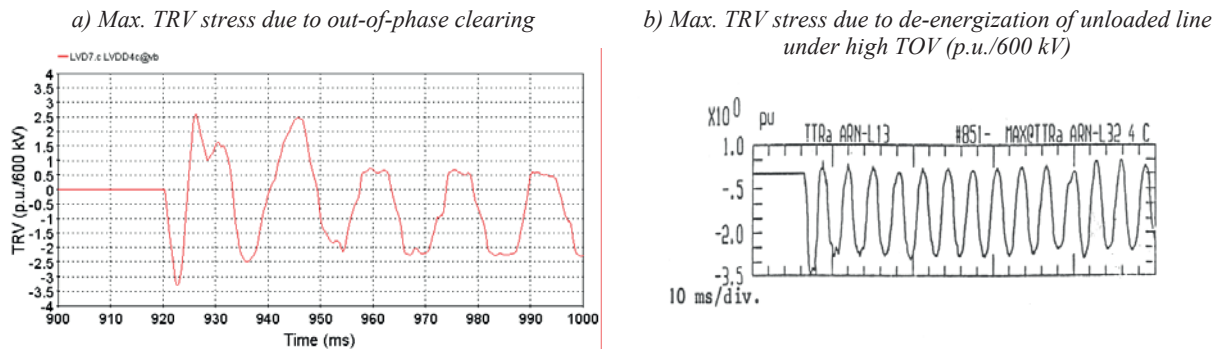


Fig. 9: Maximum TRV stresses due to out-of-phase clearing and de-energization of unloaded line under high TOV

## 6. CONCLUSIONS

- The Standards showed to be based on an out-of-phase angle substantially less than  $180^\circ$ , despite the fact that in many cases the angle will be random, ranging up to  $180^\circ$ . For generator circuit-breakers and special applications users already ask for out-of-phase angles of  $180^\circ$ .
- The RV in the Standards [1][4] is 2.0 or 2.5 pu respectively for systems with an effectively earthed neutral or a non-effectively earthed neutral with a TRV of 2.5 and 3.13 pu respectively.
- Both IEEE and IEC specify the RRRV of the TRV for out-of-phase switching to be lower than the RRRV specified for T100, whereas higher values occur in the systems. The RRRV for out-of-phase switching is considered to be covered by T30 (multi-part testing).
- Standardised TRV is based on system conditions in the absence of an earth fault. For situations with frequent out-of-phase switching and synchronisation, the Standards recommend to specify actual TRVs in the system (taking into account tripping and blocking relays for out-of-phase conditions when applied) and to adapt the requirements for the longitudinal dielectric strength accordingly.
- Under rather normal system conditions (no earth fault, no temporary overvoltages), full phase-opposition switching of a generating plant at the HV-side leads to TRV peak values in the range of 2.9 to 3.2 pu in systems with effectively earthed neutral and higher values for systems with un-earthed neutral. The peak values of the TRV as specified in the Standards, cover out-of-phase angles up to  $90^\circ$  or, in case of systems with un-earthed neutral, even less ( $75^\circ$ ).
- For out-of-phase switching of OH-lines, calculations show peak values of the TRV from 2.5 pu (100 km length,  $I_{oop} = 15\%$ ) to 4.1 pu (100 km length,  $I_{oop} = 25\%$ ) and even beyond for longer line lengths, under full phase opposition. The Standards cover out-of-phase angles up to  $90^\circ$  (line length < 100 km) or up to  $75^\circ$  (line length < 200 km).
- During synchronisation, a longitudinal power frequency withstand test voltage larger than 2.0 pu, preferably 2.5 pu or even 3.0 pu, is a reasonable requirement for circuit-breakers used for that purpose. The related auxiliary components, such as grading capacitors, MOVs, insulating materials, external insulation, should be equally specified and tested.

- Under out-of-phase switching conditions the first-pole-to-clear factor is determined by the neutral status of the systems at both sides of the circuit-breaker, as shown by the double Neptune-scheme. Depression of the generator source voltage has to be taken into account, unless the rotor is equipped with fully laminated poles and a damper winding.
- False synchronisation, mal-operation of protection equipment and erroneous switching operations by operators [7], may lead to considerable damage. Re-strikes at clearing out-of-phase currents with large out-of-phase angles will also lead to comparable consequences. Developments in modern networks lead to a higher probability of the phenomena described: distributed generation leading to large power transfers, systems separation on overloaded OH-lines, large power swings due to tripped generation, etc.

## 7. RECOMMENDATIONS

- Utilities have to look carefully for such situations and, when applicable, put forward the appropriate requirements to the protection of involved equipment and switchgear.
- The present Standards do not give users clear and adequate support in specifying TRV-values for out-of-phase conditions, for clearing of fault currents flowing through series capacitors and for dielectric withstand requirements under synchronisation conditions. The requirements should be revised or more guidance should be incorporated to improve understanding.
- Since increased TRV requirements may lead to increased costs of circuit-breakers, enhanced out-of-phase requirements should be limited in their application or countermeasures to limit TRV should be used [9].

## 8. BIBLIOGRAPHY

- [1] IEC Standard 62271-100 (Am.2, 2006) *Part 100: High-voltage Alternating-current Circuit-breakers*
- [2] IEEE Standard C37.04 (1999) *IEEE Standard Rating Structure for AC High-Voltage Circuit Breakers Rated on a Symmetrical Current Basis*
- [3] ANSI Standard C37-06 (1997) *AC High-Voltage Circuit Breakers Rated on a Symmetrical Current Basis. Preferred Ratings and Related Required Capabilities*
- [4] IEEE Standard C37-09 (1999) *IEEE Standard Test Procedures for AC High-Voltage Circuit Breakers Rated on a Symmetrical Current Basis*
- [5] TRV-Networks for the Testing of High-Voltage Equipment  
A.L.J. Janssen, P. Knol, L. van der Sluis  
CIGRE SC 13 Session 1996, Rep. 13-205
- [6] TRV's and Fault Clearing Stresses in Extra-High-Voltage Radial Networks  
E. Haginomori, e.a.  
EEJ, Vol. 114, No. 4, (1994), pp 50-61
- [7] Distributed Generation in Relation to Phase Opposition and Short-circuits  
A.L.J. Janssen, e.a.  
10th SCC Symposium 2002 in Poland
- [8] Contribution to Q. 3-15 of SC A3 Special Report  
L. Zehnder, M. Kriegel  
CIGRE Session 2006 Proceedings
- [9] Long Distance AC Power Transmission and Shunt/Series Compensation - Overview and Experiences  
Q. Bui-Van, F. Gallon, F. Iliceto, A.L.J. Janssen, B. Middleton, M. Waldron  
CIGRE SC A3 Session 2006, Rep. A3-206
- [10] IEEE Standard C37.013 (1997) *Standard for AC High-Voltage Generator Circuit Breakers Rated on a Symmetrical Current Basis*
- [11] IEC Standard 60694 (2001) *Common specifications for high voltage switchgear and controlgear standards*
- [12] IEC Standard 60071-1 (1993) *Insulation Co-ordination, Part 1: Definitions, principles and rules*
- [13] IEC Standard 60071-2 (1996) *Insulation Co-ordination, Part 2: Application guide*
- [14] Severe Duties on High-Voltage Circuit Breakers Observed in Recent Power Systems  
H.Hamada, Y.Kasahara, T.Shimato, K.Hirasawa, K.Suzuki, T.Yoshizumi  
CIGRE SC 13 Session 2002, Rep. 13-103
- [15] CIGRE Technical Brochure 305 (2006) *Guide for the application of IEC 62271-100 and IEC 60694, Part 2*
- [16] Comparison of Generator Circuit-Breaker Stresses in Test Laboratory and Real Service Condition  
I.M. Canay  
IEEE-PD, Vol.16, No.3, July 2001, pp.415-421
- [17] IEC Standard 62271-203 (2003) *Gas-insulated metal-enclosed switchgear for rated voltages above 52 kV*
- [18] Flashovers of open circuit-breakers caused by lightning strokes CIGRE TF 33.11.06  
Électra 186, Oct. 1999, pp. 114-123
- [19] Circuit-breaker Requirements for Alternative Configurations of a 500 kV Transmission System  
J. Amon, S.A. Morais, e.a.  
CIGRE SC 13 Colloquium 1995, Brazil, Rep. 2.3

Journal  
of Energy

AN  
ENERGY